**Ivane Javakhishvili**
**Tbilisi State University**

**Nana Shatashvili**

# Magneto-Hydrodynamic Flows in Two-Fluid Plasmas

(01.04.08 - Plasma Physics and Chemistry)

The Doctoral Dissertation
in Physical and Mathematical Sciences

To the memory of my father
Professor Luli Shatashvili

Tbilisi
2005

ivane javaxiSvilis saxelobis
Tbilisis saxelmwifo universiteti

nana SaTaSvili

# magnitohidrodinamiuri dinebebi orsiTxovan plazmaSi

(01.04.08 – plazmis fizika da qimia)

disertacia
fizika-maTematikis mecnierebaTa
doqtoris xarisxis mosapoveblad

naSromi eZRvneba Cemi mamis,
profesor luli SaTaSvilis
naTel xsovnas

Tbilisi
2005

## Abstract

Study of the dynamics of flowing multi-fluid plasmas embedded in the ambient magnetic fields is one of the fundamental problems of modern physics. The interest has been dramatically increased since the appearance of: latest observational evidence of fine structuring of Stellar Atmospheres; novel findings in Extra-Galactic Medium; as well as systematic investigations of the Astrophysical Jets and Radiation coming from various astrophysical objects.

Plasma "flow" could be assigned at least two connotations: 1) The flow is a primary object whose dynamics bears critically on the phenomena under investigation. The problems of the formation and the original heating of the astrophysical structures, the creation of channels for particle escape, for instance, fall in this category, 2) The flow is a secondary feature of the system, possibly created as a by-product and/or used to drive or suppress an instability. Since the generation of flows, which will eventually create the structures, is the theme of this effort, the flows here are fundamental.

In this view, it is extremely important to develop the self-consistent unified approach to the magneto-fluid coupling to study the creation of ordered structures in plasmas. An essential component of this global theory is the emphasis on including the plasma flows as a crucial component (along with the magnetic field) that dictates the dynamics of the ordered structure formation. Plasma confinement experiments, collimation of relativistic jets, large scale magnetic field openings in stellar atmospheres as well as the escape of particles from various systems are good examples of the crucial role of magnetic fields in creation of steady structures and their heating processes.

Self-organization of an ordered structure occurs in plasma under rather restrictive conditions. A new framework invokes a coercive form that results in a criterion for self--organizing relaxation of the two-fluid plasma. The constraints (constants of motion of the ideal model) are adjusted, through a weakly dissipative process, so that the relaxed state, under well-defined conditions, is a stable equilibrium independent of the direct effects of dissipation. A general solenoidal vector field, such as a magnetic field or an incompressible flow, can be decomposed into an orthogonal sum of Beltrami fields. Nonlinear dynamics of plasma induces complex couplings among these Beltrami fields. In a single-fluid magnetohydrodynamic (MHD) plasma, however, the energy condensates into a single Beltrami magnetic field

resulting in the self-organization of a force-free equilibrium, that is, the Taylor relaxed state. By relating the velocity and the magnetic fields, the Hall term in the two-fluid model leads to a singular perturbation that enables the formation of an equilibrium given by a pair of two different Beltrami fields. This new set of relaxed states, despite the simple mathematical structure, includes a variety of plasma states that could explain a host of interesting phenomena. The H-mode (high-confinement) boundary layer, where a diamagnetic structure is self-organized under the coupling of the magnetic field, flow, electric field, and pressure; high beta equilibrium are the examples.

The mechanisms for energy transport and channeling of particles are deeply connected with the challenging and exciting problems of the solar coronal heating and of the origin of the solar wind (SW). A number of recent investigations have made a strong and convincing case that neither the solar wind "acceleration" nor the numerous eruptive events (and flares of different kind and coronal mass ejections [CMEs ]) in the solar atmosphere can be treated as isolated and independent problems; they must be solved simultaneously along with other phenomena, in particular, the plasma heating that, by itself, may take place in several different stages. Several reasons (mainly the low observational resolution, and problems of resolving extremely short spatial and temporal scales in computer simulations), however, have prevented the emergence of a unified and realistic quantitative model dealing with the dynamics of energy dissipation and evolution in the solar atmosphere. Realistic transport processes are generally not included in the models that are often lower dimensional or steady state.

When the heating power exceeds a critical value, the tokamak plasmas undergo a spontaneous self-organizing transition from a low (L-mode) to a high confinement state (H-mode). The improved confinement is believed to be caused by the generation of a shear (zonal) flow, which is responsible for suppressing fluctuations and thus inhibiting transport. After this transition, a very steep pressure gradient develops at the edge. The height of the pressure pedestal is a natural figure of merit for energy confinement. Elucidation of the physics of pedestal formation, and predicting its maximum achievable height are issues crucial for magnetic fusion. To understand the physics of the formation and the properties (including the maximum sustainable pressured) of the pedestal, therefore, a two-pronged attack is strongly indicated: a systematic buildup of the database as well as the development of pertinent theories. Prediction of the height and width of the pressure profile has been actively pursued so as to provide a reliable extrapolation to future burning plasma devices.

Among the various nonlinear effects which may occur in a plasma interacting with strong laser pulses, the generation of quasistatic magnetic fields (QSMs) is found to be one of

the most interesting and significant, particularly because the presence of these fields could have considerable influence on the overall nonlinear plasma dynamics. In relativistic laboratory plasmas such immense magnetic fields can play important role in developing of the fast-ignition concept, particle acceleration schemes, etc., while in astrophysical plasmas generation of strong magnetic fields can explain many fundamental phenomena typical of extreme cosmic conditions. On the other hand, strong magnetic fields play crucial role in energy release phenomena in plasmas and plasma-like media providing effective energy sources for explosive and eruptive events as well as heating.

The relativistically hot *e–p* pairs constitute a major component of many of the astrophysical and cosmic plasmas, though a minority of cold electrons and heavy ions may also be present. For instance, outflows of $e - p$ plasma from pulsars entering low density ambient $e - i$ plasma in the inter-stellar regions form two-electron-temperature electron–positron–ion $(e - p - i)$ plasmas. The three-component plasmas, namely, the majority hot $e - p$ component with a small fraction of heavy ions, have been studied in the context of pulsar magnetospheres. On the other hand, it was demonstrated recently that the presence of minority ion species in hot $e - p$ plasma can lead to the creation of stable, localized, nondispersive and nondiffracting pulses that carry a large density excess within the region of field localization, leading to the formation of the so-called “light bullets”. Localized intense radiation pulses may be used to understand the character of AGN and pulsar radiation, as well as for particle acceleration in astrophysical situations.

The aim of the work is:

1) To develop the unified theory for the description of equilibrium structure creation and heat transfer phenomena in two-fluid plasmas due to magneto-fluid coupling.
2) To explore the Energy Transformation Mechanisms for the description of Explosive and Eruptive Events in the two-fluid plasmas.
3) To investigate the problem of magnetic field generation in underdense plasmas by super-strong short EM pulses.
4) To develop the unified analytical and numerical methods for the acceleration of plasma flows and the creation of their escape channels through the area nested with closed field structures.

The work is organized as follows: in the chapter-1, the systematic model for the interaction of two-species plasmas with the arcade-like magnetic fields has been developed; the possibility of the dynamical creation of hot quasi-equilibrium loops - of typical solar coronal structures is shown; the formation conditions for typical coronal equilibria is studied in detail; the problem of equilibrium structure creation in relativistically hot two-temperature e-p plasmas with small fraction of cold ions is investigated. In the chapter-2 we develop a basic model for coupled vortex dynamics in two-fluid MHD; study systematically the equilibrium states in incompressible Hall MHD; investigate the conditions for eruptive events in the Solar Atmosphere due to magneto-fluid coupling; suggest the novel approach for the generation of QSM fields in two-fluid plasmas embedded in super-strong EM fields for various conditions. In the chapter-3, we develop a model for the dynamical acceleration of plasma flows interacting with arcade-like ambient magnetic fields; show the applications for the Solar Atmosphere; present equilibrium analysis for the acceleration of plasma flows in the compressible two-fluid plasmas due to magneto-fluid coupling; explore the Reverse Dynamo Mechanism for the acceleration of Plasma Flows; study the process of dynamical creation of channels for the particle escape in the Solar Atmosphere; give the 1D analysis for Solar Wind origin.

At the end I emphasize the major results of the work.

# Contents

# Chapter 1

# Structure creation and heat-transfer phenomena in two-species plasmas due to Magneto-Fluid Coupling

## 1.1 Background

The TRACE observations [1, 2, 3] reveal that the solar corona is comprised of lots of thin loops that are intrinsically dynamic, and that continually evolve. These very thin strings, the observations indicate, are heated for a few to tens of minutes, after which the heating ceases, or at least changes significantly in magnitude [1]. In this study we examine a class of mechanisms, which, through the viscous–dissipation of the plasma kinetic energy, provide the primary and basic heating of the coronal structures during their very formation. The basic input of the theory is the reasonable assumption that the coronal structures are created from the evolution and re–organization of a relatively cold plasma flow [1–21] emerging from the sub–coronal region (between the solar surface and the visible corona) and interacting with the ambient magnetic field anchored inside the solar surface. During the process of trapping and accumulation, a part of the kinetic energy of the flow is converted to heat by viscous dissipation and the coronal structure is

born hot and bright. For this to happen, we must find alternative fast and efficient heating mechanisms because, for the conditions prevalent in the coronal structures, the standard viscous dissipation is neither efficient nor fast. The rates of viscous dissipation can be considerably increased by processes which either enhance the local viscosity coefficient, or induce short scale structures in the velocity field. At present we do not know of any convincing mechanism for the former possibility. This study, therefore, is limited to an examination of processes of the latter kind. We find that as long as the flow–velocity field is treated as an essential and integral part of the plasma dynamics, fast and desirable viscous dissipation does, indeed, result. Consequently, during its very formation, the coronal structure can become hot and bright.

Of the several possible mechanisms by which the flow kinetic energy may be converted into heat we emphasize the following two: The first is the ability of supersonic flows to create nonlinear perturbations which steepen to produce short scale structures which can dissipate by ordinary viscosity. The second stems from the recently established property of the magnetofluid equilibria for extreme sub–Alfvénic flows (most of the observed coronal flows fall in this category) – such flows can have a substantial, fastly varying (spatially) velocity field component even when the magnetic field is mostly smooth. Viscous damping associated with this varying component could be a major part of the primary heating needed to create and maintain the bright Corona. From a general framework describing a plasma with flows, we have been able to "derive" several of the essential characteristics of the coronal structures. Theoretical basis for both these mechanisms will be discussed. Our simulation (for which we developed a dissipative two–fluid code), however, concentrates only on the first mechanism, and preliminary results reproduce many of the salient observational features. There is clear cut evidence of nonlinearly steepened velocity fields which effectively dissipate and heat the coronal structure right through the process of formation. The numerical investigation of the second mechanism, which will require a much higher spatial resolution, will be undertaken soon.

Naturally all these processes require the existence of particle flows with reasonable

amounts of kinetic energy. There are several recent publications [1–14] cataloguing enough observational evidence for such flows in the regions between the sun and the corona to warrant a serious investigation in this direction. It must be admitted that we still have little understanding of the nature of the processes by which the relatively cool material (no hotter than about 20000K) moves upward from low altitudes (as low as a few thousand kilometers) to the outer atmosphere. For this study, we shall simply exploit the observation that the flows exist, and work out their consequences. We believe that the flows might prove to be a crucial element in solving the riddle of coronal heating.

The model for the solar atmosphere that we propose and investigate is obtained by injecting an essential new feature into several extant notions — the plasma flows are allowed to play their appropriate role in determining the evolution and the equilibrium properties of the structures under investigation. We reiterate that the distinguishing ingredient of our model is the assumption (observationally suggested) that relatively cold particles spanning an entire range of velocity spectrum — slow as well as fast, continually flow from the sub–coronal to the coronal regions. It is the interaction of these cold primary flows with the solar magnetic fields, and the strong coupling between the fluid and the magnetic aspects of the plasma that will define the characteristics of a typical coronal structure (including Coronal Holes). In this study we limit ourselves to the formation and primary heating aspects; we do not deal with instabilities, their nonlinear effects, flaring etc. These are the problems that we will confront at the next stage of the development of the model.

Below we describe in relative detail our basic model for the upper solar atmosphere, a time–dependent, two–fluid system of currents and flows. The flows are treated at par with other determining dynamical quantities, the currents and the solar magnetic fields. Next subsection is devoted to the derivation of the characteristics of typical coronal structures from the basic model. Following a general discussion, we numerically simulate the evolution of a cold plasma flow as it interacts with the solar magnetic field and gravity. We follow the fate of an initial cold supersonic flow as the particles get trapped by the

magnetic field. By the time a sizeable density is built up we also find a considerable rise in temperature. In a very short time the velocity field develops a shock–like structure which dissipates with ordinary viscosity to convert the flow kinetic energy to heat. Next we take a different approach, and describe elements of the recently investigated magneto–fluid theory (see Mahajan and Yoshida, 1998, 2000) which allows the existence of equilibrium solutions missing in the flowless MHD. We find that a short–scale velocity component is predicted to be an essential aspect of a class of magnetofluid states in terms of which a typical coronal structure could be modelled. The magnetofluid states are the equilibrium states created by the strong interaction of the magnetic and the fluid character of a plasma, and are derived from the normal two–fluid equations when the velocity field is treated at par with the magnetic field. In a somewhat detailed discussion, we argue for the relevance of these states for the solar corona. These states could be seen as a set of quasi–equilibria evolving to an eventual hot coronal structure; the dissipation of the small scale velocity component provides the necessary source of heating. Since the numerical simulation of these states requires a much finer resolution than we have in our code, their time dependent simulation is deferred to a future work.

The main results of this chapter are published in Refs.[70]-[73],[102-103],[111].

## 1.2 The basic model: general equations for the interaction of 2-species plasmas with the arcade-like magnetic fields

In this section we will develop a general theoretical framework from which the typical solar coronal structure will be "derived." In our model, the plasma flows from the Sun's surface provide the basic source of matter and energy for the myriad of coronal structures (including Coronal Holes). Although the magnetic field is, naturally, the primary culprit behind the structural diversity of the corona, the flows (and their interactions with the magnetic field) are expected to add substantially to that richness.

The primary objective of this study is to investigate how these flows are trapped and heated in the closed magnetic field regions, and create one of the typical shining coronal elements. We shall, however, make a small digression to suggest a possible fate of the fast flows making their way through the regions where the magnetic field is weak, or has open field lines. The faster particles could readily escape the solar atmosphere in the open field-line regions. They could also do so by punching temporary channels in the neighboring closed field–line structures. The flows escaping through these existing or "created" coronal holes (the coronal holes (CH) are highly dynamical structures with open and "nearly open" magnetic field regions, see e.g. [22]) may eventually appear as the fast solar wind.

In the closed field–line, the magnetic fields will trap the flows, and the trapping will lead to an accumulation of particles and energy creating the coronal elements with high temperature and density. We shall not consider the solar activity processes, since the activity regions (AR) and flares, though an additional source of particles and energy, cannot account for the continuous supply needed to maintain the corona. Moreover, in the theory we suggest, the flare is understood to be a secondary event and not the primary source for the creation of the hot corona.

To describe the entire atmosphere of the quiescent, non–flaring Sun we use the two–

fluid equations where we keep the flow vorticity and viscosity effects (Hall MHD). The general equations will apply in both the open and the closed field regions. The difference between various sub–units of the atmosphere will come from the initial, and the boundary conditions.

Let $\mathbf{V}$ denotes the flow velocity field of the plasma in a region where the primary solar magnetic field is $\mathbf{B}_s$ . It is, of course, understood that the processes which generate the primary flows and the primary solar magnetic fields are independent (say at $t = 0$ time). The total current $\mathbf{j} = \mathbf{j}_f + \mathbf{j}_s$ (here $\mathbf{j}_f$ is the self–current that generates the magnetic field $\mathbf{B}_f$ and $\mathbf{j}_s$ is the source of the solar field $\mathbf{B}_s$) is related to the total (that can be observed) magnetic field $\mathbf{B} = \mathbf{B}_s + \mathbf{B}_f$ by Ampére's law:

$$\mathbf{j} = \frac{c}{4\pi} \nabla \times \mathbf{B}. \tag{1.1}$$

Notice that in the framework we are developing (assumption of the existence of primary flows), the boundaries between the photosphere, the chromosphere and the corona become rather artificial; the different regions of each coronal structure are distinguished by just the parameters like the temperature and the density. In fact, these parameters should not show any discontinuities; they must change smoothly along the structure. At some distance from the Sun's surface, the plasma may become so hot and dense that it becomes visible (the bright, visible corona), and this altitude could be viewed as the base of the corona. But to study the creation and dynamics of bright coronal structures (loops, arches, arcades etc.) we must begin from the photosphere, and determine the plasma behavior in the closed field regions.

Assuming that the primary flows provide, on a continuous basis, the entire material for coronal structures, the solar flow with density $n$ will obey the Continuity equation:

$$\frac{\partial}{\partial t} n + \nabla \cdot (n\mathbf{V}) = 0. \tag{1.2}$$

We must add a word of caution: in the closed field regions, the trapped particle density may become too high for the confining field, resulting in instabilities of all kinds. In this study we shall not deal with instabilities and their consequences; it will constitute the next stage of development of the model.

Since the corona as well as the SW are known to be mostly hydrogen plasmas (with a small fraction of Helium, and neutrons, and an insignificant amount of highly ionized metallic atoms) with nearly equal electron and proton densities: $n_e \simeq n_i = n$ , we expect the quasineutrality condition $\nabla \cdot \mathbf{j} = 0$ to hold.

In what follows, we shall assume that the electron and the proton flow velocities are different (two–fluid approximation was used e.g. in Sturrock and Hartly, (1966). Neglecting electron inertia, these are $\mathbf{V}_i = \mathbf{V}$, and $\mathbf{V}_e = (\mathbf{V} - \mathbf{j}/en)$, respectively. We assign equal temperatures to the electron and the protons for processes associated with the quiescent Sun. For the creation processes of a typical coronal structure, this assumption is quite good. For the fast SW, however, we know from recent observations (Banaszkiewicz *et al.* 1997 and references therein), that the species temperatures are found to be different: $T_i \sim 2 \cdot 10^5\,\mathrm{K}$ and $T_e \sim 1 \cdot 10^5\,\mathrm{K}$. Since the fast SW is not the principal interest of this study, we shall persist with the equal temperatures assumption; the kinetic pressure $p$ is given by:

$$p = p_i + p_e \simeq 2\,nT, \qquad T = T_i \simeq T_e. \tag{1.3}$$

With this expression for $p$, and by neglecting electron inertia, the two–fluid equations are obtained by combining the proton and the electron equations of motion:

$$\frac{\partial}{\partial t} V_k + (\mathbf{V} \cdot \nabla) V_k =$$

$$= \frac{1}{en}(\mathbf{j} \times \mathbf{b})_k - \frac{2}{nm_i}\nabla_k(nT) + \nabla_k\left(\frac{M_\odot G}{r}\right) - \frac{1}{nm_i}\nabla_l \Pi_{i,kl}, \tag{1.4}$$

and

$$\frac{\partial}{\partial t}\mathbf{b} - \nabla \times \left[\left(\mathbf{V} - \frac{\mathbf{j}}{en}\right) \times \mathbf{b}\right] = \frac{2}{m_i}\nabla\left(\frac{1}{n}\right) \times \nabla(nT), \tag{1.5}$$

where $\mathbf{b} = e\mathbf{B}/m_i c$, $m_i$ is the proton mass, $G$ is the gravitational constant, $M_\odot$ is the solar mass, $r$ is the radial distance, and $\Pi_{i,lk}$ is the ion viscosity tensor. For flows with large spatial variation, the viscous term will end up playing an important part. To obtain an equation for the evolution of the flow temperature $T$, we begin with the energy balance equations for a magnetized, neutral, isothermal electron–proton plasma:

$$\frac{\partial}{\partial t}\varepsilon_\alpha + \nabla_k(\varepsilon_\alpha V_{\alpha,k} + {}_{\alpha,kl}V_{\alpha,l}) + \nabla \mathbf{q}_\alpha = n_\alpha \mathbf{f}_\alpha \cdot \mathbf{V}_\alpha, ) \tag{1.6}$$

where $\alpha$ is the species index. The fluid energy $\varepsilon_\alpha$ (thermal energy + kinetic energy) and the total pressure tensor ${}_{\alpha,kl}$ are given by

$$\varepsilon_\alpha = n_\alpha\left(\frac{3}{2}T_\alpha + \frac{m_\alpha V_\alpha^2}{2}\right), \qquad {}_{\alpha,kl} = n_\alpha T_\alpha \delta_{kl} + \Pi_{\alpha,kl}, \tag{1.7}$$

and

$$\mathbf{f}_\alpha = e_\alpha \mathbf{E} + \frac{e_\alpha}{c}\mathbf{V}_\alpha \times \mathbf{B} + m_\alpha \nabla \frac{GM_\odot}{r}, \tag{1.8}$$

is the volume force experienced by the fluids ($\mathbf{E}$ is the electric field). In Eq. (1.6), $\mathbf{q}_\alpha$ is the heat flux density for the species $\alpha$. After standard manipulations we arrive at the temperature evolution equation

$$\frac{3}{2}n\frac{d}{dt}(2T) + \nabla(\mathbf{q}_i + \mathbf{q}_e) = -2nT\nabla\cdot\mathbf{V} + m_i n\nu_i\left[\frac{1}{2}\left(\frac{\partial V_k}{\partial x_l} + \frac{\partial V_l}{\partial x_k}\right)^2 - \frac{2}{3}(\nabla\cdot\mathbf{V})^2\right] +$$

$$+\frac{5}{2}n\left(\frac{\mathbf{j}}{en}\cdot\nabla T\right) - \frac{\mathbf{j}}{en}\nabla(nT) + E_H + E_R \tag{1.9}$$

where $E_R$ is the total radiative loss, $E_H$ is the local mechanical heating function, and $\nu_i$ is the ion kinematic viscosity. Note that we have retained viscous dissipation in this system. If primary flows are ignored in the theory, various anomalous heating mechanisms need

to be invoked, and a corresponding term $E_H$ has to be added. The full viscosity tensor relevant to a magnetized plasma is rather cumbersome, and we do not display it here. However just to have a feel for the importance of spatial variation in viscous dissipation, we display its relatively simple symmetric form. It is to be clearly understood that this version is meant only for theoretical elucidation and not for detailed simulation. We notice that even for incompressible and currentless flows, heat can be generated from the viscous dissipation of the flow vorticity. For such a simple system, the rate of kinetic energy dissipation turns out to be

$$\left[\frac{d}{dt}\left(\frac{m_i \mathbf{V}^2}{2}\right)\right]_{\mathsf{visc}} = -m_i n \nu_i \left(\frac{1}{2}(\nabla \times \mathbf{V})^2 + \frac{2}{3}(\nabla \cdot \mathbf{V})^2\right). \tag{1.10}$$

revealing that for an incompressible plasma, the greater the vorticity of the flow, the greater the rate of dissipation.

Let us now introduce the following dimensionless variables:

$$\mathbf{r} \to \mathbf{r}\ R_\odot; \qquad t \to t\ \frac{R_\odot}{V_A}; \qquad \mathbf{b} \to \mathbf{b}\ b_\odot; \qquad T \to T\ T_\odot; \qquad n \to n\ n_\odot;$$

$$\mathbf{V} \to \mathbf{V}\ V_A; \qquad \mathbf{j} \to \mathbf{j}\ V_A e n_\odot; \qquad \mathbf{q}_\alpha \to \mathbf{q}_\alpha n_\odot T_\odot V_A; \qquad \nu_i \to \nu_i\ R_\odot V_A, \tag{1.11}$$

and parameters:

$$b_\odot = \frac{eB(R_\odot)}{m_i c}; \qquad \lambda_{i\odot} = \frac{c}{\omega_{i\odot}}; \qquad c_s^2 = \frac{2T_\odot}{m_i}; \qquad \omega_{i\odot}^2 = \frac{4\pi e^2 n_\odot}{m_i}; \qquad V_A = b_\odot \lambda_{i\odot};$$

$$r_A = \frac{GM_\odot}{V_A^2 R_\odot} = 2\beta\ r_c; \qquad r_c = \frac{GM_\odot}{2c_s^2 R_\odot}; \qquad \alpha = \frac{\lambda_{i\odot}}{R_\odot}; \qquad \beta = \frac{c_s^2}{V_A^2}, \tag{1.12}$$

where $R_\odot$ is the solar radius. Note that in general $\nu_i$ is a function of density and temperature: $\nu_i = (V_{i,th} T^2 / 12\pi n e^4)$.

In terms of these variables, our equations read:

$$\frac{\partial}{\partial t}\mathbf{V} + (\mathbf{V} \cdot \nabla)\mathbf{V} =$$

$$= \frac{1}{n}\nabla \times \mathbf{b} \times \mathbf{b} - \beta \frac{1}{n}\nabla(nT) + \nabla\left(\frac{r_A}{r}\right) + \nu_i \left(\nabla^2 \mathbf{V} + \frac{1}{3}\nabla(\nabla \cdot \mathbf{V})\right), \tag{1.13}$$

$$\frac{\partial}{\partial t}\mathbf{b} - \nabla \times \left(\mathbf{V} - \frac{\alpha}{n}\nabla \times \mathbf{b}\right) \times \mathbf{b} = \alpha\beta \ \nabla\left(\frac{1}{n}\right) \times \nabla(nT), \tag{1.14}$$

$$\nabla \cdot \mathbf{b} = 0, \tag{1.15}$$

$$\frac{\partial}{\partial t} n + \nabla \cdot n\mathbf{V} = 0, \tag{1.16}$$

$$\frac{3}{2} n \frac{d}{dt}(2T) + \nabla(\mathbf{q}_i + \mathbf{q}_e) = -2nT\nabla \cdot \mathbf{V} + 2\beta^{-1}\nu_i n \left[\frac{1}{2}\left(\frac{\partial V_k}{\partial x_l} + \frac{\partial V_l}{\partial x_k}\right)^2 - \frac{2}{3}(\nabla \cdot \mathbf{V})^2\right] +$$

$$+ \frac{5}{2}\alpha(\nabla \times \mathbf{b}) \cdot \nabla T - \frac{\alpha}{n}(\nabla \times \mathbf{b})\nabla(nT) + E_H + E_R. \tag{1.17}$$

This set of equations will now be studied for different types of magnetic field regions, in particular the regions with closed field lines.

Before we embark on a detailed theory of the formation and heating of the corona, we would like to give a short list of heating mechanisms which have been invoked to deal with this rather fundamental and still unresolved problem of Solar physics : Alfvén waves [25–32], Magnetic reconnection in Current sheets [33–46], and MHD Turbulence [47–49]. For all these schemes, the predicted temperature profiles in the coronal structures come out to be highly sensitive to the form of the heating mechanism [50,51]. Parker (1988) suggested that the solar corona could be heated by dissipation of many tangential discontinuities arising spontaneously in the coronal magnetic field that is stirred by random photospheric footpoint motions. This theory stimulated numerous searches for observational signatures of nanoflares. Unfortunately, all of these attempts fall short of providing a continuous (both in space and time) energy supply that is required to first create in a few minutes, and then support for longer periods the observed bright coronal structures (see e.g. [1, 2]).

Our attempt to solve this problem makes a clean break with the conventional approach. We do not look for the energy source within the corona but place it squarely in the primary flows emerging from the Sun (see the results of [1–3]). We propose (and will test) the hypothesis that the energy and particles associated with the primary flows,

in interaction with the magnetic field, do not only create the variety of configurations which constitute the corona, but also provide the primary heating. The flows can give energy and particle supply to these regions on a continuous basis — we will show that the primary heating takes place simultaneously with the accumulation of the corona and a major aspect of the flow–magnetic field interaction, for our system, is to provide a pathway for this to happen.

A mathematical modeling of the coronal structure (for its creation and primary heating) will require the solution of Eqs. (1.13)–(1.17) with appropriate initial and boundary conditions. We will use a mixture of analytical and numerical methods to extract, what we believe, is a reasonable picture of the salient aspects of a typical coronal structure.

## 1.3 Dynamical creation of hot quasi-equilibrium loops – Formation of a typical coronal structure

Though the solar atmosphere is highly structured, it seems that most of the constituent elements have something common in their creation and heating. In order to construct a unified theory for the entire corona, one would have to confront large variations in plasma density and temperature. It seems, however, that beyond the coronal base, the equilibrium temperature tends to be nearly constant on each one of these structures; the temperature of a specific structure increases insignificantly (about 20 p.c.) from its value at the base to its maximum reached at the top of the structure. This change is much less than the temperature change (about 2 orders of magnitude) that occurs between the solar surface and the coronal base. This observation is an outcome of the investigation of several authors (see, for example, [1,2,51–55]). Their results show that the bright elements of the corona are composed of quasi–isothermic and ultra–thin arcs (loops) of different temperature and density, situated (located) close to one other. This state is, perhaps, brought about by the isolating influence of magnetic fields which prevent the particle and energy transfer between neighboring structures.

It is safe to assume, then, that in the quasi–equilibrium state, each coronal structure has a nearly constant temperature, but different structures have different characteristic temperatures, i.e., the bright corona seen as a single entity will have considerable temperature variation. Observations tell us that the coronal temperatures are much higher than those of the primary flows (which we are proposing as the mother of the corona). For the consistency of the model, therefore, it is essential that the primary "heating" must take place during the process of accumulation of a given coronal entity.

This apparent problem, in fact, can be converted to a theoretical advantage. We distinguish two important eras in the life of a coronal structure; a hectic period when it acquires particles and energy (accumulation and heating), and the relatively calmer period when it "shines" as a bright, high temperature object.

In the first era, the most important issue is that of heating while particle accumulation (trapping) takes place in a curved magnetic field. This is, in fact, the essential new ingredient of the current approach. We plan to show:

1) that the kinetic energy contained in the primary flows can be dissipated by viscosity to heat the plasma, and 2) that this dissipation can be large enough to produce the observed temperatures.

Naturally, a time dependent treatment will be needed to describe this era.

Any additional heating mechanisms, operative after the emergence of the coronal structure, will not be discussed in this study. For an essential energy inventory of the quasi-equilibrium coronal structure, we also ignore the contributions of flares and other "activities" on the solar surface because they do not provide a continuous and sufficient energy supply [2].

The second era is that of the quasi-equilibrium of a coronal structure of given density and temperature - neither of which has to be strictly constant. The primary heating has already been performed, and in the equilibrium state, we can neglect viscosity, resistivity and other collisional effects in addition to neglecting the time dependence. The calculations in this regime will be limited to the determination of the magnetic field and the velocity–field structures that the collisionless magnetofluids can generate and we will also examine if these structures can confine plasma pressure.

### 1.3.1 Creation and heating of coronal structure

In this subsection we will concentrate on numerical methods to test our basic conjecture that the primary solar flows are responsible for the creation and heating of a typical bright coronal structure. The numerical results (obtained by modeling Eqs. (1.13)–(1.17) with viscosity tensor relevant to magnetized plasma) are extremely preliminary, but they clearly indicate that the proposed mechanism has considerable promise.

Let us first make order of magnitude estimates on the requirements that must be met for this scheme to be meaningful. It is well known that (see e.g. [56]) the rate of

energy losses $F$ from the solar corona by radiation, thermal conduction, and advection is approximately $5 \cdot 10^5\,\mathrm{erg/cm^2\,s}$. For the brightest loops the rate loss could even reach $5 \cdot 10^6\,\mathrm{erg/cm^2\,s}$. If the conversion of the kinetic energy in the primary flows were to compensate for these losses, we would require a radial energy flux

$$\frac{1}{2} m_i n_0 V_0^2 \; V_0 \geq F, \tag{1.18}$$

where $V_0$ is the initial flow speed. For $V_0 \sim 300\,\mathrm{km/s}$ this implies an initial density in the range: $(3 \cdot 10^7 - 4 \cdot 10^8\,)\mathrm{cm^{-3}}$.

For slower ($\sim 100\,\mathrm{km/s}$) velocity primary flows the starting density has to be higher ($\geq 10^9\,\mathrm{cm^{-3}}$). These values seem reasonable according to the latest observational data [1, 2, 3].

The normal viscous dissipation of the flow takes place on a time (using Eq. (1.10)):

$$t_{\mathsf{visc}} \sim \frac{L^2}{\nu_i}, \tag{1.19}$$

where $L$ is the length of the coronal structure. For a primary flow with $T_0 = 3\,\mathrm{eV} = 3.5 \cdot 10^4\,\mathrm{K}$ and $n_0 = 4 \cdot 10^8\,\mathrm{cm^{-3}}$ creating a quiet coronal structure of size $L = (2 \cdot 10^9 - 7 \cdot 10^{10})\,\mathrm{cm}$, the dissipation time can be estimated to be of the order of $(2 \cdot 10^8 - 10^{10})\,\mathrm{s}$. The shorter the structure and hotter the flow, the faster is the rate of dissipation. This estimated time is much longer than what is actually found by the latest observations by TRACE [1]. Mechanisms much faster than the one embodied in (1.19), therefore, will be needed for the model to work. In the absence of "anomalous viscosity", the only way to enhance the dissipation rates (to the observed values) is to create spatial gradients of the velocity field that are on a scale much much shorter than that of the structure length (defined by the smooth part of the magnetic field). Thus, the viability of the model depends wholly on the existence of mechanisms that induce short–scale velocity fields. Numerical simulations show that the short–scale velocity fields are, indeed, self–consistently generated in the two–fluid system.

For numerical work (to illustrate the bright coronal structure formation), we model the initial solar magnetic field as a 2D arcade with circular field lines in the $x$–$z$ plane (see Fig.1.1 for the contours of the vector potential, or the flux function). The field attains its maximum value $B_{\mathsf{max}}(x_o, z = 0)$ at $x_{\mathsf{0}}$ at the center of the arcade, and is a decreasing function of the height $z$ (radial direction). The set of model equations (12-16) was solved in 2D flat geometry (x,z) using the 2D version of Lax–Wendroff numerical scheme (Richtmyer and Morton 1967) alongwith applying the Flux–Corrected–Transport procedure [58]. Equation (1.14) was replaced with its equivalent for the y–component of the vector potential which automatically ensures the divergence-free property of the magnetic field. The equation of heat conduction was treated separately by Alternate Direction Implicit method with iterations [58]. Transport coefficients for heat conduction and viscosity were taken from Braginski, 1965. The observations revealed that the radiation losses ($n^2$ and, hence, different for the different regions and strongly varying in time dynamical parameter) are the dominant part of energy losses from the solar atmosphere that is optically very thin. The detailed calculation of radiation losses gives a strong dependence on gas composition and the accuracy of the atomic physics parameters as well as the values of the relative elemental abundances used in the calculations. In series of papers [60, 61, 62, 63, 52] [60-63,52] it was found that, "in general, the effect of including the process of dielectronic recombination and using more accurate cross sections is not very large", in the estimations of radiative losses. The most significant feature of these detailed calculations for steady state solar atmosphere "is the large peak in the cooling around $2 \cdot 10^5$ K, which is due primarily to $2s - 2p$ transitions in oxygen ions". As it was mentioned in the paper by Cox and Tucker (1969), for example, this fact must be taken into account when suggesting the theories of the production of very hot plasmas – a strong heating mechanism is required to overcome the powerful losses there. We believe that mechanism we suggest can provide such a strong and continuous heating (along with the formation) of the coronal structure. The position of the above mentioned peak is a strong function of the composition of the plasma (see, e.g., [60, 61, 62, 63, 52]

[60-63,52]). In the code bremsstrahlung radiation accounts for $E_R$, though due to the facts we discussed above we used a bit modified formula for this radiation assuming it 2 times greater,

$$E_R = 2 \cdot E_{Br} = 2 \cdot 1.69 \cdot 10^{-25} \cdot n^2 \cdot T^{1/2} Z^3 \, \mathrm{erg/cm^3\,s}, \quad \mathrm{Z} = 1.$$

Since we were exploring a particular heating mechanism, no external heating source E H was needed. A numerical mesh of $200 \times 150$ points was used for computation.

A numerical mesh of $200 \times 150$ points was used for computation.

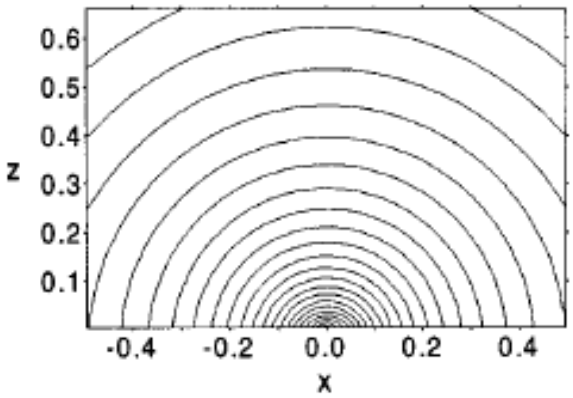


Fig.1.1 Contour plots for the vector potential $A$ (flux function) in the $x - z$ plane for a typical arcade–like solar magnetic field (initial distribution). The field has a maximum $B_{max}(x_0 = 0,\, z_0 = 0) = 7G$.

To illustrate the formation and heating of a general coronal structure, we have modelled several cases with different initial and boundary conditions for cold primary flows. The dynamical picture is strongly dependent on the relation of the initial flow pressure and the magnetic field strength. Two limiting cases are interesting: 1) the initial magnetic field is weak, and the flow significantly deforms (and in specific cases, drags) the magnetic field lines, 2) the initial magnetic field is strong, and the flow leaves the field lines practically unchanged.

For sub–Alfvénic flows, we present in Figs. 2-5 the salient features of our preliminary

results. We have plotted (as functions of $x$ and $z$) four relevant physical quantities: the flux function $A$, the density $n$, the temperature $T$, and the magnitude of the velocity field $|\mathbf{V}|$ (for specific cases, when needed, we give the radial component of velocity field $V_z$ also).

The plots correspond to two (in some cases to three) different time frames. The results are described under three separate headings, covering respectively, the fully uniform, the spatially non–uniform, and the time–dependent as well as spatially non–uniform initial flows.

### Initially uniform primary flow and an Arcade-like magnetic field structure

This case is highly idealized but illustrates the main aspects of the creation of the hot coronal structures, and of the basic heating process.

When discussing the temporally uniform initial flows, we choose the parameters to satisfy the observational constraint that, over a period of some tens of minutes, the location of the heating must have a relatively smooth evolution [1]. The final shape and location of the coronal structure (of the associated $\mathbf{B}(\mathbf{r}, t)$, for example) will be naturally defined by its material source, by the heating dynamics, and by the initial field $\mathbf{B_0}(\mathbf{r}, t)$.

For these studies, the initial flow velocity field is taken to be uniform at the surface and has only a radial component, $V_z = 300\, km/s$. Other parameters are: Maximum value of the magnetic field $B_{\mathsf{max}}(x_o, z = 0) = 7G$, initial density of the flow $4 \cdot 10^8\, cm^{-3}$ and the initial temperature $3\, eV$. Simulations yield the following results:

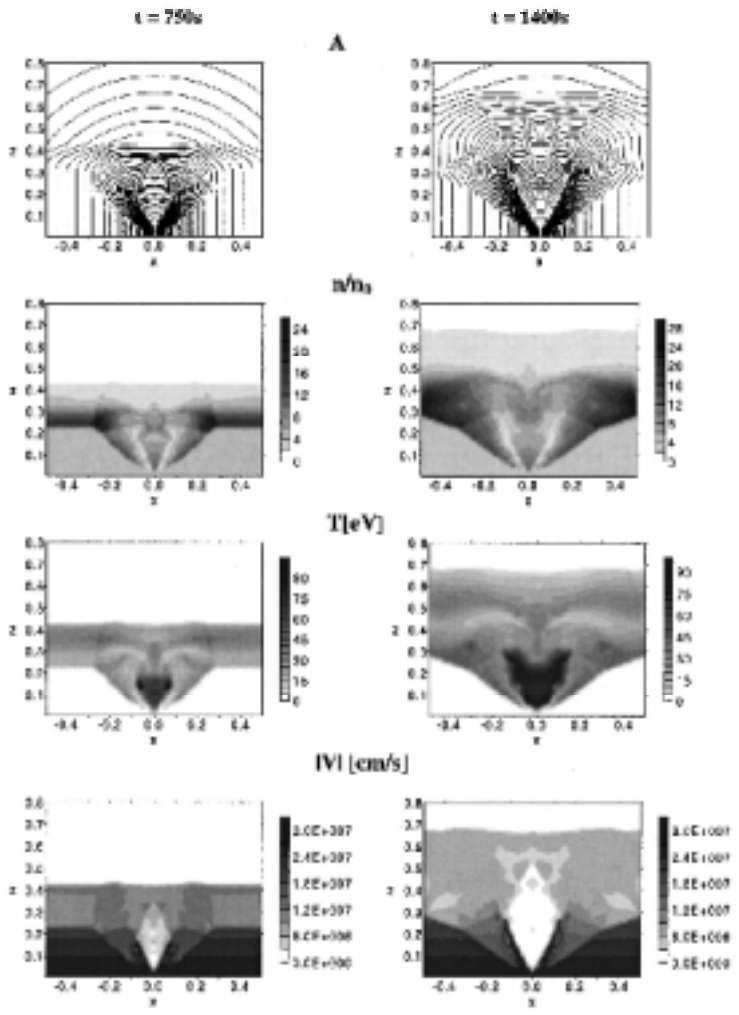


Fig.1.2 Hot coronal structure formation by the interaction of the spatially homogeneous primary flows with 2D arcade–like structure given in Fig. 1 . The initial parameters are: $V_{z0} = 300\,km/s$, the temperature and density of the flow, $T_0 = 3\,eV$ and $n_0 = 4 \cdot 10^8\,cm^{-3}$ respectively, and the background density $= 10^8\,cm^{-3}$. The vector potential $A$, the flow density $n$ (normalized to $n_0$), the flow temperature $T$ (in $eV$) and the magnitude of the flow velocity $|V|$ (in $cm/s$ ) are plotted for $t = 750s$ and $t = 1400s$ . The base of the hot structure is created at a radial distance $\sim 14000\,km$. The distance scale on the plots is $1 = 4 \cdot 10^{10} cm$ . The primary heating (and brightening) of the structure is practically stopped in about 23 minutes.

1) The flow particles begin to accumulate at the footpoints near the solar surface (Fig. 1.2, see density at $t = 750\,\mathrm{s}$). The accumulation goes on with time, and gradually the entire volume under the arcade (starting from the central short loops) is filled with particles (Fig. 1.2, density at $t = 1400\,\mathrm{s}$). First the shorter loops are filled, and then the larger ones.

2) The heating of the particles goes hand in hand with the accumulation (Fig. 1.2, plots for density and temperature).

3) The regions of stronger magnetic fields are denser in population (Fig. 1.2, plots for $A$ and $n$). In earlier stages of the formation of a coronal structure, the regions near the base (where the field is stronger) are denser and hotter than the distant regions (Fig. 2, $t = 750\,\mathrm{s}$ plots for $n$ and $T$ ); for shorter loops, the density increases (as a function of height $z$) from the bottom of the structure, and then falls — first rapidly and later insignificantly; the maximum density is much greater than the initial density of the flows.

4) The dissipation of the flow kinetic energy is faster in the first stage of formation (Fig. 1.2, $t = 750\,\mathrm{s}$ plot for $|V|$ ). The plot $|V|$ versus $z$ shows steep (shock–like) gradients near the base. Thus the bright base is created in the very first stage in the stronger magnetic field regions (shorter loops). For given parameters, the initial flow is strongly supersonic. Thus the shocks are generated with efficient transfer of kinetic energy into heat. As the mean free path of ions in the plasma is of the order of $(10^6 - 10^7)cm$ (in the direction parallel to the magnetic field) and the dimension of the structure is much greater – of the order of $10^{10}\,cm$ – efficient conditions for the kinetic energy dissipation exist. The plots for the velocity, temperature and density reveal that with increasing z, and in the regions away from the arcade center, we first find an undisturbed flow with low temperature, then see a transient area with high density and temperature, and finally a shock consistent with Hugoniot conditions. The short scale represented by the width of the shock-layer (determined by viscosity) is the main enhancer of viscous dissipation.

5) For later times, the brightening process spreads over wide regions (Fig.1. 2, $t = 1400\,\mathrm{s}$ plot for temperature).

6) In the very first stage, the shorter loops are a bit overheated, but they cool down somewhat at later times when the longer loops begin to get heated (Fig. 2, plots for temperature).

7) The base ($T \geq 100\,\mathrm{eV}$) of the bright region is at about $1.4 \cdot 10^9\,cm \sim 0.02 R_\odot$ (Fig. 1.2, $t = 1400\,s$ plots for $n$ and $T$) from the solar surface. This number is in a very good agreement with the latest TRACE results [1]. Outwards from the base, the accumulated layer has somewhat lower, but more or less uniform, insignificantly decreasing density. In the accumulated layer the kinetic energy of the flow is essentially uniform (again, decreases insignificantly); the dissipation has practically stopped (Fig. 1.2, $t = 1400\,s = 23\,min$ , plot for $|V|$ versus $z$). The temperature is practically uniform in the longer loops and increases insignificantly in shorter loops (for some special conditions these conclusions may be somewhat modified in specific regions of the arcade; see point 8) ). Outwards from the hottest region of the arcade, the temperature decreases gradually and at some radial distance the outer boundary of the bright part is reached (Fig. 2, $t = 1400\,s$ plot for temperature). Thus, in a very short time a dense and bright "coronal structure" is created — this object survives for a time much longer than was needed for its creation. The simulations show that the heating process may continue during this so–called equilibrium stage, but at a rate much slower than the earlier primary heating. This heating seems just additional and supporting to the heat content of the nascent hot structure. At this time, however, the velocity field is already much smaller in magnitude as compared to the initial values; the flows in the hot coronal structure are already subsonic. This is a possible explanation why supersonic flows may not be seen in the hot observable coronal structures.

8) When relatively dense primary flows interact with weak arcade-like magnetic fields ($B_{\mathsf{max}}(x_0, z_0 = 0) \leq 10\,G$ for our initial flow with given above parameters), the field lines begin to deform (soon after the creation of the solar base) in the central region of the arcade but far from the base (see $t = 1400\,s$ plots for density and temperature in Fig. 1.2). The particle accumulation is still strong, and the dissipation, though quite fast,

stops rather rapidly. Consequently, the temperature first reaches a maximum (up to the deformed field–line region this maximum is reached at the summit for each short loop) and later falls rapidly. Gradually one can see signs for the creation of a local gravitational potential well behind the shortest loops (see $t = 1400\,\mathrm{s}$ plot for $A$ in Fig. 1.2). This well supports a relatively dense and cold plasma in the central area of the arcade ($t = 1400\,s$ for $n$ and $T$ of Fig. 1.2). The density of this structure is considerably greater than that of the surrounding areas, and the temperature is considerably less than that of the rest of the accumulated regions at the same height of the arcade.

Our preliminary simulations show that for the same parameters of the primary outflow, such cold and dense plasma objects (confined in the so–called potential well) will not form in the regions where the initial magnetic fields are stronger ($B_{\mathsf{max}}(x_0, z_0 = 0) \geq 20\,G$).

### Spatially non–uniform primary flow interacting with an arcade–like magnetic field structure

The latest observations support the idea that the coronal material is injected discontinously (in pulses or bunches, for example) from lower altitudes into the regions of interest (e.g. spicules, jet–like structures [6, 7, 15, 16, 1, 2]. A realistic simulation, then, requires a study of the interaction of spatially non–uniform initial flows with arcade–like magnetic field structures. These "close to the actual" cases represent more vividly the dynamics of the hot coronal formation.

1) When the spatially symmetric initial flow (plot for $V_z$ at $t = 0$ in Fig.1.3a) interacts with the arcade (plots in Fig.1.3), and the initial magnetic field is rather strong ($B_{\mathsf{max}}(x_0, z_0 = 0) = 20\,G$), the primary heating is completed in a very short time ($\sim (2 - 3)\,min$) on distances ($\sim 10000\,km$) shorter than the uniform–flow case when the initial magnetic field was weaker. This is also consistent with observations. The heating is very symmetric and the resulting hot structure is uniformly heated to $1.6 \cdot 10^6\,K$.

2) Observations reveal the existence of cool material and downflows, right within the

hot coronal structures; they also show an imbalance in the primary heating on the two sides of the loops (see [15, 1]). To reproduce these characteristics, we have modelled the coronal structure formation process using an asymmetric, spatially non–uniform initial flow interacting with a strong magnetic field (see Fig.1.4).

For both of the discussed cases, the downflows can be clearly seen for the velocity field component $V_z$. In Fig. 4, the downflow is created simply by changing the initial character of the flow (initially we had only the right pulse from the velocity field distribution given in Fig.1.3a), while in Fig. 3a (plot at $t = 297\,s$), the downflows are the result of more complicated events (see explanation below, in the next paragraph). The final parameters of the downflows are strongly dependent on the initial and boundary conditions. In the pictures, the imbalance in the primary heating process is also revealed.

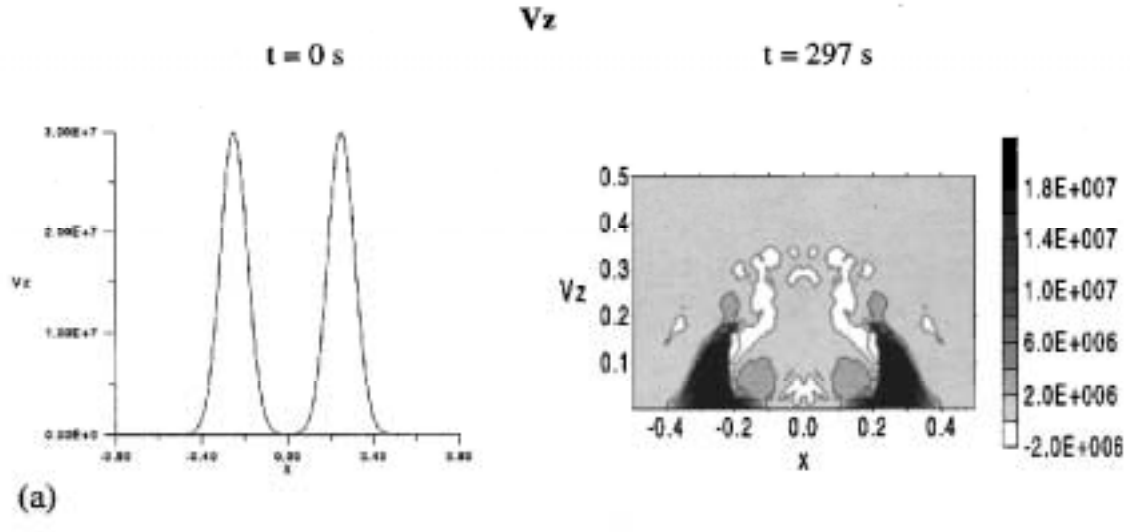


Fig.1.3a The distribution of the radial component $V_z$ (with a maximum of $300\,km/s$ at $t = 0$ ) for the symmetric, spatially non–uniform velocity field . The plot scale is $1 = 5 \cdot 10^9\,cm$. The process of interaction of such primary flows with the arcade–like magnetic fields (given in Fig. 1 with $B_{max} = 20\,G$) is accompanied by downflows much slower than the primary flows (plot for $V_z$ at $t = 297\,s$). The final parameters of downflows are strongly dependent on the initial and boundary conditions.

When two identical pulses (Fig.1.3a, plot at $t = 0\,s$) enter in succession into our

standard, arcade–like initial magnetic field, we simulate the equivalent of two colliding flows on the top of a structure. Shocks, though not very strong, are generated in a very short time ($t = 30\,s$). Such shocks, on both sides of the arcade–center, have hot fronts and cold tails. Soon ($t = 42\,s$) these shocks become "visible", a hot and dense area is created on top of the structure where these shocks (at this moment they have become stronger) collide. After the collision (and "reflection"), the entire area within the arcade becomes gradually hot. At some moment, a practically uniformly heated structure is created, and the primary heating stops. This process is accompanied by downflows much slower than the primary flows; much of the primary flow kinetic energy has been converted to heat via shock generation (the shock and downflow velocities differ significantly). It is clear that in the case of spatially assymetric initial flows, the downflows on different sides of the arcade–center will have different characteristics. Due to the high pressure prevalent in the nascent hot structure (loop), there is no more inflow of the plasma and the flow deposits its energy at the base; the base becomes overheated. Later this energy can be again transferred upwards via thermal conduction (this mechanism can work in all the discussed cases), but at that moment the flow could be also changed (see initially time–dependent flow cases below).

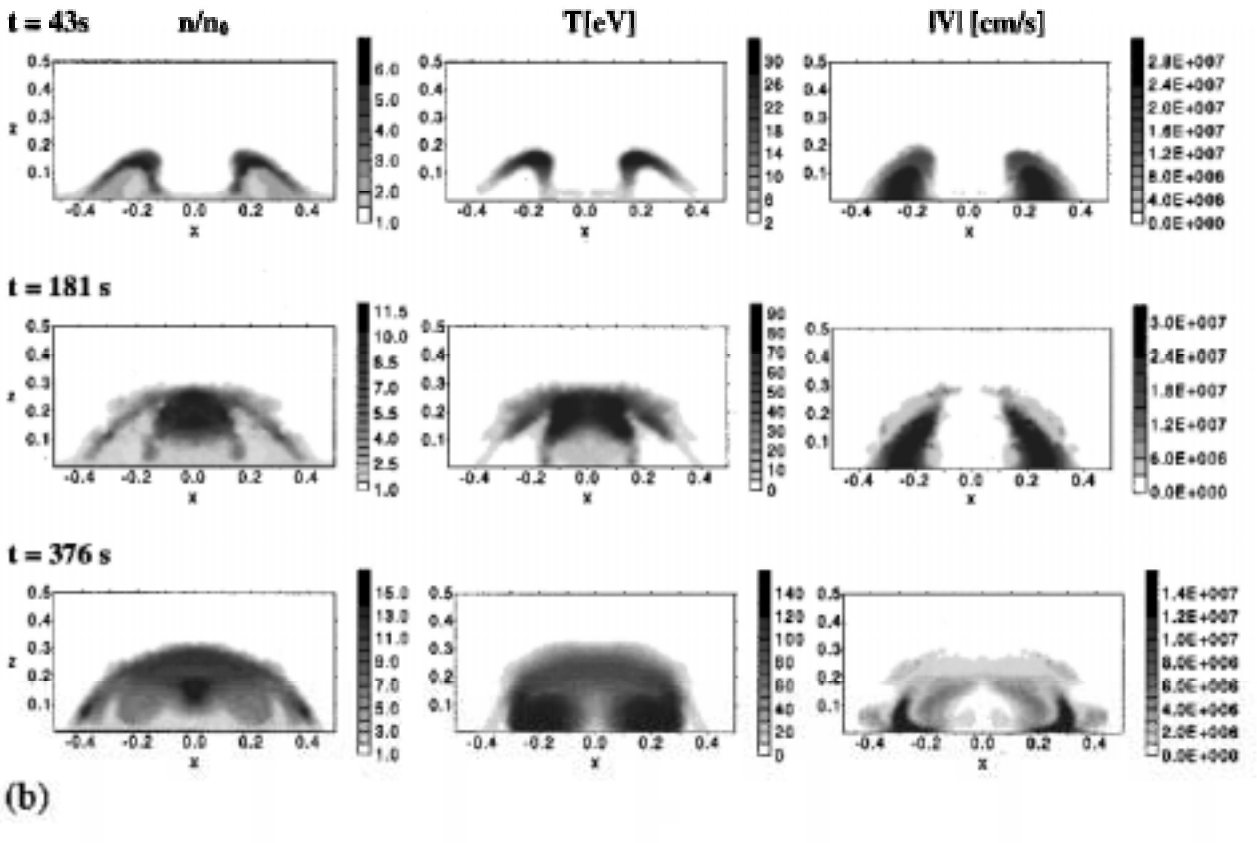


Fig.1.3b Hot coronal structure formation by the interaction of the initially symmetric spatially non–uniform primary flows (see plot for $V_z(x,z)$ in Fig. 3a ) with the 2D arcade–like structure given in Fig. 1 . Initial parameters are: the temperature and density of the flow, $T_0 = 3\,eV$ and $n_0 = 4 \cdot 10^8\,cm^{-3}$ respectively, the initial background density $= 2 \cdot 10^8\,cm^{-3}$, and the field maximum $B_{max}(x_0,\, z_0 = 0) = 20\,G$. The plot scale is $1 = 5 \cdot 10^9\,cm$. The primary heating is completed in a very short time $\sim (2-3\,)min$ on distances ($\sim 10000\,km$) shorter than the uniform–flow case when magnetic field was weaker. The heating is symmetric and the resulting hot structure is uniformly heated to $1.6 \cdot 10^6\,K$ . Much of the primary flow kinetic energy has been converted to heat via shock generation.

Plots for the temperature and velocity field in Figs.1.3b,1. 4 also indicate that some

cold particles still remain in the body of the newly created hot structure. These particles are perhaps from the slower aggregates (our initial flow was not uniform) which did not have sufficient energy to be converted to heat.

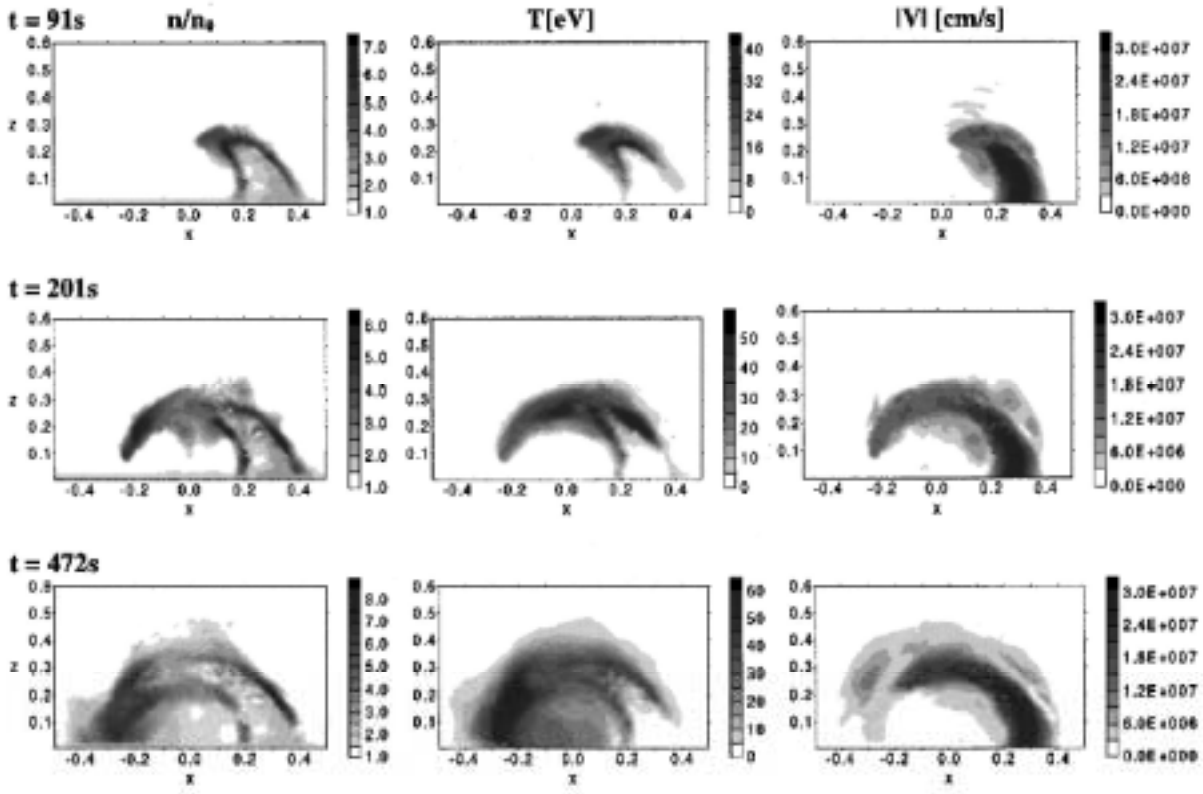


Fig.1.4 The interaction of an initially asymmetric, spatially non-uniform primary flow (just the right pulse from the distribution given in Fig. 3a ) with a strong arcade–like magnetic field ($B_{max}(x_0,\, z_0 = 0) = 20\,G$). Downflows, and the imbalance in primary heating are revealed.

### Time dependent non–uniform initial flows interacting with arcade–like magnetic field structures.

To simulate reality further we introduce time dependence in the initial primary flow velocity field. We discuss two distinct cases:

1) Initially, the velocity field has a pulse–like distribution with a time–period nearly half of the "formation time" of the quasi-equilibrium structure corresponding to the case with time–independent initial conditions. The results displayed in Fig.1.5 show that the emerging coronal structure has a rather uniform distribution of temperature along the magnetic field, and the latter is practically un–deformed during formation and heating. We see that when the basic heating ceases, the hot structure survives for the time of computation which happens to be shorter than the time necessary for losses that destroy the structure.

2) The velocity field has a fast amplitude modulation near its maximum value (for these simulations the maximum radial velocity was taken to be $300\,km/s$). We find that the dynamics of the hot coronal structure creation is quite similar to the initially time–independent, spatially symmetric case. Because of this, we don't give here the corresponding plots. We only note that for this case, the structure tends to become even hotter (by a factor 1.2 for the same parameters) and when quasi–equilibrium is established (time for this to happen is longer than for the time–independent initial flows) the base of the structure is hotter than the top although at an earlier time the top was hotter, i.e, there is a temperature oscillation with a time–period longer compared to the creation time of the hot structure.

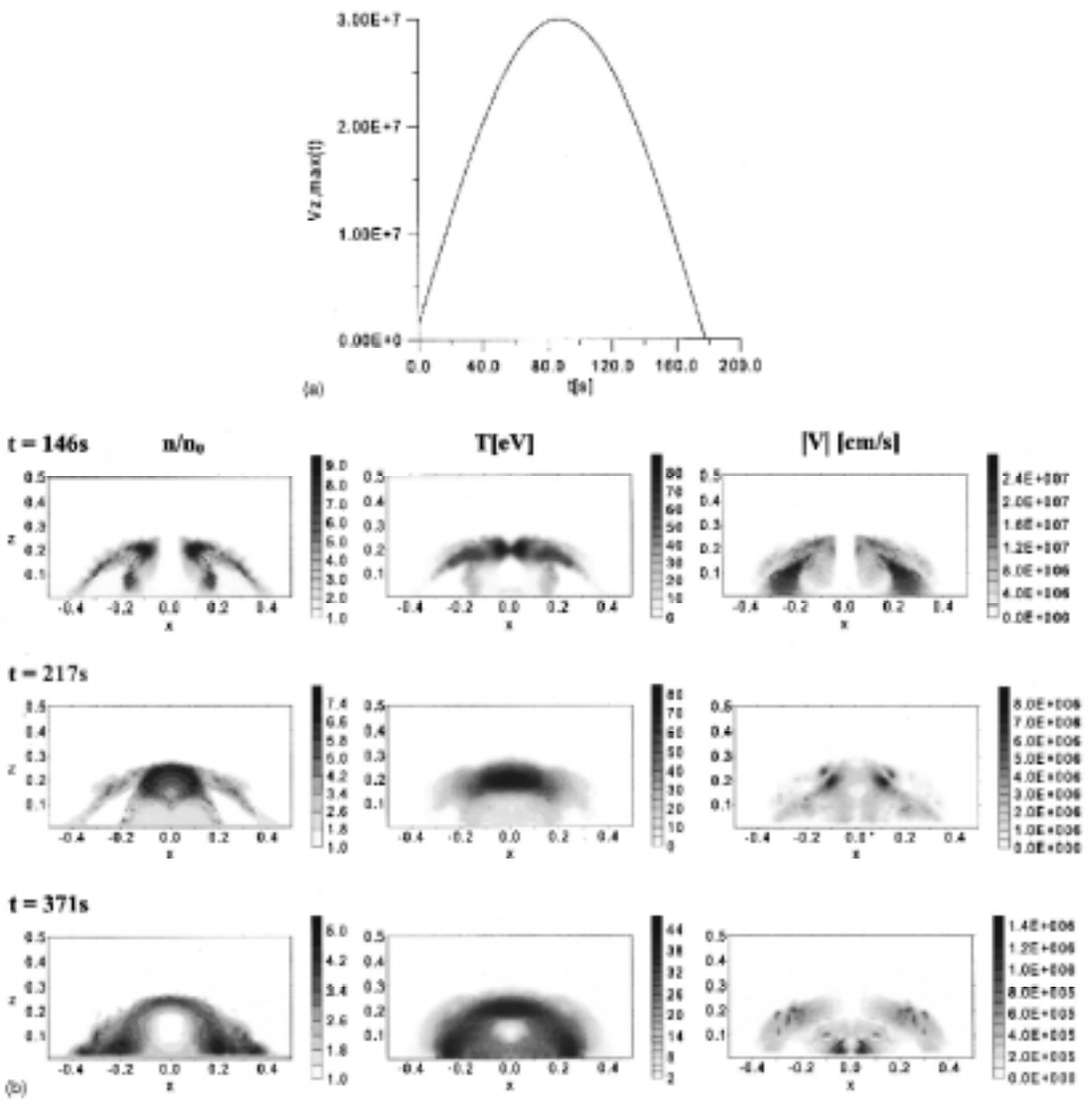


Fig.1.5 The interaction of the time–dependent non–uniform initial flow (see plot for the time–distribution of $V_z$ in this Figure; the spatial distribution of the pulse is the same as in Fig. 3a ) with the arcade–like magnetic field structure (plot in Fig.1 with $B_{max} = 20\,G$). The emerging coronal structure has uniform distribution of temperature along the magnetic field (plot for $T$ at $t = 371\,s$ ) and the latter is practically undeformed during the formation and heating.

The main message of numerical simulation is that the dynamical interaction of an initial flow with the ambient solar magnetic field leads to a re–organization of the plasma such that the regions in the close vicinity of the solar surface are characterized by strongly varying (in space and time) density and temperature, and even faster varying velocity field, while the regions farther out from the bright base are nearly uniform in these physical parameters. This phenomenon pertains generally, and not for just a set of specific structures. The creation and primary heating of the coronal structures are simultaneous, accompanied by strong shocks. These are fast processes (few tens of minutes) taking place at very short radial distances from the Sun ($\sim 10000\,km$) in the strong magnetic field regions with significant curvature. The final characteristics of the created coronal structures are defined by the boundary conditions for the coupled primary flow–solar magnetic field system. The stronger the magnetic field, the faster is the process of creation of the hot coronal structure with its base nearer the solar surface. To investigate the near surface region one must use general time–dependent 3D equations. Quasi–stationary (equilibrium) equations, on the other hand, will suffice to describe the hot and bright layers — the already existing visible coronal structures.

## 1.4 Typical Coronal Equilibria

The familiar MHD theory (single–fluid) is a reduced case of the more general two–fluid theory discussed in this study. Constrained minimization of the magnetic energy in MHD leads to force–free static equilibrium configurations [64, 65]. The range of two–fluid relaxed states, however, is considerably larger because the velocity field, now, begins to play an independent fundamental role. The presence of the velocity field not only leads to new pressure confining states [66, 67, 68, 69], but also to the possibility of heating the equilibrium structures by the dissipation of kinetic energy. The latter feature is highly desirable if these equilibria were to be somehow related to the bright coronal structures.

We begin investigating the two–fluid states by first studying the simplest, almost analytically tractable, equilibria. This happens when the pressure term in the equation of motion (1.12) becomes a full gradient, i.e, whenever an equation of state relating the pressure and density can be invoked. For our present purpose, we limit ourselves to the constant temperature states allowing $n^{-1}\nabla p \to 2\,T\nabla \ln\ n$ .

Normalizing $n$ to some constant coronal base density $n_0$ (reminding the reader that $n_0$ is different for different structures!), and using our other standard normalizations ($\lambda_{i0} = c/\omega_{i0}$ is defined with $n_0$), our system of equations reduces to:

$$\frac{1}{n}\nabla \times \mathbf{b} \times \mathbf{b} + \nabla\left(\frac{r_{A0}}{r} - \beta_0 \ln\ n - \frac{V^2}{2}\right) + \mathbf{V} \times (\boldsymbol{\nabla} \times \mathbf{V}) = 0, \tag{1.20}$$

$$\nabla \times \left(\mathbf{V} - \frac{\alpha_0}{n}\nabla \times \mathbf{b}\right) \times \mathbf{b} = 0, \tag{1.21}$$

$$\nabla \cdot (n\mathbf{V}) = 0, \tag{1.22}$$

where $r_{A0},\ \alpha_0,\ \beta_0$ are defined with $n_0,\ T_0,\ B_0$. This is a complete system of seven equations in seven variables.

Following Mahajan and Yoshida (1998) and [70, 71, 72, 73], we seek equilibrium solutions of the simplest kind. Straightforward algebra leads us to the following system

of linear equations:

$$\mathbf{b} + \alpha_0 \nabla \times \mathbf{V} = d\ n\ \mathbf{V} \tag{1.23}$$

and

$$\mathbf{b} = a\ n\ \left[\mathbf{V} - \frac{\alpha_0}{n} \nabla \times \mathbf{b}\right], \tag{1.24}$$

where $a$ and $d$ are dimensionless constants related to the two invariants: the magnetic helicity $\int(\mathbf{A}\cdot\mathbf{B})\ d^3x$ and the generalized helicity $\int(\mathbf{A}+\mathbf{V})\cdot(\mathbf{B}+\nabla\times\mathbf{V})d^3x$ (or $\int(\mathbf{V}\cdot\mathbf{B}+\mathbf{A}\cdot\nabla\times\mathbf{V}+\mathbf{V}\cdot\nabla\times\mathbf{V})\ d^3x$ ) of the system. We will discuss $a$ and $d$ later. The equilibrium solutions (1.23), (1.24) encapsulate the simple physics: 1) the electrons follow the field lines, 2) while the ions, due to their inertia, follow the field lines modified by the fluid vorticity. These equations, when substituted in (1.20), (1.21), lead to

$$\nabla\left(\frac{r_{A0}}{r} - \beta_0 \ln\ n - \frac{V^2}{2}\right) = 0, \tag{1.25}$$

giving the Bernoulli condition which will determine the density of the structure in terms of the flow kinetic energy, and solar gravity. Equations (1.23) and (1.24) are readily manipulated to yield

$$\frac{\alpha_0^2}{n}\nabla\times\nabla\times\mathbf{V} + \alpha_0\ \nabla\times\left(\frac{1}{a} - d\ n\right)\mathbf{V} + \left(1 - \frac{d}{a}\right)\mathbf{V} = 0. \tag{1.26}$$

which must be solved with (1.25) for $n$ and $\mathbf{V}$; the magnetic field can, then, be determined from (1.23).

Equation (1.25) is solved to obtain

$$n = \exp\left(-\left[2g_0 - \frac{V_0^2}{2\beta_0} - 2g + \frac{V^2}{2\beta_0}\right]\right), \tag{1.27}$$

where $g(r) = r_{c0}/r$. This relation is rather interesting; it tells us that the variation in density can be quite large for a low $\beta_0$ plasma (coronal plasmas tend to be low $\beta_0$; the latter is in the range $0.004-0.05$) if the gravity and the flow kinetic energy vary on length

scales comparable to the extent of the coronal structure. In this system of equations, as we mentioned above, the temperature (which defines $\beta_0$) has to be fixed by initial and boundary conditions at the base of the structure. Substituting (1.27) into (1.26) will yield a single equation for velocity which is quite nontrivially nonlinear. Numerical solutions of the equations are tedious but straightforward.

For analytical progress, essential to revealing the nature of the self–consistent fields and flows, we will now make the additional simplifying assumption of constant density. This is a rather drastic step (in numerical work, we take the density to be a proper dynamical variable) but it can help us a great deal in unrevealing the underlying physics. There are two entirely different situations where this assumption may be justified:

1) the primary heating of corona has already been performed, i.e., a substantial part of flow initial kinetic energy has been converted to heat. The rest of the kinetic energy, i.e., the kinetic energy of the equilibrium coronal structure is not expected to change much within the span of a given structure. Note that the ratio of velocity components will have a large spatial variation, but the variation in $V^2$ is expected to be small. It is also easy to estimate that within a typical structure, gravity varies quite insignificantly. There will be exceptional cases like the neighborhood of the Coronal holes and the streamer belts, where significant heating could still be going on, and the temperature and density variations could not be ignored. Such regions are extremely hard to model;

2) if the rates of kinetic energy dissipation are not very large, we can imagine the plasma to be going through a series of quasi–equilibria before it settles into a particular coronal structure. At each stage we need the velocity fields in order to know if an appropriate amount of heating can take place. The density variation, though a factor, is not crucial in an approximate estimation of the desired quantities.

The constant density assumption $n = 1$ will be used only in Eq. (1.26) to solve for the velocity field (or the $\mathbf{b}$ field which will now obey the same equation). These solutions, when substituted in Eq. (1.27), would determine the density profile (slowly varying) of a given structure.

In the rest of this sub–section we will present several classes of the solutions of the following linear equation:

$$\alpha_0^2 \, \nabla \times \nabla \times \mathbf{Q} + \alpha_0 \, \left( \frac{1}{a} - d \right) \nabla \times \mathbf{Q} + \left( 1 - \frac{d}{a} \right) \mathbf{Q} = 0, \tag{1.28}$$

where $\mathbf{Q}$ is either $\mathbf{V}$ or $\mathbf{b}$. To make contact with existing literature, we would use $\mathbf{b}$ as our basic field to be determined by Eq. (1.26); the velocity field $\mathbf{V}$ will follow from Eqs. (1.23) and (1.24), which for $n = 1$, become

$$\mathbf{b} + \alpha_0 \nabla \times \mathbf{V} = d\mathbf{V} \tag{1.29}$$

and

$$\mathbf{b} = a \left[ \mathbf{V} - \alpha_0 \nabla \times \mathbf{b} \right]. \tag{1.30}$$

It is worth remarking that in order to derive the preceding set of equations, all we need is the constant density assumption; the temperature can have gradients and, these are determined from the Bernoulli condition (1.25) with $\beta_0(T)$ replacing $\beta_0 \ln \, n$.

### 1.4.1 Analysis of the *Curl Curl* Equation

The Double *Curl* equation (27) was derived only recently [53] (Mahajan and Yoshida 1998); its potential, is still, largely unexplored(see [67, 68, 69, 72, 73]). The extra double *curl* (the very first) term distinguishes it from the standard force-free equation [74, 64, 75] (Woltjer 1958; Taylor 1974, 1986; Priest 1994 and references therein) used in the solar context. Since $a$ and $d$ are constants, Eq. (1.26), without the double *curl* term, reproduces what has been called the "relaxed state" [64, 75]. We will see that this term contains quantitative as well as qualitative new physics.

In an ideal magnetofluid, the parameters $a$ and $d$ are fixed by the initial conditions; these are the measures of the constants of motion, the magnetic helicity, and the fluid plus cross helicity or some linear combination thereof [48, 66, 67, 68, 69, 76]. In our

calculations, $a$ and $d$ will be considered as given quantities. The existence of two, rather than one (as in the standard relaxed equilibria) parameter in this theory is an indication that we may have, already, found an extra clue to answer the extremely important question: why do the coronal structures have a variety of length scales, and what are the determinants of these scales?

We also have the parameter $\alpha_0$, the ratio of the ion skin depth to the solar radius. For typical densities of interest ($\sim (10^7 - 10^9)\mathrm{cm}^{-3}$), its value ranges from ($\sim 10^{-7} - 10^{-8}$); a very small number, indeed. Let us also remind ourselves that the $|\nabla|$ is normalized to the inverse solar radius. Thus $|\nabla|$ of order unity will imply a structure whose extension is of the order of a solar radius. To make further discussion a little more concrete, let us suppose that we are interested in investigating a structure that has a span $\epsilon R_\odot$, where $\epsilon$ is a number much less than unity. For a structure of order 1000 km, $\epsilon \sim 10^{-3}$. The ratio of the orders of various terms in Eq. (1.26) are ($|\nabla| \sim L^{-1}$)

$$\begin{array}{lll} \frac{\alpha_0^2}{\epsilon^2}: & \frac{\alpha_0}{\epsilon}\left(\frac{1}{a} - d\right): & \left(1 - \frac{d}{a}\right) \\ (1) & (2) & (3) \end{array} . \tag{1.31}$$

Of the possible principal balances, the following two are representative:

(a) The last two terms are of the same order, and the first $\ll$ them. Then

$$\epsilon \sim \alpha_0 \frac{1/a - d}{1 - d/a}. \tag{1.32}$$

For our desired structure to exist ($\alpha_0 \sim 10^{-8}$ for $n_0 \sim 10^9\,\mathrm{cm}^{-3}$), we must have

$$\frac{1/a - d}{1 - d/a} \sim 10^5, \tag{1.33}$$

which is possible if $d/a$ tends to be extremely close to unity. For the first term to be negligible, we would further need

$$\frac{\alpha_0}{\epsilon} \ll \frac{1}{a} - d \Rightarrow \epsilon \gg \frac{10^{-8}}{1/a - d}, \tag{1.34}$$

which is easy to satisfy as long as neither of $a \simeq d$ is close to unity. This is, in fact, the standard relaxed state, where the flows are not supposed to play an important part for the basic structure. For extreme sub–Alfvénic flows, both $a$ and $d$ are large and very close to one another. Is the new term, then, just as unimportant as it appears to be? The answer is no; the new term, in fact, introduces a qualitatively new phenomenon: Since $\nabla \times (\nabla \times \mathbf{b})$ is second order in $|\nabla|$, it constitutes a singular perturbation of the system; its effect on the standard root $(2) \sim (3) \gg (1)$ will be small, but it introduces a new root for which the $|\nabla|$ must be large corresponding to a much shorter length scale (large $|\nabla|$). For $a$ and $d$ so chosen to generate a 1000 km structure for the normal root, a possible solution would be $d/a \sim 1 + 10^{-4}$, $d \simeq a = -10$ , then the value for $|\nabla|$ for the new root will be (the balance will be from the first two terms)

$$|\nabla|^{-1} \sim 10^2 \,\mathrm{cm},$$

that is, an equilibrium root with variation on the scale of 100 cm will be automatically introduced by the flows. The crucial lesson is that even if the flows are relatively weak ($a \simeq d \simeq 10$), the departure from $\boldsymbol{\nabla} \times \mathbf{B} = \alpha \mathbf{B}$, brought about by the double *curl* term can be essential because it introduces a totally different and small scale solution. The small scale solution could be of fundamental importance in understanding the effects of viscosity on the dynamics of these structures; the dissipation of these short scale structures may be the source of primary plasma heating.

We do understand that to properly explain the parallel (to the field–line) motion one must use kinetic theory since the mean free path along $\mathbf{B}$ lines can become of the order of $(10^6 - 10^7)cm$ for the hot plasma $(100\, eV)$. But since the dissipation acts on the perpendicular energy of the flow, we expect the two–fluid theory to give qualitatively (and even quantitatively) correct results.

We would like to remind the reader that by manipulating the force free state $\nabla \times \mathbf{B} = \alpha(\mathbf{x})\mathbf{B}$, Parker has built a mechanism for creating discontinuities (short scales) (Parker 1972, 1988, 1994). It is important to note that short length scales are automatically there

if plasma flows are properly treated.

(b) The other representative balance arises when we have a complete departure from the one–parameter, conventional relaxed state. In this case, all three terms are of the same order. In the language of the previous section, this balance would demand

$$\epsilon \sim \alpha_0 \, \frac{1}{1/a - d} \sim \alpha_0 \, \frac{1/a - d}{1 - d/a} \tag{1.35}$$

which translates as:

$$\left( \frac{1}{a} - d \right)^2 \sim 1 - \frac{d}{a} \tag{1.36}$$

and

$$\frac{1}{a} - d \sim \alpha_0 \, \frac{1}{\epsilon}. \tag{1.37}$$

For our example of a 1000 km structure, $\alpha_0 \cdot 1/\epsilon \sim 10^{-5}$, both $a$ and $d$ not only have to be awfully close to one another, they have to be awfully close to unity. To enact such a scenario, we would need the flows to be almost perfectly Alfvénic. However, let us think of structures which are on the km or 10 km size. In that case $\alpha_0 \cdot 1/\epsilon \sim 10^{-2}$ or $10^{-3}$, and then the requirements will become less stringent, although the flows needed are again Alfvénic. At a density of $(1 - 4) \cdot 10^8 \, \mathrm{cm}^{-3}$, and a speed $\sim (200 - 300)$ km/s, the flow becomes Alfvénic for $B_0 \sim (1 - 3)$ G. It is possible that the conditions required for such flows may pertain only in the weak magnetic field regions.

Following are the obvious characteristics of this class of flows:

(1) Alfvénic flows are capable of creating entirely new kinds of structures, which are quite different from the ones that we normally deal with. Notice that here we use the term flow to denote not the primary emanations but the plasmas that constitute the existing coronal structures, or the structures in the making.

(2) Though they also have two length scales, these length scales are quite comparable to one another: This is very different from the extreme sub–Alfvénic flows where the spatial length–scales are very disparate.

(3) In the Alfvénic flows, the two length scales can become complex conjugate, i.e.,

which will give rise to fundamentally different structures in $\mathbf{b}$ and $\mathbf{V}$.

Defining $p = (1/a - d)$ and $q = (1 - d/a)$, Eq. (1.28) can be factorized as

$$(\alpha_0 \nabla \times -\lambda)(\alpha_0 \nabla \times -\mu)\mathbf{b} = 0 \tag{1.38}$$

where $\lambda(\lambda_+)$ and $\mu(\lambda_-)$ are the solutions of the quadratic equation

$$\alpha_0 \lambda_\pm = -\frac{p}{2} \pm \sqrt{\frac{p^2}{4} - q}. \tag{1.39}$$

If $\mathbf{G}_\lambda$ is the solution of the equation

$$\nabla \times \mathbf{G}(\lambda) = \lambda \mathbf{G}(\lambda), \tag{1.40}$$

then it is straightforward to see that

$$\mathbf{b} = a_\lambda \mathbf{G}(\lambda) + a_\mu \mathbf{G}(\mu), \tag{1.41}$$

where $a_\lambda$ and $a_\mu$ are constants, is the general solution of the double *curl* equation. Using Eqs. (1.30), (1.40), and (1.41), we find for the velocity field

$$\mathbf{V} = \frac{\mathbf{b}}{a} + \alpha_0 \boldsymbol{\nabla} \times \mathbf{b} = \left(\frac{1}{a} + \alpha_0 \lambda\right) a_\lambda \mathbf{G}(\lambda) + \left(\frac{1}{a} + \alpha_0 \mu\right) a_\mu \mathbf{G}(\mu). \tag{1.42}$$

Thus a complete solution of the double *curl* equation is known if we know the solution of Eq. (1.40). This equation, also known as the 'relaxed–state', or the constant $\lambda$ Beltrami equation, has been thoroughly investigated in literature (in the context of solar astrophysics see for example Parker (1994); Priest (1994)). We shall, however, go ahead and construct a class of solutions for our current interest. The most important issue is to be able to apply boundary conditions in a meaningful manner.

We shall limit ourselves to constructing only two–dimensional solutions. For the

Cartesian two–dimensional case ($z$ representing the radial coordinate and $x$ representing the direction tangential to the surface, $\partial/\partial y = 0$) we shall deal with sub–Alfvénic solutions only. This is being done for two reasons: 1) The flows in a majority of coronal structures are likely to be sub–Alfvénic, and 2) this will mark a kind of continuity with the literature. The treatment of Alfvénic flows will be left for a future publication.

We recall from earlier discussion that extreme sub–Alfvénic flows are characterized by $a \sim d \gg 1$. In this limit, the slow scale $\lambda \sim (d-a)/\alpha_0\, d\, a$, and the fast scale $\mu = d/\alpha_0$, and the velocity field becomes

$$\mathbf{V} = \frac{1}{a}\, a_\lambda \mathbf{G}_\lambda + d a_\mu \mathbf{G}(\mu) \tag{1.43}$$

revealing that, while, the slowly varying component of velocity is smaller by a factor ($a^{-1} \simeq d^{-1}$) as compared to the similar part of the magnetic field, the fast varying component is a factor of $d$ larger than the fast varying component of the magnetic field! In a magnetofluid equilibrium, the magnetic field may be rather smooth with a small jittery (in space) component, but the concomitant velocity field ends up having a greatly enhanced jittery component for extreme sub–Alfvénic flows (Alfvén speed is defined w.r. to the magnitude of the magnetic field, which is primarily smooth, and for consistency we will insure that even the jittery part of the velocity field remains quite sub–Alfvénic). We shall come back to elaborate this point after deriving expressions for the magnetic fields.

Equation (1.40) can also be written as

$$\nabla^2 \mathbf{G}(\lambda) + \lambda^2 \mathbf{G}(\lambda) = 0, \tag{1.44}$$

and solving for one component of $\mathbf{G}(\lambda)$ determines all other components up to an integration. For the boundary value problem, we will be interested in explicitly solving for the $z$ (radial) component.

The simplest illustrative problem we solve is the boundary value problem in which

we specify the radial magnetic field $b_z(x, z = 0) = f(x)$, and the radial component of the velocity field $V_z(x, z = 0) = v_0\, g(x)$, where $v_0$ ($\simeq d^{-1} \ll 1$) is explicitly introduced to show that the flow is quite sub–Alfvénic. A formal solution of ($G_z(\lambda) = Q_\lambda$)

$$\frac{\partial^2 Q_\lambda}{\partial x^2} + \frac{\partial^2 Q_\lambda}{\partial z^2} + \frac{\lambda^2}{\alpha_0^2}\, Q_\lambda = 0 \tag{1.45}$$

may be written as

$$Q_\lambda = \int_{\lambda/\alpha_0}^{\infty} dk\, e^{-\kappa_\lambda z}\; C_k\, e^{ikx} + \int_0^{\lambda/\alpha_0} dk\;\; \cos q_\lambda z\;\, A_k\, e^{ikx} + \text{c.c.} \tag{1.46}$$

where $\kappa_\lambda = (k^2 - \lambda^2/\alpha_0^2)^{1/2}$, $q_\lambda = (\lambda^2/\alpha_0^2 - k^2)^{1/2}$, and $C_k$ and $A_k$ are the expansion coefficients. The equivalent quantities for $Q_\mu$ are $\kappa_\mu$, $q_\mu$, $D_k$, and $E_k$. The boundary conditions at $z = 0$ yield (we absorb an overall constant in the magnitude of $b_z$, and $a_\mu/a_\lambda$ is absorbed in $D_k$ and $E_k$):

$$f(x) = Q_\lambda(z = 0) + Q_\mu(z = 0), \tag{1.47}$$

$$v_0\; g(x) = \frac{1}{a}\; Q_\lambda(z = 0) + d\; Q_\mu(z = 0). \tag{1.48}$$

Taking Fourier transform (in $x$) of Eq. (1.47,1.48), we find, after some manipulation, that ($v_0 \sim d^{-1},\ |\widetilde{f}(k)| \simeq |\widetilde{g}(k)|$)

$$C_k \simeq \widetilde{f}(k), \tag{1.49}$$

$$D_k \simeq -\frac{\widetilde{f}(k)}{d^2} + \frac{v_0}{d}\, \widetilde{g}(k) \simeq d^{-2}\widetilde{f}(k), \tag{1.50}$$

and functionally (in their own domain of validity) $C_k = A_k$ and $D_k = E_k$. With the expansion coefficients evaluated in terms of the known functions (their Fourier transforms, in fact), we have completed the solution for $b_z,\ V_z$ and hence of all other field components.

The most remarkable result of this calculation can be arrived at even without a numerical evaluation of the integrals. Although $\widetilde{f}(k)$ and $\widetilde{g}(k)$ are functions, we would

assume that they are of the same order $|\widetilde{f}(k)| = |\widetilde{g}(k)|$. Then for an extreme sub–Alfvénic flow ($|\mathbf{V}| \sim d^{-1} \sim 0.1$, for example), the fastly varying part of $b_z(Q_\mu)$ is negligible ($\sim d^{-2} = 0.01$) compared to the smooth part ($Q_\lambda$). However, for these very parameters, the ratio

$$\left|\frac{V_z(\mu)}{V_z(\lambda)}\right| \simeq \frac{|C_k/a|}{|d\,D_k|} \simeq \frac{|C_k/a|}{|C_k/d|} \simeq 1; \tag{1.51}$$

the velocity field is equally divided between the slow and the fast scales. We believe that this realization may prove to be of extreme importance to Coronal physics. Viscous damping of this substantially large as well as fastly varying flow component may provide the bulk of primary heating needed to create and maintain the bright, visible Corona.

The preceding analysis warns us that neglecting viscous terms in the equation of motion may not be a good approximation until a large part of the kinetic energy has been dissipated. It also appears that the solution of the basic heating problem may have to be sought in the pre–formation rather than the post–formation era. Our time dependent numerical simulation to study the formation of coronal structures was strongly guided by these considerations.

It is evident that for extreme sub–Alfvénic flows, the magnetic field, unlike the velocity field, is primarily smooth. But for strong flows, the magnetic fields may also develop a substantial fastly varying component. In that case the resistive dissipation can also become a factor to deal with. We shall not deal with this problem in this study.

Depending upon the choice of $f(x)$ (from which $\widetilde{f}(k)$ follows) we can construct loops, arcades and other structures seen in the corona.

### 1.4.2 Spherical Solutions to the Curl Curl Equation

In this subsection we construct a 2D spherically symmetric solution of the double curl system. To accomplish this we must solve $[\boldsymbol{G}(\lambda) = \boldsymbol{P}]$

$$\boldsymbol{\nabla} \times P = \lambda \boldsymbol{P}. \tag{1.52}$$

With $(\partial/\partial\varphi = 0)$, Eq. (1.52) is equivalent to:

$$\frac{1}{r\sin\theta}\frac{\partial}{\partial\theta}(\sin\theta\, \mathrm{P}_\varphi) = \lambda \mathrm{P_r} \ , \tag{1.53}$$

$$\frac{1}{r}\frac{\partial}{\partial r}(r\, P_\varphi) = -\lambda P_\theta \ , \tag{1.54}$$

$$\frac{1}{r}\frac{\partial}{\partial r}(r\, P_\theta) - \frac{1}{r}\frac{\partial P_r}{\partial\theta} = \lambda P_\varphi \ . \tag{1.55}$$

The separable solutions can be constructed by using the ansatz

$$P_r = Q_r(r)\, f(\theta) \ , \tag{1.56}$$

$$P_\theta = Q_\theta(r)\, h(\theta) \ , \tag{1.57}$$

$$P_\varphi = Q_\varphi(r)\, h(\theta) \ . \tag{1.58}$$

Since all $Q$'s are functions of $r$ alone, we will suppress the $r$ dependence. Substituting (1.56)-(1.58) into (1.52) and (1.55), we find

$$\frac{Q_\varphi}{r\sin\theta}\,\frac{\partial}{\partial\theta}\,(\sin\theta\, \mathrm{h}(\theta)) = \lambda \mathrm{Q_r}\, \mathrm{f}_\theta \ , \tag{1.59}$$

$$-\frac{1}{r}\,\frac{\partial}{\partial r}(r\, Q_\varphi) = \lambda Q_\theta \ , \tag{1.60}$$

$$h(\theta)\frac{1}{r}\,\frac{\partial}{\partial r}(r\, Q_\theta) - \lambda h(\theta) Q_\varphi = \frac{Q_r}{r}\,\frac{d\, f}{d\,\theta} \ . \tag{1.61}$$

Equations (1.59)-(1.60) will be consistent if $f(\theta)$ and $h(\theta)$ satisfy

$$\frac{\partial f}{\partial h} = -a\, h(\theta) \ , \tag{1.62}$$

$$f(\theta) = \frac{1}{\sin\theta}\,\frac{\partial}{\partial\theta}\,(\sin\theta\, \mathrm{h}(\theta)) \ , \tag{1.63}$$

$$-a\, h(\theta) = \frac{d}{d\,\theta}\,\frac{1}{\sin\theta}\,\frac{\partial}{\partial\theta}\,(\sin\theta\, \mathrm{h}(\theta)) \ . \tag{1.64}$$

which can be solved to find a class of functions $g$ and $f$ parameterized by $a$.

Notice that $h(\theta) = \sin\theta, \mathrm{f}(\theta) = 2\cos\theta$ solve (13)-(15) if $a = 2$. For this case, the radial equations become

$$\frac{Q_\varphi}{r} = \lambda\, Q_r \ , \tag{1.65}$$

$$-\frac{1}{r}\,\frac{d}{d\,r}\,r\,Q_\varphi = \lambda\, Q_\theta \ , \tag{1.66}$$

$$\frac{Q_r}{r} = \frac{1}{2}\lambda\, Q_\varphi - \frac{1}{2}\,\frac{1}{r}\,\frac{d}{d\,r}\,r\,Q_\theta \ . \tag{1.67}$$

For the general solution, we must first solve the angular equation

$$\frac{1}{\sin\theta}\,\frac{d}{d\,\theta}\,\frac{1}{\sin\theta}\,\frac{d}{d\,\theta}\,\sin\theta\,\mathrm{h}(\theta) = -\frac{\mathrm{a}}{\sin\theta}\,\mathrm{h}(\theta) \ , \tag{1.68}$$

which, with $\cos\theta = \mathrm{y}$, becomes

$$(1-y^2)h'' - 2\,y\,h' + \left[a - \frac{1}{(1-y^2)^{1/2}}\right]\,h = 0 \ . \tag{1.69}$$

For $a = \nu\,(\nu+1)$, the solution of Eq.(1.69) is

$$h = P_\nu^1 \ , \tag{1.70}$$

where $P_\nu^1$ is the associated Legendre function. Naturally for $a = 2,\ \nu = 1$ , and $h = P_1^1 = -(1-y^2)^{1/2} = -\sin\theta$. For standard reasons, $a = n$ for good behavior at $y = \pm 1$. Then the general solution (acceptable) is

$$h = P_n^2(\cos\theta) \ . \tag{1.71}$$

The simplest nontrivial solution is with $n = 1, \Longrightarrow h = \sin\theta$. Substituting $a = n(n+1)$, the radial equations become

$$\frac{Q_\varphi}{r} = \lambda\, Q_r \ , \tag{1.72}$$

$$-\frac{1}{r}\frac{d}{d\,r}\,r\,Q_\varphi = \lambda\,Q_\theta\ , \tag{1.73}$$

$$n\,(n+1)\,\frac{Q_r}{r} = \frac{1}{r}\,\frac{d}{d\,r}\,r\,Q_\theta - \lambda\,Q_\varphi\ . \tag{1.74}$$

From these, we derive

$$\frac{d^2}{dr^2} r Q_\varphi + \left[\lambda^2 - \frac{n(n+1)}{r^2}\right]\, r\,Q_\varphi = 0 \tag{1.75}$$

which is solved as

$$r Q_\varphi = A\,r^{1/2}\,Z_{n+1/2}(\lambda r)\ . \tag{1.76}$$

where $Z$ is any Bessel function ($A$ is a constant). Thus the complete set is

$$Q_\varphi = \frac{A}{r^{1/2}}\,Z_{n+1/2}(\lambda r)\ , \tag{1.77}$$

$$Q_r = \frac{1}{\lambda}\frac{A}{r^{3/2}}\,Z_{n+1/2}(\lambda r)\ , \tag{1.78}$$

$$Q_\theta = \frac{A}{\lambda}\,\left(-\frac{A}{r}\right)\,\frac{d}{dr}\,r^{1/2} Z_{n+1/2}(\lambda r)\ . \tag{1.79}$$

From these basic units, then we can try to construct our complete solution. In the Cartesian case we had considered only the real $\lambda$ and $\mu$ solutions. We had noticed that for typical coronal plasmas (extreme sub–Alfvénic), this is the relevant case. In the low magnetic field regions, however, structures with Alfvénic flows are possible and we can run into a situation where $\mu$ and $\lambda$ may be complex ($\mu = \lambda$). We take this opportunity to work out an example ($n = 1$) of this fascinating class of solutions.

Putting all the pieces together, we find

$$\boldsymbol{G}(\lambda) = 2Q_r(\lambda)\cos\theta\ \hat{\boldsymbol{r}} + \mathrm{Q}_\theta(\lambda)\sin\theta\ \hat{\theta} + \mathrm{Q}_\varphi \sin\theta\ \hat{\varphi}\ . \tag{1.80}$$

Since the $Q$'s already have an arbitrary multiplying constant, the magnetic field will be

$$\boldsymbol{b} = \boldsymbol{G}(\lambda) + \boldsymbol{G}(\mu) = \boldsymbol{G}(\lambda) + \boldsymbol{G}^*(\lambda) \ . \tag{1.81}$$

Using Eqs. (1.77)-(1.79), all components of $\boldsymbol{b}$ can be calculated. We evaluate the radial component explicitly ($b_r = \hat{b}_r \cos\theta,\ \hat{\mathrm{A}} = \mathrm{A}/\lambda$)

$$\hat{b}_r = \frac{1}{r^{3/2}}[\hat{A}\, H_{3/2}(r\lambda) + \hat{A}^*\, H^*_{3/2}(r\lambda^*)] \ . \tag{1.82}$$

Making use of the properties of the Hankel functions and after a bit of algebra, we find ($\hat{A} = |\hat{A}|\, e^{i\hat{\varphi}}\ ,\ \lambda = k + i\kappa$)

$$\hat{b}_r = 2\,|\hat{A}|\, e^{-\kappa r} \left( \frac{\cos(\mathrm{kr} + \varphi)}{r^2} \left[ 1 - \frac{\kappa}{r(k^2 + \kappa^2)} \right] + \frac{\sin(\mathrm{kr} + \varphi)}{r^3} \frac{k}{k^2 + \kappa^2} \right) \ . \tag{1.83}$$

Other components can be readily derived.

These solutions have several interesting features:

1. They decay exponentially for large $r$.

2. In addition these solutions have $1/r^m$ dependence, and would not have been allowed if the problem was done in the entire sphere. For our system ($r > 1$), however, these solutions are perfectly acceptable.

3. The exponentially decaying (in $r$) solutions will not be available in the standard force free or relaxed cases, because then there is only one parameter $\lambda$ (or $\mu$), and it must necessarily be real.

4. The decaying solutions will tend to be localized nearer the solar surface (as opposed to the other kind) and may contribute to the near corona in the weak–field regions.

### 1.4.3 Summary

In this study we have investigated the conjecture that the structures which comprise the solar corona (for the quiescent Sun) owe their origin to particle (plasma) flows which

enter the "coronal regions" from lower altitudes. These primary transient flows provide, on a continuous basis, much of the required material and energy which constitutes the corona. From a general framework describing a plasma with flows, we have been able to "derive" several of the essential characteristics of the typical coronal structures.

The principal distinguishing component of the investigated model is the full treatment accorded to the velocity fields associated with the directed plasma motion. It is the interaction of the fluid and the magnetic aspects of the plasma that ends up creating so much diversity in the solar atmosphere.

This study has led to the following preliminary results:

(1) By using different sets of boundary conditions, it is possible to construct various kind of 2D loop and arcade configurations.

(2) In the closed magnetic field regions of the solar atmosphere, the primary flows can accumulate, in periods of a few minutes, sufficient material to build a coronal structure. The ability of the supersonic flows to generate shocks, and the viscous dissipation of these shocks can provide an efficient and sufficient source for the primary plasma heating which may take place simultaneously with the accumulation. The stronger the spatial gradients of the flow, the greater is the rate of dissipation of the kinetic energy into heat. The hot base of the structures is reached at typical distances of a $\sim 10000\,\mathrm{km}$ from the origin of simulation.

(3) A theoretical study of the magnetofluid equilibria reveal that for extreme sub–Alfvénic flows (most of the created corona flows) the velocity field can have a substantial, fastly varying (spatially) component even when the magnetic field may be mostly smooth. Viscous damping associated with this fast component could be a major part of the primary heating needed to create and maintain the bright, visible coronal structure. The far–reaching message of the equilibrium analysis is that neglecting viscous terms in the equation of motion may not be a good approximation until a large part of the kinetic energy in the primary flow has been dissipated.

(4) The qualitative statements on plasma heating, made in points 1 and 2, were

tested by a numerical solution of the time–dependent two-fluid system. For sub–Alfvénic primary flows we find that the particle-accumulation begins in the strong magnetic field regions (near the solar surface), and soon spans the entire volume of the closed magnetic field region. It is also shown that, along with accumulation, the viscous dissipation of the kinetic energy contained in the primary flows heats up the accumulated material to the observed temperatures, i.e., in the very first (and fast, $\sim (2-10)\,min$) stage of accumulation, much of the flow kinetic energy is converted to heat. This happens within a very short distance (transition region) of the solar surface $\sim 0.03 R_{\odot}$. In the transition region, the flow velocity has very steep gradients. Outside the transition layer the dissipation is insignificant, and in a very short time a nearly uniform (with insignificantly decreasing density and temperature on the radial distance), hot and bright quasi-equilibrium coronal structure is created. In this newborn structure, one finds rather weak flows. One also finds downflows with their parameters determined by the initial and boundary conditions.

The transition region from the solar surface to this equilibrium coronal structure is also characterized by strongly varying (both radial and across) temperature and density. Depending on the initial magnetic field , the base of the hot region (of the bright part) of a given structure acquires its appropriate density and temperature.

(5) The details of the ensuing dynamics are strongly dependent on the relative values of the pressure of the initial flow, and of the ambient solar magnetic field in the region. Two limiting cases were studied with the expected results: 1) The flow entering a relatively weak initial magnetic field strongly deforms (and in specific cases drags) the magnetic field lines, and 2) the flow interacting with a relatively strong magnetic field leaves it virtually unchanged.

We end this study with several qualifying remarks:

1) This study, in particular the numerical work, is preliminary. We hope to be able to extend the numerical work to make it considerably more quantitative, and to cover a much greater variety of the initial and boundary conditions to simulate the immense

coronal diversity. Then a thorough comparison with observations can be undertaken. To show the dissipation of small scale velocity component just like the dissipation of shock–like structures is postponed for future since it requires much higher resolution.

2) This study is limited to the problem of the origin, the creation and the primary heating of the coronal structures. The processes which may go on in the already existing bright equilibrium corona (secondary or supporting heating, instabilities, reconnection) etc., for example, are not considered. Because of this lack of overlap between our model and the conventional coronal heating models, we do not find it meaningful to compare our work with any in the vast literature on this subject. Led by observations alone, we have constructed and investigated the present model.

3) We do not know much about the primary solar outflows on which this entire study is based. The merit of this study, however, is that as long as they are present (see e.g. [1, 2, 3]), the details about their origin are not crucial.

4) We are just beginning to derive the consequences of according a co–primacy (with the magnetic field) to the flows in determining overall plasma dynamics. The addition of the velocity fields (even when they are small) brings in essential new physics, and will surely help us greatly in understanding the richness of the plasma behavior found in the solar atmosphere.

## 1.5 Equilibrium structure creation in relativistically hot two-temperature e-p plasmas with small fraction of cold ions

During the past few years considerable amount of papers have been devoted to the analysis of electromagnetic (EM) wave propagation in hot, pure electron-positron (e-p) plasmas since e-p pairs are thought to be a major constituent of the plasma emanating both from the pulsars and from the inner region of the accretion disks surrounding the central black holes in active galactic nuclei (AGN) [85, 77] (Michel, 1982; Begelman *et al.*, 1984). Such a plasma is formed also in the early universe [86, 87] (Rees, 1983; Tajima and Taniuti, 1980). Although the relativistically hot e-p pairs form most of astrophysical and cosmic plasmas, a minority of cold electrons and heavy ions is likely to be present [79] (Berezhiani and Mahajan, 1995). For instance, outflows of e-p plamsa from pulsars entering an interstellar cold, low density electron-ion (e-i) plamsa forms two temperature electron-positron-ion (e-p-i) plasma. The three-component plasmas - hot e-p plasma with small fraction of heavy ions - have been studied in the context of pulsar magnetospheres by Lakhina and Buti (1981) [83] and by Lominadze *et al* (1986) [84]. The creation of stable localized structures of relativistically strong EM radiation in hot e-p-i plasma have been shown by Berezhiani and Mahajan (1994,1995).

In two temperature e-p-i plasma the interesting phenomena differing from that of one temperature can exist. It is now believed that strong monochromatic waves emitted by pulsars are subject to parametric instabilities even in quite under–dence plasmas. In this context in present study we consider the propagation of strong EM radiation in a hot e-p un–magnetized plasma with small fraction of cold e-i plasma. We show, that the presence of a minority of cold electrons and ions can lead to the scattering of the pump EM wave into the electron-sound and EM wave; to the instability of hot e-p plasma against the low frequency (LF) perturbations. Hence, in contrast to the case of the pure e-p plasma, in two temperature e-p-i plasma the three wave decay instability may occur.

The possibility of the soliton formation due to the modulational instability of EM wave is also investigated.

### 1.5.1 Nonlinear Wave Dynamics In Two–Temperature Electron–Positron–Ion Plasma

Let us assume that the velocity distribution of particles is locally a relativistic Maxwellian. Then the dynamics of the fluid of species $\alpha$ ($\alpha = e, p, i$) is contained in the equation [80] (Javakhishvili and Tsintsadze, 1973):

$$\frac{\partial}{\partial x_k}(U^i_\alpha U_{\alpha k} W_\alpha) - \frac{\partial}{\partial x_i}\mathsf{P}_\alpha = \frac{1}{c}F^{ik}J_{\alpha k}, \tag{1.84}$$

where $U^i_\alpha \equiv [\gamma_\alpha,\ \gamma_\alpha \mathbf{u}_\alpha/c]$ is the hydrodynamic four velocity, $\mathbf{u}_\alpha$ is the hydrodynamic three-velocity of the hot e-p fluid, $\gamma_\alpha = (1 - u^2_\alpha/c^2)^{-1/2}$ is the relativistic factor, $J_{\alpha k}$ is the four current, $F^{ik}$ is the electromagnetic field tensor and $W_\alpha$ is the enthalphy per unit volume: $W_\alpha = (n_\alpha/\gamma_\alpha)m_\alpha c^2 G_\alpha[m_\alpha c^2/T_\alpha]$. Here $m_\alpha$ and $T_\alpha$ are the particle rest mass and temperature of species $\alpha$, respectively, $n_\alpha$ is the density in the laboratory frame of the e-p-i fluid and $G_\alpha(z_\alpha) = K_3(z_\alpha)/K_2(z_\alpha)$, ($z_\alpha = m_\alpha c^2/T_\alpha$), where $K_\nu$ are the modified Bessel functions. For the nonrelativistic temperatures ($T_\alpha << m_\alpha c^2$) $G_\alpha = 1 + 5T\alpha/2m_\alpha c^2$ and for the ultrarelativistic temperatures ($T_\alpha >> m_\alpha c^2$) $G_\alpha = 4T_\alpha/m_\alpha c^2 >> 1$. The relativistic pressure in the rest frame is $\mathsf{P}_\alpha = (n_\alpha/\gamma_\alpha)T_\alpha$.

We assume that hot electron and positron temperatures are equal and constant while the process of EM wave interaction with given fluid ($G_{\alpha h} = const$). Note that here and below the subscript "$c$" is used for cold electrons and "$h$" - for hot particles respectively.

From the set of equations (1.84) the equation of motion can be written as follows:

$$\frac{d_\alpha}{dt}(\mathbf{P}_\alpha G_\alpha) + \frac{1}{n_\alpha}\nabla \mathsf{P}_\alpha = e_\alpha \mathbf{E} + \frac{e_\alpha}{c}(\mathbf{u}_\alpha \times \mathbf{B}), \tag{1.85}$$

where $\mathbf{P}_\alpha = \gamma_\alpha m_\alpha \mathbf{u}_\alpha$ is the hydrodynamic momentum, $\mathbf{E}$ and $\mathbf{B}$ are the electric and

magnetic fields and $d_\alpha/dt = \partial/\partial t + \mathbf{u}_\alpha \cdot \nabla$ is the co–moving derivative. For cold electrons in the eq. (1.85) $G_c = 1$ and $T_{ec} \equiv T_c = const$ should be assumed.

And for all kinds of species we have the continuity equation:

$$\frac{\partial n_\alpha}{\partial t} + \nabla(n_\alpha \mathbf{u}_\alpha) = 0. \tag{1.86}$$

To study the nonlinear propagation of intense EM wave in a relativistically hot e-p plasma with small fraction of cold e–i plasma we must couple the eq.-s of motion with the Maxwell equations. In the terms of the potentials defined by:

$$\mathbf{E} = -\frac{1}{c}\frac{\partial \mathbf{A}}{\partial t} - \nabla\phi; \qquad \mathbf{B} = \nabla \times \mathbf{A}, \tag{1.87}$$

they take the form (Coulomb gauge $\nabla \cdot \mathbf{A} = 0$):

$$\frac{\partial^2 \mathbf{A}}{\partial t^2} - c^2 \triangle \mathbf{A} + c\frac{\partial}{\partial t}(\nabla\phi) - 4\pi c\mathbf{J} = 0, \tag{1.88}$$

and

$$\triangle\phi = -4\pi\rho, \tag{1.89}$$

where for the charge and current densities we have respectively:

$$\rho = \sum_\alpha e_\alpha n_\alpha; \qquad \mathbf{J} = \sum_\alpha e_\alpha n_\alpha \mathbf{u}_\alpha. \tag{1.90}$$

The equilibrium state for hot e-p plasma is characterized with charge neutrality (with unperturbed number densities of the hot electrons and positrons equal to $n_{oh}$). For small fraction of cold e-i plasma the equilibrium state is characterized also by charge neutrality (with background ion density $n_{oc}$) and

$$n_{oc} << n_{oh}. \tag{1.91}$$

Also we assume that: ions are immobile; in equilibrium state hot electrons and positrons have the same temperatures equal to $T_{oh}$ and

$$T_{oh} >> T_c; \qquad T_{oi} = 0. \tag{1.92}$$

Let us analyze the one-dimensional propagation ($\frac{\partial}{\partial z} \neq 0, \frac{\partial}{\partial x} = 0, \frac{\partial}{\partial y} = 0$) of circularly polarized EM wave with a mean frequency $\omega_o$ and a mean wave number $k_o$ along the $z$ axis. Thus

$$\mathbf{A}_\perp = \frac{1}{2}(\mathbf{x} + i\mathbf{y})A(z,t)exp(ik_o z - i\omega_o t) + c.c., \tag{1.93}$$

where $A(z,t)$ is a slowly varying function of $z$ and $t$ and $\mathbf{x}$ and $\mathbf{y}$ are the standard unit vectors. The gauge condition gives us $A_z = 0$. Then the transverse component of eq.-s of motion (1.85) are integrated yielding:

$$\mathbf{P}_{\perp\alpha} G_\alpha = -\frac{e_\alpha}{c}\mathbf{A}_\perp, \tag{1.94}$$

where the constant of integration is set equal to zero since particle hydrodynamic moments are assumed to be zero at the infinity where the field vanishes.

Now it is necessary to write the equations for longitudinal motion. This motion is driven by the ponderomotive pressure ($\sim P^2_{\alpha\perp}$) of high frequency (HF) EM fields and latter doesn't depend on the particle charge sign. In purely e-p plasma since the effective mass of the electrons and positrons are equal ($G_e = G_p = G$) the radiation pressure gives equal longitudinal moments to both the electrons and positrons and effects concentration without producing the charge separation ($n_e = n_p$ and $\phi = 0$) [78, 81]. But as it was shown by Berezhiani and Mahajan, (1995) the introduction of small fraction of heavy ions leads to "symmetry breaking" between hot electrons and positrons and it becomes possible to have finite $\phi$. As we will see below, due to the presence of small fraction of cold e-i plasma in hot e-p plasma the electrostatic potential will be surely created.

Let us redefine the electron rest mass in equations for hot e-p plasma as:

$$m \to mG_h(T_h) \equiv M. \tag{1.95}$$

Then the eq.(1.88) for transverse motion can be written as:

$$\frac{\partial^2}{\partial t^2}\mathbf{A}_\perp - c^2\frac{\partial^2}{\partial z^2}\mathbf{A}_\perp + \omega_h^2(n_{eh}+n_{ph})\frac{\mathbf{A}_\perp}{n_{oh}\gamma_h} + \omega_e^2\frac{n_c}{n_{oc}}\frac{\mathbf{A}_\perp}{\gamma_c} = 0, \tag{1.96}$$

where $\omega_h^2 = 4\pi e^2 n_{oh}/M$, $\omega_e^2 = 4\pi e^2 n_{oc}/m_e$ and $\gamma_h$ and $\gamma_c$ are the relativistic factors for hot and cold electrons respectively, $\gamma_\alpha = (1+\mathbf{P}_\alpha^2/m_\alpha^2c^2)^{1/2}$; $n_c$, $n_{eh}$ and $n_{ph}$ are the cold and hot electron and positron densities respectively.

The equations for longitudinal motion have the form:

$$\frac{\partial n_\alpha}{\partial t} + \frac{\partial}{\partial z}\left(\frac{n_\alpha P_{z\alpha}}{m_\alpha\gamma_\alpha}\right) = 0, \tag{1.97}$$

$$\left(\frac{\partial}{\partial t} + \frac{P_{z\alpha}}{m_\alpha\gamma_\alpha}\frac{\partial}{\partial z}\right)P_{z\alpha} + \frac{T_\alpha}{n_\alpha}\frac{\partial}{\partial z}\left(\frac{n_\alpha}{\gamma_\alpha}\right) = -e_\alpha\frac{\partial\phi}{\partial z} - \frac{e_\alpha^2}{2m_\alpha\gamma_\alpha c^2}\frac{\partial|A|^2}{\partial z}, \tag{1.98}$$

where for hot particles $m_{\alpha h} = M$ is assumed and in $P_{z\alpha h}$ the mass redefinition is performed (see the relation (1.95)).

In what follows we consider only the weak relativistic case assuming $\mathbf{P}_\alpha^2/m_\alpha^2c^2 << 1$. In the presence of two different temperature electron plasma for LF motion it is possible to satisfy the condition [82]: $KV_{Tc} << \Omega << KV_{Th}$, where $V_{Tc}$ and $V_{Th}$ are the cold and hot electron thermal velocities respectively and $\Omega^{-1}$ and $K^{-1}$ are the characteristic time and spacial spreads of the pulse ($\Omega << \omega_o$; $K << k_o$).

First let's find the equation for LF motion. Under the above mentioned conditions for hot particles we have:

$$-e_\alpha\frac{\partial\phi}{\partial z} = \frac{T_h}{n_{\alpha h}}\frac{\partial}{\partial z}\left(\frac{n_{\alpha h}}{\gamma_h}\right) + \frac{e^2}{2M\gamma_h c^2}\frac{\partial|A|^2}{\partial z}. \tag{1.99}$$

From eq.-s (1.99), introducing $\delta n_c = n_c - n_{oc}$ and $\delta n_{\alpha h} = n_{\alpha h} - n_{oh}$ ($\delta n_c <<$

$n_{oc}$; $\delta n_{\alpha h} << n_{oh}$), we obtain:

$$\delta n_h = \delta n_{ph} + \delta n_{eh} = -n_{oh}\frac{e^2|A|^2}{MT_hc^2} + n_{oh}\frac{e^2|A|^2}{M^2c^4}. \tag{1.100}$$

Using equations (1.89), (1.90) and (1.100) we find the relation between $\delta n_{eh}$ and $\delta n_c$ written as:

$$\delta n_{eh} = -\frac{1}{2}\delta n_c - n_{oh}\frac{e^2|A|^2}{2MT_hc^2} + n_{oh}\frac{e^2|A|^2}{2M^2c^4}. \tag{1.101}$$

Using the eq.(1.101) in the eq.(1.99) written for electrons finally we obtain:

$$\frac{\partial\phi}{\partial z} = -\frac{T_h}{2en_{oh}}\frac{\partial}{\partial z}\delta n_c. \tag{1.102}$$

Thus, as we already mentioned above, the presence of small fraction of cold e-i plasma in hot e-p plasma gives rise to electrostatic potential.

Substituting the eq.(1.102) in the eq.(1.98) written for cold electrons, after simple algebra, assuming that:

$$\frac{T_c}{T_h} << \frac{1}{2}\frac{n_{oc}}{n_{oh}}, \tag{1.103}$$

one can get the equation for $\delta n_c$:

$$\frac{\partial^2}{\partial t^2}\delta n_c - c_s^2\frac{\partial^2}{\partial z^2}\delta n_c = n_{oc}\frac{e^2}{2m^2c^2}\frac{\partial^2}{\partial z^2}|A|^2, \tag{1.104}$$

where

$$c_s^2 = \left(\frac{1}{2}\frac{n_{oc}}{n_{oh}}\frac{T_h}{m}\right)^{1/2}$$

is the so-called "electron-sound" velocity. Thus, due to the fact that the most part of electrons are relativistically hot, and consequently heavy ($G_h \neq 1$) than the small part of cold electrons, it is possible to induce the "electron-sound" wave; the exciting ponderomotive force is defined by the HF pressure on cold electrons.

The eq.(1.104) is coupled with the following equation for $A$ (for HF wave frequency

satisfying the dispersion relation: $\omega_o^2 = k_o^2 c^2 + 2\omega_h^2 + \omega_e^2$):

$$2i\omega_o \left( \frac{\partial}{\partial t} + v_g \frac{\partial}{\partial z} \right) A + \omega_o v_g' \frac{\partial^2}{\partial z^2} A$$

$$+\omega_h^2 \left( \frac{e^2|A|^2}{M^2 c^4} - \frac{\delta n_h}{n_{oh}} \right) \cdot A + \omega_e^2 \left( \frac{e^2|A|^2}{2m^2 c^4} - \frac{\delta n_c}{n_{oc}} \right) \cdot A = 0, \tag{1.105}$$

where $v_g$ is the group velocity of HF wave.

The system of equations (1.104),(1.105) together with the relation (1.100) describes the nonlinear wave dynamics in a relativistically hot e-p plasma with small fraction of cold e-i plasma. As we see we have the scattering of EM pump wave into the electron-sound and EM wave. Note that in the purely e-p plasma the three wave scattering processes do not exist. The presence of small fraction of cold e-i plasma here is a reason to have the LF longitudinal waves together with the HF EM waves. Using this result we can conclude that the radiation emanating both from the pulsars and AGN entering the cold low density e-i plasma undergoes the modification due to the scattering processes.

It is possible to find the stationary solution of the system of eq.-s (1.100), (1.104),(1.105). We look for the solutions as:

$$A = A(\xi, \tau); \quad \delta n_c = \delta n_c(\xi, \tau); \quad \xi = z - v_g t; \quad t = \tau; \quad \frac{\partial}{\partial \tau} << v_g \frac{\partial}{\partial z}. \tag{1.106}$$

In the subsonic regime: $v_g << c_s$, i.e.

$$k_o c^2 \sqrt{\frac{m}{M}} << \omega_o \sqrt{\frac{1}{2} \frac{n_{oc}}{n_{oh}}} V_{Th} \tag{1.107}$$

from the eq.(1.104) we obtain:

$$\delta n_c = -n_{oc} \frac{c^2}{c_s^2} \frac{e^2|A|^2}{2m^2 c^4} < 0 \tag{1.108}$$

and substituting the eq.(1.108) in the eq.(1.105), if we have the relativistically hot e-p

plasma ($G_h >> 1$), we get the Nonlinear Shrodinger Equation (NLSE):

$$2i\frac{\partial}{\partial\tau}A + v'_g\frac{\partial^2}{\partial\xi^2}A + \frac{\omega_e^2}{\omega_o}\frac{c^2}{c_s^2}\frac{e^2|A|^2}{2m^2c^4}\cdot A = 0. \tag{1.109}$$

As it is well–known the eq.(1.109) has the stationary solution representing the subsonic soliton of rarification (the total density variation $\delta n \equiv \delta n_h + \delta n_c < 0$).

In the case of the nonrelativistically hot e-p plasma ($G_h \cong 1$) and $k_o \to 0$ we also get the soliton solution of obtained NLSE. Under definite conditions it is possible to have the supersonic solitons too. It should be noted that for the EM waves with $v_g = 0$ in pure, hot e-p plasma the possibility to have the stable soliton–like structures was found by Kartal *et al,* 1995 [81].

Let's investigate the stability of two-temperature e-p-i plasma. For this reason we look for $A$ and $\delta n_c$ as:

$$A(z,t) = a(z,t)e^{i\theta(z,t)}; \quad \delta n_c = \delta n_c exp[ikz - i\omega t] + c.c.$$

$$a = a_o + \delta a exp[ikz - i\omega t] + c.c.; \quad \theta = \theta_o + \delta\theta exp[ikz - i\omega t] + c.c., \tag{1.110}$$

where $a(z,t)$ and $\theta(z,t)$ are the slowly varying in time and space real functions and $\delta a << a_o$, $\delta\theta << \theta_o$.

Linearizing the system of equations (1.104), (1.105) using the relation (1.100) we easily obtain the dispersion relation:

$$(\omega^2 - c_s^2k^2)[(w - v_gk)^2 - \frac{v_g'^2}{4}k^4] = \omega_e^2v_g'^2k^4\frac{e^2a_o^2}{m^2c^4}$$

$$+v'_gk^2(\omega^2 - c_s^2k^2)\frac{\omega_h^2}{2\omega_o}\frac{c^2}{V_{Th}^2}\left(\frac{m^2}{M^2} + \frac{c_s^2}{c^2}\right)\frac{e^2a_o^2}{m^2c^4}, \tag{1.111}$$

which in the limit $M >> m$ (i.e. $G_h >> 1$, the relativistically hot e-p plasma) for the coinciding roots:

$$\omega \simeq c_sk + i\Gamma \simeq v_gk + \frac{v'_gk^2}{2} + i\Gamma \tag{1.112}$$

gives the relation for increment:

$$\Gamma^2 = c_s k \frac{v_g' \omega_h^2}{V_{Th}^2} \frac{e^2 a_o^2}{m^2 c^4}. \tag{1.113}$$

Thus, the addition of even very small amount of cold e-i plasma ($n_{oc} \neq 0$, i.e. $c_s \neq 0$) leads to the instability of hot e-p plasma against the LF perturbations. Such three wave decay instability doesn't exist in pure e-p plasma. The present result shoud be useful to understand the character of the pulsar and AGN radiation.

In conclusion, we have shown that in the hot e-p plasma with small fraction of cold e-i plasma, it is possible to have the scattering of EM wave with relativistically strong amplitude into the longitudinal so-called "electron–sound" and EM wave. Under the definite conditions the possibility of soliton solution creation for EM wave is found.

### 1.5.2 Localized nonlinear structures of intense electromagnetic waves in two–electron–temperature electron–positron–ion plasmas

Nonlinear propagation of intense electromagnetic (EM) waves in electron–positron (e–p) plasmas has received a large amount of theoretical interest mainly because such plasmas are naturally produced under certain astrophysical conditions. Since e–p plasmas are thought to have been present in the early Universe [86], plasma processes are expected to have played an important role in the early history, as well as the evolution of the Universe. On the other hand, in the present epoch, electron–positron pairs are the main constituents of the plasma emanating both from pulsars and from the inner regions of the accretion disks surrounding the central black holes in active galactic nuclei (AGN)[89, 90, 85, 77]. Recent progress in the production of pure positron plasmas now makes it possible to consider performing laboratory experiments on e–p plasmas [91, 92, 93].

During the past few years, a considerable amount of theoretical work has been de-

voted to the analysis of nonlinear EM wave processes in pure e–p plasmas [87, 94, 88, 96, 97, 98, 99]. In such plasmas, wherein both the constituent species possess the same magnitude of charge to mass ratio, important symmetries manifest themselves and one cannot distinguish the high–frequency (hf) and low-frequency (lf) motions, unlike in conventional electron–ion (e–i) plasmas. On the other hand, when a small amount of electron–ion component is present, e–p plasmas admit lf density fluctuations associated with longitudinal modes, such as the electron–acoustic mode. The self–consistent coupling between the pump EM wave and the electron–acoustic mode can cause the onset of the modulational instability of the pump wave. On the application side, modulational instability may be a potential mechanism for the phenomena of pulsar radiation in terms of nonlinear effects. For example, nonlinear structure formation in e–p plasmas has been extensively investigated by Tajima and Taniuti [87]. Their results show that e–p plasmas are more "plastic" than the usual e–i plasmas. This has been ascribed to the fact that e–p plasmas do not lead to charge separation electric fields, which provide the self–consistent restoring force. It is known [100] that the interaction of a large amplitude EM wave with strongly magnetized e–p plasmas can lead to the formation of nonlinear localized wave structures, such as the envelope solitons, which could be associated with the observed pulsar and AGN radiation.

The relativistically hot e–p pairs constitute a major component of many of the astrophysical and cosmic plasmas, though a minority of cold electrons and heavy ions may also be present. For instance, outflows of e–p plasma from pulsars entering low density ambient e–i plasma in the inter–stellar regions form two–electron–temperature electron–positron–ion (e–p–i) plasmas. The three–component plasmas, namely, the majority hot e–p component with a small fraction of heavy ions, have been studied in the context of pulsar magnetospheres [83, 84]. On the other hand, it was demonstrated recently [79] that the presence of minority ion species in hot e–p plasma can lead to the creation of stable, localized, non–dispersive and non–diffracting pulses that carry a large density excess within the region of field localization, leading to the formation of the so-called

"light bullets".

It should be pointed out that in un–magnetized, cold pure e–p plasmas there is no amplitude modulation of the high-frequency electromagnetic field [98]. On the other hand, when finite thermal effects are included, e–p plasmas are known to be modulationally unstable [99, 100, 83, 84, 79, 101]. Moreover, two-electron-temperature e–p–i plasmas exhibit many interesting phenomena, which are significantly different from those found in the usual plasmas with single electron species. It is now believed that strong monochromatic waves emitted by pulsars are subject to parametric instabilities even in quite under–dense plasmas. In this context, it has been shown [102, 103] recently that, in contrast to the case of pure e–p plasmas, two–electron–temperature e–p–i plasmas are susceptible to three-wave decay instabilities. The addition of even a very small amount of cold e–i component leads to the scattering of the pump EM wave into the electron–acoustic and EM wave, which leads to the instability of hot e–p plasma against the lf perturbations. However, in this analysis, the lf response of the plasma was described by means of a driven linear wave equation, which is valid for near–static propagations and when the amplitude of the density fluctuation is small. On the other hand, coupled mode propagations in the near–sonic regime typically lead to large amplitude density fluctuations [100]. In such cases, the latter are to be described by means of a suitable nonlinear (driven) wave equation, such as the Korteweg–de Vries or, more generally, the Boussinesq equation.

In the present study, we investigate the problem of soliton formation due to the modulational instability of EM waves in e–p–i plasmas by including leading order nonlinearities in the low-frequency response of the plasma. This is the main motivation for the present work. Specifically, we discuss the coupled propagation of electromagnetic and electron–acoustic waves in a two–lectron–temperature e–p–i plasma by deriving a generalized system of coupled Schrödinger–Boussinesq system. For slow modulations, the EM wave amplitude is governed by a Schrödinger–type equation which includes self–nonlinear terms. For finite amplitudes, the lf cold electron density perturbation is governed by a

nonlinear evolution equation of the Boussinesq type for the so–called "electron–sound" wave driven by the time–averaged, low–frequency nonlinear ponderomotive force on the cold electrons. We explicitly obtain exact solutions for the coupled waves for the case of stationary propagation and show that for finite amplitudes only the supersonic compressional solitons can exist in such plasmas, while in the quasi–neutral, linear lf response case, both the sub– and super–sonic solitons may occur.

Below we formulate the problem and derive the governing equations leading to generalized Schrödinger–Boussinesq equations for weakly relativistic amplitudes. Then we consider the stationary propagation of coupled waves and obtain exact analytical solutions in different parameter regimes.

To study the nonlinear propagation of intense EM wave in a relativistically hot e–p plasma with a small fraction of cold e–i plasma, we start from the Maxwell equations, which are coupled to the relativistic fluid equations for the various species. In the terms of the vector and scalar potentials defined by parameter regimes.

$$\mathbf{E} = -\frac{1}{c}\frac{\partial \mathbf{A}}{\partial t} - \nabla\phi; \qquad \mathbf{B} = \nabla \times \mathbf{A} \ , \tag{1.114}$$

the wave equation takes the form (after using the Coulomb gauge $\nabla \cdot \mathbf{A} = 0$),

$$\frac{\partial^2 \mathbf{A}}{\partial t^2} - c^2 \Delta \mathbf{A} + c\frac{\partial}{\partial t}(\nabla\phi) - 4\pi e \mathbf{J} = 0 \ , \tag{1.115}$$

and

$$\Delta\phi = 4\pi\rho \ , \tag{1.116}$$

where the charge and the current densities are given, respectively, by

$$\rho = \sum_\alpha e_\alpha n_\alpha; \qquad \mathbf{J} = \sum_\alpha e_\alpha n_\alpha \mathbf{u}_\alpha \ . \tag{1.117}$$

Here, $\alpha(= e, p, i$ for electrons, positrons, ions, respectively) indicates particle species; $e_\alpha$ is the charge and $n_\alpha$ is the density (in the laboratory frame) of species $\alpha$; $\mathbf{u}_\alpha$ is the hydrodynamic three–velocity of the particles.

The equilibrium state of the hot e–p plasma is characterized by charge neutrality (with unperturbed number densities of the hot electrons and positrons equal to $noh$). We assume also that ions are immobile; for a small fraction of cold e–i plasma, the equilibrium state is characterized by charge neutrality (with background ion density $n_{oc}$) and

$$n_{oc} \ll n_{oh}. \tag{1.118}$$

In the equilibrium state, hot electrons and positrons have the same temperatures equal to $T_{oh}$, and

$$T_{oh} \gg T_{oc} \ ; \qquad\qquad T_{oi} = 0 \ . \tag{1.119}$$

Note that here and in the following, the subscript c is used for cold electrons and h for the hot particles, respectively.

Equations (1.115) and (1.116) are coupled to the relativistic hydrodynamic equations. The continuity equation for all the species has the form

$$\frac{\partial n_\alpha}{\partial t} + \nabla \cdot (n_\alpha \mathbf{u}_\alpha) = 0 \ . \tag{1.120}$$

Before considering the equations of motion, we may point out here that there are two types of relativistic regimes in e–p–i plasma that are important. In space and astrophysical situations, the electromagnetic radiation of luminous objects serves as a source of intense EM fields because of which the plasma particles may attain relativistic quiver velocities. Hence, the particle masses become functions of the respective speeds, while the relativistic mass variation leads to a host of important physical effects even in ordinary e–i plasmas [100]. On the other hand, at very high temperatures, the thermal energy of the plasma particles is of the order of, or larger than the energy at rest and this is another type of relativistic regime that may be specifically relevant in the early epochs

of the Universe. These two relativistic effects contribute important nonlinear terms to the relevant dynamical equations we include in the present work. We shall assume in the following that the velocity distribution of particles is locally a relativistic Maxwellian.

Then, from the set of relativistic hydrodynamic equations [80, 104] the equation of motion can be written as follows:

$$\frac{d_\alpha}{dt}(\mathbf{p}_\alpha G_\alpha) + \frac{1}{n_\alpha}\nabla\mathcal{P} = e_\alpha\mathbf{E} + \frac{e_\alpha}{c}(\mathbf{u}_\alpha \times \mathbf{B}) \ , \tag{1.121}$$

where $\mathbf{p}_\alpha = \gamma_\alpha m_\alpha \mathbf{u}_\alpha$ is the hydrodynamic momentum, $\gamma_\alpha = (1 - u_\alpha^2/c^s)^{-1/2}$ is the relativistic factor, $\mathcal{P} = (n_\alpha/\gamma_\alpha)T_\alpha$ is the relativistic pressure in the rest frame and $d_\alpha/dt = \partial/\partial t + \mathbf{u}_\alpha \cdot \nabla$ is the comoving derivative. Here, $m_\alpha$ and $T_\alpha$ are the particle rest mass and temperature of species $\alpha$, respectively, and $G_\alpha(z_\alpha) = K_3(z_\alpha)/K_2(z_\alpha)$ and $z_\alpha = m_\alpha c^2/T_\alpha$ , where $K_\nu$ is the modified Bessel function of order $\nu$. It may be noted that for nonrelativistic temperatures $(T_\alpha \ll m_\alpha c^2)$ one has $G_\alpha = 1 + 5T_\alpha/2m_\alpha c^2$ , while for ultrarelativistic temperatures $(T_\alpha \gg m_\alpha c^2)$ we find $G_\alpha = 4T_\alpha/2m_\alpha c^2 \gg 1$ .

To keep the analysis tractable, as well as amenable for analytical investigations, we assume that the hot electron and positron temperatures are equal and constant, while the process of EM wave interaction with the cold electron component takes place at nonrelativistic temperatures. Thus, for the cold electrons in (1.121), we have $G_c = 1$ and, hence, $T_{ec} \equiv T_c = const$ should be assumed.

We are interested in localized solutions of the above system of equations for a circularly polarized EM wave with a mean frequency $\omega_0$ and a mean wave number $k_0$ along the $z$–axis. Accordingly, the hf pump field is represented by

$$\mathbf{A}_\perp = \frac{1}{2}(\mathbf{x} + i\mathbf{y})\, A(z,t) \exp(ik_0 z - i\omega t) + c.c. \ , \tag{1.122}$$

where $A(z,t)$ is a slowly varying function of $z$ and $t$, and $\mathbf{x}$ and $\mathbf{y}$ are the standard unit vectors. The gauge condition gives us $A_z = 0$. Then the transverse component of the

equations of motion (1.121) are integrated to yield

$$\mathbf{p}_{\perp\alpha} G_\alpha = -\frac{e_\alpha}{c}\mathbf{A}_\perp \ , \tag{1.123}$$

where the constant of integration is set equal to zero, since particle hydrodynamic momenta are assumed to be zero at infinity where the field vanishes.

The role of hot particle mass is now played by the quantity $m_h G_h(T_h)$. Thus, the effective mass of hot electrons and positrons depends on the temperature. We now redefine the electron rest mass $(m_e \equiv m)$ in the equations for the hot e-p component as $\mu = m G_h(T_h)$ . The wave equation (1.115) for the transverse motion can then be written as

$$\frac{\partial^2}{\partial t^2}\mathbf{A}_\perp - c^2\frac{\partial^2}{\partial z^2}\mathbf{A}_\perp + \omega_h^2\left(n_{eh} + n_{ph}\right)\frac{\mathbf{A}_\perp}{n_{0h}\gamma_h} + \omega_e^2\,\frac{n_c}{n_{0c}}\,\frac{\mathbf{A}_\perp}{\gamma_c} = 0 \ , \tag{1.124}$$

where $\omega_h^2 = 4\pi e^2 n_{0h}/\mu$ ; $\omega_e^2 = 4\pi e^2 n_{0c}/m$ and $\gamma_h$ and $\gamma_c$ are the relativistic factors for the hot and the cold electrons, respectively, and $\gamma_\alpha^2 = (1 + \mathbf{p}_\alpha^2/m_\alpha^2 c^2)^{1/2}$ ; the quantities $n_c$ , $n_{eh}$ , and $n_{ph}$ denote the cold electron, the hot electron and the positron number densities, respectively.

One can easily derive the equations for longitudinal motion from Eqs. (1.120) and (1.121) using the relation (1.123) after performing the mass redefinition in the hot component momenta parallel to the magnetic field, namely, $p_{zeh}$ and $p_{zph}$ . This motion is driven by the ponderomotive pressure $(\sim \mathbf{p}_{\alpha\perp}^2)$ of hf EM fields, which does not depend on the sign of the particle charges. One of the manifestations of the pure e–p plasma symmetry is that the effective mass of the electrons and positrons are equal and, hence, the radiation pressure gives equal longitudinal momenta to both the electrons and positrons, and affects the particle concentration density with- out producing the charge separation ($n_e = n_p$ and $\phi = 0$). But, as shown earlier [79], the introduction of a small fraction of heavy ions leads to "symmetry breaking" between hot electrons and positrons, and hence it becomes possible to have finite space charge potential $\phi$. The electrostatic potential is also known to be created in a two–electron–temperature e–p–i plasma due to

the presence of small fraction of cold e–i plasma in hot e–p plasmas [102, 103].

In the presence of two different electron temperatures in the plasma, for lf motion it becomes possible to satisfy the condition (for comparison to the two-temperature e–i plasma see the [82]) $KV_{Tc} \ll \Omega \ll KV_{Th}$ , where $V_{Tc}$ and $V_{Th}$ are the cold and hot electron thermal velocities, respectively, and $\Omega^{-1}$ and $K^{-1}$ are the characteristic time and spatial spreads of the pulse ( $\Omega \ll \omega_0$ ; $K \ll k_0$ ). We shall consider in the following the weakly relativistic case by assuming $p_\alpha^2/m_\alpha^2 c^2 \ll 1$ . We first define the number density perturbations, $\delta n_c = n_c - n_{0c}$ and $\delta n_{\alpha h} = n_{\alpha h} - n_{0h}$ and, to the lowest order in the field amplitudes, obtain following relations:

$$\delta n_h = n_{ph} + n_{eh} = -n_{0h}\,\frac{e^2|\mathbf{A}|^2}{\mu T_h c^2} + n_{0h}\,\frac{e^2|\mathbf{A}|^2}{\mu^2 c^4} =$$

$$= \frac{1}{2}\,\delta n_c - n_{0h}\,\frac{e^2|\mathbf{A}|^2}{2\mu T_h c^2} + n_{0h}\,\frac{e^2|\mathbf{A}|^2}{2\mu^2 c^4} + \frac{1}{8\pi e}\,\frac{\partial^2\phi}{\partial z^2} \tag{1.125}$$

and

$$\frac{\partial\phi}{\partial z} = -\frac{T_h}{2e}\,\frac{\partial}{\partial z}\,\left(\frac{\delta n_c}{n_{0h}}\right) - \frac{T_h}{2e}\,\left(\frac{\delta n_c}{n_{0h}}\right)\frac{\partial}{\partial z}\,\left(\frac{\delta n_c}{n_{0h}}\right)$$

$$-\frac{T_h}{4e}\,\frac{T_h}{\mu\omega_h^2}\,\frac{\partial^3}{\partial z^3}\,\left(\frac{\delta n_c}{n_{0h}}\right) \tag{1.126}$$

Using these relations and the assumptions (1.118) and (1.119) together with

$$\frac{T_c}{T_h} \ll \frac{1}{2}\,\frac{n_{0c}}{n_{0h}}\ , \tag{1.127}$$

we get the driven Boussinesq equation for lf cold electron density perturbation ( $\delta n_c$ )

$$\frac{\partial^2}{\partial t^2}\,\delta n_c - C_s^2\,\frac{\partial^2}{\partial z^2}\,\delta n_c - \frac{1}{2}\,C_s^2\,r_{dh}^2\,\frac{\partial^4}{\partial z^4}\,\delta n_c$$

$$-\frac{1}{2}\,\frac{C_s^2}{n_{0c}}\,\frac{\partial^2}{\partial z^2}\,(\delta n_c)^2 - \frac{1}{6}\,\frac{C_s^2}{n_{0c}n_{0h}}\,\frac{\partial^2}{\partial z^2}\,(\delta n_c)^3$$

$$= n_{0c}\,\frac{e^2}{2m^2c^2}\,\frac{\partial^2}{\partial z^2}|A|^2\ , \tag{1.128}$$

where $r_{dh}^2 = (T_h/\mu\omega_h^2) = T_h/4\pi e^2 n_{oh}$ , and

$$C_s = \left(\frac{1}{2}\,\frac{n_{0c}}{n_{0h}}\,\frac{T_h}{m}\right)^{1/2}$$

denotes the so-called "electron–acoustic" speed. Equation (1.128) describes the bidirectional propagation of the driven electron–acoustic waves. On the other hand, for unidirectional propagation in the near–sonic regime, it can be reduced to a generalized driven Korteweg–de Vries equation. The reduction procedure is similar to that in the case of the usual e–i plasmas with two–electron–temperatures [105], and hence we omit the details here.

Equation (1.128) is coupled to the equation for the EM field amplitude ($A$) given by

$$2i\omega_0\left(\frac{\partial}{\partial t} + v_g\,\frac{\partial}{\partial z}\right) A + \omega_0\, v_g^{''}\,\frac{\partial^2}{\partial z^2}\,A$$

$$+\omega_e^2\left[\left(1 + \frac{m^2}{\mu^2}\,\frac{c^2}{C_s^2}\right)\frac{e^2|A|^2}{2m^2c^4} - \frac{\delta n_c}{n_{0c}}\right]\cdot A = 0\ , \qquad (1.129)$$

where $v_g$ is the group velocity of the hf wave, $v_g^{''} = \partial v_g/\partial k$ is the group dispersion, and hf wave frequency $\omega_0$ satisfies the linear dispersion relation, $\omega_0^2 = k_0^2c^2 + 2\omega_h^2 + \omega_e^2$ .

The system of equations 1.118) and (1.129) describes the nonlinear wave dynamics in two–electron–temperature un–magnetized e–p–i plasma. Since most of the electrons are relativistically hot, and consequently heavy ( $G_h \neq 1$ ), it is possible to induce the electron.acoustic waves. Thus, we have here the three-wave scattering process, which does not exist in pure e–p plasmas. Hence, the radiation emanating both from the pulsars and AGN entering the cold low density e–i plasma may undergo modifications due to such scattering processes and the observed radiation could be defined by these nonlinear processes. It is useful to recall here that the nonlinear coupling between the electrons, the positrons and the photons arises when a relativistic e–p plasma is immersed in a photon gas, while the acoustic modes can be driven by the ponderomotive force due to the photon gas [87].

### 1.5.3 Stationary Coupled Waves

Equations similar to (1.128) and (1.129) were obtained in [105] for the two-electron-temperature e–i plasmas, where the addition of second electron species gave us the possibility to have the quadratic nonlinear term in the Boussinesq equation with changing sign. This leads, as shown in [105], to certain new classes of localized stationary solutions. In our case, the presence of second electron species leads to wave coupling itself. Furthermore, because of the relativistic effects, (1.129) has a new type of nonlinear term, which is cubic in the field amplitude and which arises from the self interaction of the waves [100]. On the other hand, the quadratic term in (1.128) is with a fixed sign. We shall obtain below exact analytical solutions of the derived system of equations for stationary propagation of the form

$$A = A(\xi) \exp\left[i \left\{X(z) + T(t)\right\}\right] ; \qquad \delta n_c = \delta n_c(\xi) \ , \tag{1.130}$$

where $\xi z - Vt$ is the stationary coordinate, $A(\xi)$ is a real function and propagation velocity $V < V_{Th}$ . Using (1.130) in (1.128) and (1.129), we get the coupled set of stationary governing equations,

$$\eta \frac{d^2 A}{d\xi^2} = \lambda A - \frac{\Lambda}{2} A^3 + \theta \, N \, A \ , \tag{1.131}$$

$$\frac{d^2 N}{d\xi^2} = 2(M^2 - 1) \, N - N^2 - \frac{\beta}{3} N^3 - \alpha A^2 \ , \tag{1.132}$$

where

$$\lambda = \frac{2\delta}{\omega_0} + \frac{(M^2 C_s^2 - v_g^2)}{\omega_0^2 r_{dh}^2 \eta} \ . \tag{1.133}$$

Note that $\delta = dT/dt$ denotes the nonlinear frequency shift and is treated as a free parameter of the problem, and $M = V/C_s$ denotes the Mach number normalized with respect to the electron.acoustic speed ($C_s$). In (1.131) and (1.132), we have introduced

the following dimensionless variables:

$$N \to \frac{\delta n_c}{\delta n_{0c}} , \qquad \xi \to \frac{\xi}{r_{dh}} , \qquad A \to \frac{eA}{mc^2} , \qquad T_\alpha \to \frac{T_\alpha}{mc^2} \quad .$$

Other quantities are defined as,

$$\alpha = \frac{c^2}{C_s^2} \gg 1 , \qquad \beta = \frac{n_{0c}}{n_{0h}} , \qquad \Lambda = \frac{\omega_e^2}{\omega_0^2} , \qquad \eta = \frac{v_g^{\,0}}{\omega_0 r_{dh}^2} , \qquad \theta = \frac{\omega_e^2}{\omega_0^2} < 1 \quad . \quad (1.134)$$

Note that all these quantities are positive definite. From (1.134) it follows that for nonrelativistically hot ( $G_h > 1$ ) e–p plasmas, $\Lambda \gg 1$ and, hence the relativistic nonlinearity (the $\sim A^3$ term), can not be neglected in (1.131). On the other hand, for ultrarelativistic temperatures, $G_h \gg 1$ , and it is possible that $\Lambda \sim \theta$ , so that once again we cannot ignore the $A^3$ term in (1.131), while the cubic nonlinear term $\beta N^3/3$ may be neglected in (1.132). This is consistent with the fact that, in the lowest order, relativistic nonlinear effects lead to cubic nonlinearity in the governing equation for the modulated field amplitude [100].

### Exact localized solutions

We now look for the localized solutions of Eqs. (1.131) and (1.132). Since $\beta \ll 1$, we drop the cubic nonlinear term in (1.132). To this end, we follow the method of solution discussed in [105]. Omitting the details, which are cumbersome but straightforward, we note that for Mach numbers given by

$$M^2 = 1 + \frac{2\lambda}{\eta} + \frac{\alpha}{3\Lambda}\,(3\theta + \eta) , \qquad M < \sqrt{\frac{2}{G_h \beta}} . \quad (1.135)$$

Eqs. (1.131) and (1.132) (without the $N^3$ term) admit exact analytical solutions given by,

$$N(\xi) = \frac{6\lambda}{\eta}\, sech^2(\kappa\xi) , \quad (1.136)$$

$$A(\xi) = \pm sech(\kappa\xi) , \quad (1.137)$$

where the amplitude $A_0$ is given by

$$A_0^2 = \frac{4\lambda}{\eta\Lambda}\,(\eta + 3\theta) \tag{1.138}$$

and $\kappa = \sqrt{\lambda/\eta}$ . Since $\eta$ is positive, $\lambda > 0$ is required and, hence, only supersonic ($M > 1$) solutions are admissible. The total number density perturbation $\delta n \equiv \delta n_h + n_{0c}N$ is then obtained as

$$\delta n = n_{0h}\left[-\frac{m\alpha\beta}{2\mu} + \frac{m^2}{\mu^2} + \frac{3\beta\Lambda}{2(\eta + 3\theta)}\right] A^2 \ . \tag{1.139}$$

For ultrarelativistic temperatures ($G_h \gg 1$), we find $\delta n_h \to 0$ and, therefore, $\delta n \sim n_{0c}N > 0$ . Thus, the localized solutions are accompanied by compressional number density perturbations. On the other hand, for weakly relativistic temperatures, we have the soliton solutions consisting of rarefaction density profiles ( $\delta n \sim \delta n_h < 0$ ).

The wave amplitudes $A_0$ and $N_0$ satisfy the relation

$$A_0^2 = \frac{2}{\alpha}\left[(M^2 - 1) - \frac{2\lambda}{\eta}\right] N_0 \ . \tag{1.140}$$

For the above solutions, $M$ and $\lambda$ are not free but are related by the "parametric relation" (1.135). Using the well–known stability criterion of Vakhitov and Kolokolov [106], it can be shown that the soliton solutions obtained above are stable against small perturbations. Note that localized structures were found in one-temperature unmagnetized e–p plasma in [81] for the near static regime ($M \ll 1$) . Soliton structures were also reported in [87] for the nonresonant, as well as resonant interactions of photons and phonons in e–p plasmas. Stable localized solutions, as discussed in [107, 108, 109], could provide a potential mechanism for the production of micro–pulses in pulsars and in AGNs.

### Quasineutral, linear low–frequency response case

We shall now discuss briefly the quasineutral, linear low-frequency case by neglecting in (1.132) the nonlinear terms (in $N$), as well as the dispersive term (the left–hand side),

while retaining the self–nonlinear cubic term in (1.131). This is valid when the coupled mode propagation is not in the near–sonic regime, and hence the low–frequency density perturbation is small. Equation (1.132) thus yields,

$$N = \frac{\alpha A^2}{2(M^2 - 1)} \ . \tag{1.141}$$

Using (1.141) in (1.131), we obtain the localized solution,

$$A(\xi) = \pm A_0 \, sech(\kappa\xi) \ , \tag{1.142}$$

$$N(\xi) = N_0 \, sech(\kappa\xi) \ , \tag{1.143}$$

where

$$A_0^2 = \frac{4\lambda(M^2 - 1)}{\Lambda(M^2 - 1) - \alpha\theta} \ , \tag{1.144}$$

$$N_0 = \frac{\alpha}{2(M^2 - 1)} \ . \tag{1.145}$$

From (1.144), it follows that the near-sonic regime $1 \leq M^2 \leq 1 + \alpha\theta/\Lambda$ is forbidden. Subject to this restriction, both sub– as well as super–sonic solutions are permissible. In the present case, both $\lambda$ and $M$ are free parameters, while in the previous case they are related by (1.135) and only the supersonic values for Mach numbers are admissible to lead to localized solutions.

Note that the amplitude relation (1.140) exactly reduces to (1.145) in the limit $\lambda \to 0$ . This is consistent with the fact that the solutions (1.142) and (1.143) follow from the exact stationary solutions when both the amplitudes $A_0$ and $N_0$ are much smaller than in the previous case.

It should be pointed out that in the above discussions we have ignored wave–particle interactions. Using the results obtained for conventional e–i plasmas, one can expect that the induced electron–acoustic wave undergoes Landau damping on electrons, which is strong in near–sonic regime. The propagating nonlinear wave structures obtained above

can interact with electrons and thus decelerate, transferring part of the energy to hot electrons (see [111] for e–i plasma). The heat transfer mechanism to plasma particles is an interesting process in the astrophysical context, and needs to be investigated separately in detail.

## Summary

To conclude, we have investigated the nonlinear propagation of intense electromagnetic waves in hot relativistic e–p plasmas containing a small component of cold e–i plasma with the aim of finding possible mechanisms for structure formation. Specifically, we have discussed the possibility of the existence of stable localized wave structures by deriving a nonlinear system of governing equations consisting of Schrödinger–Boussinesq equations, which describes the hf and lf wave coupling. This system takes into account the effects that result from the relativistic electron velocity distribution [111]. In the lowest order, the relativistic effects lead to a cubic nonlinear term in the Schrödinger equation arising from the self–interaction of the hf waves. Explicit analytical solutions of the coupled system of equations have been obtained. These solutions can survive in a plasma, since their propagation velocity is not near the thermal velocities of electrons, and hence they may be associated with the observed pulsar radiation. For the stationary propagation of finite amplitude electromagnetic wave only supersonic solitons exist, while in quasineutral linear lf response case both the sub–, as well as supersonic, solitons occur giving rise either to total electron density humps (solitons) or to density holes (cavitons). These structures represent the localization of intense electromagnetic radiation arising due to the selfinteraction of the waves, as well as relativistic nonlinearities. Such localized intense radiation pulses may be used to understand the character of AGN and pulsar radiation, as well as for particle acceleration in astrophysical situations.

# Chapter 2

# Energy Transformation Mechanisms in the two–fluid plasmas associated with the Magnetofluid Coupling; Explosive and Eruptive Events

## 2.1 Background

The mechanisms for energy transport and channeling of particles are deeply connected with the challenging and exciting problems of the solar coronal heating, and of the origin of the solar wind (SW). A number of recent investigations have made a strong and convincing case that neither the solar wind "acceleration" nor the numerous eruptive events (and flares of different kind and Coronal Mass Ejections (CMEs)) in the solar atmosphere can be treated as isolated and independent problems; they must be solved simultaneously along with other phenomena, in particular, the plasma heating that, by itself, may take place in several different stages. Several reasons (mainly the low observational resolution, and problems of resolving extremely short spatial and time scales in computer simulations), however, have prevented the emergence of a unified and

realistic quantitative model dealing with the dynamics of energy dissipation and evolution in the solar atmosphere. Realistic transport processes are generally not included in the models that are often lower dimensional or steady state. Recently, in [120] the necessity to account for transport processes was emphasized; It was also shown (based on estimates of energy fluxes required to heat the chromosphere and the corona) that the mechanism which transports mechanical energy from the convection zone to the chromosphere (to sustain its heating rate) could also supply the energy to heat the corona, and accelerate the SW. A model for the general global dynamics that may operate in a given atmospheric region was proposed in [70, 72].

An essential component of this global theory is the emphasis on including the plasma flows as a crucial component (along with the magnetic field) dictating the dynamics of the solar atmosphere. A systematic treatment of loop models that include flows was developed by Orlando, Peres and Serio (1995a, 1005b) and Mahajan et.al. (1999, 2001) even though, at that time, there did not exist abundant evidence for a widespread occurrence of flows in the inner corona. More recently a variety of investigators have begun to argue for the existence of flows in the solar atmosphere, and have begun to speculate about the mechanisms of their creation. There has appeared convincing evidence that particle flows are common features of both the coronal structures and the chromosphere (see e.g. [1, 140, 139] and references therein). Different mechanisms for the origin of flows as well as of the sudden explosive and eruptive events in the atmosphere, have been suggested. Wilhelm (2001) proposed that the spicule generation is related to an explosive event occurring during the magnetic reconnection phase of a network loop system, with another such system or with a unipolar–field region of appropriate polarity. The results of [119] supported the belief that magnetic field or other forces play important role in the generation of spicules and the source functions and the velocity fields play a fundamental role in the appearance of mottles and spicules. On the other hand, though the reconnection processes that can happen both in the corona and the chromospheric network (flares, microflares, nanoflares) are studied very thoroughly, it is still not proved

that the energy thrown out by these processes is sufficient either to create small scale spicules of different kind, and/or to heat the corona (see e.g. [114, 139, 140]).

Along with the evidence for flows there are several other recent observations that provide some guidance for constructing theories of energy transfer mechanisms in the solar atmosphere. The latest *Transition Region and Coronal Explorer (TRACE)* and *Solar and Heliospheric Observatory (SOHO)*/EUV Imaging Telescope high resolution observations reveal : 1) that the structures that form the solar corona are in constant motion, extremely dynamical and full of fast–moving gas, heated primarily at the footpoints of visible structures (base of the hot structure). The heating does not happen throughout the loops, or preferentially near the top as some theories predict; it rather takes place very close to the solar surface. In addition, most of this heating occurs in few minutes in the first ten to twenty thousand kilometers above the surface, that is, in a fairly small fraction of the bright part of the anchored structure. "Moreover, not only heat is deposited low down, but the gas is often actually thrust upward very rapidly. It does not merely 'evaporate' into the coronal structures, it is often actually thrown up there. Exactly how that happens is still a puzzle" [1], 2) that the loops are composed of clusters of filamentary structures and they are not (as believed before) static structures supported by interior gas pressure and heated along their lengths (the model given in [134]) but they fill and drain so quickly that the gas in them must be moving nearly ballistically (see latest TRACE observational data and e.g. [1] along the substructures, rather than being "quiescently heated". From a detailed study of the loops with different characteristic parameters the authors of [113] conclude that the heating process is quite non-uniform with a high degree of spatio–temporal variability. Loops evolve rapidly in temperature with associated changes in density. This variability requires that heating can turn on and off (for a specific structure) on a time scale of minutes or less along the field–line bundles with cross sections at or below the instrumental resolution. Due to diverse initial conditions for the flow–magnetic field system, the dynamical evolution of different structures will be different and so will be the eventual parameters they acquire

in the "quasi–equilibrium" state. The observations also indicate two important eras in the life of a coronal structure: a hectic period when it acquires particles and energy, and the relatively calmer period when it shines as a bright, high temperature object (note that mottles belong to that class of quiescent structures that are considerably darker compared to the shiny coronal structures).

Transient brightenings, with their associated flows of cool and hot material, are also a very common phenomenon in the TRACE movies. These relatively fast (violent) happenings vary from small events in the quiet Sun to major flares in active regions; brightenings which are more than $10^5$ km apart often occur within the same exposure that typically lasts for 10 to 30 s [1]. This kind of a coincidence in the events at distant locations is suggestive of fast particle beams propagation along separate magnetic loops which come together at the flaring site. The flaring sites are generally assumed to be reconnection sites although observations have not establish a causal connection: "Direct evidence for reconnection in flares is difficult to find, despite the fact that it is thought to be the primary process behind flares" [1]. It is remarkable that often the post–flare loop systems begin to glow at the TRACE EUV wavelengths without substantial distortion: reconnection that probably took place appears to be (largely) completed by the time the loops are detected by TRACE.

Based on the recent TRACE observations, the existence of outflows in coronal loops (above the active regions) was reported in [140]. It was found that events are observable for several minutes as they move outward; the projected velocities lie in the range $(5 - 17) km/s$. The authors show that the events are characterized by both temporal brightenings and apparent motions, and are similar in spatial scales and lifetimes to microflares and explosive events. They conclude that these events are mass outflows driven by localized events in the footpoint region of the loops (suggesting reconnection as a possible mechanism). However, they also report that by examining the simultaneous TRACE $1600 A^o$ images and Michelson Doppler Imager observations, they could not see signs of jets or flux cancellation within the resolution of the instruments; they recommend

better studies of these flows. Whether the transient brightenings occur in addition to steady flows, or are the causes of the observed flows, is still unclear.

The observations and their natural interpretations seem to suggest the need for a unified magneto–fluid model of the kind mentioned earlier [72]; a model in which the plasma flows play an essential role in determining the structure and dynamics of the solar atmosphere. Once the importance of flows is recognized, one could further enquire whether the mechanisms underlying the formation and primary heating of the coronal structures could also explain the more violent events (possibly flares, erupting prominences and coronal mass ejections (CMEs)). In the context of the solar corona, a first step in this enquiry was taken recently [218]. We would like to suggest now that the same very dynamics could be readily exploited to understand the explosive events and mass outflows in the chromosphere of the Sun.

We take this opportunity to remind the reader that the general unified model of [72] is based on the stipulation that the coronal structures are created from the evolution and re–organization of a relatively cold plasma flow emerging from the sub–coronal regions and interacting with the ambient solar magnetic field. It is likely that this interaction may be the cause of the immense diversity of the observed coronal structures [72, 67, 128]. Preliminary results from this magneto–fluid approach reproduce several of the salient observational features of the typical loops: the structure creation and primary heating are simultaneous – the heating takes place (by the viscous dissipation of the flow kinetic energy) in a few minutes, is quite non–uniform, and the base of the hot structure is hotter than the rest. What we call primary heating is, perhaps, the first stage of the two–stage heating process strongly indicated by observations. As opposed to the fast initial heating, the second stage of additional, supporting heating may last for much longer time, at least for quasi–equilibrium structures. It needs to be emphasized that, in the approach of [72, 67, 128] and this study, the flows are not extraneous to the structure but are an integral part of it – it is not the thermalization of an external flow which heats a preformed structure; the same flow provides the matter as well as the energy (eventually

seen as heat) contained in the structure. This distinction is important.

Having stressed the fundamental importance of flows in the dynamics and diversity of the solar atmosphere, we must examine the question of their origin. Although we have mentioned a few mechanisms like the reconnection processes in the chromospheric network, there is as yet no satisfactory theory of the genesis of the flows; much work needs to be done for a desirable understanding of their existence and nature. In this study we explore some possible processes for the flow-origin. And if the mechanisms that create these flows (of different initial parameters) are independent of the mechanisms which produce the ambient magnetic field, and are random in time and space (one can expect that, for separate structures, the up–flows can last for specific periods of time but such events can happen randomly all over the solar surface) we will have a recipe for a very diverse and dynamic corona.

Following Ohsaki et. al. (2001) we wish to further extend the scope of the magneto–fluid theory beyond the creation of the semi-quiescent coronal structures by seeking answers to the following: a) can the basic framework of this model predict the possibility of, and the pathways for the occurrence of sudden, explosive, eruptive, and catastrophic events (such as flares, eruptive prominences, CMEs, chromospheric mass outflows, spicules) in the solar atmosphere, b) does the eventual fate, possibly catastrophic reorganization, of a given structure lie in the very conditions of its birth, c) is it possible to identify the range and relative values of identifiable physical quantities that make a given structure prone to bulk motion, eruption (flaring), d) will a fast outflow/eruption be the result of the conversion of excess magnetic energy into heat and bulk plasma motion as is generally believed to happen in the solar atmosphere [135, 132, 115, 116, 118, 133] ? It is hoped that this quest will also provide us with some clues to the origin of the flows.

Below we begin by identifying the quasi–equilibrium state of a typical chromospheric/coronal structure with a slowly changing Double–Beltrami (DB) state (one of the simplest, non–trivial magnetofluid equilibrium). The slow changes may be due to changes in the sun

which affect the local magnetic fields, the interaction of various nearby structures, or disturbances in the solar atmosphere. The parameter change is assumed to be sufficiently slow that, at each stage, the system can find its local DB equilibrium (adiabatic evolution). The slow evolution must conserve the dynamical invariants: the helicity $h_1$, the generalized helicity $h_2$, and the total (magnetic plus the fluid) energy $E$. The problem of predicting sudden events (e.g. catastrophic eruptive/explosive events) then reduces to finding the range, if any, in which the slowly evolving structure may suffer a loss of equilibrium. The signature of the loss of equilibrium is quite easy to identify for the DB states. The transition may occur in one of the following two ways: 1) when the roots of the quadratic equation, determining the length scales for the field variation, go from being real to complex (implying change in the topology of the magnetic and the velocity fields — boundary separating the paramagnetic from the diamagnetic), or 2) the amplitude of either of the two states ceases to be real. For our current problem, the sudden change is likely to follow the second route.

By analyzing a simple analytically tractable model, we find affirmative answers to all the four questions we posed. We show that the invariants $h_1, h_2$ , and $E$ , which label and (along with the initial and boundary conditions) determine the original state, hold the key to the eventual fate of a structure. If for a given equilibrium sequence, the total energy $E$ is larger than some critical value (given in terms of $h_1$, and $h_2$), the catastrophic loss of equilibrium could certainly occur. The trigger for the equilibrium loss could come, for instance, from nearby structures getting close to each other with an increase in their interaction energy. The catastrophe pushes a DB state to relax to a minimum energy single Beltrami field. For coronal structures, the transition transfers almost all the short–scale magnetic energy to the flow energy. Then we give our conclusions and summary.

The main results of this chapter are published in Refs.[70-72],[141],[191-192],[218-219].

## 2.2 Basic Model and Equations for Coupled Vortex Dynamics in Two–Fluid MHD

Any model of the heliosphere must attempt to answer the following fundamental issues of the storage–release paradigm, the dominant framework for models of solar eruptions for over four decades [117]: (1) How does sufficient energy gets stored in the 3D corona to power eruptions, (2) Does a realistic solar magnetic structure undergoing quasi–static motion of the footpoints possess a critical point beyond which no equilibrium or stability exists, (3) Can a specific footpoint motion be directly and causally related to observed eruptions. There is, as yet, no model based on the storage–release paradigm that can correctly describe the observed dynamics of both CMEs and their heliospheric consequences. To answer some of these questions, a new paradigm, where the eruptions are the end products of dynamic Alfénic relaxation (time scale is neither quasi–static nor impulsive) of magnetic energy propagating outward from the solar dynamo, was proposed by Chen (2001).

The principal new element in our approach is the co-primacy (along with the magnetic field) accorded to the plasma flows [72]. The flows influence the occurence of the explosive/eruptive events rather directly: it happens due to their ability to deform (and in specific cases, distort) the ambient magnetic field – to temporarily stretch (shrink, destroy) the closed field lines so that the flow can escape the local region acquiring a considerable kinetic energy converted either to heat or to bulk motion.

Within the framework of our approach, there are two distinct scenarios for explosive/eruptive events : a) when a "slowly" evolving structure finds itself in a state of no equilibrium, and b) when the process of creating a long–lived structure is prematurely aborted; the flow shrinks/distorts the structure which suddenly shines and/or releases energy or ejects particles. The latter mechanism requires a detailed time–dependent treatment and is not the subject matter of this study. The following semi–equilibrium, collisionless magneto–fluid treatment pertains only to the former case [218] .

In our analysis we keep the temperature varying, but we assume the density to be constant for a given structure. This is a rather drastic step but it can help us in unveiling the underlying physics. There are two entirely different quasi–equilibrium situations where this assumption may be justified: (i) the primary heating of the structure has already been performed, i.e. a substantial part of initial kinetic energy of the primary flow has been converted to heat, (ii) if the rates of kinetic energy dissipation are not very large, we can imagine the plasma to be going through a series of quasi–equilibria before it settles into a state which can be identified with a typical closed structure. The density variation, though a factor, is not crucial in an appropriate estimation of the desired quantities. The constant density assumption is being used only for simplicity - extension to varying density is straightforward [72].

### 2.2.1 Double Beltrami Fields

A given structure is supposed to correspond to the equilibrium solutions of the two–fluid system (neglecting electron inertia and transport processes) written in dimensionless variables:

$$\frac{\partial}{\partial t}\boldsymbol{A} = (\boldsymbol{V} - \nabla \times \boldsymbol{B}) \times \boldsymbol{B} - \nabla\left(\phi - p_e\right), \tag{2.1}$$

$$\frac{\partial}{\partial t}(\boldsymbol{V} + \boldsymbol{A}) = \boldsymbol{V} \times (\boldsymbol{B} + \nabla \times \boldsymbol{V}) - \nabla\left(V^2/2 + p_i + \phi\right). \tag{2.2}$$

where the magnetic field $\boldsymbol{B}$ is normalized to an appropriate measure $B_0$, the fluid velocity $\boldsymbol{V}$ to the corresponding Alfvén speed, distances to the collisionless ion skin depth $l_i (= c/\omega_{pi})$, where $c$ is the speed of light and $\omega_{pi}^2 = 4\pi n_0 e^2/m_i$, $m_i$ is the ion mass), the intrinsic length for two–fluid or Hall MHD; $\boldsymbol{A}$ and $\phi$ are the vector and scalar potentials and $p_e$, $p_i$ are the normalized electron and ion pressures. This set of equations can be

cast in the Vortex dynamics form ([67] and references therein)

$$\frac{\partial}{\partial t}\boldsymbol{\omega}_j - \nabla \times (\boldsymbol{U}_j \times \boldsymbol{\omega}_j) = 0 \quad (j = 1, 2) \tag{2.3}$$

written in terms of a pair of generalized vorticities:

$$\boldsymbol{\omega}_1 = \boldsymbol{B},\ \boldsymbol{\omega}_2 = \boldsymbol{B} + \nabla \times \boldsymbol{V},$$

and effective flows

$$\boldsymbol{U}_1 = \boldsymbol{V} - \nabla \times \boldsymbol{B},\ \boldsymbol{U}_2 = \boldsymbol{V}.$$

Notice, that the system allows general steady state solutions

$$\boldsymbol{U}_j \times \boldsymbol{\omega}_j = \nabla \varphi_j \quad (j = 1, 2),$$

where the scalar fields $\varphi_j$ correspond to the fluid energy densities:

$$\varphi_1 = \phi - p_e\ , \qquad \varphi_2 = V^2/2 + \phi + p_e\ .$$

The simplest and perhaps the most fundamental equilibrium solution to (2.3) is given by the "Beltrami condition", i.e, by alignment of the vorticities along the corresponding flows ($\boldsymbol{\omega}_j // \boldsymbol{U}_j$). A well–known example of a single Beltrami field is the so called Taylor relaxed state $\nabla \times \boldsymbol{B} = \lambda \boldsymbol{B}$ [112, 137]. Notice, that the Double Beltrami (DB) conditions are statements of the simple physics: the electrons follow the field line, while the massive ions follow the field–lines modified by their vorticity. For constant $a$ and $b$, the Beltrami conditions yield a system of simultaneous linear equations in $\boldsymbol{B}$ and $\boldsymbol{V}$

$$\boldsymbol{B} = a(\boldsymbol{V} - \nabla \times \boldsymbol{B}), \tag{2.4}$$

$$\boldsymbol{B} + \nabla \times \boldsymbol{V} = b\boldsymbol{V}. \tag{2.5}$$

Combining (2.4) and (2.5) yields a second order partial differential equation

$$\nabla \times (\nabla \times \boldsymbol{B}) - (b - \tilde{a})\, \nabla \times \boldsymbol{B} + (1 - \tilde{a}b)\, \boldsymbol{B} = 0, \tag{2.6}$$

where $\tilde{a} = 1/a$. Denoting the curl derivative $\nabla\times$ by "curl", (2.6) is written as

$$(\mathrm{curl} - \lambda_+)(\mathrm{curl} - \lambda_-)\boldsymbol{B} = 0, \tag{2.7}$$

where

$$\lambda_\pm = \frac{1}{2}\left[(b - \tilde{a}) \pm \sqrt{(b + \tilde{a})^2 - 4}\right]. \tag{2.8}$$

For sub–Alfvénic flows (the flows we generally encounter in the solar atmosphere), the length scales ($\lambda_\pm^{-1}$) are quite disparate. Depending on the values of $\tilde{a}$ and $b$, one of these will signify the macro while the other will signify the micro scale. The general solution to the "double Beltrami equations" (2.6) is a linear combination of the single Beltrami fields $\boldsymbol{G}_\pm$ satisfying $(\mathrm{curl} - \lambda)\boldsymbol{G} = 0$. Thus, for arbitrary constants $C_\pm$, the sum

$$\boldsymbol{B} = C_+\boldsymbol{G}_+ + C_-\boldsymbol{G}_-, \tag{2.9}$$

solves (2.7). The corresponding velocity field is given by

$$\boldsymbol{V} = (\lambda_+ + \tilde{a})\, C_+\boldsymbol{G}_+ + (\lambda_- + \tilde{a})\, C_-\boldsymbol{G}_-. \tag{2.10}$$

The double Beltrami field encompasses a wide class of steady states of mathematical physics — from the force–free paramagnetic to the fully diamagnetic field expressed by the London equation of superconductivity.

It may be significant to note that the Beltrami conditions demand "generalized Bernoulli condition" ($\varphi_j = const$) signifying the homogeneity of the energy density. Substituting (2.4) and (2.5) into the original two–fluid equations, and combining them

we find get

$$\beta + V^2 = \text{const}, \tag{2.11}$$

where $\beta = 2(p_e + p_i)$ is the ratio of the total pressure to the magnetic pressure. This relation shows that the double Beltrami equilibrium is no longer zero–beta (force–free; for statistical mechanical treatments see [129, 124, 121]), but it can confine an appreciable pressure when an appropriately sheared flow, measured in the Alfvén units, is driven [67].

In order to place the DB configuration in perspective, we show in FIG.2.1 a possible hierarchy of the relaxed states accessible to a magneto–fluid system. We may distinguish three distinct stages: 1) the harmonic (zero Beltrami) state associated with the vacuum magnetic field, 2) the single Beltrami state brought about by the interaction of plasma currents with the external field, and 3) the Double Beltrami states in which the plasma flows become co–determinants (with the currents and the external field) of the overall dynamics. Each stage corresponds to a different "energy level" with energy increasing as we advance in the hierarchy. The vacuum magnetic field is the absolute minimum energy state. A plasma immersed in a static magnetic field will eventually disappear leaving only the harmonic magnetic field. When a plasma current is added to sustain magnetic helicity, the plasma may relax into the Taylor or the single Beltrami field configuration. If, in addition, a flow is induced (or charge injected) to sustain what will be called the generalized helicity (see below), the relaxed state will correspond to the double Beltrami field. These generalized states, which contain the Taylor (force–free) states [137] as a sub–class, have a very rich structure and can be qualitatively different from the widely used Taylor states.

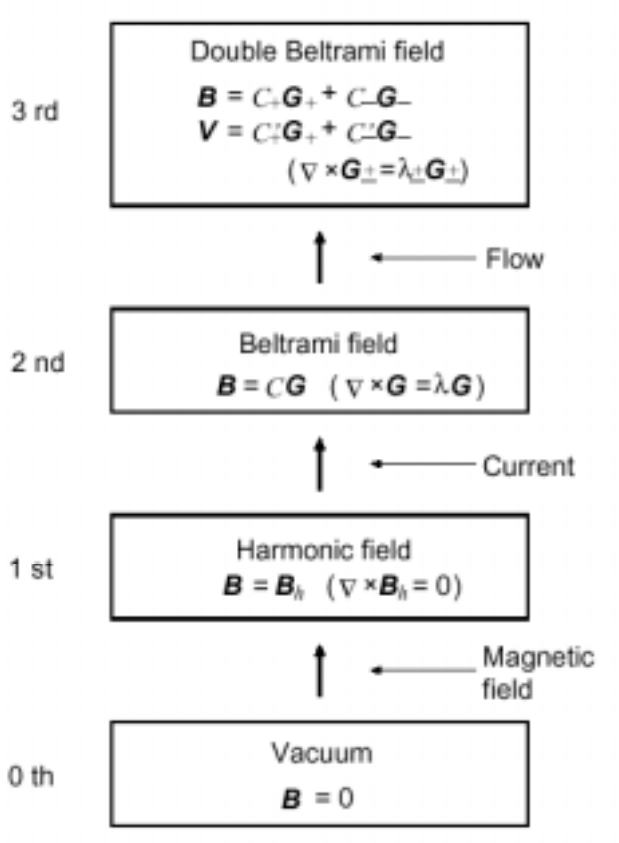


Fig. 2.1 Hierarchy of relaxed states. The upper relaxed state has more complicated structure and higher energy. The absolute minimum energy state is the vacuum. In supplying a magnetic field, current, and flow to the plasma, the energy of the system rises successively with the harmonic, the first, and the second Beltrami fields.

### 2.2.2 Conservation laws and algebraic structure

The general DB field is characterized by four parameters, two eigenvalues and two amplitudes,

$$\begin{cases} \lambda_+,\ \lambda_-, \\ C_+,\ C_-. \end{cases} \tag{2.12}$$

The three invariants ([136]): the helicity $h_1$, the generalized helicity $h_2$,

$$h_1 = \frac{1}{2}\int (\boldsymbol{A}\cdot\boldsymbol{B})\,\mathrm{d}\mathbf{r}, \tag{2.13}$$

$$h_2 = \frac{1}{2}\int (\boldsymbol{A}+\boldsymbol{V})\cdot(\boldsymbol{B}+\nabla\times\boldsymbol{V})\,\mathrm{d}\mathbf{r}, \tag{2.14}$$

($\boldsymbol{A}$ is the vector potential), and the total energy

$$E = \frac{1}{2}\int (\boldsymbol{B}^2+\boldsymbol{V}^2)\,\mathrm{d}\mathbf{r} \tag{2.15}$$

will provide three algebraic relations between them ([141]). It is worthwhile to remark here that Steinhauer and Ishida (1997) proposed a variational principle using the total energy $E$ and two helicities and derived the equations (2.4), (2.5) as an Euler–Lagrange equation describing the relaxed state in two–fluid MHD [1]. We remind the reader that $E$ , the magnetic helicity $h_1$ , and the generalized helicity $h_2$ are the three rugged bilinear invariants of the collisionless two–fluid dynamics and their conservation will provide three algebraic relations between the four parameters $\lambda_+$, $\lambda_-$ (eigenvalues), and $C_+$, $C_-$ (amplitudes) characterizing the DB field [141]. To predict the possibility of an eruptive event, interpreted as the termination of an equilibrium sequence (for solar flares, this kind of an approach, albeit in different contexts, has been followed in numerous investigations, (see e.g. [122, 123, 126, 127] and references therein), we analytically investigate this system using the macro–scale of the closed structure as a control parameter. This choice is physically sensible and is motivated by observations because in the process of structure–structure interactions, "initial" shapes do undergo deformations/distortions

[1] For the two–fluid MHD, the setting up of a satisfactory variational which is both physically sound and mathematically well–posed is a rather demanding problem both conceptually and technically. The minimum energy principles (as distinct from minimum potential energy principles) with or without compression, have, in general, very little conceptual justification. One has, thus, to find a physically meaningful and mathematically justifiable target functional (the functional whose constrained minimization leads to a relaxed state). This can be and has been done and is the subject of [128]. The final result, fortunately is the same: we obtain the set of Double Beltrami–Bernoulli states (used in this study) as the expression of self–organization. The system is amenable to the same treatment even for varying density as long as a polytropic equation of state is allowed (see [72])

with rates strongly dependent on the initial and boundary conditions.

For simplicity we explicitly work out the system in a Cartesian cube of length $L$. We take $\boldsymbol{G}_{\pm}$ to be the simple 2-D ABC field (a solution of the beltrami equation) [112],

$$\boldsymbol{G}_{\pm} = g_{x\pm} \begin{pmatrix} 0 \\ \sin \lambda_{\pm} x \\ \cos \lambda_{\pm} x \end{pmatrix} + g_{y\pm} \begin{pmatrix} \cos \lambda_{\pm} y \\ 0 \\ \sin \lambda_{\pm} y \end{pmatrix}, \tag{2.16}$$

with the normalization

$$(g_{x\pm})^2 + (g_{y\pm})^2 = 1. \tag{2.17}$$

the ratio of $g_{x\pm}$ and $g_{y\pm}$ defines the shape of an arcade–magnetic field structure. In FIG.2.2 we show the field line structure of a 2-D ABC vector field that resembles interacting loops. If $\lambda_{\pm}$ are complex in (2.16), the equilibrium solution will have the spatially decaying (or growing) component initially. Such regions are extremely hard to model and it is beyond the scope of the present study. In this study we restrict ourselves to real $\lambda_{\pm}$.

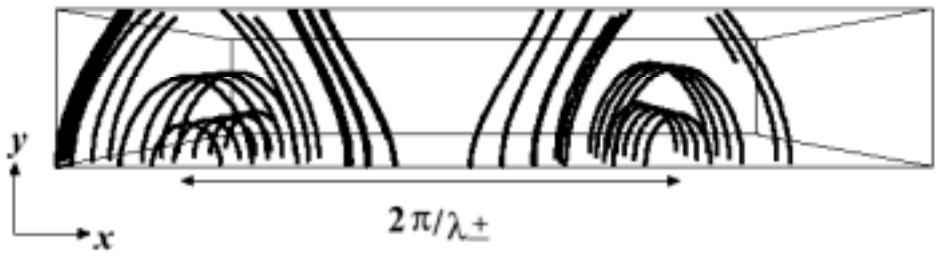


Fig. 2.2 Magnetic field line structure of a 2-D ABC map resembling a coronal arcade.

Assuming periodic boundary conditions,

$$L = n_{+} \frac{2\pi}{\lambda_{+}} = n_{-} \frac{2\pi}{\lambda_{-}}, \tag{2.18}$$

($n_{\pm}$ are integers)

we evaluate $\boldsymbol{G}_{\pm}$ of (2.16) to be,

$$\int \boldsymbol{G}_{\pm}^2 \mathrm{d}\mathbf{r} = L^2 \left[ (g_{x\pm})^2 + (g_{y\pm})^2 \right] = L^2,$$
$$\int \boldsymbol{G}_{+} \cdot \boldsymbol{G}_{-} \mathrm{d}\mathbf{r} = 0,$$

where $\int \mathrm{d}\mathbf{r} = \int_0^L \int_0^L \mathrm{d}x\mathrm{d}y$.

As a result, the constants of motion $h_1$, $\tilde{h}_2 (= h_2 - h_1)$ and $E$ read

$$h_1 = \frac{L^2}{2} \left[ \frac{C_+^2}{\lambda_+} + \frac{C_-^2}{\lambda_-} \right], \tag{2.19}$$

$$\tilde{h}_2 = \frac{L^2}{2} \left\{ \left[ 2 + \lambda_+ \left( \lambda_+ + \tilde{a} \right) \right] \left( \lambda_+ + \tilde{a} \right) C_+^2 + \left[ 2 + \lambda_- \left( \lambda_- + \tilde{a} \right) \right] \left( \lambda_- + \tilde{a} \right) C_-^2 \right\}, \tag{2.20}$$

$$E = \frac{L^2}{2} \left\{ \left[ 1 + \left( \lambda_+ + \tilde{a} \right)^2 \right] C_+^2 + \left[ 1 + \left( \lambda_- + \tilde{a} \right)^2 \right] C_-^2 \right\}. \tag{2.21}$$

Reminding the reader that the parameter set ($\tilde{a}$, $b$) is entirely equivalent to $\lambda_{\pm}$ we write down here a variety of relations connecting them,

$$\left( \lambda_+ + \tilde{a} \right)^{-1} = \left( \lambda_- + \tilde{a} \right), \tag{2.22}$$

$$\lambda_+ + \lambda_- = b - \tilde{a}, \tag{2.23}$$

$$\lambda_+ \lambda_- = 1 - b\tilde{a}, \tag{2.24}$$

$$\tilde{a} = \frac{1}{2} \left[ - \left( \lambda_+ + \lambda_- \right) \pm \sqrt{\left( \lambda_+ - \lambda_- \right)^2 + 4} \right], \tag{2.25}$$

$$b = \frac{1}{2} \left[ \left( \lambda_+ + \lambda_- \right) \pm \sqrt{\left( \lambda_+ - \lambda_- \right)^2 + 4} \right]. \tag{2.26}$$

Using these relations, we may express $\tilde{h}_2$ of (2.20) in terms of $h_1$, $E$, $\lambda_+$, $\lambda_-$ ($h_1$, $E$, $\tilde{a}$, $b$),

$$\tilde{h}_2 = \frac{L^2}{2} \left\{ \left[ 2 \left( \lambda_- + \tilde{a} \right) + \lambda_+ \right] \left( \lambda_+ + \tilde{a} \right)^2 C_+^2 \right.$$

$$
\begin{aligned}
& + \left[2\left(\lambda_+ + \tilde{a}\right) + \lambda_-\right]\left(\lambda_- + \tilde{a}\right)^2 C_-^2 \Big\} \\
= \; & b\frac{L^2}{2}\left\{\left[1 + \left(\lambda_+ + \tilde{a}\right)^2\right] C_+^2 + \left[1 + \left(\lambda_- + \tilde{a}\right)^2\right] C_-^2\right\} \\
& -\lambda_+\lambda_-\frac{L^2}{2}\left[\frac{C_+^2}{\lambda_+} + \frac{C_-^2}{\lambda_-}\right] \\
= \; & bE - \lambda_+\lambda_- h_1, \qquad (2.27)
\end{aligned}
$$

which can be cast in several equivalent forms

$$
\begin{aligned}
h_2 &= h_1 + \tilde{h}_2 = b\left(E + h_1\tilde{a}\right), \qquad (2.28) \\
\tilde{h}_2 &= \frac{E}{2}\left[\left(\lambda_+ + \lambda_-\right) \pm \sqrt{\left(\lambda_+ - \lambda_-\right)^2 + 4}\right] \\
& \qquad -\lambda_+\lambda_- h_1. \qquad (2.29)
\end{aligned}
$$

For given $h_1$, $E$, $\tilde{h}_2$ ($h_2$) and one of the $\lambda_\pm$ (control parameter), we can solve (2.29) to find variations of other $\lambda_\mp$. Here we assume that $L$ is sufficiently large, so that $\lambda_\pm$ ($= n_\pm/L$) can take continuous real values. From (2.28), we can derive that the equilibrium we consider corresponds to zero free energy [68, 136];

$$
E + \tilde{a}h_1 - \frac{1}{b}h_2 = 0. \qquad (2.30)
$$

From (2.19) and (2.21), we find $C_+$ and $C_-$ to be

$$
\begin{aligned}
\frac{L^2}{2}C_+^2 &= D^{-1}\left\{E - \left[1 + \left(\lambda_- + \tilde{a}\right)^2\right]\lambda_- h_1\right\}\lambda_+, \qquad (2.31) \\
\frac{L^2}{2}C_-^2 &= -D^{-1}\left\{E - \left[1 + \left(\lambda_+ + \tilde{a}\right)^2\right]\lambda_+ h_1\right\}\lambda_-, \qquad (2.32)
\end{aligned}
$$

where

$$
\begin{aligned}
D &= \left[1 + \left(\lambda_+ + \tilde{a}\right)^2\right]\lambda_+ - \left[1 + \left(\lambda_- + \tilde{a}\right)^2\right]\lambda_- \\
&= \left(\lambda_+ - \lambda_-\right) b\left(b + \tilde{a}\right) \qquad (2.33)
\end{aligned}
$$

Naturally, $D^{-1}$ diverges at the coalescence of the roots (when $\lambda_+ = \lambda_-$).

For an acceptable equilibrium the amplitudes $C_\pm$ and the micro–length (corresponding to one of the $\lambda_\pm$) must remain real as the other $\lambda_\pm$ goes over real values. Therefore $C_\pm^2$ must remain positive. There are, then, two possible scenarios for losing equilibrium: (1) Either of $C_\pm^2$ becomes zero (starting from positive values) for real $\lambda_\pm$, (2) The roots $\lambda_\pm$ coalesce ($\lambda_- \leftrightarrow \lambda_+$) for real $\lambda_\pm$ and $C_\pm$. For the Solar atmosphere problem, where we deal with equilibria with vastly separated scales (sub–Alfvénic flows [72]), the second possibility is not of much relevance; there are no slow adiabatic changes which will make such vastly different $\lambda_\pm$ to coalesce. Thus, it is the loss of equilibrium through the first mechanism that will be primarily investigated for the present problem. The second mechanism can be operative and may be of serious importance for other special structures; we shall briefly deal with it in the sections below.

## 2.3 Equilibrium States in Incompressible Hall MHD

The Beltrami fields, eigenfunctions of the curl operator, may be used to represent the essential characteristics of sheared, spiral, chiral, or helical structures in various vector fields. Since the magnetic field is the key player in labelling and determining the state of a typical plasma, it stands to reason that one could describe and understand the possible self–organized states of a plasma in terms of Beltrami fields.

A general solenoidal (divergence–free) vector field, such as a magnetic field or the velocity field of an incompressible flow, can be decomposed into an orthogonal sum of Beltrami fields [138]. In the dynamical evolution of a general plasma, the nonlinearities in the equations of motion will necessarily induce couplings among the constituent Beltrami fields (into which the initial field may be composed), making the resultant dynamics rather complicated [124]. It is remarkable, however, that in the single–fluid magnetohydrodynamics (MHD, a simple but a very important plasma model), the energy of the system tends to condensate into a single Beltrami magnetic field, leading to a self-organized, force–free equilibrium — the well-known Taylor relaxed state satisfying $\nabla \times \boldsymbol{B} = \lambda \boldsymbol{B}$ [137]. It is equally remarkable that a more general equilibrium, a relaxed state described by a pair of different Beltrami fields, is available even in a two–fluid description of a plasma. The relevant double Beltrami (DB) fields are a well–defined combination of the magnetic and flow-velocity fields [67, 128]. The essential new physics is due to the Hall term that relates the kinematic and the magnetic aspects of a magnetofluid. The resulting relaxed states, with a tight coupling between the velocity and the magnetic fields, span a far richer set of plasma conditions than the conventional single Beltrami states. For instance, the DB states can exhibit diamagnetism and pressure confinement that is not allowed in a single Beltrami state. In this study, among other applications, we show that the strongly sheared boundary layer associated with the high confinement mode (H-mode) of a plasma could be viewed as a self–organized double Beltrami diamagnetic structure, where the magnetic field, flow velocity, electric field, and pressure are self–consistently related. We will also discuss the potential of DB states as

high-beta equilibria.

### 2.3.1 Generalized Bernoulli condition

In the vortex dynamics equation (2.3), the general steady states are given by

$$\boldsymbol{U}_j \times \boldsymbol{\omega}_j = \nabla \varphi_j \quad (j = 1, 2),$$

where the $\varphi_j$ is a certain scalar field. Going back from (2.3) to the original (decurled) equations (2.1) and (2.2), we find that $\varphi_j$ corresponds to the energy density of each fluid;

$$\varphi_1 = \phi - p_e \ , \tag{2.34}$$

$$\varphi_2 = V^2/2 + \phi + p_e \ . \tag{2.35}$$

The Beltrami condition $\boldsymbol{U}_j = \mu_j \boldsymbol{\omega}_j$, thus, gives a special class of solution such that

$$\boldsymbol{U}_j \times \boldsymbol{\omega}_j = \nabla \varphi_j \quad (j = 1, 2),$$

The former equality is the Beltrami condition, while the latter, demanding that the energy density is homogeneous, is a "generalized Bernoulli condition". Subtracting (2.34) from (2.35) under the Bernoulli condition, we obtain [in the normalized unit, the beta ratio is given by $\beta = 2(p_e + p_i)$]

$$V^2 + \beta = const. \tag{2.36}$$

This relation shows that the double Beltrami equilibrium is no longer zero beta, but it can confine an appreciable pres- sure when an appreciable flow (in the Alfvén unit) is driven [67]. It is perhaps more pertinent to state that the double Beltrami equilibria are instruments for maintaining pressure gradients (plasma confinement) through the Bernoulli condition, i.e., by creating sheared velocity fields.

### 2.3.2 High-beta Toroidal equilibrium

Due to the simple mathematical structure of the double Beltrami fields, it is rather easy to find analytical solutions of various equilibria in slab or cylindrical geometry. By choosing an appropriate set of parameters, we can construct very high–beta solutions concomitant with highly sheared flow velocity fields. In this section, we present a numerical solution of a high–beta toroidal equilibrium. By the representations ($r, \theta, z$ are the standard cylindrical coordinates)

$$\boldsymbol{B} = \nabla\Psi(r,z) \times \nabla\theta + rB_\theta(r,z)\nabla\theta \tag{2.37}$$

$$\boldsymbol{V} = \nabla\Phi(r,z) \times \nabla\theta + rV_\theta(r,z)\nabla\theta \tag{2.38}$$

the double curl Beltrami equations translate to coupled Grad-Shafranov equations;

$$\mathcal{L}\begin{pmatrix}\Psi\\ \Phi\end{pmatrix} = \begin{pmatrix}1-\tilde{a}^2 & (\tilde{a}-b)\\ (b-\tilde{a}) & 1-b^2\end{pmatrix}\begin{pmatrix}\Psi\\ \Phi\end{pmatrix} - \begin{pmatrix}\tilde{a}\,C_1 + C_2\\ C_1 + b\,C_2\end{pmatrix}, \tag{2.39}$$

where

$$-\mathcal{L} = r\frac{\partial}{\partial r}\left(\frac{1}{r}\frac{\partial}{\partial r}\right) + \frac{\partial^2}{\partial z^2} \tag{2.40}$$

and $C_1$ and $C_2$ are constants to be determined by boundary (or flux) conditions. We note that the "vacuum fields" satisfying $\mathcal{L}\phi_v = 0$ can be included both in $\Psi$ (magnetic flux function) and $\Phi$ (approximately, the electrostatic potential) as inhomogeneous terms. Choosing appropriate vacuum fields, we can control the radial position and the shape of the toroidal equilibrium. Fig.2.3 shows a typical solution with a high–beta value.

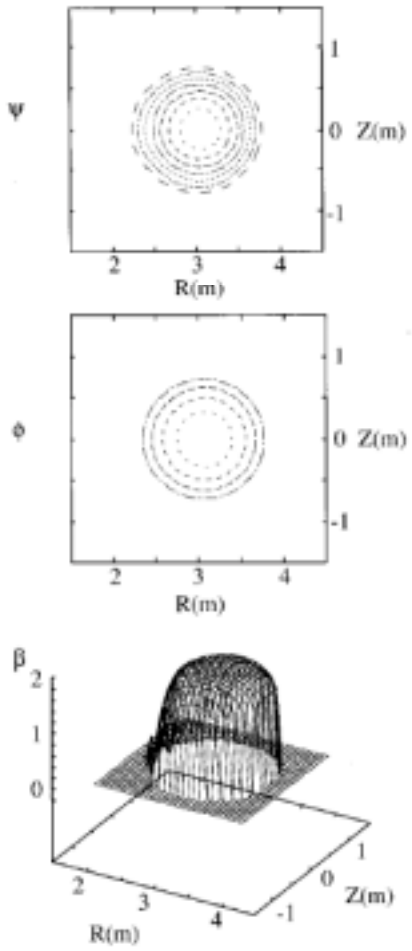


Fig.2.3 Toroidal equilibrium of the high-beta double Beltrami field.

### 2.3.3 H–mode Boundary Layer

In this section, we apply the theory to analyze the boundary layer in a H-mode tokamak plasma [68]. Since the H–mode is so extensively studied and analyzed, it is important that we clarify the scope of this effort for a proper perspective. The theory we present is a purely equilibrium theory, that is, we will try to examine if a double Beltrami diamagnetic state can capture and predict the essential character of the strongly sheared edge layer associated with the H–mode. No attempts will be made to suggest a pathway or a mechanism that leads to the transition to a H-mode. Nor will we describe the process of

transition. The reader may find representative literature. Our goals are rather modest ?– to understand the distribution of fields and pressure in the transition layer once it has been created. It is hoped that the final characteristics of the layer, which are viewed as an expression of plasma self–organization, are independent of the processes that led to the self–organization.

For a proper analysis of a tokamak plasma (embedded in a strong external magnetic field), it is appropriate to decompose the magnetic field $\boldsymbol{B}$ into the self–field component $\boldsymbol{B}_s$, and the externally rooted component $\boldsymbol{B}_h$ with $|\boldsymbol{B}_h| = B_0 (\gg |\boldsymbol{B}_s|)$. Only $\boldsymbol{B}_s$ is produced by the plasma current $\boldsymbol{j}$ in the region of our interest (a thin boundary layer of the core plasma), while $\boldsymbol{B}_h$ is current–free (harmonic) in that region. From now on, the dynamical part of the field, $\boldsymbol{B}_s$ , will be normalized by its representative value $\boldsymbol{B}_*$ . The velocities are, then, normalized by the corresponding Alfvén velocity $\boldsymbol{V}_{A*}$. The pressure gradient across the boundary layer is maintained by the diamagnetic pressure of the magnetic field, and hence, we have an estimate for the variation of the pressure and the magnetic field across the layer; $\delta p = \delta(|\boldsymbol{B}|^2)/2\mu_0 \simeq (B_0 B_*)/\mu_0$ (in physical units), which reads as

$$\frac{B_*}{B_0} = \frac{\beta}{2} \qquad (\ll 1), \tag{2.41}$$

where $\beta$ is the conventional beta ratio evaluated for the pressure maintained at the inner edge of the boundary layer. Formally, we define

$$\hat{\boldsymbol{B}}_s = \left(\frac{B_0}{B_*}\right) \hat{\boldsymbol{B}}_s, \ \hat{\boldsymbol{V}} = \left(\frac{B_0}{B_*}\right) \hat{\boldsymbol{V}}, \ \hat{\nabla} = \nabla,$$

$$\hat{p} = \left(\frac{1}{\beta^2}\right) p, \hat{\Phi} = \left(\frac{1}{\beta^2}\right) \Phi,$$

with the idea that all the normalized dynamical variables are of order unity.In what follows, we shall drop $\hat{}$ to simplify the notation. We consider a one–dimensional system where the fields vary only in the "radial" direction, perpendicular to the magnetic surfaces, i.e., $\boldsymbol{B}_h \cdot \nabla = 0$ . We also assume that $\boldsymbol{V}$ is incompressible ($\nabla \cdot \boldsymbol{V} = 0$). Then, we

find $\nabla \times \boldsymbol{V} \times \boldsymbol{B}_h = 0$ , which allows us to write

$$\boldsymbol{V} \times \boldsymbol{B}_h = \left(\frac{\beta}{2}\right)^{-1} \nabla P_i \ , \tag{2.42}$$

where $P_i$ is a potential field. Similarly,

$$\boldsymbol{V}_e \times \boldsymbol{B}_h = (\boldsymbol{V} - \nabla \times \boldsymbol{B}) \times \boldsymbol{B}_h = -\left(\frac{\beta}{2}\right)^{-1} \nabla P_e \ , \tag{2.43}$$

with

$$P_e = -P_i - \left(\frac{\beta}{2}\right) \boldsymbol{B}_h \cdot \boldsymbol{B}_s. \tag{2.44}$$

Equations (2.42) and (2.43) represent the zeroth–order diamagnetism. We may, now, rewrite the system (2.1) and (2.2) as

$$\frac{\partial}{\partial t}\boldsymbol{A}_s = (\boldsymbol{V} - \nabla \times \boldsymbol{B}_s) \times \boldsymbol{B}_s + \left(\frac{\beta}{2}\right)^{-1} \nabla (p_e - P_e - \Phi), \tag{2.45}$$

$$\frac{\partial}{\partial t}(\boldsymbol{V} + \boldsymbol{A}_s) = \boldsymbol{V} \times (\boldsymbol{B}_s + \nabla \times \boldsymbol{V}) - \left(\frac{\beta}{2}\right)^{-1} \nabla \left[p_i - P_i + \phi + \left(\frac{\beta}{2}\right) \frac{V^2}{2}\right]. \tag{2.46}$$

where $\nabla \times \boldsymbol{A}_s = \boldsymbol{B}_s$. For the self–field components, the Beltrami and Bernoulli conditions, respectively, read as

$$\boldsymbol{B}_s = a(\boldsymbol{V} - \nabla \times \boldsymbol{B}_s), \tag{2.47}$$

$$\boldsymbol{B}_s + \nabla \times \boldsymbol{V} = b\, \boldsymbol{V} \tag{2.48}$$

and ($c_i, c_e$ : constants)

$$p_i - P_i + \phi + \left(\frac{\beta}{2}\right) \frac{V^2}{2} = c_i, \tag{2.49}$$

$$p_e - P_e - \Phi = p_e + P_i + \left(\frac{\beta}{2}\right) \boldsymbol{B}_h \cdot \boldsymbol{B}_s - \Phi = c_e \tag{2.50}$$

relating the plasma pressure and the electrostatic field with the self– and the externally

applied fields.

The general features of the structure represented by (2.47-2.48), and (2.49-2.50) can be illustrated by an analysis in slab geometry (the coordinate $x$ is radial, $y$ is poloidal, and $z$ is toroidal). The double Beltrami fields are explicitly expressed by sinusoidal functions (2.17). We consider a boundary layer $0 < x < \Delta$ in contact with a "core plasma" ($x < 0$). The exterior region ($x > 0$) is scraped off by a physical boundary. The layer thickness $\Delta$ is to be determined by the theory. The fields $\boldsymbol{B}_s$ and $\boldsymbol{V}$ in the boundary layer are determined by solving (2.47-2.48) with appropriate boundary conditions on $\boldsymbol{B}_s$ and $\boldsymbol{V}$, as well as assuming values for $a, b$ and the width $\Delta$.

We note that these equations can be solved without ref-erence to the Bernoulli conditions (2.49-2.50). Then, the Bernoulli conditions relate the field $\boldsymbol{B}_s$ and $\boldsymbol{V}$ to the pressures $p_e$, $p_i$ and the electrostatic potential $\Phi$. When we prescribe the "jumps" of these quantities across the layer, $\boldsymbol{B}_s$ and $\boldsymbol{V}$ must be set to yield the given jumps, and these conditions will demand a consistent set $a$, $b$, and $\Delta$, resulting in a totally self–consistent model of the boundary layer [68]. The solution gives a poloidal shear flow and layer width of order

$$|V_y| = O(\sqrt{\beta}\, V_T) = O(\sqrt{\beta_p}\, \frac{B_p}{B_0}\, V_T), \tag{2.51}$$

$$\Delta = O(\lambda_i) = O(\rho_i/\sqrt{\beta}) = O(\rho_{ip}/\sqrt{\beta_p}), \tag{2.52}$$

where $V_T$ is the ion thermal speed, $B_p$ ($\beta_p$) is the poloidal field ($\beta$), $\rho_i$ ($\rho_{ip}$) is the ion gyroradius (poloidal gyroradius). In standard nomenclature, (2.51) implies that the magnitude of the velocity corresponds to the "poloidal Mach number" ($V/[V_T(B_p/B_0)$) of order $\sqrt{\beta_p} = O(1)$. Since, typically, A bp 5O(1), the layer width is also of the order of the poloidal gyroradius. The given potential yields a negative electric field ($E_x < 0$), as well as $dE_x/dx < 0$. These predictions are in good agreement with experimental observations.

### 2.3.4 Summary

Thus, the two–fluid model of a plasma describes the strong coupling between the magnetic and the fluid aspects of a plasma. The resulting system can be cast in the form of a pair of vortex dynamics equations. The simplest equilibrium solution of this system consists of two simultaneous Beltrami conditions signifying the alignment of generalized vorticities with flows that transport them. Combining these equations yields the double curl Beltrami equation. The set of solutions contains field configurations that can be qualitatively different from the conventional single Beltrami fields (Taylor relaxed states). The larger new set may help us understand a variety of structures generated in plasmas. A double Beltrami field is characterized by four parameters (two eigenvalues and two amplitudes). By relating these parameters with conserved physical quantities, we obtain a set of algebraic relations that can be investigated to predict the characteristics of the equilibrium state as a control parameter is slowly changed. One such ex-ample is worked out in detail, evaluating the Beltrami field parameters in terms of the macroscopic constants of motion  helicities and energy. It is found that under certain conditions the ambient equilibrium can be catastrophically lost. The double Beltrami equilibria are shown to be capable of confining pressure – the diamagnetic and high-beta structures, thus, lie within the scope of the current theory. The generalized Bernoulli condition, implying that the energy density of the field is fully relaxed, gives a simple relation among the flow velocity, potential, and the static pressure. When we drive a strong flow (of order unity in the Alfvénic units), very high–beta equilibrium may be obtained. On the other hand, when diamagnetism is imposed (as a jump condition at the boundary), a flow and electric field naturally emerge to sustain the pressure. The self–consistency of the fields and pressure is the defining attribute of the DB self-organized states. Finally, we make a small catalog of the known relaxed state equilibria and also point out how one may arrive at them. In Fig.2.1, we may see a hierarchy determined by the increasing complexity of the final state. In supplying a magnetic field, current, and flow to the plasma, the energy of the system rises successively with the harmonic, the first, and the

second Beltrami fields. These "energy levels" are explained as follows. Suppose that a plasma is produced in an external magnetic field (harmonic field). In the absence of a drive, such a plasma will disappear and the system will relax into the pure harmonic magnetic field ($\nabla \times \boldsymbol{B} = 0$). When a drive in the form of a plasma current is added, it sustains the total helicity, and the plasma relaxes into the Taylor state corresponding to the single Beltrami magnetic field. When a strong flow exists in addition to the current in a two–component plasma, the system must conserve two distinct helicities and the self–organized state becomes qualitatively different from the Taylor relaxed state. The new states represent a "singular perturbation" to the MHD accessible states because the two–fluid effect induces a coupling among the flow, magnetic field, electric field, and the pressure. To access these states one must also maintain the second helicity invariant by driving and sustaining an appropriate flow. It is equivalent to giving an internal electric field or applying a steep gradient in pressure, because these fields are tightly coupled. As the final state becomes more and more complex, greater and greater care is needed for its creation and maintenance. However, if all the requirements are met, the more complex states can display a tremendously variegated and rich structure in field variations.

## 2.4 Magnetofluid Coupling: Eruptive Events in the Solar Atmosphere

Let's examine the solutions expressed by (2.29), (2.31) and (2.32). We first show that either of the $\lambda_{\pm}$ can correspond to the macroscopic length. Vastly separated roots of (6) require $(b+\tilde{a})^2 \gg 4$. Then

$$\lambda_+ \simeq b - \frac{1}{\tilde{a}+b}, \quad \lambda_- \simeq -\tilde{a} + \frac{1}{\tilde{a}+b}.$$

There are two distinct cases (more complicated cases can also be constructed): (i) Both $a$ and $b$ are small and very near ($\tilde{a} = a^{-1} \gg 1$). Then $\lambda_+ \sim b - a,\ \lambda_- = \tilde{a}$ implying that $\lambda_+$ corresponds to long–scale and $\lambda_-$ to short one. (ii) both $a$ and $b$ are large and very close to one another, then $\lambda_+ \sim b - (1/b) \sim b,\ \lambda_- \sim (1/b) - \tilde{a}$. Thus, here the long scale is $\lambda_-$ and the short one is $\lambda_+$.

From now onwards, $\lambda$ will denote the long or the macro scale, and $\mu$ , the short or the micro scale.

We are now ready to study the behavior of $C_{\lambda,\mu}$ and $\mu$ as the control parameter $\lambda$ is varied for a given equilibrium characterized by specified values of the invariants. For two sets $h_1 = 1,\ h_2 = 1.5,\ E = 0.4$ and $h_1 = 1,\ h_2 = 1.5,\ E = 1.3$, the results are plotted in FIG.2.4(a) and FIG.2.4(b), respectively ($\lambda$ corresponds to $\lambda_-$ in Fig.2.4(a) and $\lambda_+$ in Fig.2.4(b)). Here $L^2/2$ has been normalized out and we set $C_{\lambda,\mu} > 0$. Notice that the dashed lines in the $\mu$ and $C_\lambda$ plots in Fig.2.3(b) correspond to the region of imaginary $C_\mu$, where the "solution" can not be defined.

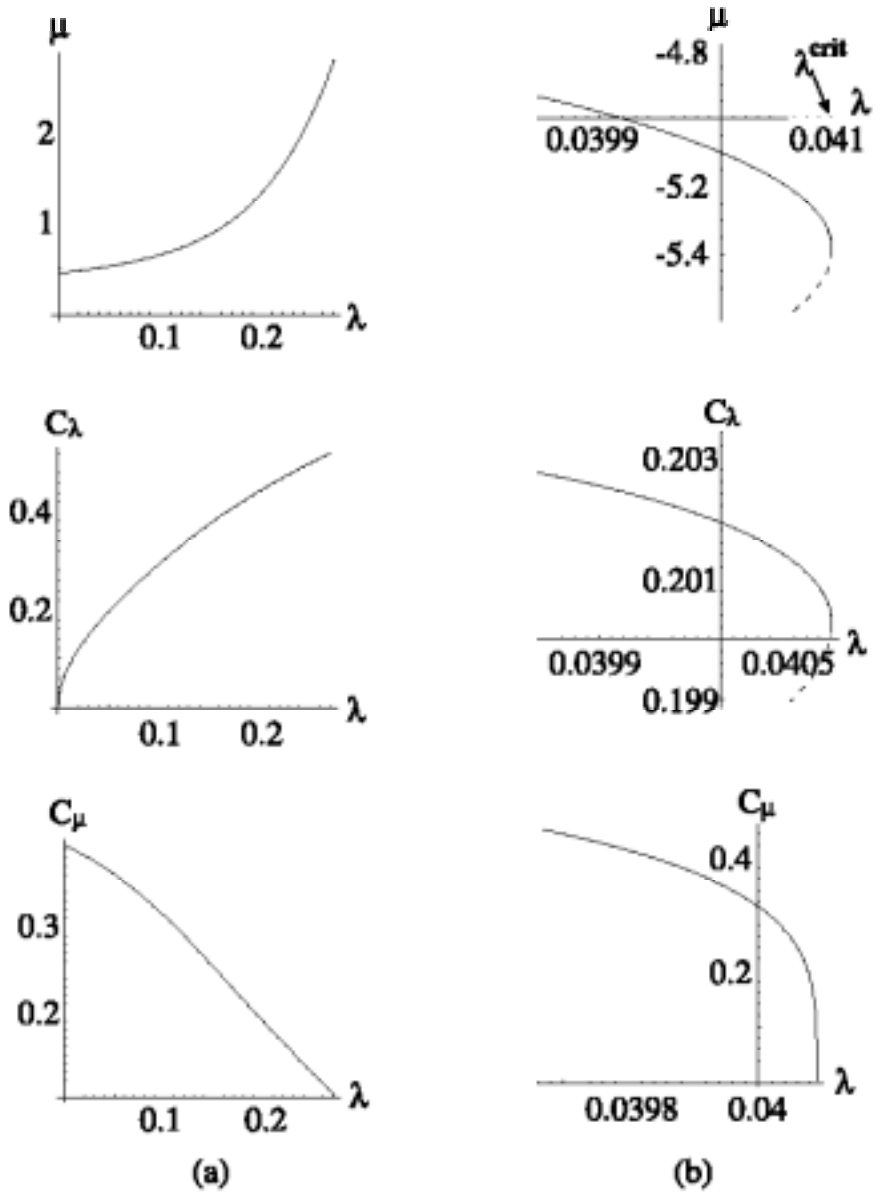


Fig.2.4 Plots of $\mu$ and $C_{\lambda,\mu}$ versus $\lambda$ for: (a) $E = 0.4 < E_c \simeq 0.45$, the critical energy; no catastrophe. (b) $E = 1.3 > E_c$ . There is a critical point at $\lambda \simeq 0.041$.

From these figures we conclude that the nature of the system changes drastically as $E$ is changed. For the parameters of FIG.2.4(a), $\mu$ and $C_{\lambda,\mu}$ remain real and change continuously with varying $\lambda$ implying that as the macroscopic scale of the structure $(1/\lambda)$ changes continuously the equilibrium expressed by (2.16) persists; there is no qualitative

change in the state of the system. The plots in FIG.2.4(b) reveal a totally different situation. With $E$ changing from 0.4 to 1.3 (for the same $h_1$, $h_2$), the system displays a qualitatively different behavior; when $\lambda$ exceeds a critical value $\lambda^{\mathsf{crit}}$, i.e, the macro–scale becomes smaller than a critical size, the physical determinants of the equilibrium cease to be real; the sequence of equilibria is terminated.

Note that in [125], where the "generating function" approach was applied to model catastrophes ("loss of equilibria"), it was argued that in the solar context, one often arrives at unphysical results. They conclude that the physical parameters defining the solution may become unphysical at the catastrophe points when one simply varies the amplitude while keeping a fixed functional form for the force–free field. Our model, due to its deeper physical content, does not suffer from this problem. Since in the DB equilibria, there exists an additional length-scale that changes with the adiabatic evolution, the parameters of the system like the temperature, density and velocity field are clearly defined at the critical point (see e.g. [72] for the dynamical evolution).

### 2.4.1 Catastrophe - Reduction to a single Beltrami state

The first route to a catastrophic transformation of DB is through the disappearance of one of the constituent single–Beltrami states. This is the path followed by the catastrophe illustrated in Fig.2.4(b). It is remarkable that , for this model problem, we can derive the conditions for the catastrophe as well as the critical value of the control parameter. We shall now show that if the curve $\lambda(\mu)$ implied by (2.29) has an extremum, i.e. $d\lambda/d\mu = 0$ for real $\lambda$ and $\mu$, then it implies the disappearance of the micro–scale constituent of the DB field.

For analysis, it is more convenient to use the equivalent equation (2.28)

$$b = \frac{h_2}{E + h_1 \tilde{a}} \tag{2.53}$$

with $b$ expressed in terms of $\lambda$ and $\mu$. Since $\lambda$ and $\mu$ are fully determined in terms of

$b$ and $\tilde{a}$, and $b$ is fully known (the invariants are given) in terms of $\tilde{a}$ through (2.53), the extremum condition $\mathrm{d}\lambda/\mathrm{d}\mu = 0$ may be easily replaced by having $\mathrm{d}\lambda/\mathrm{d}\tilde{a} = 0$. From (2.8), we find

$$\begin{aligned}\frac{\mathrm{d}\lambda}{\mathrm{d}\tilde{a}} &= \frac{1}{2}\left[\left(-1+\frac{b+\tilde{a}}{\sqrt{(b+\tilde{a})^2-4}}\right)\right. \\ &\left.+\frac{\mathrm{d}b}{\mathrm{d}\tilde{a}}\left(1+\frac{b+\tilde{a}}{\sqrt{(b+\tilde{a})^2-4}}\right)\right] = 0, \end{aligned} \tag{2.54}$$

leading to

$$\begin{aligned}\frac{\mathrm{d}b}{\mathrm{d}\tilde{a}} &= \frac{-\left[-1+(b+\tilde{a})/\sqrt{(b+\tilde{a})^2-4}\right]}{\left[1+(b+\tilde{a})/\sqrt{(b+\tilde{a})^2-4}\right]} \\ &= -\frac{1}{4}\left[(b+\tilde{a})-\sqrt{(b+\tilde{a})^2-4}\right]^2 \\ &= -(\mu+\tilde{a})^2. \end{aligned} \tag{2.55}$$

Combining it with

$$\frac{\mathrm{d}b}{\mathrm{d}\tilde{a}} = \frac{-h_1 h_2}{(E+h_1\tilde{a})^2}, \tag{2.56}$$

a simple corollary of (2.53), we find that the product

$$h_1 h_2 = \left[(\mu+\tilde{a})(E+h_1\tilde{a})\right]^2 \geq 0, \tag{2.57}$$

is positive implying that when the two helicities $h_1$ and $h_2$ have opposite signs, there is no extremum and, therefore, no loss of equilibrium.

Our next task is to extract a relationship or a condition which insures that all the parameters are real at the extremum, i.e, the extremum is physically allowed. We first eliminate $\mu(\lambda_-)$ in favor of $\tilde{a}$ and $b$, and then rearrange the equation as a quadratic in $\tilde{a}$ with the coefficients written entirely in terms of the invariants. The two steps are

explicitly spelled out:

$$\mp 2\sqrt{h_1 h_2} = \left[(b+\tilde{a}) - \sqrt{(b+\tilde{a})^2 - 4}\right](E + h_1\tilde{a})$$
$$= h_2 + \tilde{a}\,(E + h_1\tilde{a})$$
$$-\sqrt{[h_2 + \tilde{a}\,(E+h_1\tilde{a})]^2 - 4\,(E+h_1\tilde{a})^2}, \tag{2.58}$$
$$\left(h_1^2 \pm h_1\sqrt{h_1 h_2}\right)\tilde{a}^2 + \left(2h_1 \pm \sqrt{h_1 h_2}\right)E\tilde{a}$$
$$+E^2 + h_1 h_2 \pm h_2\sqrt{h_1 h_2} \;=\; 0\;. \tag{2.59}$$

Then $\tilde{a}$ is real at $\mathrm{d}\lambda_+/\mathrm{d}\tilde{a} = 0$, if

$$\left[\left(2h_1 \pm \sqrt{h_1 h_2}\right)E\right]^2$$
$$-4\left(h_1^2 \pm h_1\sqrt{h_1 h_2}\right)\left(E^2 + h_1 h_2 \pm h_2\sqrt{h_1 h_2}\right)$$
$$= h_1 h_2 E^2 - 4h_1 h_2\left(h_1 \pm \sqrt{h_1 h_2}\right)^2 \;\geq\; 0\;. \tag{2.60}$$

Simplifying (2.60), we may conclude that the extremum is physical when

$$E^2 \geq E_c^2 = 4\left(h_1 \pm \sqrt{h_1 h_2}\right)^2, \tag{2.61}$$

that is, when the energy of the system exceeds a critical energy $E_c$ defined by the helicities $h_1$ and $h_2$. We shall soon relate the existence of this physical extremum to the possibility of a catastrophic rearrangement of the original state.

The system behavior at the critical point $\lambda = \lambda^{\mathsf{crit}}$ is better studied by resorting to (2.29) ($\lambda_+ = \lambda, \lambda_- = \mu$) ; the extremum condition $\mathrm{d}\lambda/\mathrm{d}\mu = 0$ implies

$$\left(1 \mp \frac{(\lambda-\mu)}{\sqrt{(\lambda-\mu)^2 + 4}}\right)E - 2\lambda h_1 = 0. \tag{2.62}$$

which, when coupled with equations (22–26), yields

$$E = \lambda h_1 \left[1 + (\tilde{a} + \lambda)^2\right]. \tag{2.63}$$

This is precisely the condition for $C_\mu^2 = 0$ (see (2.32)). Thus, the existence of a physically allowed extremum in the $\lambda(\mu)$ curve is a necessary and sufficient condition for the micro-scale component of the DB field to vanish, $C_\mu^2 \to 0$ . Since $C_\mu^2$ is positive to begin with, the extremum does represent a critical transition point; if the system is pushed beyond this point, $C_\mu^2$ will become negative ($C_\mu$ becomes imaginary) resulting in a loss of equilibrium.

The critical $\lambda = \lambda^{\mathsf{crit}}$ at which the transition happens can be determined from a simultaneous solution of (2.53) and (2.63). The process is straightforward but a bit tedious. The following relations derived from (22)-(26),

$$(\tilde{a} + \lambda)^2 = \frac{E - \lambda h_1}{\lambda h_1}$$

and

$$(\tilde{a} + \lambda)[\tilde{h}_2 - \lambda(E - \lambda h_1)] = 2(E - \lambda h_1).$$

are combined to give

$$(\tilde{h}_2 - Q)^2 = 4h_1 Q, \quad \text{where} \quad Q = \lambda(E - \lambda h_1), \tag{2.64}$$

from which we first derive $Q = \left[\sqrt{h_1} \pm \sqrt{h_2}\right]^2$, and then find:

$$\lambda^{\mathsf{crit}} = \frac{1}{2h_1}\left(E \pm \sqrt{E^2 - E_c^2}\right) . \tag{2.65}$$

where $E_c$ has been defined earlier by (2.61).

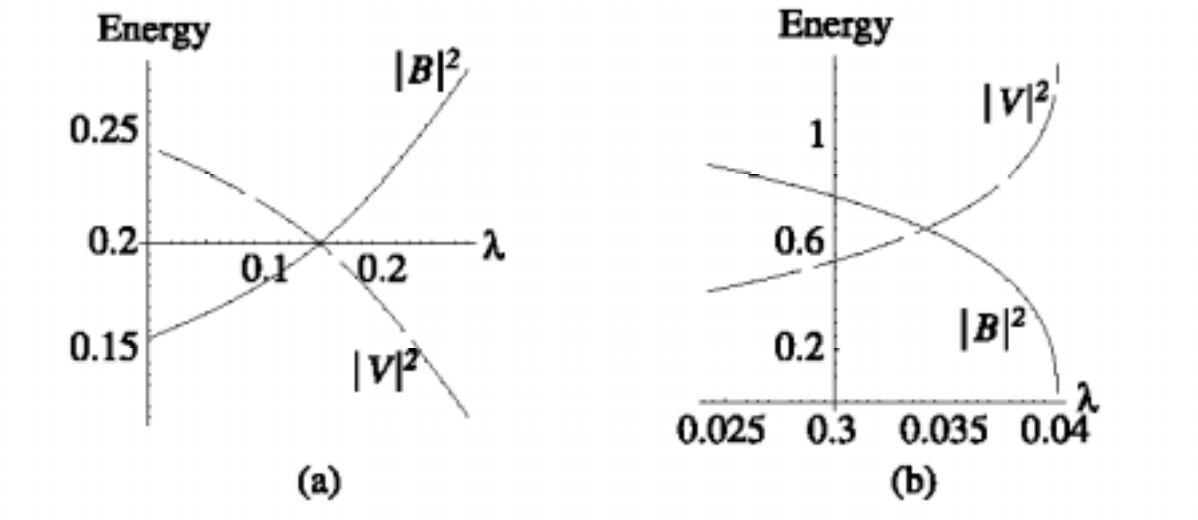


Fig.2.5 Plots for $\mu$, the magnetic and the flow energies versus $\lambda$ for the (a) catastrophe–free set, (b) catastrophe–prone set; the parameters are the same as in Fig.2.3.

Using this value of $\lambda^{\mathsf{crit}}$, we may confirm that, at the critical point, the coefficient $C_\mu$ which measures the strength of the short scale fields, identically vanishes, and the equilibrium changes from Double Beltrami to a single Beltrami state labelled by $\lambda = \lambda^{\mathsf{crit}}$, i.e., $\boldsymbol{B} = C_\lambda \boldsymbol{G}_\lambda$ or $\nabla \times \boldsymbol{B} = \lambda \boldsymbol{B}$ with $\boldsymbol{V}$ parallel to $\boldsymbol{B}$. The amplitude of the macro–scale component (the only one remaining) turns out to be $C_\lambda^2 = \lambda^{\mathsf{crit}} h_1$. The transition leads to a magnetically more relaxed state with the magnetic energy reaching its minimum with an appropriate gain in the flow kinetic energy. At the transition, the kinetic energy is far in excess of the magnetic energy with the ratio $(B^2/V^2) \sim 1/(\tilde{a} + \lambda)^2 \ll 1$ (see Fig. 2.5(b)). In Fig.2.6, we clearly see the redistribution of the magnetic energy as the system responds to changes in the control parameter. In (Fig.2.6(b)) we show the history of a catastrophe–prone sequence; starting from vastly separated scales, the initial magnetic energy is transferred mainly to flow energy in the macroscopic scale, i.e., to the bulk plasma motion. In the opposite case where the initial conditions are not favorable

to a catastrophic change (Fig.2.6(a)), one can see that even though the large scale flow–energy can increase for some part of the sequence of adiabatic changes (slow "breathing" of the structure), eventually it is the magnetic energy that increases feeding on the flow–energy (Fig.2.5(a)).

From these figures it is clear that physical parameters of the system are precisely defined at the critical point. Note, that since we assume that changes are slow and transport processes can be ignored in our model, the representation of a changing structure by a local DB field persists. It is remarkable, however, that even as the system is pushed to the catastrophe stage, the length scales do remain vastly separated (see Fig.2.5(b)).

Notice that there are several other auxiliary conditions that have to be satisfied in order that these mechanisms may operate. It is straightforward to approximate $-D^{-1}\mu \sim 1/b\tilde{a}$ and $D^{-1}\lambda \simeq (1/b\tilde{a}) \cdot (b-a)/\tilde{a}$. The condition for well–separated length–scales requires that $b$ and $a$ must have the same sign $\Longrightarrow$ $b\tilde{a} > 0$. The amplitudes may be conveniently written as

$$C_\mu^2 \simeq \frac{1}{b\tilde{a}} \left[ E - (b-a)h_1[1 + (\tilde{a}+\lambda)^2] \right],$$

$$C_\lambda^2 \simeq \frac{b-a}{\tilde{a}} \frac{1}{b\tilde{a}} \left[ E + \tilde{a}h_1[1 + (\tilde{a}+\mu)^2] \right]$$

revealing that if $C_\mu^2$ has to go to zero, one must demand $(b-a)h_1 > 0$. The condition is naturally satisfied if $h_1 > 0$, $(b-a) > 0$, and for this case, $C_\mu^2$ is guaranteed to be positive if $a$ and $b$ are both positive. Appropriate conditions for a physical equilibrium state for various domains of $a$ and $b$ can be readily calculated. Note that the system is invariant to $b \to -\tilde{a}$ and $\tilde{a} \to -b$.

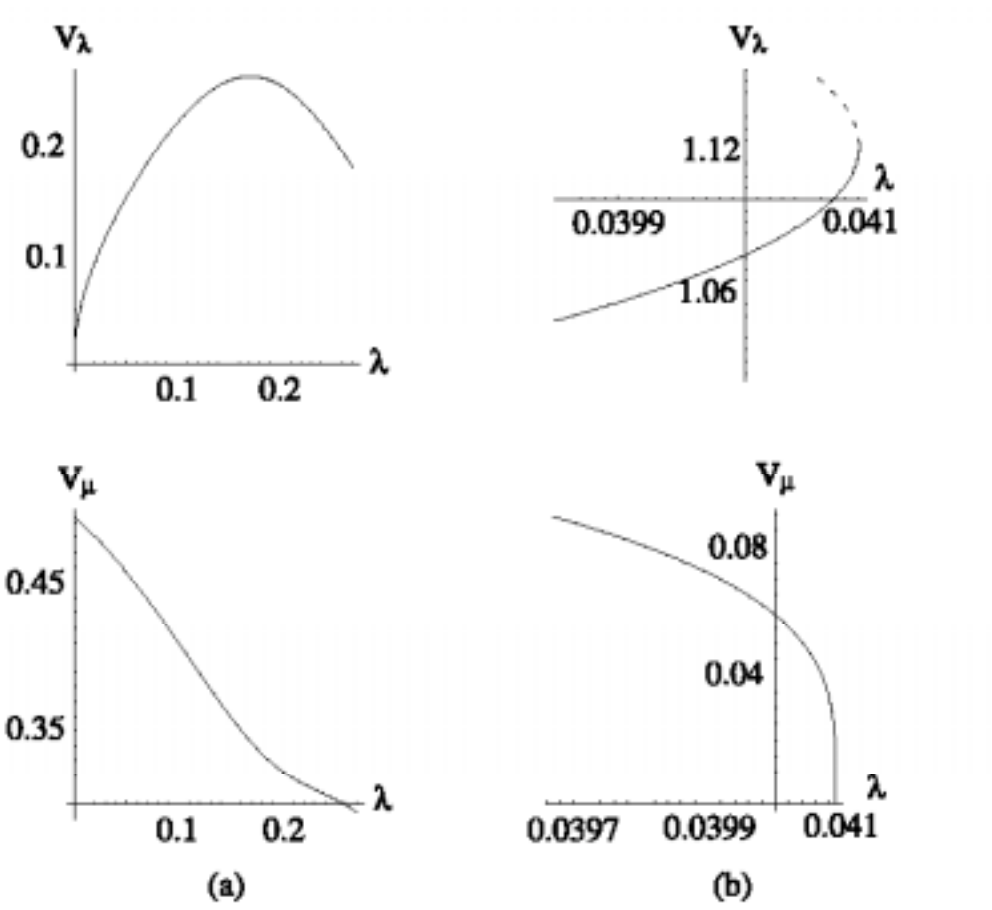


Fig.2.6 Plots of the velocity amplitudes $V_\mu$ and $V_\lambda$ versus $\lambda$ for (a) the catastrophe free set of parameters (Fig.2.3(a)), and (b) the catastrophe–prone set (Fig.2.3(b)). It is clearly seen that at the catastrophe point the large scale velocity component acquires most of the transferred magnetic energy.

In order to apply the present model to explore the conditions for the occurrence of explosive/eruptive events in the solar atmosphere, we may proceed as follows. The macroscopic scale of a structure (measured by $|\lambda^{-1}|$) will dictate the value of $\lambda$ ; this must be quite small with $|\lambda| \ll |\mu|$. The structure is then viewed as a DB state in which a macro–scale field is superposed by a small scale ($|\mu^{-1}|$) one. Using (2.31) and (2.32) we may estimate $C_\lambda \sim O\left(\lambda_\lambda/\lambda_\mu\right) \ll 1$ and $C_\mu \sim O\left(\lambda_\mu/\lambda_\mu\right) \sim 1$ from. If any interaction increases $\lambda$ (the size of the structure shrinks) the critical point ($\lambda = \lambda^{\mathsf{crit}}$) will

be reached at which $C_\mu$ is zero. The magnetic field energy ($\propto C_\lambda^2 + C_\mu^2$) decreases to a very small value since $C_\lambda^2 \ll 1$. Since the total energy is conserved, almost all the initial magnetic energy is transferred to the flow causing an eruption (see Fig.2.7). Notice that for coronal plasma, the skin depth $l_i$ , for a typical density $\sim 10^9\,\mathrm{cm}^{-3}$, is small $\sim$ 100cm ($l_i/\lambda \sim 10^3$km) .

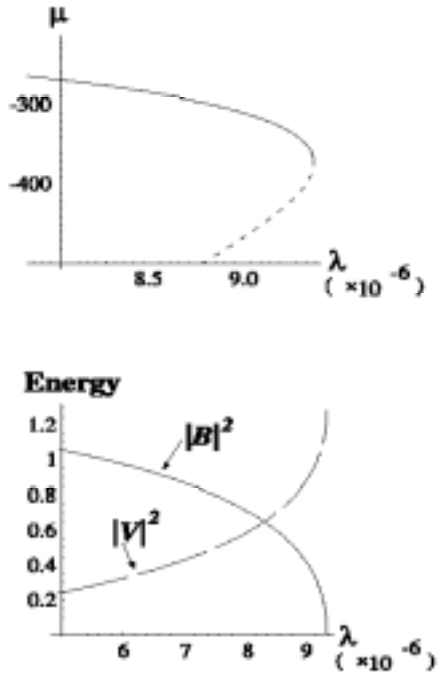


Fig.2.7 Plots for $\mu$, the magnetic and the flow energies versus $\lambda$ for the catastrophe–prone set $h_1 = 1$, $h_2 = 1.007$ and $E = 1.3 > E_c = 7 \cdot 10^{-3}$ (these conditions can be used to model the explosive/eruptive events in solar atmosphere). The scale lengths are highly separated $\lambda_+ << \lambda_-$. The initial choice makes $C_\lambda \sim O(\lambda/\mu) \ll 1$ and $C_\mu \sim O(\mu/\lambda) \sim 1$ from (2.31) and (2.32). If any interaction increases $\lambda$ (the size of the structure shrinks) the critical point ($\lambda = \lambda^{\mathsf{crit}}$) will be reached at which $C_\mu$ is zero. Magnetic field energy ($\propto C_\lambda^2 + C_\mu^2$) decreases to a very small value since $C_\lambda^2 \ll 1$. Total energy is conserved, almost all the initial magnetic energy is transferred to the flow.

### 2.4.2 Catastrophe through coalescence

The slowly evolving DB states may suffer a catastrophe in which the two constituent states become degenerate on their way to changing the basic topological structure of the fields. Although at the critical point we are still left with only one of the original independent fields, the pathway to this catastrophe (as well as the parameter range where it happens) is fundamentally different. In the previous example the DB state relaxed to a single Beltrami state when the amplitude of one of original states went to zero (Root Disappearance Mode (RDM)). An equally striking change may occur when the original states coalesce to a single independent state (Root Coalescence Mode (RCM)), that is, the two real characteristic length–scales degenerate to one. The critical point will define the boundary between the real and a pair of complex conjugate roots of the Double Beltrami equation which translates into a boundary between what may be called paramagnetic and diamagnetic structures of the magnetic field. We remind the reader that a single Beltrami field with real $\lambda$ defines the conventional paramagnetic structure, while a purely imaginary $\lambda$, leading to the London Equation, signifies complete diamagnetism.

The conditions for an RCM catastrophe are satisfied when the parameters of the system are such that the $\lambda(\mu)$ curve intersects the $\lambda = \mu$ line for real $\lambda$. By definition, the root coalescence means that at the critical point, there is no scale–separation implying that the parameter space for RCM to occur will be quite different from the space in which RDM occurs. This will also imply different astrophysical or solar structures where RCM may pertain. Naturally at and near the critical point, parameter changes are not slow, and the system is pushed to the dynamical evolution stage exactly like the situation discussed in the previous section.

At the root coalescence critical point ($\lambda = \mu = \lambda_o$), following relations hold

$$b = \lambda_o \pm 1, \quad \tilde{h}_2 = E\left(\lambda_o \pm 1\right) - \lambda_o^2 h_1;$$

the latter is solved for critical $\lambda_o$ ,

$$\lambda_o = \frac{1}{2}\left[E \pm \sqrt{E^2 - 4h_1(\tilde{h_2} \pm E)}\right],$$

which must be real for the catastrophe to occur. The necessary condition for the root coalescence catastrophe is

$$E^2 > E_o^2, \qquad E_o^2 = 4\left(h_1 \pm \sqrt{h_1 h_2}\right)^2, \tag{2.66}$$

an inequality which the invariant determinants of the system must obey. From the critical energy $E_o$ and critical $\lambda_o$ , it is easy to find that at the transition, the amplitudes $C_\mu^2 \leftrightarrow C_\lambda^2$ . When $\lambda \to \mu$ , both the numerator and the denominator vanish in (2.32) and (2.31); the amplitudes are obtained by a limiting process

$$C_\lambda^2 = D^{-1}\lambda\left[E - \mu[1 + (\tilde{a} + \mu)^2]h_1\right] \to$$

$$\to D^{-1}\lambda h_1\left[\lambda[1 + (\tilde{a} + \lambda)^2 - \mu[1 + (\tilde{a} + \mu)^2\right] \longrightarrow \lambda h_1$$

$$C_\mu^2 = -D^{-1}\mu h_1\left[\mu[1 + \tilde{a} + \mu)^2 - \lambda[1 + (\tilde{a} + \lambda)^2\right] \longrightarrow \lambda h_1$$

and are found to be equal, $C_\mu^2 = C_\lambda^2$, as it must be because there is no way to distinguish between the two states. The ratio of the magnetic to the kinetic energy $b^2/V^2 = (\tilde{a} + \lambda)^{-2} =\sim O(1)$ because in this case there is no separation between the roots! The structure relaxes to a Single Beltrami state with a well–defined relationship between the magnetic and the velocity field.

In Fig.2.8, we display the contents of (2.53) in $\tilde{a}$-$b$ plane for different values of $E$: (a) $E = 0.4$, (b) $E = 1.3$, where $h_1 = 1$ and $h_2 = 1.5$. From this figure and (2.53), we find that, with $E$ increasing (or $h_1$ increasing, $h_2$ decreasing), the solutions enter the region where $\lambda$ and $\mu$ are complex, i.e., $(b + \tilde{a})^2 < 4$. Since the ABC map is not valid for complex $\lambda$ and $\mu$, the critical point $\lambda = \mu$ defines the end of the domain of applicability

of the current theory.

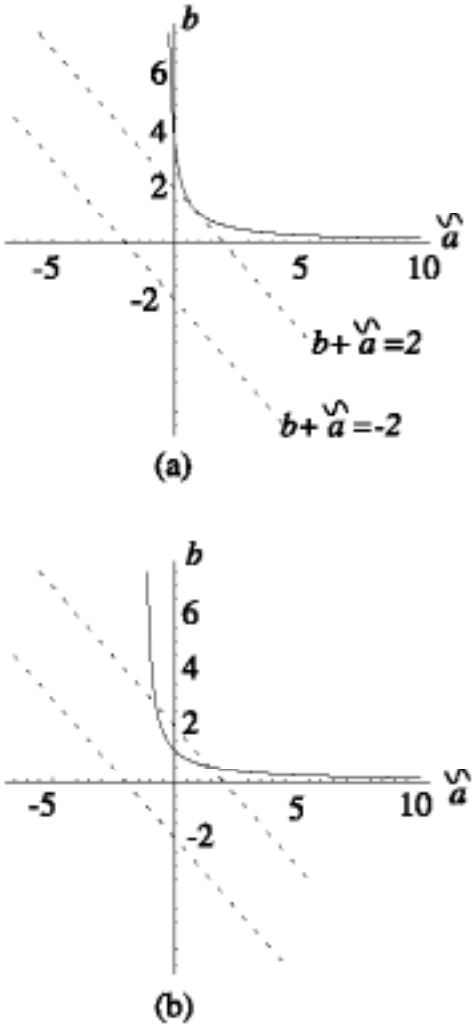


Fig.2.8 Plots for the catastrophe conditions trough coalescence of the roots. (a) $E = 0.4$, (b) $E = 1.3$ and $h_1 = 1$, $h_2 = 1.5$ in both cases. We see that there exist regions where $\lambda$ and $\mu$ are complex.

The sudden transformation of a DB state to a single Beltrami state (the standard one parameter, one scale–length relaxed state) with qualitatively different physical properties from the original state (kinetic and magnetic energies, the relative orientation of the magnetic and the velocity fields etc.) signifies a genuine catastrophe – a sudden change

in the defining physical attributes of the system. This is quite different from the thought experiment discussed in [125] where it was argued that the specification of appropriate photospheric boundary conditions for the magnetic field governed by the force–free equation, could lead to a well–behaved evolutionary sequence without exhibiting any catastrophic behavior.

In our model, even at the critical point of the catastrophe we can define physical parameters like the flow kinetic energy and the magnetic energy. The assumptions of the model like the vastly separated scales hold throughout and up to the critical point. It should also be stressed that energy transformations do take place during the slow evolution era (Figures 3a,b) for both the catastrophe–free and the catastrophe–prone cases. Only the rates and direction of the transformations are dictated by the initial conditions of the system. An appropriate choice of initial values of the invariants can lead to a desired transformation.

Needless to say that as the system approaches the critical point, the quasi–equilibrium considerations are just an indicator of what is happening and they must be replaced by a dynamical description including the transport processes to capture the changes which are no longer slow.

### 2.4.3 Conclusions and Summary

The theoretical foundation of this subsection rests on the Double Beltrami magneto–fluid states which represent plasma self–organization (relaxation) under the combined action of interacting magnetic and velocity fields. The DB states contains field configurations which can be qualitatively different from the conventional single Beltrami fields (Taylor relaxed states, for instance) and are likely to help us understand the diversity of structures generated in a variety of plasmas.

The crucial step we take in the solar physics context is to model the quasi–equilibrium, slowly evolving solar atmosphere structures as a sequence of Double–Beltrami magnetofluid states. As a consequence of this identification, we have been able to show

the possibility of, and derived the conditions for catastrophic changes leading to a fundamental transformation of the initial state which is a superposition of two states — one with a microscopic and the other with a macroscopic length–scale. The critical condition comes out as an inequality involving the three invariants of the collisionless magnetofluid dynamics. When the total energy exceeds a critical energy, the DB equilibrium may suddenly relax to a single Beltrami state corresponding to the large macroscopic size. All of the short–scale magnetic energy is lost having been transformed to the flow energy and partly to heat via the viscous dissipation of the flow energy.

We have also discussed another route to catastrophe within the broad theoretical framework when the characteristic length scale are not separable into micro and macro lengths. Physical situations where this mechanism may pertain will be discussed in future work.

This general mechanism in which the flows (and their interactions with the magnetic field) play an essential role could certainly help in advancing our understanding of a variety of sudden (violent) events in the solar atmosphere like the flares, the erupting prominences, and the coronal mass ejections, particle outflows in chromosphere. The connection of flows with explosive/eruptive events is rather direct: it depends on their ability to deform (in specific cases distort) the ambient magnetic field lines to temporarily stretch (shrink, destroy) the closed field lines so that the flow can escape the local region with a considerable increase in kinetic energy in the form of heat/bulk motion.

It is certainly tempting to speculate that though diverse phenomena like the chromospheric mass outflows, spicules, explosive events in chromosphere, micro– and nano–flares, large coronal flares, erupting prominences and CMEs do appear to be disconnected, they could all be the manifestations of different aspects of a more global dynamics pertinent to a specific coronal region. The mechanism for energy transformation presented in this work and other mechanisms inherent in the basic model can work in various regions of the Solar atmosphere dictating different patterns of dynamical evolution depending on the intial and boundary conditions for a specific region.

We end this section with a word of caution: this quasi–equlibrium model is incapable of handling processes that are not slow. Events in the neighbourhood of the catastrophe, the creation and primary heating of the hot coronal structures, and the magnetic energy release from the emerging flux or the dynamics of the magnetic flux emergence are a few examples of a vast number of processes that require a careful and proper time dependent treatment.

## 2.5 Generation of QSM Fields in Two-Fluid Plasmas Embedded in Super-Strong EM Fields

Recently considerable progress has been achieved in the development of compact terawatt laser sources [142]. Such laser sources generate sub-picosecond pulses of electromagnetic (EM) radiation with focal intensities $I > 10^{18} W/cm^2$. One of the most powerful Neodymium-glass laser system, "Vulcan" at Rutherford Appleton Laboratory, delivers $35TW$ to target at an intensity of $I = 10^{19} W/cm^2$ [143] in the short pulse mode. Preliminary reports from several other centers seem quite promising and in very near future, it will be possible to design petawatt laser facilities which will produce even higher intensity ($\sim 10^{21-23} W/cm^2$) pulses of EM radiation [144, 145]. In the field of such strong sub-picosecond pulses, it is expected that the character of the nonlinear response of the medium would radically change [146, 147].

In the wake of these far-reaching developments, it is natural that the interaction of ultrashort, relativistically strong pulses has become a subject of intense theoretical and experimental investigation. In the field of such strong radiation, the electron oscillation energy could be comparable or even larger than its rest energy. The relativistic nonlinear effect, which is basically associated with the dependence of the electron mass on the EM field amplitude, determines the dynamics of EM pulses. At intensities $10^{18} W/cm^2$ and higher, a whole set of new phenomena were predicted and some of them have already been confirmed by experiments [148, 149, 150]. Bulk of the investigations have been connected with: 1) electrostatic wake-field generation due to the displacement of plasma electrons from the region occupied by the laser pulse under the action of the ponderomotive force [151, 152, 153, 154, 155], and 2) the relativistic self-focusing of the laser beam itself [156, 157, 158, 159, 160, 161, 162, 163].

Among the various nonlinear effects which may occur in a plasma interacting with strong laser pulses, the generation of quasistatic magnetic fields (QSM) is found to be one of the most interesting and significant, particularly because the presence of these

fields could have considerable influence on the overall nonlinear plasma dynamics. In the past, although much effort has been devoted to studying the mechanisms leading to magnetic field generation in laser plasmas (for a review see [164]), there does not exist a well-established and satisfactory theory. Indeed, numerical simulations carried out by Wilks et al. [165], carried out for the interaction of an ultra-intense laser pulse with an overdense plasma target, predict extremely high self-generated magnetic fields $\sim 250MG$; these immense fields can not be properly explained on the basis of existing theories. Sudan [166] suggested that the spatial gradients, and the nonstationary character of the ponderomotive force, may lie at the origin of the strong magnetic fields discovered in numerical simulations [165]. Several other analytical attempts have been made to understand the results of the simulation [167, 168]. All these theoretical attempts use a hydrodynamical formulation. It must, however, be pointed out that the conditions prevalent in the simulation experiments (for example, the thermal speed $v_{th} > v_p$, where $v_p$ is a characteristic low-frequency phase speed) may not yield to a hydrodynamical description. The heat generated during the interaction further strengthens the inequality as time goes on, and the transverse fields are pushed to the anomalous skin region making it necessary to employ a kinetic treatment [169].

The hydrodynamic treatment (which we will follow in this section) can be quite adequate provided $v_p >> v_{th}$. In the problem of magnetic field generation in underdense plasmas, this condition is likely to prevail. We would like to point out, here, that relatively strong magnetic fields can also be generated in underdense plasmas; this has been definitively demonstrated in the numerical simulations of Askar'yan et al. [170, 171] who were studying the relativistic self-focusing of the laser beam in such plasmas. In [172, 173], it was shown that due to the resonant excitation of plasma waves the generation of QSM field occurs both in the body of the linearly polarized EM pulse, and also in its wake (region of the wakefield). The simulation as well as experimental results strongly indicate, that the problem of the generation of QSM fields by EM pulses is ripe for a serious and careful theoretical investigation.

In the present work we deal with the generation of QSM fields by relativistically strong EM pulses propagating in an underdense plasma. Laser pulses are assumed to be short, with time duration ($T_l$) less than the characteristic time for the ion response $\omega_i^{-1}$ ($\omega_i$ is the ion Langmuir frequency) so that the ion motion can be neglected. At the same time we assume that the pulse is sufficiently long, i.e. $T_l >> \omega_e^{-1}$ ($\omega_e$ is the electron Langmuir frequency) that the complications due to the excitation of Langmuir waves are absent. For simplicity, the analysis is restricted to beams with a narrow crossection i.e. $L_\parallel(\sim cT_l) >> L_\perp$, where $L_\perp$ and $L_\parallel$ are respectively the characteristic transverse and longitudinal spacial dimensions of the beam. This assumption is not particularly restrictive and holds for the parameters pertinent to the experiment, for example, by Borisov et. al. [148], where the propagation of relativistic high-intensity, linearly polarized pulses is explored. In fact, [148, 149, 150] reports the observation of self-channeled propagation of EM pulses from a sub–picosecond $KrF^*$ ($\lambda = 0.248\mu m$, $T_l \sim 500fs$) excimer laser over a distance up to $2mm$ which is two orders longer than the corresponding diffraction (Rayleigh) length ($\sim \pi r_o^2/\lambda$, where $r_o \sim 3.5\mu$ is a initial focal radius of the EM beam). The diameter of the channel ($\sim L_\perp$) was $\sim 1\mu m$, and the peak intensity of the channeled radiation reached $I \sim 10^{19} W/cm^2$. Note that the generation of QSM fields was not reported in [148, 149, 150].

### 2.5.1 QSM Field Generation in Initially Uniform Plasma

Although it is not definite that linearly polarized pulses do not generate a magnetic field, it is likely that the effect may be small. In this study, therefore we concentrate on the circularly polarized pulses for which QSM fields should appear due to the inverse Faraday effect. The mechanism (originally found in [174] using a phenomenological approach) of excitation is the rotation of the polarization vector of the external radiation. In several later papers, the evolution of QSM fields had been studied using the hydrodynamic approach for both the weak and as well as the relativistically strong EM radiation. The basic approach consists in using a relation which describes the conservation (at each

instant) of the generalized vorticity, and then calculating a low frequency (LF) drag current excited by the EM radiation [175, 176, 177, 178]. However, there are several inconsistencies, and contradictions in the final expressions of the drag current obtained in these publications. We believe that these contradictions stem from the following fact: in the cold plasma limit (i.e. when the characteristic phase velocities of LF perturbations are much bigger than the electron thermal velocity) the expression for the LF drag current is derived by taking the time average (over the fast scale associated with the laser frequency) of the product of two high frequency quantities, one of which is $\sim \nabla \cdot \tilde{\mathbf{E}}$, where $\tilde{\mathbf{E}}$ is the HF part of the EM field. It is well known that the laser field in a plasma is predominantly transverse ($\tilde{\mathbf{E}}_\perp$), i.e., the longitudinal field $\tilde{\mathbf{E}}_\parallel << \tilde{\mathbf{E}}_\perp$ for $k >> L^{-1}$, where $k$ is the wave number and $L$ is the characteristic spatial spread of the pulse. Since $\nabla \cdot \tilde{\mathbf{E}} \sim \nabla_\perp \cdot \tilde{\mathbf{E}}_\perp + ik\tilde{\mathbf{E}}_\parallel$ is nearly zero (is proportional to the high frequency density perturbation), its replacement by $\nabla \cdot \tilde{\mathbf{E}}_\perp$ (which most of these references do) can lead to a gross overestimate of the drag current. We shall correct this serious error in this study, and evaluate $\nabla \cdot \tilde{\mathbf{E}}$ much more accurately and derive a correct expression for the drag current for arbitrary amplitude laser pulses. We show that QSM field generation takes place due to the strong plasma inhomogeneity caused by the intense laser beam itself, and that the amplitude of QSM field increases in the ultrarelativistic case. We also discuss the possibility of electron cavitation, and its influence on the effect of magnetic field generation.

We use the Maxwell equations which, under the above-mentioned assumptions, can be written as:

$$\boldsymbol{\nabla} \times \mathbf{B} = \frac{1}{c}\frac{\partial \mathbf{E}}{\partial t} - \frac{4\pi e}{c}\, n\, \frac{\mathbf{p}}{m\gamma}, \tag{2.67}$$

$$\boldsymbol{\nabla} \times \mathbf{E} = -\frac{1}{c}\frac{\partial \mathbf{B}}{\partial t}, \tag{2.68}$$

$$\boldsymbol{\nabla} \cdot \mathbf{E} = 4\pi e(n_o - n), \tag{2.69}$$

where - $e$ , $m$ , $n$ , $\mathbf{p}$ are the electron charge, mass, density and momentum respectively, $c$ is the speed of light, $n_o$ is the ion background density, and $\gamma = (1 + \mathbf{p}^2/m^2c^2)^{1/2}$ is the

relativistic factor.

The motion of the cold unmagnetized electron fluid is described by the standard special–relativistic hydrodynamical equations. These consist of the equation of motion

$$\frac{\partial \mathbf{p}}{\partial t} + mc^2 \boldsymbol{\nabla}\gamma = -e\mathbf{E}, \tag{2.70}$$

and the continuity equation

$$\frac{\partial n}{\partial t} + \boldsymbol{\nabla} \cdot \left( n \frac{\mathbf{p}}{m\gamma} \right) = 0. \tag{2.71}$$

The absence of the magnetic part of the Lorenz force in Eq.(2.70) is due to the assumption that generalized vorticity is zero in the body of the electron fluid; this assumption relates the magnetic field with the electron momentum (London equation of super conductivity),

$$\mathbf{B} = \frac{c}{e} \boldsymbol{\nabla} \times \mathbf{p}. \tag{2.72}$$

For laser plasma interactions, the hydrodynamic equations in this form were displayed, for the first time, in [179, 180]; more complete discussion can be found in [181]. Equations (2.70–2.72) are in an extremely convenient form for further manipulation. Substituting $\mathbf{E}$ from Eq. (2.70) in Eqs.(2.67) and (2.69), and using (2.72), we obtain our first equation relating $\mathbf{p}$ ($\gamma$ is just a function of $\mathbf{p}^2$) and the density $n$,

$$c^2 \boldsymbol{\nabla} \times \boldsymbol{\nabla} \times \mathbf{p} + \frac{\partial^2 \mathbf{p}}{\partial t^2} + mc^2 \frac{\partial}{\partial t} \boldsymbol{\nabla}\gamma + \omega_e^2 \frac{n}{n_o} \frac{\mathbf{p}}{\gamma} = 0. \tag{2.73}$$

The second equation relating $n$ and $\mathbf{p}$ is derived by a combination of Eqs.(2.69) and (2.70),

$$\frac{n}{n_o} = 1 + \frac{1}{m\omega_e^2} \left( \frac{\partial}{\partial t} \boldsymbol{\nabla} \cdot \mathbf{p} + mc^2 \Delta\gamma \right). \tag{2.74}$$

Equations (2.73) and (2.74) are a closed set to which the system of Maxwell and hydrodynamical equations has been reduced [182]. Note that this very set of equations was

derived in our recent publication [78] dealing with the problem of wake field generation in semiconductor plasmas. Before proceeding further, it is worthwhile to remark that the continuity equation (2.71) was totally ignored in the derivation of (2.73) and (2.74). It is evident, however, that Eq.(2.71) is not really independent, and is readily derived by taking the divergence of (2.73) and using (2.70). In fact, any two of the set (2.71), (2.73) and (2.74) can be used as independent equations for $n$ and $\mathbf{p}$. Our goal in this study is to calculate the relatively slow-varying (quasistatic) magnetic field induced by a specified high frequency laser pulse. In response to the laser field, all the fields in the plasma will contain both the slow and the fast time dependence (with characteristic time $\tau \sim \omega^{-1}$ ). Therefore, we may decompose each of the variables $A \equiv (\mathbf{E}, \mathbf{B}, \mathbf{p}, n, \gamma)$ into an averaged and a varying part,

$$A = < A > + \tilde{A}, \tag{2.75}$$

where the brackets $< ... >$ denote averaging over the time interval $\tau$. With this prescription, the averaged equation for $< n >$ and $< \mathbf{p} >$ become

$$\frac{< n >}{n_o} = 1 + \frac{1}{m\omega_e^2}\left(\frac{\partial}{\partial t}\boldsymbol{\nabla}\cdot < \mathbf{p} > + mc^2\Delta < \gamma >\right) \tag{2.76}$$

and

$$c^2\boldsymbol{\nabla}\times\boldsymbol{\nabla}\times < \mathbf{p} > + \frac{\partial^2}{\partial t^2} < \mathbf{p} > + mc^2\frac{\partial}{\partial t}\boldsymbol{\nabla} < \gamma > + \omega_e^2\frac{< n >}{n_o}\frac{< \mathbf{p} >}{< \gamma >} =$$

$$-\frac{\omega_e^2}{n_o < \gamma >} < \tilde{n}\tilde{\mathbf{p}} >, \tag{2.77}$$

where it is assumed (to be justified later) that $< \gamma >= \gamma$. The averaged Eq.(2.72),

$$< \mathbf{B} >= \frac{c}{e}\boldsymbol{\nabla}\times < \mathbf{p} > \tag{2.78}$$

allows us to relate the generated magnetic field with the averaged momentum. Electric

field of the HF radiation can be written in the form:

$$\tilde{\mathbf{E}} = [(\mathbf{x} + i\mathbf{y})E_{\perp}(\mathbf{r}, t) + \mathbf{z}E_{\parallel}(\mathbf{r}, t)]\ exp(-i\omega t + ikz) + c.c.\ , \tag{2.79}$$

where the transverse ($E_{\perp}$) and the longitudinal ($E_{\parallel}$) amplitudes are slowly varying.

Since we are using $\tilde{\mathbf{p}}$, rather than $\tilde{\mathbf{E}}$ as our dynamical variable, let us find the corresponding expression for $\tilde{\mathbf{p}}$. It can be shown that if $r_E/\lambda << 1$, where $r_E$ is a characteristic displacement of the oscillating electrons due to HF field, and $\lambda$ is the EM field wave length, the relation between $\tilde{\mathbf{p}}$ and $\tilde{\mathbf{E}}$ has the form:

$$\frac{\partial \tilde{\mathbf{p}}}{\partial t} = -e\tilde{\mathbf{E}}, \tag{2.80}$$

which, coupled with (2.79), yields

$$\tilde{\mathbf{p}} = [(\mathbf{x} + i\mathbf{y})p_{\perp}(\mathbf{r}, t) + \mathbf{z}p_{\parallel}(\mathbf{r}, t)]exp(-i\omega t + ikz) + c.c. \tag{2.81}$$

after a simple integration over the fast time ($\omega^{-1}$). The slowly varying amplitudes (kept constant during the integration), $p_{\perp}$ and $p_{\parallel}$, are given by

$$p_{\perp} = -\frac{ie}{\omega}E_{\perp}, \quad p_{\parallel} = -\frac{ie}{\omega}E_z. \tag{2.82}$$

Our next order of business is to evaluate the driving term proportional to $< \tilde{n}\tilde{\mathbf{p}} >$ in Eq. (2.77). For this we must begin by deriving an expression for $\tilde{n}$ in terms of $\tilde{\mathbf{p}}_{\perp}$, which we are assuming is a 'given' quantity. We could use the high frequency version of either Eq.(2.71) or (2.74) to accomplish this. We choose to use Eq.(2.74) primarily to show, in a very perspicuous manner, how our treatment differs from, and corrects earlier treatments. From (2.74), we find ($\gamma$ has only an averaged part)

$$\frac{\tilde{n}}{n_o} = \frac{1}{m\omega_e^2}\frac{\partial}{\partial t}(\nabla \cdot \tilde{\mathbf{p}}) \tag{2.83}$$

Since $\nabla \cdot \tilde{\mathbf{p}}$ for a basically transverse wave is very small, extreme care must be taken in its evaluation. It is conventional to replace $\nabla \cdot \tilde{\mathbf{p}}$ by $\nabla \cdot \tilde{\mathbf{p}}_\perp$ because $|p_\parallel|$ is much smaller than $|p_\perp|$. This, in our opinion, is a serious mistake. Although $|p_\parallel| << |p_\perp|$, $|\nabla \cdot \tilde{\mathbf{p}}_\perp| \sim |p_\perp|/R$ may be (and is) of the same order as $|\nabla \cdot \tilde{\mathbf{p}}_\parallel| \sim k|p_\parallel|$ because $kR >> 1$, where $R$ is the transverse scale length associated with the laser pulse. Replacing $\nabla \cdot \tilde{\mathbf{p}}$ with $\nabla \cdot \tilde{\mathbf{p}}_\perp$ results in a gross overestimate of $\tilde{n}$ and hence of the driving term. There is a general lesson to be learnt here: whenever the end results depend on $\nabla \cdot \tilde{\mathbf{E}}$ ($\sim \nabla \cdot \tilde{\mathbf{p}}$), as they do in the magnetic field generation problem, one must not neglect the contributions from $p_\parallel$ and one must find an appropriate (generally indirect) way of evaluating this small quantity.

We now calculate $\nabla \cdot \tilde{\mathbf{p}}$ by taking the divergence of the high frequency version of Eq.(2.73), and obtain for a transparent plasma ($\omega > \omega_e$), [2]:

$$\boldsymbol{\nabla} \cdot \tilde{\mathbf{p}} = \frac{\omega_e^2}{\omega^2} \tilde{\mathbf{p}}_\perp \cdot \boldsymbol{\nabla}_\perp \left( \frac{< n >}{n_o \gamma} \right) \tag{2.84}$$

where we have used the fact that, for circular polarized radiation, the particle energy does not depend on the "fast" time, and there is no generation of high harmonics of the EM field (Note that effects of high harmonic generation, which take place due to longitudinal part of HF field, are negligibly small). This indeed is the reason for the equality $\gamma =< \gamma >$, which is approximately given by

$$\gamma = \left( 1 + \frac{|p_\perp|^2}{m^2 c^2} \right)^{1/2} \tag{2.85}$$

The LF drag current, which appears in the right hand side of Eq. (2.77), can now be computed using Eqs. (2.83) and (2.84). One can already see that for circularly polarized radiation, it is non vanishing provided the quantity $< n > \gamma^{-1}$ depends on the radial variable $\mathbf{r}_\perp$. If the radially inhomogeneous beam propagates in an initially uniform plasma,

[2]It should be mentioned that the relation (2.84) is the relativistic version of well-known equation from the courses of the continuous media electrodynamics: $\epsilon \nabla \cdot \mathbf{E} = -(\mathbf{E} \cdot \nabla)\epsilon$ where $\epsilon$ is the dielectric permitivity of a medium.

the ponderomotive force of the EM radiation ($\sim \nabla\gamma$) pushes out the plasma electrons from the region of its localization, and creates an effective plasma density inhomogeneity. Notice that $< n >$ and $\gamma$ have the same characteristic radial scales length, and their contributions in the creation of the drag current are equally important. At this junction it is worthwhile to mention that if the EM beam has a spatially constant amplitude, an initial inhomogeneity of plasma density will be required. Thus in a homogeneous plasma, contrary to a statement made in [175], the constant amplitude EM beam can not generate the QSM field by "magnetization currents". It was shown in [183] that the physical reason, for the absence of the QSM field generating source in the homogeneous case, is the mutual compensation of the circular electron currents.

Now, for simplicity we consider an axisymetric electromagnetic pulse propagating along the $z$ axis: $p_\perp = p_\perp(r, z - v_g t, t)$ , where $v_g = c(1 - \omega_e^2/\omega^2)^{1/2}$ is the group velocity of the laser radiation. Using Eqs.(2.83)-(2.85), the $\phi$ component of Eq.(2.77) can be written as

$$\frac{2}{c}\frac{\partial^2 < p_\phi >}{\partial\xi\partial\tau} + \frac{1}{r}\frac{\partial}{\partial r}r\frac{\partial < p_\phi >}{\partial r} - \left(\frac{< n >}{n_o}\frac{k_e^2}{\gamma} + \frac{1}{r^2}\right) < p_\phi >=$$

$$= -2\frac{\omega}{mc^2}\frac{\omega_e^2}{\omega^2}\frac{|p_\perp|^2}{\gamma^2}\left[\frac{\partial}{\partial r}\left(\frac{< n >}{n_o}\right) - \left(\frac{< n >}{n_o}\right)\frac{\partial}{\partial r}ln\gamma\right] \tag{2.86}$$

where $\xi = z - v_g t$ and $k_e = \omega_e/c$. Notice that exactly the same expression for the driving term (right hand side of Eq.(2.86)) could be derived by using the high frequency version of Eq.(2.71) to evaluate $\tilde{n}$. In this case one could avoid the possibility of going wrong since $\tilde{n}$ can be calculated without having to evaluate $\nabla \cdot \tilde{\mathbf{p}}$. We followed this path for historical reasons.

For a narrow laser beam, within the approximations used in this study, Eq.(2.74) can be approximated by

$$\frac{< n >}{n_o} = 1 + \frac{1}{k_e^2}\left(\frac{1}{r}\frac{\partial}{\partial r}r\frac{\partial\gamma}{\partial r}\right) \tag{2.87}$$

It is now clear that using Eqs. (2.85) and (2.87), Eq.(2.86) can be viewed as an inho-

mogeneous differential equation (the driving term is fully known because $p_\perp$ is supposed to be specified) for $< p_\phi >$. If we can solve Eq.(2.86) for $< p_\phi >$, then the required components of the QSM field are readily determined by

$$\frac{e}{c}B_z = \frac{1}{r}\frac{\partial}{\partial r}r < p_\phi >, \tag{2.88}$$

$$\frac{e}{c}B_r = -\frac{\partial}{\partial z} < p_\phi > . \tag{2.89}$$

The explicit form for the driving term (drag current) in Eq.(2.86) allows us to substantiate the discussion following Eq.(2.83) in clearer terms: For the nonrelativistic case ($\mathbf{p}^2 << m^2c^2$), an equation similar to Eq.(20) was derived in Ref. [19]. However they used the relation $\boldsymbol{\nabla} \cdot \tilde{\mathbf{p}} \sim \boldsymbol{\nabla} \cdot \tilde{\mathbf{p}}_\perp$ and consequently, the source term came out to be proportional to $|p_\perp|^2$. This is in marked contrast to our result; the nonrelativistic limit of our source term is, in fact, proportional to $|p_\perp|^4$, because both the terms in the square brackets of the right hand side of Eq.(2.86) are also proportional to $|p_\perp|^2$. Since $|p_\perp|^4 << 1$, the magnetic field strength will be considerably smaller than what was found in [178]. In [176, 177] the spatial structure of the magnetic field was analyzed for the case in which the pump wave intensity and the plasma density have axisymetric distributions and it was shown that the growth of the strength of these fields reaches saturation with increasing pump intensity in the ultrarelativistic limit. But the expression for the drag current is not correct.

As we will see below the problem is self consistent - If the pulse amplitude $p_\perp$, and therefore $\gamma$, has strong space dependence, then the inhomogeneity of $< n > \gamma^{-1}$ will always lead to the generation of QSM field. Thus the system of Eqs. (2.86)-(2.89) with (2.85) is an acceptable model for describing the magnetic field generation process by narrow relativistic short laser beams. In what follows we assume that during the interaction time of interest, the laser beam profile remains unchanged, and can be presumed to be

Gaussian [3]:

$$|p_\perp|^2 = p_o^2 \; exp\left[-\frac{r^2}{R^2} - \frac{\xi^2}{L^2}\right] \tag{2.90}$$

where $R$ and $L$ are the transverse and longitudinal dimensions of the pulse ($R << L$). For the pulse shape represented by (2.90) we find

$$N = \frac{< n >}{n_o} = 1 - \frac{1}{k_e^2 R^2}\frac{(\gamma^2 - 1)}{\gamma}\left(2 - \frac{r^2}{R^2}\frac{(\gamma^2 + 1)}{\gamma^2}\right). \tag{2.91}$$

From Eq. (2.91) one can see that the plasma electrons are expelled from the central part of the pulse ($r \approx 0$), creating a density hump away from the beam axis ($r \sim R$); with a final ($r \to \infty$) exponential decay to the equilibrium value $n_o$. However, as it was shown in [159, 160, 161, 162, 163], under certain condition, the electrons can be fully expelled from the central part of EM beam (electron cavitation). To derive this condition, let us first define a critical radius

$$R_c^2 = \frac{1}{k_e^2}\frac{2(\gamma_o^2 - 1)}{\gamma_o}, \tag{2.92}$$

where $\gamma_o = \gamma(r = 0) = (1 + p_o^2/m^2c^2)^{1/2}$. For $R > R_c$, Eq.(2.91) reveals that $N > 0$ for all $r$, and consequently, the electron cavitation does not occur. However if $R = R_c$, the density does vanish at $r = 0$. Thus $R_c$ defines the minimum beam radius for the beginning of cavitation. Notice that within the framework of current model equations (which are being widely exploited for the problem of relativistic self-focusing of EM beams), one can not prevent the occurrence of unphysical, negative values for the electron density when $R < R_c$. This failure of hydrodynamical model of a plasma is generally corrected by putting $N = 0$ in the entire spacial region where $N < 0$ [159, 160, 161, 162, 163]. For the current study, we will follow this arbitrary, though, workable ansatz. In future, more detailed work, we will examine if this unphysical feature is basic to the hydrodynamical description or is a consequence of the approximations made. (It has also been argued ([184] that in the case of cavitation, an alternative to the fluid models, the particle in

[3]This assumption can be justified until the pulse passes the self-focusing length or the Rayleigh length in the case of diffraction spreading.

cell (PIC) technique should be used).

Algebraic complications prohibit a general analytical solution of Eq. (2.86). In the non relativistic case ($p_o^2 << m^2c^2$) Eq. (2.86) reduces to an equation which can be solved by taking a Fourier-Bessel transform. However the fields produced are uninterestingly small, and are not presented here. The interested reader can consult [178], remembering that they have overestimated the fields by a factor $m^2c^2/p_\perp^2 >> 1$.

Concentrating on the relativistic case, we first neglect the first term on the l.h.s (because $c^{-1}\partial^2/\partial\tau\partial\xi << \partial^2/\partial r^2$), of Eq. (2.86) arriving at an ordinary differential equation in $r$. For this ordinary differential equation, we can get an analytical solutions in two different limits, for arbitrary amplitudes. Indeed, in the limit of a smoothly inhomogeneous laser beam, $k_e^2R^2 >> \gamma_o$, for which the electron cavitation does not occurs, Eq.(2.86) yields (derivative terms are neglected)

$$< p_\phi >= 2\frac{mc^2}{\omega}\frac{(\gamma^2-1)}{\gamma}\frac{\partial}{\partial r}ln\left(\frac{N}{\gamma}\right) \tag{2.93}$$

The profile for the magnetic field $B_z(r)$ can be calculated using Eqs. (2.88) and (2.93). $B_z(r)$ has a maximum on the beam axis, then it decreases with increasing $r$, changing polarity near the beam edge ($\sim R$), and decaying rapidly to zero when $r \to \infty$. The central maximum can be conveniently expressed as

$$\Omega_c(0) = 4\frac{\omega_e^2}{\omega}\frac{\gamma_o}{k_e^2R^2}\left(1-\frac{1}{\gamma_o^2}\right)^2, \tag{2.94}$$

where $\Omega_c(r) = eB_z(r)/mc$ is an effective cyclotron frequency. Remembering that Eq.(2.94) is valid only for $\gamma_o << k_e^2R^2$, we conclude that $\Omega_c < \omega_e$ even in the relativistic case.

Note that the final value of $\Omega_c$ (Eq.(2.94)) does not depend on the equilibrium plasma density $n_o$. However, for this calculation to be valid, certain ($\omega > \omega_e$, $\gamma_o << k_e^2R^2$) constraints on the density have to be imposed. Let us now estimate the strength of the magnetic field for a relativistically strong pulse. For this purpose we choose the wavelength and intensity in the experimentally range (see Borisov et al. in [161]), $\lambda =$

$0.248\mu m$, $I = 1.3 \times 10^{20} W/cm^2$ ($\gamma_o = 2$). For representative values of $R = 1\mu m - 3\mu m$, the maximal value of the magnetic field is found to be $3MG - 0.4MG$. Corresponding plasma densities needed to satisfy the aforementioned constraint must lie in the range $n_o = 5 \times 10^{19} - 10^{21} cm^{-3}$ for $R = 3\mu m$, and $n_o = 5 \times 10^{20} - 10^{21} cm^{-3}$, for $R = 1\mu m$.

In the opposite case of a narrow pulse, $k_e^2 R^2 << 1$, the differential term dominates, and Eq.(2.86) can be readily integrated to give

$$\Omega_z(r) = 2\frac{\omega_e^2}{\omega} \int_r^\infty dr' \left(\frac{\gamma^2 - 1}{\gamma}\right) \frac{\partial}{\partial r'} \left(\frac{N}{\gamma}\right), \tag{2.95}$$

from which, with the aid of Eq.(2.91), one can obtain the radial structure of $B_z(r)$ for given $R$ and $\gamma_o$. However, in the relativistic case when $R_c^2 k_e^2 > 1$, electron cavitation occurs ($R < R_c$). In order to incorporate this phenomena, we must put $N = 0$ for $0 < r < r_c$ where $r_c$ is the solution of $N(r_c) = 0$, and use Eq.(2.91) for $N$ for $r > r_c$. Thus for $r < r_c$, we obtain a constant magnetic field (the source is zero). For this case it is straightforward to see that the strength of the magnetic field has a maximum on the beam axis $r = 0$, remains unchanged up to $r = r_c$, then drops down, changes polarity and rapidly tends to zero as $r \to \infty$. This behavior closely resembles the field produced by a solenoid! Indeed, the induced current is located on the "wall" of the cavitating plasma cylinder with radius $r \approx r_c (< \sqrt{2}R)$; there is no current in the body of the cylinder ($r < r_c$). The magnetic field, created by this current formation, remains uniform inside the "cylinder". The maximum value of $B_z = B_z(0)$ can be found from Eq.(2.95) by replacing the lower limit $r$ by $r_c$. Let us estimate the strength of the magnetic field. For $\lambda = 0.248\mu m$, $\gamma_o = 2$, $R = 3\mu m$ and plasma density $n_o = 10^{17} cm^{-3}$ ($k_e^2 R^2 = 0.03$). For the magnetic field we get $B_z(0) \approx 0.1MG$. We would like to emphasize, that if we were to neglect the effects of cavitation, and try to obtain $B_z(0)$ by integrating from $r = 0$, we may badly overestimate the strength of the generated magnetic field.

A caveat is in order here. For the narrow beam (with cavitation and $\gamma_o > 1$) case, the term proportional to $N/\gamma$ (Eq.(2.86)) is not smaller than the differential term for all $r$. Equation (2.95), therefore, should be just viewed as a very approximate indicator of

the field strength and structure. For a proper and accurate evaluation, Eq.(2.86) should be solved numerically.

The above Eqs.(2.94-2.95) provide us with estimations at the focal spot area. The radiation pulse, after it has passed the focal area, either diffract (in the case of narrow beam $R^2k_e^2 << 1$) or enters the self-focusing regime (for $R^2k_e^2 >> 1$) provided that the laser radiation power exceeds of critical value ($\sim 1.6 \times 10^{10}(\omega/\omega_e)^2 W$). In the latter case the beam intensity is concentrated in a narrow channel of the radius $R \sim 2k_e^{-1}$. Note that Eqs.(2.94-2.95) are invalid for evaluation the magnetic field in channel since all the terms in the left-hand side of Eq.(2.86) are of the same order. In order to evaluate the magnetic field in the channel we have solved Eq.(2.86) numerically. In Fig.2.9, typical behavior of $B_z(r)$ is displayed for $p_o/mc = 3$. One can see that in the region of electron cavitation the magnetic field is constant. Outside of the cavitating channel it changes polarity.

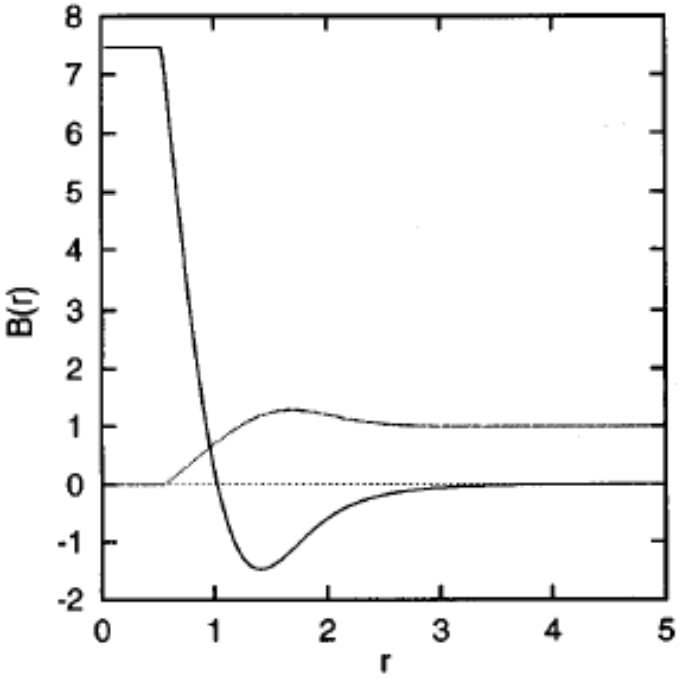


Fig.2.9 The magnetic field $B(r)[= \Omega_c(r)\,\omega/\omega_e^2]$ (solid line), and the density $N(r)$ (dashed line) profiles as functions of the dimensionless radius $r[= r/R]$.

For arbitrary strong laser radiation it is convinient to present the maximal strength of the magnetic field ($B_m = B_z(0)$), which is generated in the self-guiding channal, as

$$\frac{B_m}{B_1} = \frac{\omega_e^2}{\omega^2} b(p_o^2) \tag{2.96}$$

where $B_1$ is the high frequency magnetic field's strength of the laser pulse, and $b(p_o^2)$ is the dimensionless function. In Fig.2.10 we plot $b$ versus $p_o^2/m^2c^2$. We can see that $b$ is fast growing function and whenever $p_o^2$ reaches the value when electron cavitation occurs, further grow of $b$ becomes considerably weaker. If we neglect the effect of electron cavitation we may overestimate the strength of the generated magnetic fields. The maximal value of magnetic field $B_m$, as it follows from Eq.(2.96) and Fig.2.10, can not be as high as the magnetic field of laser radiation (at least for the EM fields intensities which can be created in the channel nowadays). However it can be quite strong in a dense plasma for high intensities of the laser radiation. Indeed, for $\lambda = 0.248\mu m$ and $I = 4 \times 10^{20} W/cm^2$ (i.e. $p_o = 3mc$) and for the plasma density $n_o = 10^{20} - 10^{21} cm^{-3}$ ($(\omega_e/\omega) = 0.07 - 0.24$) for the maximal value of the magnetic field we get $B_m = 13 - 130MG$.

In this study, we have attempted to develop a systematic treatment of the phenomenon of the generation of quasistatic magnetic fields by relativistically strong circu-larly polarized laser pulses propagating in an initially uniform underdense cold electron plasma. We show that because of the strong plasma inhomogeneity caused by the intense laser beam, a low-frequency drag current is induced, which, due to the inverse Faraday effect, produces a quasis tatic magnetic field in the beam propagation area. We derive an expression for the drag current valid for arbitrary amplitude laser pulses, and show that for the weakly relativistic (or nonrelativistic) laser radiation, the QSM field is smaller than what was found in previous publications. In the case of ultrarelativistic pulses, however, the generated QSM fields can reach considerable magnitudes. In all of these cases, the fields peak on the beam axis. We have also calculated the QSM field generation in the self-channeling regimes of intense laser pulses, and found that the electron

cavitation makes the QSM field resemble closely the field produced by a solenoid. The maximum value of the generated magnetic field in the channel increases rapidly with the beam intensity, and when cavitation occurs the rate of growth of $B_m$ with the intensity becomes slower. Finally, we show that for high-density plasma, the strength of the QSM field, which can be generated in the channel, can be $\sim 100$ MG and greater for currently available laser pulses.

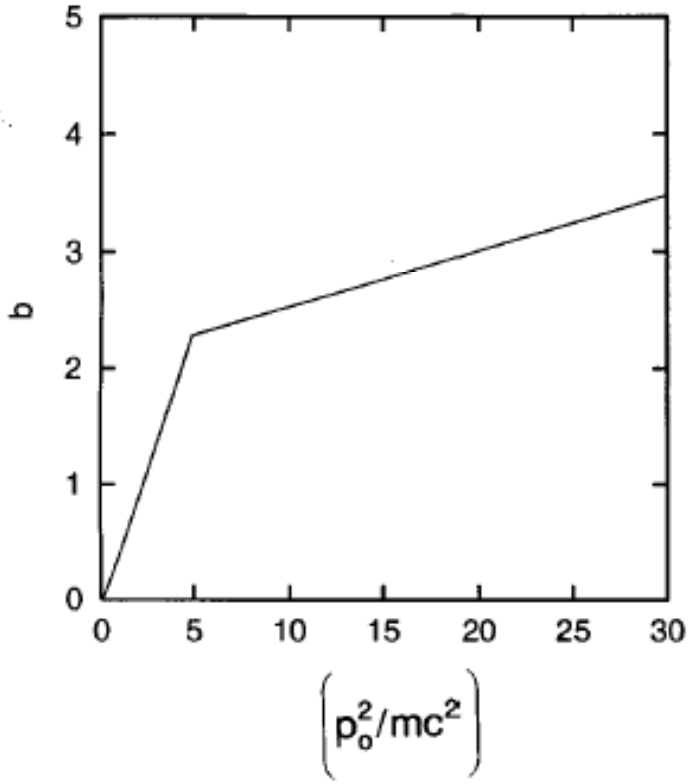


Fig.10 The dimensionless measure $b$, indicating the excess of the calculated over the simply estimated field, vs $p_0^2/m^2c^2$.

### 2.5.2 QSM Field Generation in Initially Non–Uniform Plasma

In this subsection we concentrate on the circularly polarized pulses for which QSM fields should appear due to the inverse Faraday effect. The mechanism (originally found in

[174] using a phenomenological approach) of excitation is the rotation of the polarization vector of the external radiation. The plasma in a very strong circularly polarized field of laser radiation exhibits some of features of magnetized (gyrotropic) plasma which lead to the creation of avarage current. The sum of circular electron currents in inhomogeneous (given initially or created due to the ponderomotive effects) infinite underdense plasma generating the summary "magnetization current" gives rise to the low frequency (LF) drag current appearance, which is the source of the QSM field.

The evolution of QSM fields has been studied using the hydrodynamic approach for both the weak as well as the relativistically strong pulses of circularly polarized field. The basic approach consists in using a relation which describes the conservation (at each instant) of the generalized vorticity, and then calculating a LF drag current excited by the EM radiation [187, 188, 175, 189, 176, 177, 178, 190, 191]. However, in most of the publications several inconsistencies and contradictions in the understanding of the QSM field generating source and the final calculation of drag current are presented. Just recently the magnetic field generation through inverse Faraday effect and its effects on the propagation of a circularly polarized light wave were studied by Sheng *et al.* [190] in a self–consistent way for relativistic intensities introducing, however, again two generating sources: plasma magnetization and the inhomogeneity of both the electron density and light intensity, which produces the nonzero current in the azimuthal direction. In our paper [191] we derived a correct expression for the drag current for arbitrary amplitude laser pulses. It was shown that QSM field generation in intially uniform underdense plasma takes place due to the strong plasma inhomogeneity caused by the intense inhomogeeous laser beam itself, and that the amplitude of QSM field increases in the ultrarelativistic case. In both papers [190, 191]] the possibility of electron cavitation and its influence on the effect of magnetic field generation was discussed. In self–channeling regime the magnitude of generated QSM fields can reach $100MG$ and greater values.

In initially strongly nonuniform plasma having the inhomogeneous distribution of circular electron magnetization currents which can not compansate each other it becomes

possible to generate the QSM fields of ruther high values even with arbitrarily strong circularly polarized laser radiation of constant amplitude (we will present below), while with linearly polariazed laser radiation of constant amplitude the generation of QSM fields is doubtful [186]. The initial inhomogeneity of plasma was not considered in above subsection [191], here we show that the formalism given there is applicable for the general case, when the density and the laser radiation have spacial gradients initially. We find below that the wrong formalism used in many earlier publications sometimes could lead to the right results obtained for inverse Faraday effect. The advantage of the initial convex density profile (rather than concave one) to get the high value generated magnetic fields is found.

Let us assume that laser beam with the electric field amplidude of the high frequency (HF) radiation: $\tilde{\mathbf{E}} = [(\mathbf{x}+i\mathbf{y})E_\perp(\mathbf{r},t)+\mathbf{z}E_\parallel(\mathbf{r},t)]exp(-i\omega t+ikz)+c.c.$ (here the transverse ($E_\perp$) and the longitudinal ($E_\parallel$) amplitudes are slowly varying in time $\tau \sim \omega^{-1}$ values) propagates in the initially inhomogeneous underdense plasma.

Following the derivation procedure similar to that made in the paper [191], within the approximations given there, considering the axisymmetric circularly polarized EM pulse propagating along the $z$ axis: $p_\perp = p_\perp(r, z - v_g t, t)$ , where $v_g = c(1 - \omega_e^2/\omega^2)^{1/2}$ is the group velocity of the laser radiation, we find for the LF electron density:

$$\frac{< n >}{n_{oo}} = \frac{n_o(\mathbf{r})}{n_{oo}} + \frac{1}{k_e^2}\left(\frac{1}{r}\frac{\partial}{\partial r}r\frac{\partial \gamma}{\partial r}\right), \tag{2.97}$$

where the brackets $< ... >$ denote the averaging over the time $\tau$; $n_o(\mathbf{r})$ is the plasma electron density in equilibrium state and $n_{oo} \equiv n_o(r = 0)$ (here $k_e^2 = \omega_e^2/c^2$ and $\omega_e^2 = 4\pi e^2 n_{oo}/m_e$); And for the $\phi$ component of the LF electron momentum (ions are assumed immobile) we get:

$$\frac{2}{c}\frac{\partial^2 < p_\phi >}{\partial\xi\partial\tau} + \frac{1}{r}\frac{\partial}{\partial r}r\frac{\partial < p_\phi >}{\partial r} - \left(\frac{< n >}{n_{oo}}\frac{k_e^2}{\gamma} + \frac{1}{r^2}\right) < p_\phi >=$$

$$= -2\frac{\omega}{mc^2}\frac{\omega_e^2}{\omega^2}\frac{|p_\perp|^2}{\gamma}\left[\frac{\partial}{\partial r}\left(\frac{< n >}{n_{oo}\gamma}\right)\right], \qquad (2.98)$$

where $\xi = z - v_g t$ and $< n >$ is given by the eq.(2.97), $\gamma = (1 + |p_\perp|^2/m^2c^2)^{1/2} =< \gamma >$ . We have used the fact that for circularly polarized radiation the particle energy does not depend on the "fast" time and there is no generation of high harmonics of EM field.

We have to note here that calculating the driving term in the eq.(2.98) we used the relativistic version of well–known equation from the courses of the continuous media electrodynamics: $\epsilon\nabla\cdot\mathbf{E} = -(\mathbf{E}\cdot\nabla)\epsilon$ (where $\epsilon$ is the dielectric permitivity of a medium) since replacing $\nabla\cdot\tilde{\mathbf{E}}$ $(\sim \nabla\cdot\tilde{\mathbf{p}})$ with $\nabla\cdot\tilde{\mathbf{E}}_\perp$ $(\sim \nabla\cdot\tilde{\mathbf{p}}_\perp)$ results in a gross overestimate of $\tilde{n}$ and hence of the driving term $\sim< \tilde{n}\cdot\tilde{\mathbf{p}} > /\gamma$ (as most of the references do in the magnetic field generation problem neglecting the contributions from $E_\parallel$).

If the pulse amplitude $p_\perp$ , and therefore $\gamma$ , has strong space dependence, then the inhomogeneity of $< n > /\gamma$ will always lead to the generation of QSM fields in the uniform infinite underdense plasma. Now, in initially inhomogeneous plasma, in the limit of weak laser pulse inhomogeneity ( $\nabla N_0(\mathbf{r}) >> \nabla\gamma(\mathbf{r})$, $< n(\mathbf{r}) > \simeq n_o(\mathbf{r})$ ), one can find the spatial structure of the magnetic field $B_z = (c/e)(1/r)(\partial/\partial r)r < p_\phi >$ from the following equation (provided that $n_o(\mathbf{r}) \neq 0$ in the pulse propagation area):

$$B_z - \frac{1}{r}\frac{\partial}{\partial r}\left[\frac{\gamma}{N(r)k_e^2}\left(r\frac{\partial}{\partial r}B_z\right)\right] = \frac{2mc^3}{e\omega}\frac{1}{r}\frac{\partial}{\partial r}\left[\frac{(\gamma^2-1)}{\gamma}r\frac{\partial}{\partial r}ln\ \left(\frac{N(r)}{\gamma}\right)\right], \qquad (2.99)$$

where $N(r) \equiv< n(r) > /n_{oo}$.

From the eq.(2.99) it is clear, that even in case of nonrelativistic laser radiation ($\gamma \simeq 1$) or spatially constant amplitude laser pulse for initially inhomogeneous plasma the drag current is significant if the electron density inhomogeneity (given initially!) is large and, consequently, the quasistatic magnetic field generation becomes possible. While in the limit of initially homogeneous plasma ($n_o(\mathbf{r}) = n_{oo}$) the inhomogeneity of laser pulse is required to generate the QSM fields.

(i). In the limit when the initial density inhomogeneity scale length $L$ is much larger than the skin depth $\sim \gamma^{1/2}/k_e$ the maximal value (reached on the beam axis) is com-

pletely defined by $L$. Calculating the QSM field for radially concave (convex) density profile $N_o(r) = 1 \mp r^2/L^2$ we find that $B_z(r)$ has maximum on the beam axis and then decreases to zero when $r \to \infty$ , having different polarity depending on the initial profile type. The central maximum, introducing the expression for the effective cyclotron frequency $\Omega_z(r) = eB_z/mc$ , can be expressed as:

$$\mid \Omega_{max}(0) \mid = 8\frac{\omega_e^2}{\omega}\frac{\gamma_o}{k_e^2 L^2}\left(1 - \frac{1}{\gamma_o^2}\right), \tag{2.100}$$

where $\gamma_o = \gamma(\mathbf{r} = 0)$. Simple estimations give us $\mid \Omega_{max} \mid < \omega_e$.

(ii). In the opposite case of $k_e^2 L^2 << 1$ from the eq.(2.100), in the case of strongly nonuniform plasma, when the EM amplitude spatial gradients are completely negligible, taking into account that fields vanish in the infinity, we find the folowing expression for the effective cyclotron frequency $\Omega_z(r)$ :

$$\Omega_z(r) = -2\frac{\omega_e^2}{\omega}\left(1 - \frac{1}{\gamma^2}\right) N_o(r). \tag{2.101}$$

which for the nonrelativistic laser radiation coincides with that of obtained by Pitaevskii in 1960 for the magnetic induction generated by the inverse Faraday effect [174] using the phenomenological approach. Later this effect was found experimentally [193], it was shown that in the low intensity limit the produced magnetic field is proportional to the intensity of the incident wave.

We have to mention here, that the expression for $\Omega_z(r)$ given by the eq.(2.101), found under the proper conditions using the only source for magnetic filed induction — the LF drag current, is valid for the strongly inhomogeneous plamsa only (for nearly constant amplitude laser pulse). In this case the maximal value of magnetic field doesn't depend on inhomogeneity scale length, is the same for all type initial inhomogeneity, and is defined just by the laser beam intensity. For ultra–relativistic laser radiation it reaches saturation giving $\Omega_{max,u} \sim -\omega_e^2/\omega < \omega_e$ . Such result was obtained by Abdulaev *et al.* (1986) in [177], although they used the incorrect expression for drag current again neglecting the

contributions from $p_{\|}$. Thus, taking the limit of constant amplitude ultrarelativistic laser radiation using the wrong formalism one can get the correct result. However, using the formalism of several other publications, even in this case, it is impossible to obtain the above correct result and understanding for the inverse Faraday effect [187, 188, 178].

(iii). In case of $k_e^2 L^2 \sim \gamma$ it is necessary to solve the Eq.(2.100). For both (concave and convex) shapes of initial density distribution it is possible to perform by the numerical simulations. The generated magnetic field profiles are similar to those found in the (i) case, only the maximal values are increased significantly.

Generally, in laser-produced plasmas the density gradient scale length is typically of the order of that of for the beam amplitude, $L \geq R$ ($R$ is the laser beam radius), i.e. $\nabla n_o(\mathbf{r}) \leq \nabla\gamma(\mathbf{r})$ and we have to take into acoount the spatial gradients of EM apmlitude. Thus, it is necessary to solve the system of equations (2),(3) with (1) keeping in mind that $< n >$ changes additionally because of ponderomotive effects. Now the characteristic radial scale lengths of $< n >$ and $\gamma$ can be of same order and, consequently, their contributions in the creation of the drag current are equally important. For the relativistically strong laser radiation, when the electron cavitation occurs, to prevent the unphysical, negative electron density existance, we have to put instead of $N$ the following (using the accepted in previous papers ansatz):

$$N(r) = \theta[< n(r) >]\cdot < n(r) >, \tag{2.102}$$

where $\theta(x)$ is the Heaviside function and ($\theta(x) = 0$ for $x < 0$ ; $\theta(x) = 1$ for $x \geq 0$).

The system of equations (2.97),(2.98),(2.99) with (2.102) is the acceptable self–consistent model to describe the QSM field generation process in the initially inhomogeneous plasma by the narrow relativistic laser beams. Estimating the generated magnetic field value for the Gaussian profile laser pulse propagation at the focal spot area we find (in both concave and convex cases) that the maximal value is reached on the beam axis. The profiles are similar to those found in case of the initially homogeneous plasma (see the results of paper [191]), only the maximal values are changed a little corresponding to the final

density distribution. In the self–focusing regime the structure of the generated QSM field closely resembles that of the field produced by a solenoid : the field is maximum and uniform in the cavitation region, then it falls, changes polarity and vanishes (see Fig.2.11). The cavitation region is either wider (concave initial density) or narrower (convex) than in initially homogeneous plasma and, hence, the maximal strength of the magnetic field is greater in case of initial convex density profile, although in the latter case we get a less steep density gradient but, what is essential, a more narrow channel empty of electrons and a wide "wall" of electron cylinder (the spatial gradients of the initial density distribution and the density variation caused by the ponderomotive effects have the same signs yielding an increased maximal strength of the magnetic field).

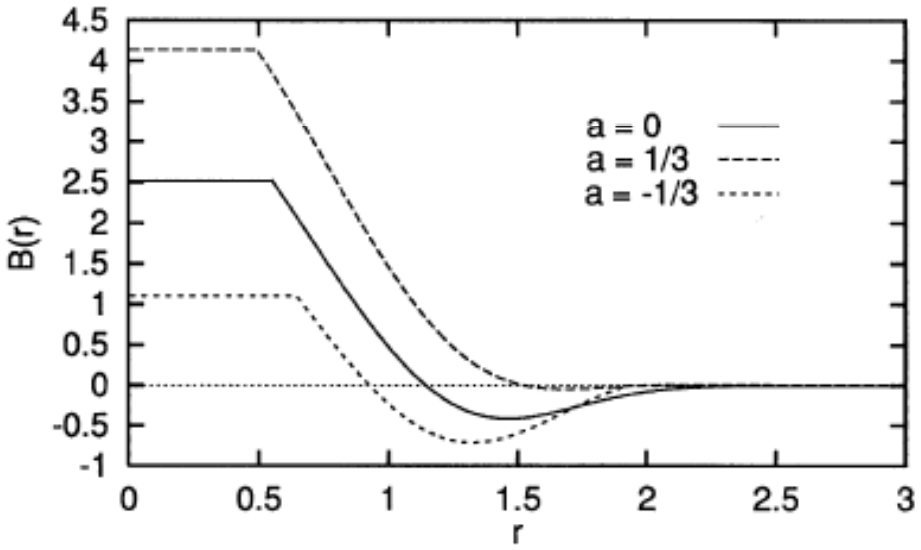


Fig.11 The magnetic field profiles as functions of the $B(r)[\Omega_z(r)\,\omega/\omega_e^2]$ dimensionless radius $r[= r/R]$ for different initial densities $N_0(r) = 1 + ar^2[a = R^2/L^2]$. Pulse intensity in the channel: $I = 4 \cdot 10^{20}\, W/cm^2$, $n_{00} = 10^{20} - 10^{21} cm^{-3}$ $(\omega_e/\omega = 0.07 - 0.24)$.

Thus, a strong electron density inhomogeneity is profitable to generate immense magnetic field strengths but at the same time it would be better to provide this inhomogeneity

in a wide region of the beam propagation area. Remembering that for an initially convex density distribution plasma less energy is required to drive the self-focusing (and the more energy of the incident pulse is trapped in the channel) than in the homogeneous plasma (see the results obtained by Bonnaud et al. [194], we conclude that such plasma have advantages also in obtaining higher values of generated QSM fields in the channel.

In the present study, applying the correct formalism found in our previous paper [191], we have shown the possibility of quasistationary magnetic field generation by spatially uniform circularly polarized laser radiation in initially strongly inhomogeneous underdense plasma. We conclude that the only source of magnetic field generation is the low frequency drag current induced due to the plasma inhomogeneity (given initially or produced by the ponderomotive force of the incident wave). The advantage of a convex initial density profile compared to a concave one (or to a homogeneous plasma) to generate huge magnetic fields ($\sim$ 200 MG and greater) in the self-focusing regime by the currently available intense laser pulses is found.

### 2.5.3 On the Generation of Generalized Vorticity and Quasi–static Magnetic Fields In Dissipative Plasmas

As discussed above, the self–generated magnetic fields in laser–produced plasmas are induced by a variety of mechanisms depending on both the laser and plasma characteristics (see e.g. [177, 191, 192, 195, 196, 197] and references therein). Recently, ultrahigh self–generated magnetic fields have been revealed in experiments [198] and in numerical simulation [190]. Also the work on QSM field generation due to Inverse Faraday (IF) effect was performed in dissipative isotropic plasma by a hydrodynamic approach. There are several reasons why dissipative processes and the relativistic increase in electron mass caused by an intense EM field should be taken into account when studying the QSM field generation problem. Most of them are based on the observational evidence of the dependence of plasma heating and particle acceleration processes on the self–consistent

processes of QSM field generation in both the plasma confinement experiments and astrophysical environments. In this study we concentrate on the circularly polarized pulses for which QSM fields should appear due to the inverse Faraday effect. The mechanism (see [174]) of excitation is the rotation of the polarization vector of the external radiation. Then plasma in a very strong circularly polarized field of laser radiation exhibits some features of a magnetized plasma which lead to the creation of average magnetization current – the sum of circular electron currents in inhomogeneous (given initially or created due to the ponderomotive effects) infinite under–dense plasma; this low frequency (LF) drag current itself represents the source of the QSM field. We now develop further the QSM field generation theory [191] with account of dissipation.

We start with the equations for the collissional un–magnetized relativistic plasma embedded in the strong electromagnetic field [199] (where $\mathbf{p}$ is the electron momentum, $n$ – electron density and ions are assumed immobile with density $n_0$):

$$\frac{\partial \mathbf{p}}{\partial t} + mc^2 \nabla\gamma = e\mathbf{E} + \frac{\mathbf{p}}{\gamma} \times \mathbf{\Omega} + \mathbf{f}, \tag{2.103}$$

$$\frac{\partial n}{\partial t} + \nabla \left( \frac{\mathbf{p}}{m\gamma} \cdot n \right) = 0, \tag{2.104}$$

where ($\nu = \nu(\mathbf{r})$ is the collision frequency):

$$\mathbf{f} = -\nu \mathbf{p}, \qquad \gamma = \left( 1 + \frac{\mathbf{p}^2}{m^2 c^2} \right)^{1/2} \tag{2.105}$$

and for generalized vorticity $\mathbf{\Omega} = \frac{e\mathsf{B}}{mc} + \frac{1}{m} \nabla \times \mathbf{p}$ we have the relation:

$$\frac{\partial \mathbf{\Omega}}{\partial t} = \nabla \times \left[ \frac{\mathbf{p}}{m\gamma} \times \mathbf{\Omega} \right] + \frac{1}{m} \nabla \times \mathbf{f} \tag{2.106}$$

that describes the nonlinear interaction of vortices (and generation of magnetic fields). In non–dissipative plasma generalized vorticity is conserved ($\mathbf{\Omega}(t) = 0$ everywhere) .

We take $\mathbf{f}(t=0) \neq 0$ . From Maxwell equations and the equations of motion we get:

$$\nabla \times \nabla \times \mathbf{p} + \frac{1}{c^2}\frac{\partial^2}{\partial t^2}\mathbf{p} + m\frac{\partial}{\partial t}\nabla\gamma + \frac{{\omega_p}^2}{c^2}\frac{n}{n_0}\frac{\mathbf{p}}{\gamma} = m\nabla \times \mathbf{\Omega} + \frac{1}{c}\frac{\partial}{\partial t}\left[\frac{\mathbf{p}}{\gamma} \times \mathbf{\Omega}\right] + \frac{1}{c}\frac{\partial}{\partial t}\mathbf{f}, \quad (2.107)$$

$$\frac{n}{n_0} = 1 + \frac{1}{m\omega_p^2} div(e\mathbf{E}) = 1 + \frac{1}{m\omega_p^2}\left[\left(\frac{\partial}{\partial t} + \nu\right)\nabla \cdot \mathbf{p} + mc^2\Delta\gamma - \nabla \cdot \left(\frac{\mathbf{p}}{\gamma} \times \mathbf{\Omega}\right)\right] \quad (2.108)$$

and representing all $A(\mathbf{E}, \mathbf{B}, \mathbf{\Omega}, \mathbf{p}, n)$ as $A =< A > +\tilde{A}$ in the presence of transverse field: $\tilde{\mathbf{E}} = \frac{1}{2}\tilde{\mathbf{E}}_\perp(\mathbf{r}, t)e^{-i\omega t} + c.c.$ ($\tilde{\mathbf{E}}_{||} \ll \tilde{\mathbf{E}}_\perp$; $k_0 \sim \nabla_{||} \gg \nabla_\perp \sim L^{-1}$ and $< \gamma > \simeq \gamma$ for c.p. radiation; $\mathbf{F}_E \equiv \gamma^{-1} < \tilde{\mathbf{p}} \times \tilde{\mathbf{\Omega}} >$) we arrive to following relations:

$$\frac{\partial < \mathbf{\Omega} >}{\partial t} = \nabla \times \left[\frac{< \mathbf{p} >}{m\gamma} \times < \mathbf{\Omega} >\right] + \frac{1}{m}\nabla \times < \mathbf{f} > + \frac{1}{m}\nabla \times \mathbf{F}_E \ . \quad (2.109)$$

Note that for c.p. radiation the last term in Eq.(2.108) has LF part only (there is no generation of harmonics). For the fast components we have:

$$\frac{\partial\tilde{\mathbf{\Omega}}}{\partial t} = \frac{1}{m}\nabla \times \tilde{\mathbf{f}} \ , \qquad \frac{\partial\tilde{\mathbf{p}}}{\partial t} = e\tilde{\mathbf{E}} + \tilde{\mathbf{f}}. \quad (2.110)$$

In general theory there are the fastly and slowly varying collision frequencies and $\nu_h \neq \nu_s$. We will ignore this effect since for our case $\gamma \gg 1$. Then $< \mathbf{f} >= -\nu < \mathbf{p} >$, $\tilde{\mathbf{f}} = -\nu\tilde{\mathbf{p}}$. From Eq.-s (2.107),(2.108) one gets the following relations (to the lowest order):

$$\left(\frac{\partial^2}{\partial t^2} - \nu^2\right)\tilde{\mathbf{p}} = e\left(\frac{\partial}{\partial t} - \nu\right)\tilde{\mathbf{E}} \ , \qquad \frac{\tilde{n}}{n_0} = \frac{1}{m\omega_p^2}\left(\frac{\partial}{\partial t} + \nu\right)\nabla \cdot \tilde{\mathbf{p}}. \quad (2.111)$$

Now we have to find correctly the expression for $\tilde{n}$. Following [191], taking *div* of the Eq.(2.107) we get: $\nabla \cdot \tilde{\mathbf{p}} \sim (\mathrm{Re}\,\epsilon)^{-1}\tilde{\mathbf{p}} \cdot \nabla(\mathrm{Re}\,\epsilon)$ , where $\mathrm{Re}\,\epsilon = 1 - \omega_p^2 < n > /[n_0\gamma\,(\omega^2 + \nu^2)]$. Then the drag current: $\mathbf{j}_E =< \tilde{n}\,\tilde{\mathbf{p}} > e/m\gamma$ can be found as:

$$\mathbf{j}_E = \frac{e}{m\gamma} < \tilde{n}\tilde{\mathbf{p}} >= \frac{e}{m\gamma\,(\omega^2 + \nu^2)} \ < \tilde{\mathbf{p}}\left[\left(\frac{\partial}{\partial t} + \nu\right)\tilde{\mathbf{p}}_\perp \cdot \nabla_\perp\left(\frac{< n >}{\gamma}\right)\right] > \quad (2.112)$$

with $\tilde{\mathbf{p}}$ calculated for collisional plasma. It is clear, that $\mathbf{j}_{||} \ll \mathbf{j}_\perp$ and drag current can

be responsible mainly for axial QSM field generation. As shown in [191, 192], without initial inhomogeneity external field has to be strong to create drag current via induced inhomogeneity. This is the manifestation of both ponderomotive and Faraday effects.

To find the influence of dissipation ($\mathbf{F}_E$ is absent in collisionless limit)we use Eq.(2.110):

$$\tilde{\mathbf{\Omega}} = -\frac{i}{m\omega}[(\nabla\nu(\mathbf{r}) \times \tilde{\mathbf{p}}) + \nu\nabla \times \tilde{\mathbf{p}}] \ , \tag{2.113}$$

$$\mathbf{F}_E = < \frac{\tilde{\mathbf{p}}}{\gamma} \times \tilde{\mathbf{\Omega}} > = -\frac{i}{m\omega\gamma}[< \tilde{\mathbf{p}} \times (\nabla\nu(\mathbf{r}) \times \tilde{\mathbf{p}}) > + \nu < \tilde{\mathbf{p}} \times \nabla \times \tilde{\mathbf{p}} >]. \tag{2.114}$$

Thus, when $\nu \to 0$, $\tilde{\mathbf{\Omega}} \to 0$ and $\mathbf{F}_E \to 0$, $\mathbf{j}_E \to \mathbf{j}_{collisionless}$. From the equations (2.109), (2.112) and (2.113) to the lowest order we derive, that $\tilde{\mathbf{\Omega}}_{||} \gg \tilde{\mathbf{\Omega}}_{\perp}$ and $\mathbf{F}_{E||} \gg \mathbf{F}_{E\perp}$, while $< \mathbf{\Omega}_{||} > \ll < \mathbf{\Omega}_{\perp} >$ $(\partial_z \ll \partial_x; \partial_y)$. After straightforward algebra, using $< \mathbf{\Omega}_{||} > \to 0$ and equations (2.107), (2.112) in stationary limit for the cylindrical geometry, the equations for the components of generated QSM field are derived (there is no $\phi$ dependence):

$$\frac{e}{c} < B_z > = -\frac{1}{r}\frac{\partial}{\partial r}\ r < p_\phi >; \tag{2.115}$$

$$\frac{1}{r}\frac{\partial}{\partial r}(r < B_\phi >) = \frac{\omega_p^2}{c^2}\ \frac{c}{e}\ \frac{< n >}{n_0}\frac{< p_z >}{\gamma} + \frac{4\pi}{c}\, j_{Ez}\ . \qquad (j_{Ez} \to 0) \tag{2.116}$$

The equations for $< p_\phi >$ and $< n >$ can be easily derived from the Eq.-s (2.107),(2.108) for steady state (to the lowest order):

$$\frac{1}{r}\frac{\partial}{\partial r} r \frac{\partial}{\partial r} < p_\phi > - \left(\frac{{\omega_p}^2}{c^2}\frac{< n >}{n_0\gamma} + \frac{1}{r^2}\right) < p_\phi > = \frac{\omega_p^2}{c^2}\, j_{E\phi}\ , \tag{2.117}$$

$$\frac{< n >}{n_0} = 1 + \frac{1}{m\omega_p^2}\left[mc^2\Delta\gamma - \nabla \cdot \mathbf{F}_E\right], \tag{2.118}$$

$$\text{where} \qquad j_{E\phi} \sim \frac{e}{m\omega}\frac{|\tilde{\mathbf{p}}_\perp|^2}{\gamma}\nabla_\perp\left(\frac{< n >}{\gamma}\right).$$

We need now to derive the equation for $< p_z >$. The $\phi$–component of Eq.(2.109) in

stationary case gives:

$$\frac{\partial}{\partial r}(< f_z > + F_{Ez} >) = 0. \tag{2.119}$$

Then, assuming that all fields vanish at $r \to \infty$, we have:

$$< p_z >= \frac{1}{\nu} < F_{Ez} > . \qquad ( \ \nu = const \quad \Rightarrow \quad F_{Ez} \sim \frac{\nu k_0}{2m\omega} \frac{|\tilde{\mathbf{p}}_\perp|^2}{\gamma} \ ) \tag{2.120}$$

And since $\tilde{\mathbf{p}} \sim \tilde{\mathbf{p}}_\perp$ $(\tilde{p}_z = k_0^{-1}\partial_r \tilde{p}_\perp)$ and $j_{Ez} \to 0$ , the axial component of QSM field $< B_z >$ is defined by $< j_{E\phi} >$ only (exactly as it is in non–dissipative plasma) while azimuthal component of QSM field is completely defined by dissipation (note, that for $\nu = const$ the latter is absorbed in final relation for $< B_\phi >$). Due to the existence of this $\phi$–component the QSM field is helice–type.

In conclusion, we have shown that since the generalized vorticity is not conserved in dissipative plasma there exists the rotational part of the LF force in addition to drag current. It is determined by the interaction of HF oscillations of plasma electrons and HF vorticity (present is such plasma). There exists also the axial component of this LF force that generates the quasi–static axial current. This current later becomes the source for azimuthal component of QSM field. Due to the existence of this component the structure of magnetic field represents the helices. This component is completely defined by the friction effect and exists even in weakly relativistic case. Hence, in such plasmas, for the generation of QSM fields there is no need in strong inhomogeneity (initially given or created by the strong relativistic laser pulse). The establishment of the helical structure of QSM field is fully determined by collision frequency and less sensitive to the scale of plasma inhomogeneity. The generated vortices of magnetic field may strongly influence the dynamics of both the laser field and electrons (e.g. leading to efficient acceleration of electrons) in the self–focusing regime.

# Chapter 3

# Acceleration of Plasma Flows and Their Escape Due to Magneto–Fluid Coupling

## 3.1 Background

In astrophysics (particularly in the physics of the solar atmosphere), plasma "flow" could be assigned at least two connotations: 1) The flow is a primary object whose dynamics bears critically on the phenomena under investigation. The problems of the formation and the original heating of the coronal structures, the creation of channels for particle escape, for instance, fall in this category, 2) The flow is a secondary feature of the system, possibly created as a by–product and/or used to drive or suppress an instability. Since the generation of flows which will eventually create the coronal structures [70, 72] is the theme of this effort, the flows here are fundamental.

By exploiting a simple two–fluid model in the solar context, several recent studies [67, 236] have revealed the breadth of phenomena made possible by the combined action of the flow–velocity and the magnetic fields. The flow–based approach will prove, perhaps, crucial in the study of solar corona, observationally found to be a highly dynamic

arena replete with multiple–scale spatiotemporal structures (Aschwanden *et al.* 2001a); the approach gains immense credibility with the discovery that strong flows are found everywhere – in the subcoronal (chromosphere) as well as in the coronal regions (see e.g. [1, 140, 200, 201, 247, 232, 207, 202] and references therein). Recent phenomenology strongly emphasizes that the solar atmosphere is an extremely inhomogeneous (in all parameters) area in which small– and large–scale closed magnetic field structures with different temperatures co–exist in nearby regions. For example, two-temperature coronal models constructed from *SOHO/EIT* observations indicate complicated magnetic topology and fine–scale structuring of corona (including Coronal Holes) [234, 203]. It is also clear that the mechanisms for energy transport and channeling of particles in Solar atmosphere are deeply connected with the challenging and exciting problems of the solar coronal heating and of the origin of the solar wind (SW) [233].

Exploring the mechanisms for flow–generation is the main theme of this study. We begin, however, by presenting illustrative examples for the evidence/speculation on the existence of flows, as well as their possible role in the processes taking place in the solar vicinity:

1) Goodman (2001) has shown that the mechanism which transports mechanical energy from the convection zone to the chromosphere (to sustain its heating rate) could also supply the energy needed to heat the corona, and accelerate the SW. The coronal heating problem, hence, is shifted to the problem of the dynamic energization of the chromosphere. In the latter process the role of flows is found to be critical as warranted by the following observations made in soft X–rays and extreme ultraviolet (EUV) wavelengths, and recent findings from the *Transition Region and Coronal Explorer (TRACE)*: the over–density of coronal loops, the chromospheric up–flows of heated plasma, and the localization of the heating function in the lower corona (Schrijver, *et al.* 1999; Aschwanden *et al.* 2001a; Aschwanden 2001b).

2) The connection/coupling of transient events like up–flows and different types of jet–like structures to the photosphere dynamics was reported in numerous studies (see e.g.

[246] and references in). In [210] it was demonstrated that the eruption of a coronal mass ejection is triggered from the low solar atmosphere (photosphere/chromosphere) as seen in TRACE $1600 A^o$ images and with SOHO Michelson Doppler Imager. The data of this latest research favor the idea that the rapid ejection may be attributed to a catastrophic loss of MHD equilibrium. The process takes place in 3 important stages - a relatively stable equilibrium, a loss (fast, impulsive) stage, and the final rapid eruption (associated with substantive changes in the photospheric magnetic flux and white–light morphology). The results of [226] suggest a strong coupling between magnetic fields and the convective processes that pervade the solar photosphere. The correlation between photospheric shear flows and flares is also reported in [235]; several current models suggest that the former can be responsible for the energy build up in the flares.

3) In [217], the authors report on the low coronal signatures of major solar energetic particle (SEP) events focusing on flare–associated motions (observed in soft X–rays). It was underlined that these motions may provide an important link between small–scale energy release and large–scale explosive events; the existence of a continuum of acceleration timescales was also pointed out. In [211] the detailed investigation of the dynamical behavior of the emerging magnetic flux was carried out ( using three–dimensional MHD numerical simulation) to show that the flux-emergence generates not only vertical but also horizontal flows in the photosphere; both of these components contribute to the injection of the magnetic energy and helicity. The contributions of vertical flows are dominant in the early phase while horizontal flows become a dominant in later stages. In [206] it was shown that solar corona is mainly heated by the magnetic activity in the edges of the network flux clumps that are observed to be riddled with the fine-scale explosive events. They present that: (1) at the edges of the network flow clumps there are many transient sheared-core bipoles of the size and lifetime of granules and having transverse field strengths greater than $\sim 100\, G$, (2) $\sim 30$ of these bipoles are present per supergranule, and (3) most spicules are produced by explosions of these bipoles.

Recent observations also suggest that the energy for coronal heating is very likely

a by–product of the outflow of heat from Sun's interior through the convection zone. The convection zone acts as a heat engine, converting some of the thermal energy into mechanical and magnetic energy; some of this energy (mechanical and magnetic ) enters the corona, and finally dissipates into heat. There are only two obvious energy sources that could power significant flow generation in the chromosphere: the magnetic field (both large scale and short–scale including turbulence), and the thermal pressure of the plasma. The main message then, is that in order to solve the coronal heating problem, the inclusion of processes taking place in the chromosphere and the transition region may be essential. One must carefully study the march of the primary flow as it passes through specific regions of the solar atmosphere populated by ambient magnetic field structures of varying scale lengths. In short, the dynamics of the flow must be thoroughly understood.

Finding sources and mechanisms for the creation of flows has been an active industry for some time. Catastrophic models of flow production in which the magnetic energy is suddenly converted into bulk kinetic energy (and thermal energy) are rather well–known; various forms of magnetic reconnection (flares, micro and nano–flares) schemes permeate the literature (E.g. (Wilhelm 2001; Christopoilou, Georgakilas and Koutchmy 2001) for chromosphere up–flow generations). A few other mechanisms of this genre also exist: Uchida *et al.* (2001) proposed that the major part of the supply of energy and mass to the active regions of the corona may come from a dynamical leakage of magnetic twists produced in the sub-photospheric convection layer; Ohsaki *et al.* (2001, 2002) have shown how a slowly evolving closed structure (modelled as a double–Beltrami two–fluid equilibrium) may experience, under appropriate conditions, a sudden loss of equilibrium with the initial magnetic energy appearing as the mass flow energy. Another mechanism, based on loop interactions and fragmentations and explaining the formation of loop threads, was given in Sakai and Furusawa (2002); the suggestion based on cascade of shock wave interactions was made in [246]. A more quasi–static mechanism for flow generation in sub–coronal regions taking into account the density in–homogeneity of the structures was given in [240]. Mahajan *et al.* (2005) have recently proposed and explored

the "Reverse-Dynamo" mechanism– the amplification/generation of plasma flows by micro scale (turbulent) magnetic fields via the magneto-fluid coupling enhanced by the Hall effect [214]. The basic result is that macroscopic magnetic fields and flows are generated simultaneously and proportionately from microscopic turbulence (magnetic and kinetic). The mechanisms based on the wave–energy transformation and instabilities can be operative at later stages of the flow evolution; these mechanisms could have additional importance for acceleration [220].

Our investigations on flow acceleration/generation in the Solar atmosphere are based on the dynamical two–fluid model suggested in [72]. We find that the acceleration process unfolds in two distinct stages: an extremely fast stage (right at the lower chromosphere heights) giving rise to a significant flow acceleration followed by a quasi–static stage in which the newly created fast flows are further accelerated via the magnetofluid coupling (by the Reverse Dynamo mechanism, perhaps). The detailed nature of the accelerated flows is found to depend on the initial and boundary conditions.

The main results of this chapter are published in Refs.[70]-[71],[212-214],[240-241].

## 3.2 Dynamical Acceleration of Plasma Flows interacting with arcade-like ambient magnetic fields - applications for the Solar Atmosphere

In the simplified two–fluid model used here, the plasma is quasi–neutral — electron and proton number densities are nearly equal: $n_e \simeq n_i = n$ ($\nabla \cdot \mathbf{j} = 0$), but the electron and the proton flow velocities are allowed to be different. Neglecting electron inertia the ion ( electron) velocity is approximately $V_i = V$ ( $V_e = (V - j/en)$). We assign equal temperatures to the two specie so that the kinetic pressure $p$ is given by: $p = p_i + p_e \simeq 2\,nT$, $T = T_i \simeq T_e$. The analysis can be readily extended to the more realistic case of unequal temperatures [215, 229, 230]. We understand that, when solving the solar wind problem, one should use the multi–fluid, multi–dimensional descriptions (see e.g. [229, 230, 209] and references therein). We believe, however, that the essential physics of acceleration of the primary flow can be captured within the relatively simple basic two-fluid model. Very near the photospheric surface, the influence of neutrals and ionization (and processes of flux emergence etc.) would be out side the scope of the two–fluid approach. A little farther distance down stream ($\Delta r \geq 500\,\mathrm{km}$), however, we expect that there exist fully ionized and magnetized plasma structures such that the dynamical two–fluid model will constitute an adequate description.

The dimensionless two–fluid equations describing the flow–field interaction processes can be read off from (Mahajan *et al.* 1999, 2001):

$$\frac{\partial}{\partial t}\mathbf{V} + (\mathbf{V}\cdot\nabla)\mathbf{V} = \frac{1}{n}\nabla\times\mathbf{b}\times\mathbf{b} - \beta_0\,\frac{1}{n}\nabla(nT) + \nabla\left(\frac{r_{A0}}{r}\right) + \nu_i(n,T)\left(\nabla^2\mathbf{V} + \frac{1}{3}\nabla(\nabla\cdot\mathbf{V})\right), \tag{3.1}$$

$$\frac{\partial}{\partial t}\mathbf{b} - \nabla\times\left(\mathbf{V} - \frac{\alpha_0}{n}\,\nabla\times\mathbf{b}\right)\times\mathbf{b} = \alpha_0\,\beta_0\,\nabla\left(\frac{1}{n}\right)\times\nabla(nT), \tag{3.2}$$

$$\nabla\cdot\mathbf{b} = 0, \tag{3.3}$$

$$\frac{\partial}{\partial t}n + \nabla\cdot n\mathbf{V} = 0, \tag{3.4}$$

$$\frac{3}{2}n\frac{d}{dt}(2T)+\nabla(\mathbf{q}_i+\mathbf{q}_e) = -2nT\nabla\cdot\mathbf{V}+2\beta_0^{-1}\,\nu_i(n,T)\,n\left[\frac{1}{2}\left(\frac{\partial V_k}{\partial x_l}+\frac{\partial V_l}{\partial x_k}\right)^2-\frac{2}{3}\left(\nabla\cdot\mathbf{V}\right)^2\right] +\frac{5}{2}\alpha_0\left(\nabla\times\mathbf{b}\right)\cdot\nabla T-\frac{\alpha_0}{n}\left(\nabla\times\mathbf{b}\right)\nabla(nT)+E_H-E_R. \qquad (3.5)$$

where the notation is standard with the following normalizations: the density $n$ to $n_0$ at some appropriate distance from the solar surface, the magnetic field to the ambient field strength at the same distance, and velocities to the Alfvén velocity $V_{A0}$. The parameters $r_{A0}=GM_\odot/V_{A0}^2R_\odot=2\beta_0/r_{c0},\ \alpha_0=\lambda_{i0}/R_\odot,\ \beta_0=c_{s0}^2/V_{A0}^2$ are defined with $n_0,\ T_0,\ B_0$. Here $c_{s0}=\sqrt{2T_0/m_i}$ is the sound speed, $R_\odot$ is the solar radius, $r_{c0}=GM_\odot/2c_{s0}^2R_\odot$, $\lambda_{i0}=c/\omega_{i0}$ is the collisionless ion–skin depth, $\nu_i(n,T)$ is the ion kinematic viscosity, $q_e$ ( $q_i$) is the dimensionless electron ( ion) heat flux densities, $E_H$ is the local mechanical heating function and $E_R$ is the total radiative loss. We note that the full viscosity tensor relevant to a magnetized plasma is rather cumbersome, and we do not display it here. Just to have a feel for the importance of spatial variation in viscous dissipation, we display its relatively simple symmetric form. It is to be clearly understood that this version is meant only for theoretical elucidation and not for detailed simulation. We also note that in general, the Hall current contributions are expected to become significant when the dimensionless Hall coefficient $\alpha_0$ satisfies $\alpha_0>\eta$, where $\eta$ is the inverse Lundquist number for the plasma. For a typical coronal plasma as well as for plasmas in the low chromosphere and transition region (TR) this condition is easily satisfied ($\alpha_0$ is in the range $10^{-10}-10^{-7}$ for densities within $(10^{14}-10^{8})\,cm^{-3}$ and $\eta=c^2/(4\pi V_{A0}R_\odot\sigma)\sim10^{-14}$, where $\sigma$ is the plasma conductivity).

To establish the relevant parameter regime for simulation, we resort to recent observational data (e.g. [120, 200, 224] and references therein). At $\sim(500-5000)\,km$, the observations yield the average plasma density and temperature to be respectively $n\sim(10^{14}-10^{11})\mathrm{cm}^{-3}$ , and $T\sim(1-6)\,\mathrm{eV}$. For simplicity, we have assumed $T_e=T_i=T$.

The information about the magnetic field is hard to extract due to the low sensitivity and lack of high spatial resolution of the measurements. The inhomogeneity and co–

existence of small– and large–scale structures with different temperatures, (observational evidence of small scale mixtures of weak and strong fields [228]) in nearby regions makes the task even harder. The observation of pixel–to–pixel variations in the magnetic field indicates that small–scale (sub–pixel) distribution of fields changes considerably at larger spatial scales [225, 227]. At these distances we have different values for the network and for the internetwork fields: (i) The *network* plasmas have typically *short-scale* fields in the range $B_0 \sim (700 - 1500)$ G, and have more or less $n \sim const$ . (ii) The *internetwork fields* are generally weaker (with some exceptions [224]) — $B_o \leq 500$ G, and are embedded in *larger–scale plasma structures* with $n \neq const$ . For different classes of magnetic field structures, different physical processes may be dominant.

In our investigation we shall assume that the processes that generate the primary flows and the primary solar magnetic fields are independent. The plasma flows begin to interact with the ambient field at time t=0. The choice of initial conditions for our numerical work is guided by the observational evidence presented in the introduction. Our approach is consistent with that of Woo, Habbal and Feldman (2004) who have argued that the flow of the solar wind is influenced by the closed field structures stressing the self–consistent process of acceleration and trapping/heating of plasma particles in the finely structured atmosphere. We will dwell, in this study, on the representative problem of the trapping and acceleration of the primary flow impinging on a single closed-line structure. The simulation was performed for a variety of initial and boundary conditions and essential aspects of the typical results will be presented below.

The general set of Eqs. (3.1–3.5) was solved numerically in Cartesian Geometry for 2.5 Dimensions ($\partial_y = 0$). Note that the 2.5D Cartesian nature of our code does not allow us to explore large distances from the surface due to interference with the boundaries.

Fortunately that does not translate into a serious shortcoming because much of the action is found to be limited to regions very close to the surface; the simulation results, therefore, are quite trustworthy in the revelation of the basic processes of interest. In carrying out the simulations an important assumption was made: the diffusion time of magnetic field is longer than the duration of the interaction process (the Hall term is important in the parameter range relevant to this study).

A short summary of our numerical methods is in order:
We use the 2.5D version of Lax–Wendroff finite difference numerical scheme along with applying the Flux–Corrected–Transport procedure [222, 58]. The predictor–corrector type of approximation was used. Equation (3.3) was replaced by its equivalent for the y–component of the vector potential to ensure the divergence–free property of the magnetic field. The equation of heat conduction was treated separately by the alternate direction implicit method with iterations. Transport coefficients for heat conduction and viscosity are taken from Braginski, 1965. Our estimates show that the magnetic field doesn't develop components with sufficient microscopic fluctuations to make the diffusion term important. Also, the force term in Eq.(3.2) is very small and there was no need to use numerical resistivity in the code. The numerical viscosity was still included as an aid for smoothing. For the main goal of the present study, (to show the fast acceleration low in the atmosphere) these assumptions seem to be satisfactory. Resistivity will be included in a later more comprehensive work.

Observations reveal that the radiation losses ($\sim n^2$ and, hence, different for the different regions and strongly varying in time dynamical parameter) form the dominant part of energy loss from the solar atmosphere that is optically very thin. Radiation losses are strongly dependent on gas composition, and the accuracy of the atomic physics parameters as well as the values of the relative elemental abundances. "In general, the effect of including the process of dielectronic recombination and using more accurate cross sections is not very large" on radiative loss estimates [60]. In [204] for a collisionally ionized plasma at equilibrium it is found that "for $T < 2.5 \cdot 10^4$K and low densities

($< 10^4 cm^{-3}$), forbidden and semi-forbidden coefficients dominate the cooling. At higher densities ($> 10^8\, cm^{-3}$), much of the forbidden-line radiation is suppressed". In [221] it is emphasized that "below $3 \cdot 10^4$ K temperature plasma (due to hydrogen collisional excitation peak) the forbidden-line cooling coefficient is strongly density and model dependent". Drawing from this wealth of information, we believe that for the parameters of interest, the $E_R$ term in the code could be simply approximated by Bremsstrahlung radiation [72]. We use a somewhat modified formula assuming it to be 2 times greater, $E_R = 2 \cdot E_{Br} = 2 \cdot 1.69 \cdot 10^{-25} \cdot n^2 \cdot T^{1/2} \cdot Z^3\, erg/cm^3\, s,\ (Z = 1)$. Since we were exploring a particular and inherent heating mechanism , no external heating source $E_H$ was needed. A numerical mesh of $280 \times 220$ points was used for computation. The corresponding scheme is characterized by second order accuracy with respect to the chosen grid.

Latest observations support the idea that the coronal material is injected discontinuously (in pulses or bunches, for example) from lower altitudes into the regions of interest (e.g., spicules, jet–like structures). We now follow the dynamical trajectory of such a flow (spatially and temporally localized, initially a Gaussian, Fig.-s 3.1; 3.3) as it enters a region nested with arcade–like closed field line structures with varying scales.

For better visualization of the results we take the symmetric case. The flow is assumed to be initially weak ($|\mathbf{V}|_{0max} \ll C_{s0}$). The initial ambient magnetic field was modelled as a single 2D arcade with circular field lines in the $x$–$z$ plane (Fig.3.2 for the vector potential/flux function). The arcade field attains its maximum value $B_{max}(x_o, z = 0) \equiv B_{0z}$ at $x_0$ at its center, and is a decreasing function of the height $z$ (radial direction). This field was assumed to be initially uniform in time. When doing so, we choose the parameters to satisfy the observational constraint that, over a period of some tens of minutes, the location of the trapping/acceleration must have a relatively smooth evolution. The final shape and location of the structure of the associated $\mathbf{B}(\mathbf{r}, t)$, for example will be naturally defined by its material source, by the process dynamics, and by the initial field $\mathbf{B_0}(\mathbf{r}, t)$. We use the following representation for the magnetic field:

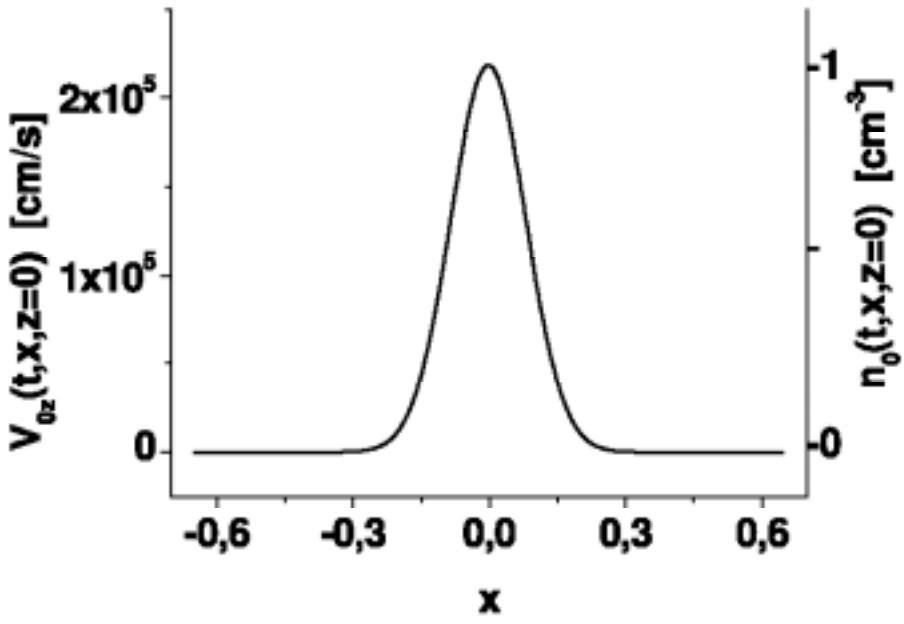


Figure 3-1: Initial symmetric profiles of the radial velocity $V_z$, and density $n$. The respective maxima (at $x$=0) are $\sim 2\,km/s$ and $10^{12}\,cm^{-3}$ .

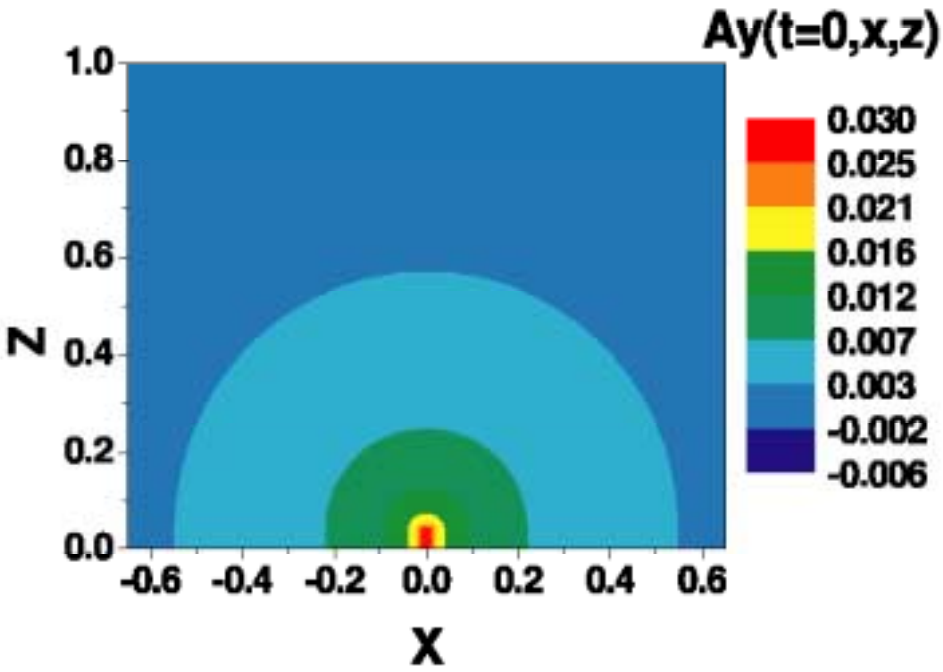


Figure 3-2: Contour plots for the $y$– component of vector potential $A$ (flux function) in the $x-z$ plane for a typical ambient arcade–like solar magnetic field (initial distribution). The field has a maximum $B_{max}(x_0 = 0, z_0 = 0) = 100\,\mathrm{G}$ .

$\mathbf{B} = \boldsymbol{\nabla} \times \mathbf{A} + B_z\,\hat{\mathbf{z}}$ and for the given geometry $\mathbf{A}(0; A_y; 0)$; $\mathbf{b} = \mathbf{B}/B_{0z}$; $b_x(t, x, z \neq 0) \neq 0$. From numerous runs on the flow–field evolution, we have chosen to display pictorially the results corresponding to the following initial and boundary conditions: $B_{0z} = 100\,G$, the flow parameters: are $V_{max}(x_o, z = 0) = V_{0z} = 2.18 \cdot 10^5\,cm/s$; $n_{0max} = 10^{12}\,cm^{-3}$; $T(x, z = 0) = const = T_0 = \mathbf{3}\,eV$. The background plasma density is $n_{bg} = 0.2 n_{0max}$. In simulations, the initial density ratio $n(x, z, t = 0) = n/n_{0max}$ is an exponentially decreasing function of $z$. Experienced gained from numerous runs taught us that the processes under study are localized within a small area of interaction. As a result we are able to settle on the following boundary condition, $\partial_x(x = \pm\infty, z, t) = 0$ which was used with sufficiently high accuracy for all parameters $(\mathbf{A}, T, \mathbf{V}, \mathbf{B}, n)$ .

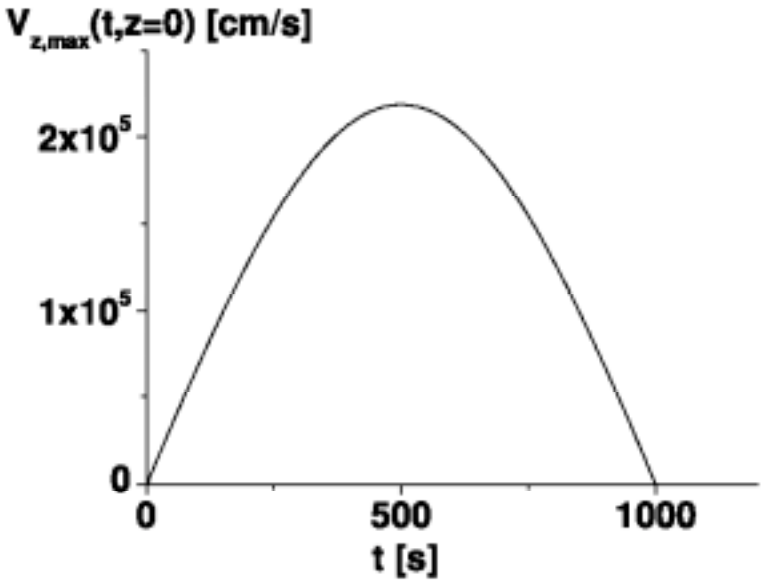


Figure 3-3: The original pulse is limited in time. A time plot of $V_{z,max}(t, z = 0)$ corresponding to the shape $V_z(t, z = 0) = V_{0z}\, sin(\pi t/t_0)$; $V_z(t > t_0) = 0$. The parameter $t_0$ (1000 s for this pulse) can be interpreted as the "life–time" of the pulse.

Observations further guided us to assume that the initial velocity field has a pulse–like distribution (Fig.3.3) with a time duration (life–time) $t_0$ & $50\, s$.

To illustrate the acceleration of initial flows (extremely weak), we have modelled several cases with different initial and boundary conditions. The dynamical picture is strongly dependent on the relative strengths of the initial flow pressure and the magnetic field strength.

Our typical representative example is the evolution of a symmetric weak up–flow with its peak located in the central region of a single closed magnetic field structure (location of field maximum $B_{0z} = 100\, G$) (Figs.3.1-3.3). Figs. (3.4-3.8), in which we give the $x - z$ contour plots of all the relevant fields ($A_y$; $|\mathbf{b}|$; $n$; $|\mathbf{V}|$; $T$), contain the essence of the simulation. We find that the acceleration is significant in the vicinity of the field–maximum with strong deformation of field lines and energy re–distribution. In this

very region, the simulations show cooling of the flow with serious density redistribution: part of the flow is trapped in the maximum field localization area, accumulated, cooled and accelerated. The accelerated flow reaches & 100 km/s value in less than 100 s (in agreement with recent observations [246, 247, 1] and references therein). The accelerated flow is decoupled from the mother flow, and is localized in a distinguishable region with dimensions . $0.05\,R_s$ starting at a distance $\sim$ $0.01\,R_s$ from the interaction surface. The time for reaching the quasi–equilibrium parameters is determined by the initial and boundary conditions (this conclusion holds in general).

In a stationary analysis to be presented in the next sub–section, we will attempt to derive the characteristic steady state parameters (like the distance from the surface) of the simulated system.

Extensive simulation experiments show that, when viscosity and heat flux effects are included, the flow acceleration evolution parameters depend strongly on $\alpha_0$, the parameter measuring the strength of the Hall term in the two-fluid equations. A very interesting and far–reaching result is that the final parameters of the accelerated flow are practically independent of the initial flow–characteristics (Fig.-s 3.4-3.8); only the initial fast stage of acceleration up to $\sim 200\,km/s$ is slightly different for different life–time primary flows. Simulation results for 2 different initial life–times of the flow ($t_0 = 1000\,s$ – left panel and $t_0 = 100\,s$ – right panel in Fig.-s 3.4-3.8) illustrate this feature.

We also found that at some critical time, the solutions split into two parts; all fields, the magnetic (Fig.-s 3.4,3.5), the density (Fig.3.6), the velocity (Fig.3.7) and temperature (Fig.3.8) exhibit bifurcation. This process persists as initial conditions vary. In Fig.3.9, we give time evolution plots of the maximum values of all fields ($A_y,\ |\mathbf{b}|,\ b_p,\ b_z,\ n,\ |\mathbf{V}|,\ V_p,\ V_z,\ T$) for a pulse–like flow interacting with a single arcade–structure for different initial life–times ($t_0$) of the flow ($t_0 = 100\,s(black);\ t_0 =$

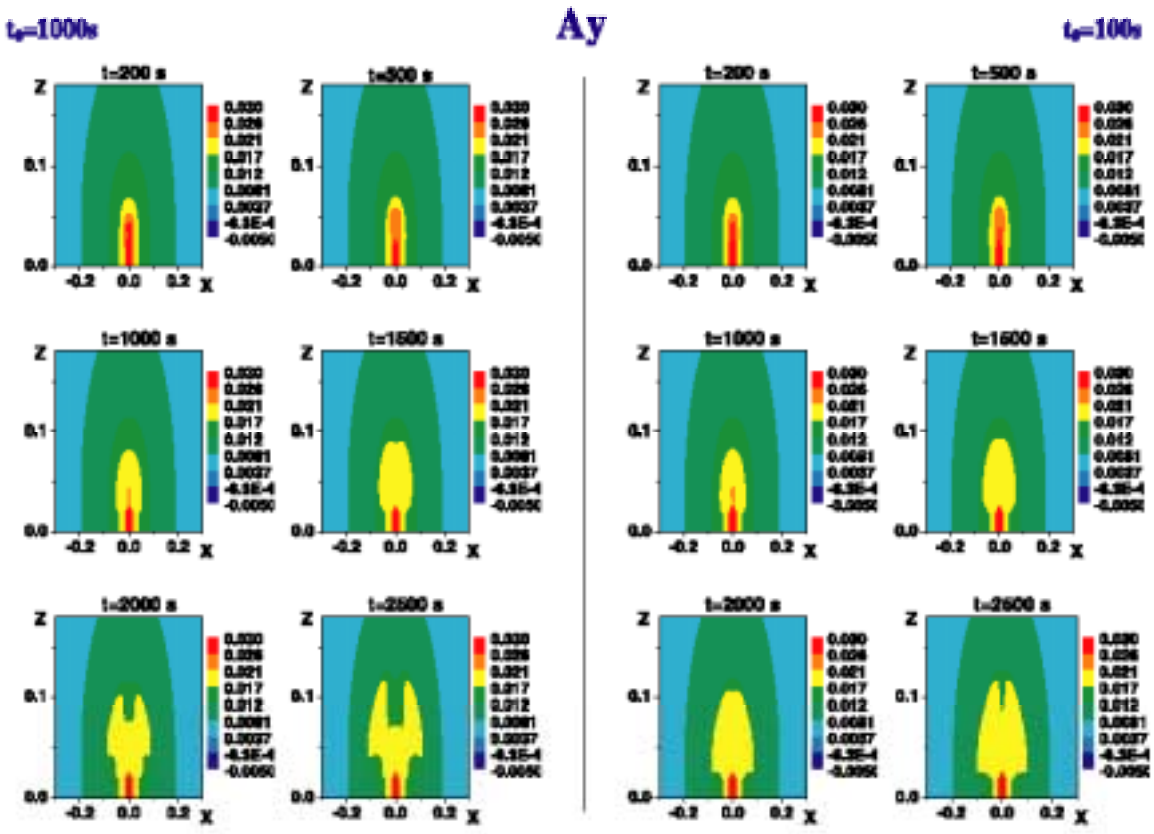


Figure 3-4: $x - z$ contour plots at various time–frames: $t = 200\,s$; $500\,s$; $1000\,s$; $1500\,s; 2000\,s$; $2500\,s$ for the dynamical evolution of $A_y$ for flows with two different initial life–times. The spatially and temporally inhomogeneous (type displayed in Fig.3.1, Fig.3.3) primary flows are accelerated as they make their way through the magnetic field with an arcade–like structure (Fig.3.2). The realistic viscosity and heat–flux effects as well as the Hall term ($\alpha_0 = 3.3 \cdot 10^{-10}$ realistic) are included in the simulation. Left panel corresponds to the case of initial flow life–time: $t_0 = 1000\,s$, right panel — for $t_0 = 100\,s$. There is a critical time ( . $1000\,s$) when the accelerated flow bifurcates in 2; the original arcade field is deformed correspondingly.

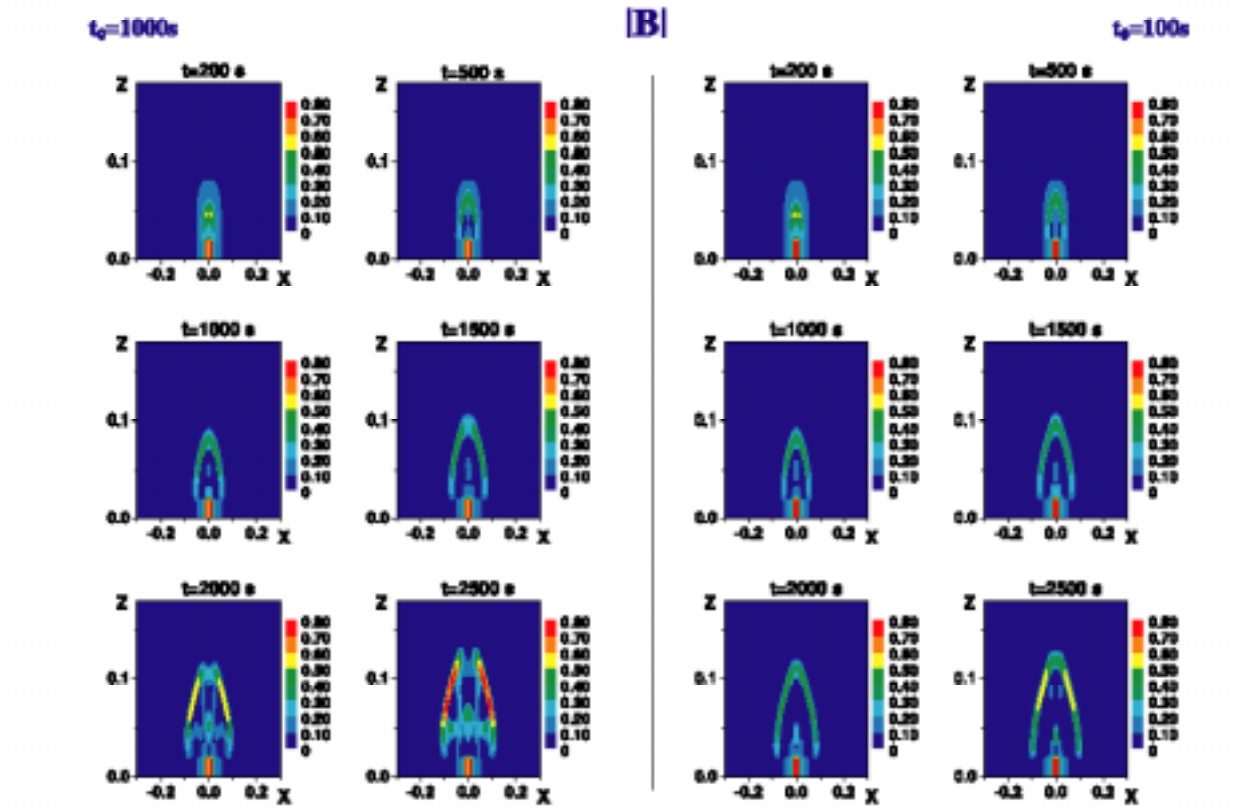


Figure 3-5: $x - z$ contour plots for the dynamical evolution of $|\mathbf{b}|$ exactly following the pattern of Fig.4. After the bifurcation (read caption of Fig.3.4), strong magnetic field localization areas, carrying currents, are created symmetrically about $x = 0$.

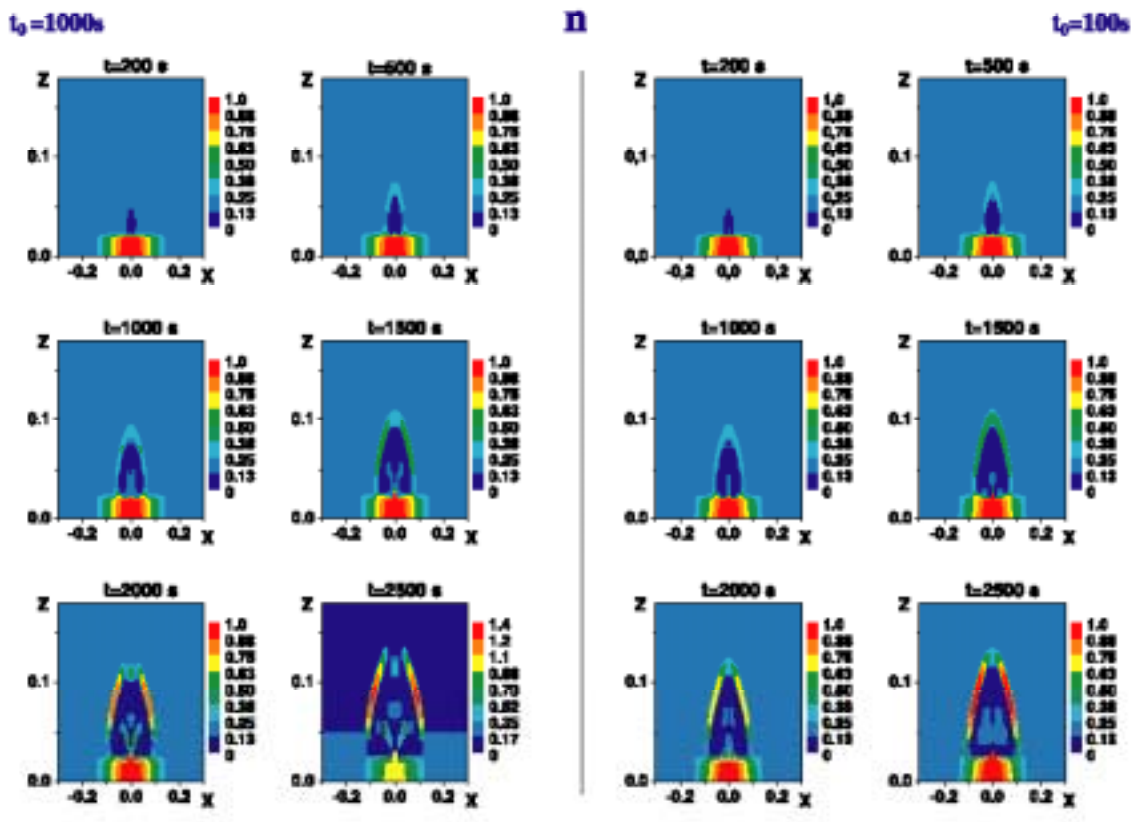


Figure 3-6: $x - z$ contour plots for dynamical evolution of density $n$ exactly following the pattern of Fig.3.4. Post–bifurcation daughter flows are localized in the newly created magnetic field localization areas. The maximum density of each daughter flow is of the order of the density of the mother–flow. Daughter–flows have distinguishable dimensions $\sim 0.05\, R_s$

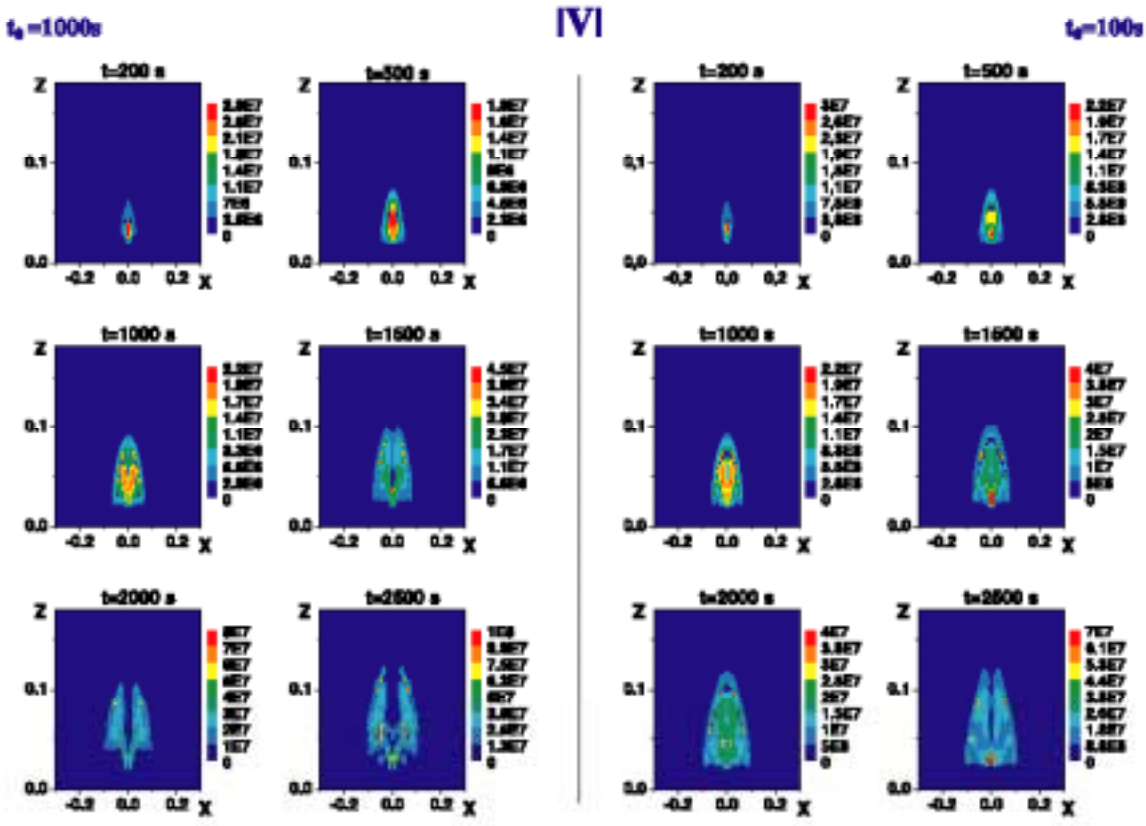


Figure 3-7: $x - z$ contour plots for the dynamical evolution of $|\mathbf{V}|$ exactly following the pattern of Fig.3.4. The initial flow, locally sub–Alfvénic, is accelerated reaching significant speeds (& 100 km/s) in a very short time (& 100 s). The effect is strong in the strong field region (center of the arcade). At $t$ & 1000 s, the velocities reach $\sim 500$ km/s or even greater ( . 800 km/s) values. The distance from surface where it happens is & 0.01 $R_s$ .

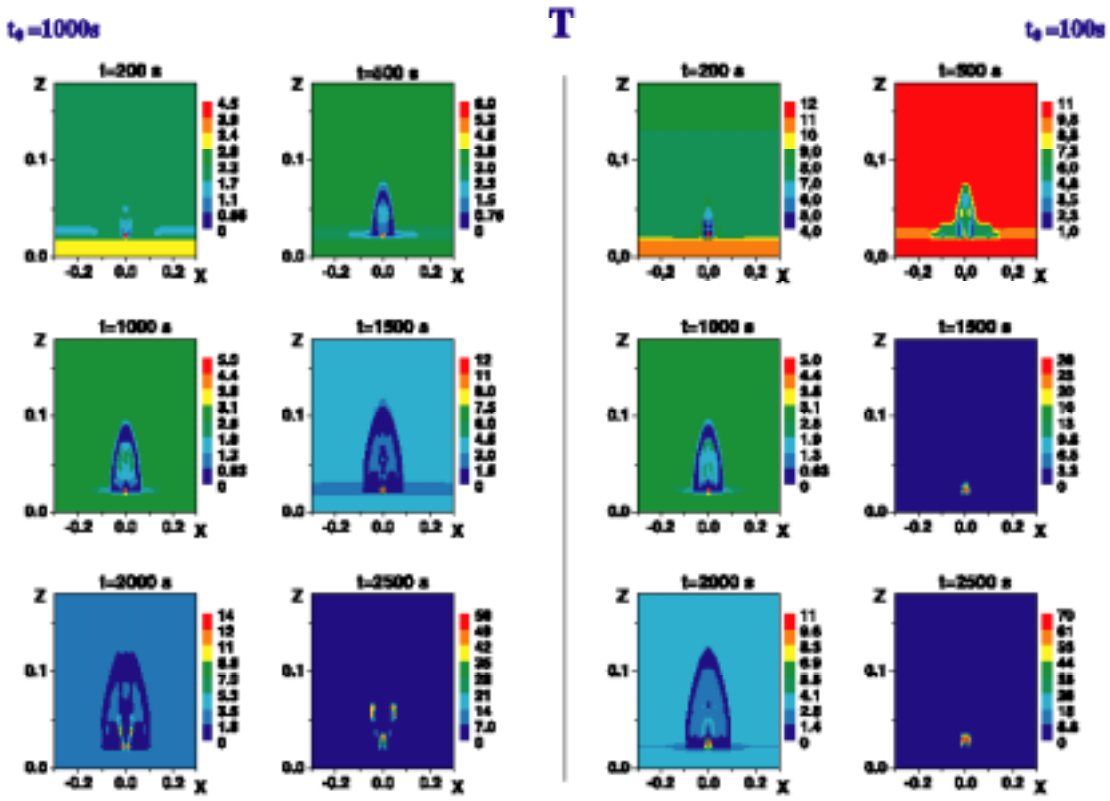


Figure 3-8: $x-z$ contour plots for dynamical evolution of temperature $T$ exactly following the pattern of Fig.3.4. In the regions of localization of the daughter flow the cooling is more significant compared to the nearby regions — the latter areas are heated.

$1000\,s(red);\ t_0 = 2000\,s(blue);\ t_0 \to \infty$ (green)). In Fig.3.10, the same maximum values of all fields are plotted versus the initial life–time ($t_0$) of the flow for different time–frames ($t = 200\,s(black);\ 500\,s(red);\ 1000\,s(blue);\ 1500\,s(green); 2000\,s(lightgreen);\ 2500\,s$ (rose)).

These pictures clearly demonstrate that the accelerated mother flow bifurcates into two separate, fast daughter–flows (after an initial acceleration stage) modifying significantly the original arcade structure. The characteristic fields undergo rather similar dynamics for flow pulses with different initial life–times. It should be emphasized that now the maxima of these parameters are localized not around the initial B–maximum but on both sides of it, and are shifted along height (in the localization areas of each accelerated daughter flow with newly created B–maxima and currents (the reason could be explained by RD mechanism [214]).

After the initial acceleration stage, the magnetic energy maxima remain practically unchanged up to some "blow–up" time ($\& \ 2000\,s$) at which the gradients become too steep and the simulation results cease to be meaningful. The same result holds for the maxima of the transverse and parallel magnetic field energies (with . 10% accuracy). For a given ambient field $\mathbf{b}_0(\boldsymbol{r}, t)$ and fixed $T_0(\beta_0)$ the spatial maximum of each parameter exhibits practically similar dynamics (independent of the initial flow life–time) reaching similar values as the critical time is approached. This picture persists for different initial $T_0(\beta_0)$ indicating the controlling effect of magnetic fields, and the robustness of the results (see Fig.3.11). Testing the conservation of total energy of the system as it evolves in time also shows that the simulation results can be trusted only up to the blow–up time; in its vicinity the energy conservation no longer holds. To study longer time dynamics, the code will need improvement.

At this stage of our work, we are not in a position to pinpoint the dominant mechanisms which restructure the magnetic field and impart energy to the flow; the standard

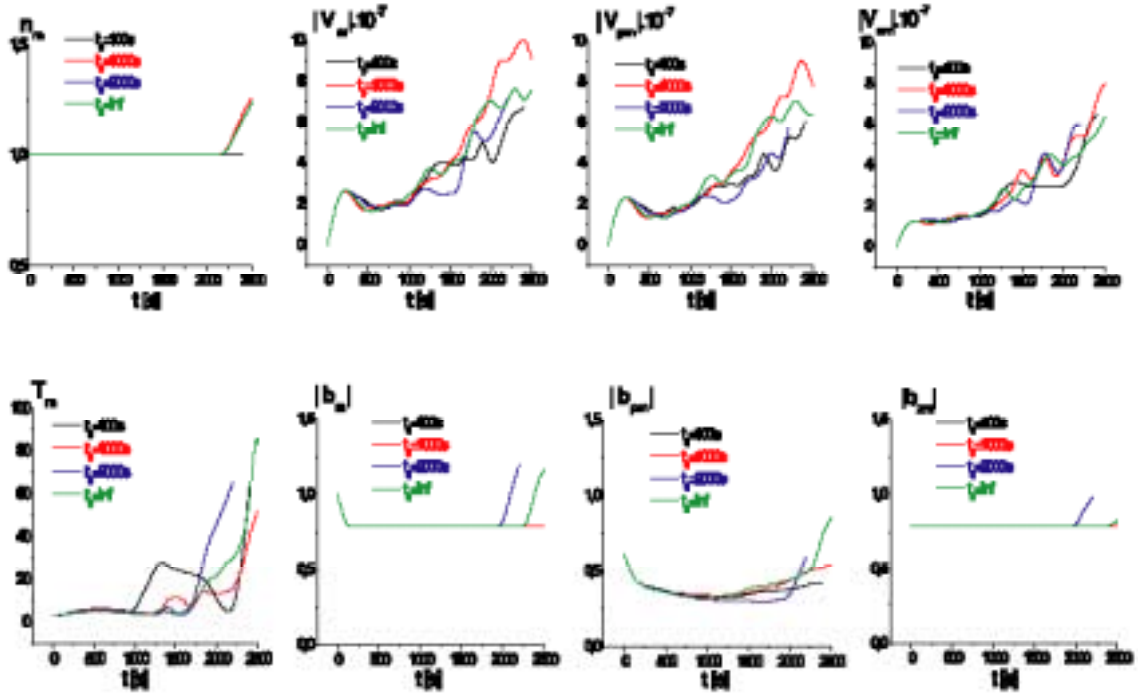

Figure 3-9: Dynamical evolution of the characteristic fields (their maximum values), $|\mathbf{b}|$; $b_x$; $b_y$; $n$; $|\mathbf{V}|$; $V_x$; $V_y$; $T$, defining the interacting flow–magnetic field system (their $x-z$ contour plots are shown in Fig.-s 3.4–3.8) for different initial flow life–times ($t_0 = 100\,s$ (black); $1000\,s$ (red); $2000\,s$ (blue); $\infty$ (green)). The code ceases to be dependable for times at which very steep gradients emerge; the blow–up time for this simulation is ( . $2500\,s$)

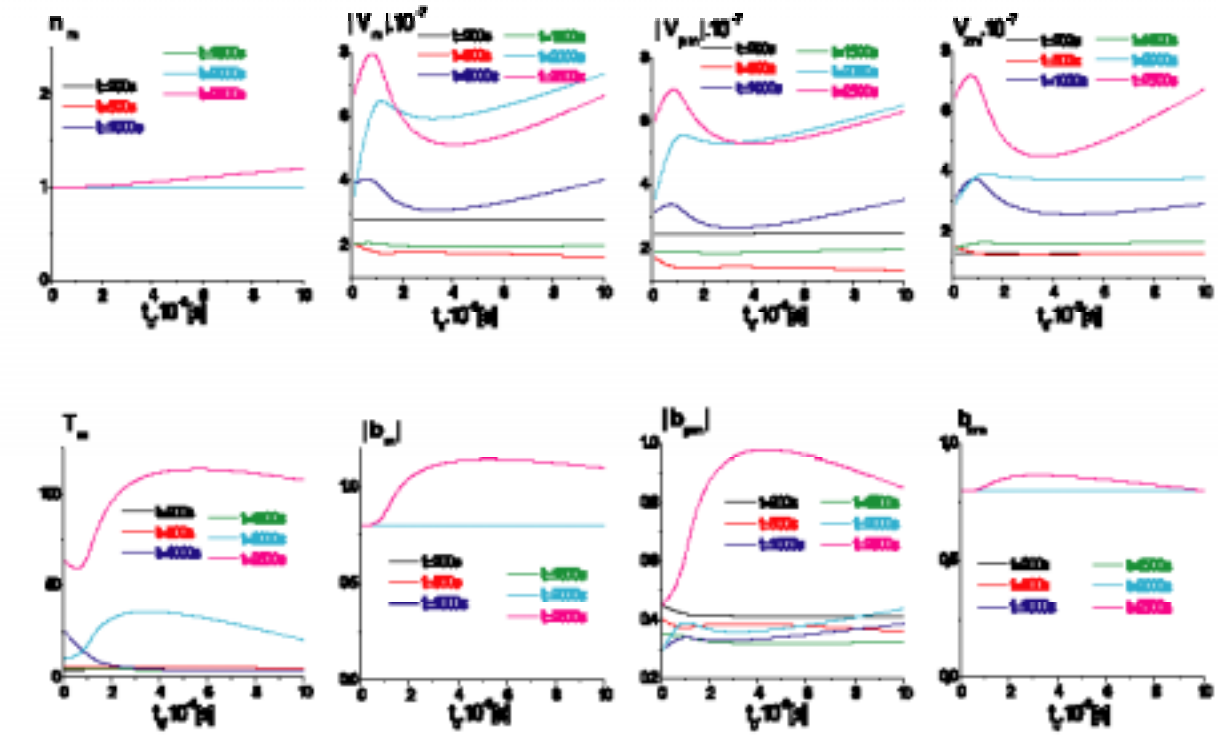

Figure 3-10: Maximum values of $|\mathbf{b}|; b_x; b_y; n; |\mathbf{V}|; V_x; V_y; T$ (their $x - z$ contour plots are shown in Figs.3.4–3.8) versus the initial life–time ($t_0$) of the primary outflow for different time–frames ($t = 200\,s$ (black); $500\,s$ (red); $1000\,s$(blue); $1500\,s$ (green); $2000\,s$(lightgreen); $2500\,s$ (rose)). The code ceases to be dependable for times at which very steep gradients emerge; the blow–up time for this simulation is ( . $2500\,s$).

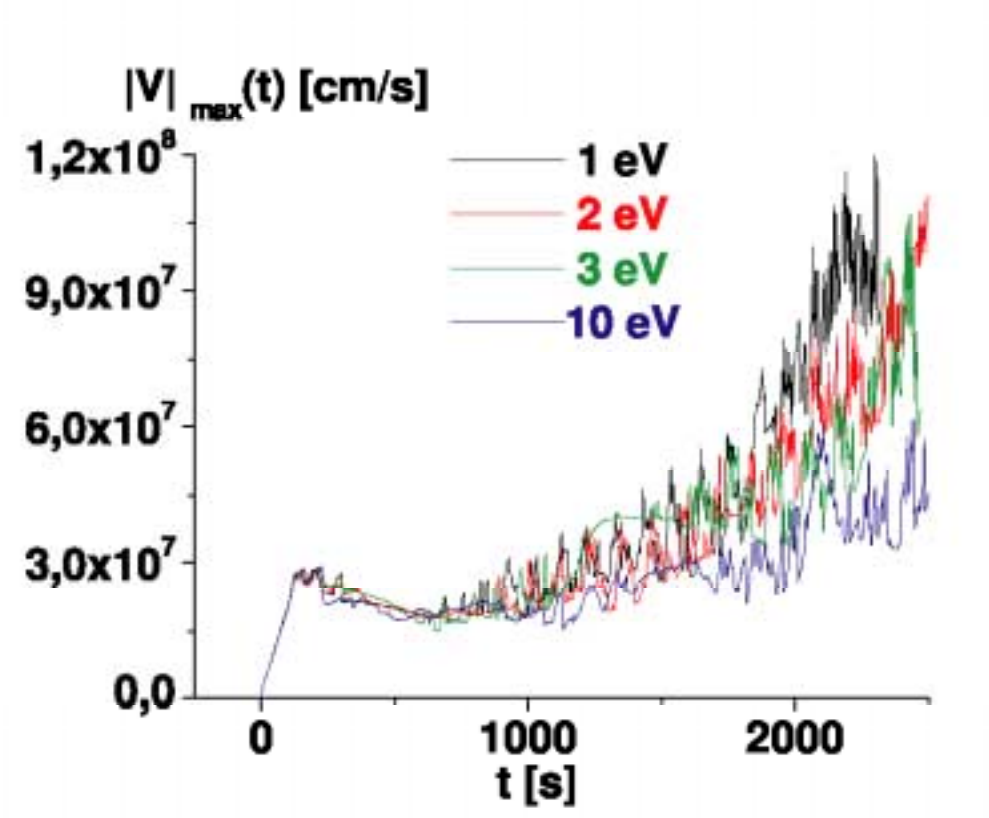


Figure 3-11: Time evolution of the maximum of $|\mathbf{V}|$ for a given magnetic field structure (Fig.3.2) but for different initial temperatures ($T_0 = 1\,eV$(black); $T_0 = 2\,eV$(red); $T_0 = 3\,eV$(green); $T_0 = 10\,eV$(blue)) of flow (Fig.3.1). Several distinct phases of the acceleration process can be discerned.

MHD reconnection may or may not be the key player. It would appear that different aspects of the magneto–fluid coupling control the dynamics at different stages/phases of development. In particular the role of Hall term which provides a singular perturbation to the conventional MHD (and introduces a characteristic intrinsic small length scale (the ion skin depth) breaking the scale–invariance of the ideal nonlinear system) may turn out to be crucial. The macroscopic structures could still be accessible within MHD but their coupling to the microscopic structures (dominated by the Hall term) will be an essential part of the controlling dynamics. Since the Hall term is nonlinear, the coupling of the macroscopic and microscopic scale hierarchies is rather complicated (in comparison with the well–known viscosity effect perturbing the ideal fluid–dynamics equations).

We will soon (in the next section) offer a possible explanation of simulation results through an equilibrium analysis similar to the one invoked in [214] to account for the specific phases of the acceleration process; the analysis is limited to an ideal Hall MHd system.

The two–fluid system model used for simulation does have dissipation. The presence of viscosity destroys the ideal invariance of the generalized ion vorticity making it into a dynamical parameter [177] ; the modification of magnetic fields and even the creation of micro scales (shocks or fast fluctuations) could, thus, result from viscosity. Then, the magneto–fluid coupling [1] (with frozen in condition for electrons) causes redistribution of accelerated particles to the regions of the maximum magnetic field localization in a 2D compressible plasma [214].

In the simulation, the magnetic and the generalized helicity densities are dynamical parameters. Even if they are not (initially) in the required range for efficient flow generation, their evolution could, subsequently, bring them in the appropriate range where they could satisfy conditions needed for efficient acceleration. In fact, the favorable conditions

[1] What we call magneto–fluid coupling in this study is a direct consequence of the fact that $\mathsf{V_e} = (\mathsf{V} - \mathsf{j}/en)$ and not just $\mathsf{V}$ as in standard MHD; it is the $\mathsf{j}$ part that separates the electron from the ion fluid. In the non–dissipative limit the magnetic field is frozen in the electron fluid and the ion fluid (due to its finite inertia) moves distinctly.

could occur at several stages in the evolution. This could, perhaps, explain the existence of several phases of acceleration. If it is true, then the dissipation would have played a fundamental role in setting up these distinct stages.

The most interesting and distinguishable new results found in the 2.5D simulation of the two–fluid equations (containing various dissipative and short–scale effects) solved for different initial and boundary conditions are listed below:

1. A primary flow, even with a very slow initial speed ($V_{0z} \sim 1\,\mathrm{km/s}$ locally sub–Alfvénic) is accelerated when it interacts with an arcade–like closed magnetic field structure. The effect is strong in the strong field region (initially the arcade center). This is a common feature independent of the arcade–characteristics, and the shape of the initial flow.

2. For realistic $\alpha_0$ (measuring the strength of the Hall term), when the heat flux and viscosity effects are not ignored, there is a re–distribution of magnetic, flow kinetic and thermal energies in the arcade region in reasonable times $\sim 100\,\mathrm{s}$ .

3. When viscosity and heat–flux are ignored, the time needed for the flow to acquire a reasonable amount of energy is significantly longer. This is probably due to the fact that without dissipation, the energy transfer through the short–scales introduced by the two–fluid effects is not highly effective. Unless the initial conditions are close to the ones necessary for the onset of a catastrophic process [218, 219], the acceleration will be relatively slow.

4. During the redistribution, the arcade field is modified; the thermal and magnetic field energies are converted locally to the flow energy. The time–scale for generating a reasonably fast flow ($V_{0z}$ & $100\,\mathrm{km/s}$) is dictated by $\alpha_0$. For a given initial $T_0(\beta_0)$, the larger the $\alpha_0$ , the faster the flow generation (for a given ambient field). The density is non–uniformly redistributed within the arcade span.

5. At some specific "critical time" $\sim 1000\,s$ the accelerated flow bifurcates into two separate fast flows. At this moment the arcade is also split in two, each with its share of the accumulated particles. Two fast spicule–like structures, carrying vorticity and current, are decoupled from the mother flow. Their densities are similar to the initial density of the mother–flow.

6. Initially the amplification of the flow depends on the flow $\beta_0$, the ratio of the thermal and the magnetic field energy.

7. The distance from the interaction surface where the bifurcation occurs is $\sim 0.01\,R_s$. It is interesting to mention that this height is lower than the heights of the base of a typical hot coronal structure ([1, 72] and references therein) and it seems to be comparable to the latest observational findings [202, 233]. Initially the fast flow localizes in the center of the original arcade. After the bifurcation several flows appear with distinguishable dimensions ($\sim 0.05\,R_s$) practically on similar heights.

8. For fixed initial $T_0$, $n_0$, the final speed of the accelerated flow and the picture of the modified field structure are independent of the initial flow life–time. This result seems extremely important in connection with the observed flows in the lower atmosphere. At $t \gtrsim 1000\,\mathrm{s}$ the flow acquires $\sim 500\,\mathrm{km/s}$ or even greater ($\sim 800\,\mathrm{km/s}$) velocities. Such results persist for different $T_0(\beta_0)$ for a given ambient field (and $n_0$) suggesting the controlling effect of magnetic fields.

We note here that at any quasi–equilibrium stage of the acceleration process, the nascent intermittent flows will blend and interact with pre–existing varying scale closed field structures (recall the fine structure of the solar atmosphere); the "new" flows could be trapped by other structures with strong/weak magnetic fields and participate in creating different dynamical scenarios: heating of the new structure [72] could result, or an escape channel could be created [212, 233]. Instabilities, generation of waves could also be triggered.

## 3.3 Equilibrium Analysis for the Acceleration of Plasma Flows in the Compressible Two–Fluid Plasmas – Magneto–Fluid Coupling

Both the observational evidence and the results of dynamical simulation point out that a typical solar structure passes through a quasi–equilibrium stage (possibly even a series of quasi–equilibria) before it reaches the final explosive or distortion/deformation stage leading to particle escape. Let us try to understand the physics of these quasi–equilibrium structures in terms of equilibrium two–fluid equations. We analyze the simplest two–fluid equilibria with $T = \text{const} \longrightarrow \mathrm{n}^{-1}\nabla \mathrm{p} \rightarrow \mathrm{T}\nabla \ln \mathrm{n}$ (generalization to a homentropic fluid: $p = \text{const} \cdot \mathrm{n}^{\gamma}$ is straightforward and was performed in numerical work [240]). The dimensionless equations describing the model equilibrium can be written as:

$$\frac{1}{n}\nabla \times \mathbf{b} \times \mathbf{b} + \nabla\left(\frac{r_{A0}}{r} - \beta_0 \ln\, n - \frac{V^2}{2}\right) + \mathbf{V} \times (\boldsymbol{\nabla} \times \mathbf{V}) = 0, \tag{3.6}$$

$$\nabla \times \left[\left(\mathbf{V} - \frac{\alpha_0}{n}\nabla \times \mathbf{b}\right) \times \mathbf{b}\right] = 0, \tag{3.7}$$

$$\nabla \cdot (n\mathbf{V}) = 0, \tag{3.8}$$

$$\nabla \cdot \mathbf{b} = 0, \tag{3.9}$$

where $\mathbf{b} = \mathbf{B}/B_0$ and the following normalizations were used: $n \rightarrow n_0$ – the density at some appropriate distance from the solar surface ($\geq 2000\,km$), $B \rightarrow B_0$ – the ambient field strength at the same distance, $|V| \rightarrow V_{A0}$ and the dimensionless parameters are defined with $n_0,\ T_0,\ B_0$ taken at the same distance. In the non–dissipative limit, the system allows the well–known double Beltrami solutions :

$$\mathbf{b} + \alpha_0 \nabla \times \mathbf{V} = d\ n\ \mathbf{V}, \qquad \mathbf{b} = a\ n\ \left[\mathbf{V} - \frac{\alpha_0}{n}\,\nabla \times \mathbf{b}\right], \tag{3.10}$$

where $a$ and $d$ are the dimensionless constants related to ideal invariants: the magnetic $h_1 = \int (\mathbf{A}\cdot\mathbf{b})\, d^3x$ and the generalized $h_2 = \int (\mathbf{A}+\mathbf{V})\cdot\nabla\times(\mathbf{A}+\mathbf{V}) d^3x$ helicities [67, 72]. Substituting (3.10) into (3.6)–(3.8) one obtains the Bernoulli Condition

$$\nabla\left(\frac{2\beta_0 r_{c0}}{r} - \beta_0 \ln\, n - \frac{V^2}{2}\right) = 0, \tag{3.11}$$

relating the density with the flow kinetic energy, and solar gravity.

Equations (3.6), (3.10),(3.11) represent a close system. They may be easily manipulated to yield an alternative form $(g(r) = r_{c0}/r)$

$$\frac{\alpha_0^2}{n}\nabla\times\nabla\times\mathbf{V} + \alpha_0\,\nabla\times\left[\left(\frac{1}{a\,n} - d\right) n\,\mathbf{V}\right] + \left(1 - \frac{d}{a}\right)\mathbf{V} = 0, \tag{3.12}$$

$$\alpha_0^2\nabla\times\left(\frac{1}{n}\nabla\times\mathbf{b}\right) + \alpha_0\,\nabla\times\left[\left(\frac{1}{a\,n} - d\right)\mathbf{b}\right] + \left(1 - \frac{d}{a}\right)\mathbf{b} = 0. \tag{3.13}$$

$$n = \exp\left(-\left[2g_0 - \frac{V_0^2}{2\beta_0} - 2g + \frac{V^2}{2\beta_0}\right]\right). \tag{3.14}$$

Equations (3.12), and (3.14) can be solved for the density and the velocity field $\mathbf{V}$ and then $\mathbf{b}$ could be determined from (3.10).

### 3.3.1 Simulation for 1-Dimensional case

In the Solar atmosphere one observes quasi–equilibrium magnetic structures with both homogeneous (practically anywhere) and inhomogeneous (especially in the Chromosphere and TR) densities. By invoking appropriate variational principles (see subsection below) , one can show that the generic double Beltrami class of equilibria are accessible in all cases of interest: constant density, constant temperature, or when the plasma obeys an equation of state. Maximum analytical headway, however, is possible for constant density. In that case the Beltrami–Bernoulli system consists of a set of linear equations and has two well–defined scales of variation. Non–constant density does not lead to a linear chain (see (3.12), and (3.14)), but allows phenomena peculiar to nonlinear systems. It is the

latter class of systems that we will deal with now.

We have to resort to numerical methods to obtain detailed solutions for the coupled non–linear system (3.12), (3.13), and (3.14). We have carried out a 1D simulation (the relevant dimension being the height "Z" from the center of Sun; $Z_0 = R_\odot + \Delta r$ is the surface at which the boundary conditions are applied) for a variety of boundary conditions. The boundary surface is so chosen that at this height $Z_0$ the influecne of ionization can be neglected. For observational estimates of $\Delta r$ given earlier, the relevant heights lie higher than $(1 + 2.8 \cdot 10^{-3})\, R_\odot$.

The simulation results are presented in Figs.1-2. These are the plots of various physical quantities as functions of the height. The first figure consists of three frames (a-b, c-d, and e-f) each consisting of two pictures – one for the density and the magnetic field and the other for the velocity field. The parameters defining different frames are (we will give them in the order $(n_0;\ B_0;\ T_0;\ V_{A0})$): 1) a-b frame: $(10^{12}\, cm^{-3};\ 200\, G;\ 2\, eV;\ 440\, km/s)$ implying $\beta_0 \sim 0.002 \ll 1$ and $r_{c0} = 225$; 2) c-d frame: $(10^{11}\, cm^{-3};\ 100\, G;\ 5\, eV;\ 600\, km/s)$ implying $\beta_0 \sim 0.007 \ll 1$ and $r_{c0} = 40$; 3) e-f frame: $(10^{11}\, cm^{-3};\ 50\, G;\ 6\, eV;\ 330\, km/s)$ implying $\beta_0 \sim 0.04 < 1$ and $r_{c0} = 30$. In each frame there are three sets of curves labelled by $\alpha_0$ (1-2-3 corresponding respectively to $\alpha_0 = 0.000013;\ 0.005;\ 0.1$), the measure of the strength of the two–fluid Hall currents.

For all our runs the boundary conditions, $|b_0| = 1, \quad V_0 = 0.01\, V_{A0}$ (with $V_{x0} = V_{y0} = V_{z0}$) were imposed; we begin with just a small residual flow speed. The choice, $d \sim a \sim 100$ and $(a - d)/a^2 \sim 10^{-6}$ for the parameters characterizing the double Beltrami state, reflects the physical constraint that we are dealing with a sub–Alfvenic flow with a very small $\alpha_0$ ([70]). We must admit that the values of $\alpha_0$ chosen for the simulation are much larger than their actual values ($\sim 10^{-8}$ for corona and smaller for sub–coronal regions); our present code cannot resolve the equivalent short lengths, though, we hope to do better in future. We believe, however, that the nature of the final results is properly captured by these artificial values of $\alpha_0$.

The most remarkable result of the simulation is that for small and realistic values of $\alpha_0$

(curves labelled 1), there exists some height where the density begins to drop precipitously with a corresponding sharp rise in the flow speed. The effect is even stronger for the low beta (a-b are the lowest beta frames) plasmas. It is also obvious that at very short distances, the stratification is practically due to gravity but as we approach the velocity "blow–up" height, the self–consistent Magneto–Bernoulli processes take over and control the density (and hence the velocity) stratification.

An examination of the Bernoulli condition (3.14) readily yields an indirect estimate for the height at which the observed shock–formation may take place. For a low beta plasma, the sharp fall in density is expected to occur when (this is true for all $\alpha_0$), i.e,

$$|\mathbf{V}|^2 - V_0^2 > 2\,\beta_0. \tag{3.15}$$

For the current simulation, at $\beta_0 = 0.04$, it occurs approximately at $|\mathbf{V}|^2 > 0.08$ or at $|V| \sim 0.28$; This analytically predicted value is very close to the simulation result (see Fig.2(b)). Simulation results also confirm that the velocity blow–up distance depends mainly on $\beta_0$, and that the final velocity is greater for greater $\beta_0$ (Fig.2). The data presented in Fig.1 and Fig.2 corresponds to a uniform temperature plasma. For this case, the variations in plasma pressure are entirely due to the variations in density. Since the magnetic energy remains practically uniform over the distance, sharp decrease in density with a corresponding sharp rise in the flow–speed (of the order of $n^{-1/2}$) is nothing but the expression of the commonly understood Bernoulli effect. We must emphasize that the general results remain unchanged in our extensive simulations in which the temperature is allowed to vary (but we have to use a homentropic equation of state to analytically derive the beltrami states. The final parameters, naturally, depend upon the adiabaticity index $\gamma$).

To check whether the generated flows are predominantly radial or somewhat more isotropic (to explain the observational constraints) we studied in detail the different $\beta_0$ and $\alpha_0$ cases (fixing $\beta_0$ is quite difficult due to complications like ionization) and found that the flows tend to be mostly radial only for large $\alpha_0$ (see, for example, plots labeled

2 and 3 in Fig.1(b,d,f)). The situation could change considerably when we deal with a more inclusive time–dependent dynamical model with dissipation. Plasma heating, then, could result from the dissipation of the perpendicular energy so that at larger distances, the flows would have larger radial components. Heating would also keep $\beta(\mathbf{r}, t)$ large at upper heights shifting the velocity blow–up distance further or eliminating it all together; we know from Fig.1 that as $\beta_0$ goes up, the density fall (velocity amplification) becomes smoother. These issues will be dealt with later in a more detailed work. Notice, that final velocities go up with $V_0 \sim d^{-1}$. An initial flow with speed $3.3\,km/s$ (e-f frame of Fig.1) ends up acquiring a high speed $\sim 100\,km/s$ at the height $(Z - Z_0) \sim 0.09\,R_\odot$ but at a lower density $\sim 10^{9.5}\,cm^{-3}$.

If one were to ignore the flow term in (3.11) (a totally wrong assumption commonly used in many studies), we will end up finding essentially radial flows. The magnitude of these flows, however, remains small; there is no region of sharp rise (3.15), and the generated flows achieve reasonable energies at heights typically 10 times greater than the heights at which the correct Bernoulli condition would do the trick.

We have shown a possible pathway for a steady generation of flows in the quasi–equilibrium structures established in the sub-coronal regions. These structures consist of fully ionized two–species plasma trapped in magnetic fields. The suggested mechanism is a straightforward application of the recently developed magneto–fluid model [67, 70, 72]; a generalized Bernoulli mechanism (a necessary condition for the double–beltrami magneto–fluid equilibrium) allows the conversion of thermal energy into kinetic energy and/ or a readjustment of the kinetic energy from a high density–low velocity to a low density–high velocity plasma. Numerical results show, for realistic plasma parameters, a significant density fall with a sharp amplification of the flow speed. In the presence of dissipation, these flows are likely to play a fundamental role in the heating of the upper chromosphere and TR, although our explicit purpose in this study was to create a steady source of matter and energy for the formation and primary heating of the corona. Our preliminary results agree with the observational data, and lend promise to attempts,

based on the existence of sub–coronal flows, to tackle unresolved problems like the coronal heating and origin of the Solar wind.

### 3.3.2 Variational Principle

Let's introduce target functional:

$$W = \frac{1}{2}\int (B + \nabla \times V)^2 d^3x. \tag{3.16}$$

To the constants of motion $h_1, h_2$ one should add the total energy (for simplicity we ignore the gravity)

$$E = \int d^3x \left[\frac{1}{2} n V^2 + B^2 + \frac{p}{\gamma - 1}\right], \tag{3.17}$$

and the normalized total fluid mass

$$\widehat{M} = \frac{M}{m_i n_0} = \int n d^3x. \tag{3.18}$$

In order to derive some of these equations we have assumed that the pressure follows the adiabatic law

$$p = n^\gamma p_0, \tag{3.19}$$

which also implies that $T = p/n = p_0 n^{\gamma-1}$. The last equation allows the pressure term $\nabla p/n$ in the force equation to become a perfect gradient. The variations principle is

$$\delta\left[W - \mu_0 E - \mu_1 H_1 - \mu_2 H_2 - \mu\widehat{M}\right] = 0 \tag{3.20}$$

where the variation is to be done on the three–dynamical variables $A(\boldsymbol{B})$, $\boldsymbol{V}$ and $n$.

$$\delta W = \langle (B + \nabla \times \boldsymbol{V})) \cdot (\delta \boldsymbol{B} + \nabla \times \delta \boldsymbol{V})\rangle = \langle [\nabla \times (B + \nabla \times V)] \cdot [\delta \boldsymbol{A} + \delta \boldsymbol{V}]\rangle \tag{3.21}$$

$$\delta E = \left\langle (\boldsymbol{\nabla} \times \boldsymbol{B}) \cdot \delta \boldsymbol{A} + n \boldsymbol{V} \cdot \delta \boldsymbol{V} + \frac{1}{2} V^2 \delta n + \frac{\gamma}{\gamma - 1} T \delta n \right\rangle \tag{3.22}$$

$$\delta H_1 = \langle \boldsymbol{B} \cdot \delta \boldsymbol{A} \rangle \, \delta H_2 = \langle (\delta \boldsymbol{A} + \delta \boldsymbol{V}) \cdot (\boldsymbol{B} + \nabla \times \boldsymbol{V}) \rangle \tag{3.23}$$

$$\delta \widehat{M} = \langle \delta n \rangle \, . \tag{3.24}$$

Using Eq.-s (3.21)-(3.24) in (3.20) and demanding $\delta n, \delta \boldsymbol{A}$ and $\delta \boldsymbol{V}$ to be independent and arbitrary, we must have: the standard two (with $n$ a variable)

$$\nabla \times [\boldsymbol{B} + \nabla \times \boldsymbol{V}] - \mu_0 (\nabla \times \boldsymbol{B}) - \mu_1 \boldsymbol{B} - \mu_2 (B + \nabla \times \boldsymbol{V}) = 0 \tag{3.25}$$

$$\nabla \times [\boldsymbol{B} + \nabla \times \boldsymbol{V}] - \mu_0 n \boldsymbol{V} - \mu_2 (B + \nabla \times \boldsymbol{V}) = 0 \tag{3.26}$$

and the new equation

$$-\mu_0 \left[ \frac{1}{2} V^2 + \frac{\gamma}{\gamma - 1} T \right] - \mu = 0. \tag{3.27}$$

Concentrating on eq. (3.27) first $[T = p_0 n^{\gamma - 1}]$

$$\frac{1}{2} V^2 + \frac{\gamma}{\gamma - 1} T = -\frac{\mu}{\mu_0} = \text{Const.}$$

or

$$\nabla \left[ \frac{1}{2} V^2 + \frac{\gamma}{\gamma - 1} T \right] = \nabla \frac{1}{2} V^2 + \frac{\nabla p}{n} = 0 \tag{3.28}$$

which is precisely the Bernoulli condition that came from the uncurled equation as a subsidiary condition to the Beltrami conditions. Eq.-s (3.25) and (3.26) may be combined as usual to

$$\begin{aligned} &-\mu_0 n \boldsymbol{V} + \mu_0 \nabla \times B + \mu_1 \boldsymbol{B} = 0 \\ &\boldsymbol{B} = \frac{\mu_0}{\mu_1} \left[ n \boldsymbol{V} - \nabla \times \boldsymbol{B} \right] . \end{aligned} \tag{3.29}$$

We could, of course, now deal with any case: constant density, constant temperature, or a given equation of state.

### 3.3.3 Analysis for 1D case

We will now calculate the amplification conditions for inhomogeneous density flows in the chromosphere. We restrict to one–D variation (along the height $Z$) and choose the constants $a \sim d = 100$ so that $(a-d)/a\,d \sim 10^{-6}$. This choice insures that two homogeneous Beltrami scales will be vastly different. Detailed algebraic derivation of the approximate formulas used below can be found in Sub–subsection 3.3.4.

The principal results of Sub–subsection 3.3.4 are that if $n \gg (a\,d)^{-1}$ (density fall in the region of interest is not more than 3 orders of magnitude), then

1) the transverse components of magnetic field vary keeping $b_x^2 + b_y^2 = b_{0\perp}^2 = const.$

2) The density and the velocity fields are related approximately by $|V|^2 = 1/d^2n^2$ so that the magnetic energy does not change much, $|\mathbf{b}|^2 = const$ to leading order.

3) The Bernoulli condition transforms to the defining equation for density:

$$\left(-2\,\beta_0\,n^2 + \frac{1}{d^2}\right)\frac{\partial n}{\partial z} = n^3\,g. \tag{3.30}$$

We notice that for the density to drop with height, it has to be larger than $n_{min} = (2\beta_0)^{-1/2}d^{-1}$. The existence of $n_{min}$ also implies via $V^2 = 1/d^2n^2$ that the maximum allowed velocity is

$$|V_{max}| = \frac{1}{d\,n_{min}} = (2\beta_0)^{1/2}. \tag{3.31}$$

As one approaches the singularity at $n = n_{min}$, the spatial variation of density (and in particular of the velocity) becomes very large. In such a region of the steep density fall (and velocity rise), the time–independent dissipationless approach will not be valid. The Bernoulli equation (3.30), however, clearly reveals the origin of the very fast first stage of dynamical acceleration found in the simulations. From Eq.(3.30) we also see that the distance over which the catastrophe appears is determined by the strength of gravity, $g(z)$ . Eventual amplification of the flow (for a given ambient magnetic field) is determined by the local value of $\beta_0$. These simple consequences of the Bernoulli equation explain one of the most important findings of the simulation: for a fixed initial temperature, the

final characteristic parameters of the accelerated flow (quasi–equilibrium after the fast stage of acceleration) do not depend on its initial state. For these gross features of the system, the value of $\alpha_0$ as long as it is finite, is also quite irrelevant, it just determines how fast the transverse components of magnetic and velocity fields oscillate. However when dissipation is present, $\alpha_0$ , through the mediation of short-scale physics, plays a crucial role in the acceleration/heating processes.

In connection with this result it is interesting to mention that according to latest observations on the quasi–equilibrium coronal loops, the so called quasi–periodic intensity oscillations are found to propagate upwards with speeds of the order of the (adiabatic/isothermal) coronal sound speed ([205] and the references therein).

For structures with ($n = const$), there are two distinct scenarios for eruptive events in the current framework : (1) when a "slowly" evolving structure finds itself in a state of no equilibrium and (2) when the process of creating a long–lived hot structure is prematurely aborted; the flow shrinks/distorts the structure that suddenly shines and/or releases energy or ejects particles. The latter mechanism requires a detailed time–dependent treatment. The semi–equilibrium, collisionless magnetofluid treatment pertains only to the former case [218, 219]. In the references cited, the conditions for catastrophic transformations of an original DB (double Beltrami state) were investigated. It was shown that when the total energy of the original state exceeds a critical value, the DB equilibrium suddenly relaxes to a single Beltrami state corresponding to the larger macroscopic scale; at the transition, much of the magnetic energy $|\mathbf{b}|^2$ of the original state is converted to heat/flow kinetic energy.

### 3.3.4 Detailed equilibrium analysis of particle acceleration for non–uniform density case due to Magneto–fluid coupling

Let's rewrite DB equations (3.10) in following way:

$$\alpha_0 \nabla \times \boldsymbol{b} = -\frac{1}{a}\,\boldsymbol{b} + n\,\boldsymbol{V}, \qquad\qquad \alpha_0 \nabla \times \boldsymbol{V} = -\boldsymbol{b} + d\,n\,\boldsymbol{V}, \tag{3.32}$$

Let's define a vector:

$$\boldsymbol{Q} = \begin{pmatrix} \boldsymbol{b} \\ \boldsymbol{V} \end{pmatrix}, \tag{3.33}$$

then (3.32) may be written as:

$$\alpha_0 \nabla \times \boldsymbol{Q} = M\ \boldsymbol{Q}, \tag{3.34}$$

where

$$M = \begin{pmatrix} -a^{-1}\,, & n \\ -1\,, & d\,n \end{pmatrix}. \tag{3.35}$$

$M$ can be diagonalized by a similarity transformation:

$$S\ M\ S^{-1} == \begin{pmatrix} \lambda_+\,, & 0 \\ 0\,, & \lambda_- \end{pmatrix}, \tag{3.36}$$

where $[\lambda^2 - (d\,n - a^{-1})\lambda + n\,(1 - d\,a^{-1}) = 0]$ $\quad \lambda_\pm = \frac{1}{2}[(d\,n - a^{-1}) \pm \sqrt{(d\,n + a^{-1})^2 - 4\,n}\,]$ are standard roots. $S$ is found to be ($n$ is a slowly varying parameter, see the Bernoulli condition – $V^2$ and $g$ are slowly varying):

$$S = \begin{pmatrix} 1\,, & -(\lambda_+ + a^{-1}) \\ 1\,, & -(\lambda_- + a^{-1}) \end{pmatrix}. \tag{3.37}$$

Then, if density fall is at a much slower rate than the slow scale of the Beltrami system ( $\lambda_-/\alpha_0$, ), rewriting (3.34) as:

$$\alpha_0 \nabla \times S\,\boldsymbol{Q} = (S\,M\,S^{-1})\,S\;\boldsymbol{Q} = \begin{pmatrix} \lambda_+\,, & 0 \\ 0\,, & \lambda_- \end{pmatrix}\; S\,\boldsymbol{Q}\;, \tag{3.38}$$

one finds:

$$S\;\boldsymbol{Q} = \begin{pmatrix} \boldsymbol{Q}_+ \\ \boldsymbol{Q}_- \end{pmatrix} = \begin{pmatrix} \boldsymbol{b} - (\lambda_+ + a^{-1})\;\boldsymbol{V} \\ \boldsymbol{b} - (\lambda_- + a^{-1})\;\boldsymbol{V} \end{pmatrix} \tag{3.39}$$

each obeying its own independent (fully de–coupled) equation:

$$\nabla \times \boldsymbol{Q}_\pm = \frac{\lambda_\pm}{\alpha_0}\;\boldsymbol{Q}_\pm. \tag{3.40}$$

Let's find the amplification conditions for flows (say in the chromosphere, where $a \sim d = 100$ so that $(a-d)/a\,d \sim 10^{-6}$). Assuming (this is found to be a restriction) $n \gg (a\,d)^{-1}$ — density fall is not more than 3 orders of magnitude, then

$$\lambda_+ \sim d\,n\;, \qquad\qquad \lambda_- \sim \frac{a-d}{a\,d}\;. \tag{3.41}$$

Notice, that for realistic solar atmosphere parameters (chromosphere, TR, corona) $\alpha_0 \sim 10^{-9} - 10^{-11}$ and the fast Beltrami scale $\lambda_+/\alpha_0 \sim 10^{11} - 10^{13}$ is very oscillatory and its amplitude must go to zero. This gives a relation between the velocity and the magnetic field;

$$\boldsymbol{Q}_+ = \boldsymbol{b} - (d\,n - a^{-1})\,\boldsymbol{V} \simeq \boldsymbol{b} - d\,n\,\boldsymbol{V} = 0, \tag{3.42}$$

and the approximate equation for the pertinent solution takes the form

$$\nabla \times \boldsymbol{Q}_- = \frac{a-d}{a\,d\,\alpha_0}\;\boldsymbol{Q}_- \qquad\qquad \text{with} \qquad\qquad \boldsymbol{Q}_- = \boldsymbol{b} - \frac{\boldsymbol{V}}{d} \simeq \boldsymbol{b}. \tag{3.43}$$

Let's consider a 1D problem ($Z$ along height, $b_0 = 1$ when normalized). Eq.(3.43) leads to:

$$\frac{\partial}{\partial z}\left(b_x^2 + b_y^2\right) = 0 \qquad \Longrightarrow \qquad b_x^2 + b_y^2 = b_{0\perp}^2. \tag{3.44}$$

Then, using eq.(3.42), one has: $V_x^2 + V_y^2 = b_{0\perp}^2/d^2\,n^2$ . From Continuity Equation and DB condition: $V_z = V_{0z}/n \sim b_{0z}/d\,n$ . Thus,

$$V^2 = \frac{1}{d^2\,n^2}. \tag{3.45}$$

Eq.(3.45) converts the Bernoulli condition ($T_0 = const$) to:

$$\left(-2\,\beta_0\,n^2 + \frac{1}{d^2}\right)\frac{\partial n}{\partial z} = n^3\,g. \tag{3.46}$$

Notice, that maximum allowed velocity for this mechanism is (compare with the condition (10) of [240]):

$$|V_{max}| = \frac{1}{d\,n_{min}} = (2\beta_0)^{1/2}. \tag{3.47}$$

Analysis gives similar results for varying temperature ($T = n^{-\mu}, \quad 0 < \mu < 1$).

### 3.3.5 Summary for Dynamical and Steady Generation of Flows

We have developed a 2.5 Dimensional dynamical code for two-fluid equations. The two fluid equations contain the Hall term ($\alpha_0 \neq 0$), the ion vorticity, heatflux and viscosity effects. We have used the code for a systematic study of particle acceleration and energy re–distribution phenomena associated with the interaction of a primary plasma flow with closed field–line magnetic structures. We also developed simple analytical arguments to explain and understand essential features of the simulation results. The simulation and analytical effort have led us to several far–reaching results for the understanding of the solar atmosphere. Even at the cost of some repetition, we list the most important ones: (1) A primary plasma flow (locally sub-Alfvénic) is accelerated when it impinges on an emerging/ambient arcade–like closed magnetic field structure. The effect is strong in the

strong field region. It is found that the final state of the flow is quite insensitive to the details of initial and boundary conditions; the latter simply dictate the time–scale at which significant flow–energy is generated.
(2) It is shown that there is a redistribution of magnetic, flow- kinetic and thermal energies in the arcade region so that the original arcade field is modified. The time–scale of the fast (& 100 km/s) flow generation is dictated by $\alpha_0$, the measure of the Hall term.
(3) It is found that at some specific time the accelerated flow bifurcates into 2 separate fast flows with an accompanying split of the arcade; each component has its share of the accumulated particles.
(4) Initially the amplification of the flow depends on $\beta_0$ as proven by the 1D analysis. To the best of our knowledge, this is first demonstration that major part of the acceleration takes place within a distance $\sim 0.01\, R_s$ (independent of $\alpha_0$) from the interaction surface. Later the fast flow localizes (with dimensions . $0.05\, R_S$) in the upper center of the original arcade.
(5) It is shown that for a given ambient magnetic field and fixed initial $T_0$, $n_0$ , the final speed (& $500\, km/s$) of the accelerated flow, and the shape of the modified field structure are independent of the initial flow life–time. Many of these parameters can be approximately calculated by analysis.

We have shown possible pathways for both dynamical and steady generation of fast flows. The cold flows originating, for example, in the lower chromosphere acquire energy as they meet and interact with emerging/ ambient magnetic fluxes; the trapping of an ionized (& 3 eV ) plasma by network/ inter–network structures takes place at the same time. In the presence of dissipation, these flows are likely to play a fundamental role in the heating of the finely structured solar atmosphere. The explicit purpose of this study, however, was to demonstrate the generation of flows in the lower atmosphere feeding on the ambient magnetic energy. The flows, in turn, provide a steady and assured source of matter and energy for the formation and primary heating of the corona as well as for the

creation of the solar wind. The agreement of our preliminary results with the observation data lends credence and promise to attempts, based on the exploitation of sub–coronal flows, to tackle unresolved problems like the coronal heating and origin of the solar wind. We believe that although the chromospheric mass outflows, spicules, explosive events in chromosphere, micro– and nano–flares, large coronal flares, erupting prominences and CMEs appear to be disconnected and independent, they, in all probability are simply the manifestations of region-specific responses to similar dynamical causes.

## 3.4 Acceleration of Plasma Flows Due to Reverse Dynamo Mechanism

The generation of macroscopic magnetic fields (primarily from microscopic velocity fields) defines the standard "dynamo" mechanism. The dynamo action seems to be a very pervasive phenomenon; in fusion devices as well as in astrophysics (stellar atmosphere, MHD jets) one sees the emergence of macro–scale magnetic fields from an initially turbulent system. The relaxation observed in the Reverse Field pinches is a vivid illustration of the dynamo in action. Search for interactions that may result in efficient dynamo action is one of the most flourishing fields in plasma astrophysics. The myriad phenomena taking place in the stellar atmospheres (heating of the corona, the stellar wind etc.) could hardly be understood without knowing the origin and nature of the magnetic field structures weaving the corona.

The conventional dynamo theories concentrate on the generation of macroscopic magnetic fields in charged fluids. With time the dynamo theories have invoked more and more sophisticated physics models — from the kinematic to the magneto hydrodynamic (MHD) to, more recently, the Hall MHD (HMHD) dynamo. In the latter theories the velocity field is not specified externally (as it is in the kinematic case) but evolves in interaction with the magnetic field. Naturally both MHD and HMHD "dynamo" theories encompass, in reality, the simultaneous evolution of the magnetic and the velocity fields. If the short–scale turbulence can generate long–scale magnetic fields, then under appropriate conditions the turbulence could also generate macroscopic plasma flows. In this context, a quotation from a recent study is rather pertinent: the structures/magnetic elements produced by the turbulent amplification are destroyed/dissipated even before they are formed completely [237, 248, 239] creating significant flows or leading to the heating.

If the process of conversion of micro–scale kinetic energy to macro–scale magnetic energy is termed "dynamo" (D) then the mirror image process of the conversion of micro–scale magnetic energy to macro–scale kinetic energy could be called "reverse dynamo"

(RD). It is convenient to somewhat extend the definitions – the D (RD) process connotes the generation of the macroscopic magnetic field (flow) independent of the mix of the microscopic energy (magnetic and kinetic).

Within the framework of a simple HMHD system, we demonstrate in this study that the Dynamo and the Reverse Dynamo processes operate simultaneously — whenever a macroscopic magnetic field is generated there is a concomitant generation of a macroscopic plasma flow. Whether the macroscopic flow is weak (sub–Alfvénic) or strong (super–Alfvénic) with respect to the macroscopic field will depend on the composition of the turbulent energy. We shall derive the relationships between the generated fields and the flows and discuss the conditions under which one or the other process is dominant. In Sec.1 we display an analytical calculation based on the conversion of micro scale magnetic and kinetic energy into macroscopic fields and flows. In particular, we dwell on the reverse dynamo mechanism: the permanent dynamical feeding of the flow kinetic energy through an interaction of the microscopic magnetic field structures with weak flows (seed kinetic energy). In Sec.2 we illustrate that the theoretically derived processes do indeed take place by presenting simulation results from a general two fluid code that includes dissipation.

### 3.4.1 Theoretical Model Analysis

The physical model exploited for flow generation/acceleration is simplified HMHD – a minimal model that entertains two interacting scales that can be quite disparate; the macroscopic scale of the system is generally much larger than the ion skin depth, the intrinsic micro scale of HMHD at which ion kinetic inertia effects become important [67, 72, 219, 236]. In HMHD the ion ($\boldsymbol{v}$) and electron ($\boldsymbol{v}_e = (\boldsymbol{v} - \boldsymbol{j}/en)$) flow velocities are different even in the limit of zero electron inertia. In its dimensionless form, HMHD comprises of

$$\frac{\partial \boldsymbol{b}}{\partial t} \;=\; \boldsymbol{\nabla} \times \Big[ [\boldsymbol{v} - \alpha_0 \, \boldsymbol{\nabla} \times \boldsymbol{b}] \times \boldsymbol{b} \Big], \tag{3.48}$$

$$\frac{\partial \boldsymbol{v}}{\partial t} = \boldsymbol{v} \times (\boldsymbol{\nabla} \times \boldsymbol{v}) + (\boldsymbol{\nabla} \times \boldsymbol{b}) \times \boldsymbol{b} - \boldsymbol{\nabla} \left( p + \frac{v^2}{2} \right). \tag{3.49}$$

with the standard normalizations: the density $n$ to $n_0$ , the magnetic field to the some measure of the ambient field $B_0$ and velocities to the Alfvén velocity $V_{A0}$. We assign equal temperatures to the electron and the protons so that the kinetic pressure $p$ is given by: $p = p_i + p_e \simeq 2\,nT,\ T = T_i \simeq T_e$. We note that the Hall current contributions become significant when the dimensionless Hall coefficient $\alpha_0 = \lambda_{i0}/R_0$ ($R_0$ – the characteristic scale length of a system and $\lambda_{i0} = c/\omega_{i0}$ is the collisionless skin depth) satisfies the condition: $\alpha_0 > \eta$, where $\eta$ is the inverse Lundquist number for the plasma. For a typical solar plasma, in the corona, the chromosphere and the transition region (TR), this condition is easily satisfied ($\alpha_0$ is in the range $10^{-10} - 10^{-7}$ for densities within $(10^{14} - 10^{8})\,cm^{-3}$ and $\eta = c^2/(4\pi V_{A0} R_\odot \sigma) \sim 10^{-14}$, where $R_\odot$ is solar radius, $\sigma$ is the plasma conductivity). In such circumstances, the Hall currents modifying the dynamics of the microscopic flows and fields could have a profound impact on the generation of macroscopic magnetic fields [244] and fast flows [240, 241].

In the following analysis $\alpha_0$ will be absorbed by choosing the normalizing length scale to be $\lambda_{i0}$. Let us now assume that our total fields are composed of some ambient seed fields and fluctuations about them,

$$\boldsymbol{b} = \boldsymbol{H} + \boldsymbol{b}_0 + \tilde{\boldsymbol{b}}, \qquad \boldsymbol{v} = \boldsymbol{U} + \boldsymbol{v}_0 + \tilde{\boldsymbol{v}} \tag{3.50}$$

where $\boldsymbol{b}_0,\ \boldsymbol{v}_0$ are the equilibrium fields and $\boldsymbol{H},\ \boldsymbol{U}$ and $\tilde{\boldsymbol{b}},\ \tilde{\boldsymbol{v}}$ are, respectively, the macroscopic and microscopic fluctuations.

Notice that our ambient fields are allowed to have a component at a microscopic scale. For analytical work, we choose for the ambient fields a special class of equilibrium solutions to Eqs. (1-2). These solutions, also known as the Double Beltrami (DB) pair [67], come into existence because of the interaction of flows and fields; the Hall term is essential for their formation. The DB configurations are known to be robust and accessi-

ble, through a variational principle, for a variety of conditions including inhomogeneous densities. Non constant density cases do display many interesting phenomena [240, 241], but the dynamo and reverse dynamo actions can be very adequately described by the analytically tractable constant density system. We shall, therefore, choose the following DB pair (obeying the concomitant Bernoulli condition $\boldsymbol{\nabla}(p_0 + \boldsymbol{v}_0{}^2/2) = const$ [218, 219])

$$\frac{\boldsymbol{b}_0}{a} + \boldsymbol{\nabla} \times \boldsymbol{b}_0 = \boldsymbol{v}_0, \qquad\qquad \boldsymbol{b}_0 + \boldsymbol{\nabla} \times \boldsymbol{v}_0 = d\boldsymbol{v}_0, \tag{3.51}$$

as a representative ambient state. The general solution is expressible in terms of the single Beltrami fields $\boldsymbol{G}_\pm$ that satisfies $\boldsymbol{\nabla} \times \boldsymbol{G}(\lambda) = \lambda \boldsymbol{G}(\lambda)$:

$$\boldsymbol{b}_0 = C_+ \boldsymbol{G}_+(\lambda_+) + C_- \boldsymbol{G}_-(\lambda_-), \tag{3.52}$$

$$\boldsymbol{v}_0 = (a^{-1} + \lambda_+)\, C_+ \boldsymbol{G}_+(\lambda_+) + (a^{-1} + \lambda_-)\, C_- \boldsymbol{G}_-(\lambda_-). \tag{3.53}$$

Here $C_\pm$ are the arbitrary constants and the parameters $a$ and $d$ are set by the invariants of the equilibrium system; the magnetic helicity $h_{10} = \int (\boldsymbol{A}_0 \cdot \boldsymbol{b}_0)\, d^3x$ and the generalized helicity $h_{20} = \int (\boldsymbol{A}_0 + \boldsymbol{v}_0) \cdot \nabla \times (\boldsymbol{A}_0 + \boldsymbol{v}_0) d^3x$ [67, 72]; here $\boldsymbol{A}_0$ is the vector potential of the ambient field. The inverse scale lengths $\lambda_+$ and $\lambda_-$ are fully determined in terms of $a$ and $d$: $\lambda_\pm = \frac{1}{2}[(d - a^{-1}) \pm \sqrt{(d + a^{-1})^2 - 4}\,]$. As the DB parameters $a$ and $d$ vary, $\lambda_\pm$ can range from real to complex values of arbitrary magnitude[2].

Our primary interest is the creation of macro fields from the ambient micro fields. Some what later we will assume, for simplicity, that our zeroth order fields are wholly at the microscopic scale. This allows us to create a hierarchy in the micro fields, the ambient fields are much greater than the fluctuations at the same scale ($|\tilde{\boldsymbol{b}}| \ll |\boldsymbol{b}_0|,\ |\tilde{\boldsymbol{v}}| \ll |\boldsymbol{v}_0|$). Following [244], we may derive the following evolution equations:

$$\partial_t \boldsymbol{U} = \boldsymbol{U} \times (\boldsymbol{\nabla} \times \boldsymbol{U}) + \boldsymbol{\nabla} \times \boldsymbol{H} \times \boldsymbol{H}$$

[2] In the analysis below we will use $\lambda$ for the micro–scale and $\mu$ for the macro–scale structures.

$$+\left\langle \boldsymbol{v}_0 \times (\boldsymbol{\nabla} \times \tilde{\boldsymbol{v}}) + \tilde{\boldsymbol{v}} \times (\boldsymbol{\nabla} \times \boldsymbol{v}_0) + (\boldsymbol{\nabla} \times \boldsymbol{b}_0) \times \tilde{\boldsymbol{b}} + (\boldsymbol{\nabla} \times \tilde{\boldsymbol{b}}) \times \boldsymbol{b}_0 \right\rangle$$

$$- \langle \boldsymbol{\nabla}(\boldsymbol{v}_0 \cdot \tilde{\boldsymbol{v}}) \rangle - \boldsymbol{\nabla} \left( p + \frac{\boldsymbol{U}^2}{2} \right), \tag{3.54}$$

$$\frac{\partial \tilde{\boldsymbol{v}}}{\partial t} = -(\boldsymbol{U} \cdot \boldsymbol{\nabla}) \boldsymbol{v}_0 + (\boldsymbol{H} \cdot \boldsymbol{\nabla}) \boldsymbol{b}_0, \tag{3.55}$$

$$\frac{\partial \tilde{\boldsymbol{b}}}{\partial t} = (\boldsymbol{H} \cdot \boldsymbol{\nabla}) \boldsymbol{v}_{e0} - (\boldsymbol{U} \cdot \boldsymbol{\nabla}) \boldsymbol{b}_0, \tag{3.56}$$

$$\frac{\partial \boldsymbol{H}}{\partial t} = \boldsymbol{\nabla} \times \left\langle [\tilde{\boldsymbol{v}}_e \times \boldsymbol{b}_0] + \boldsymbol{v}_{e0} \times \tilde{\boldsymbol{b}} \right\rangle + \boldsymbol{\nabla} \times [(\boldsymbol{U} - \boldsymbol{\nabla} \times \boldsymbol{H}) \times \boldsymbol{H}], \tag{3.57}$$

where the brackets $< .. >$ denote the spatial averages and $\boldsymbol{v}_{e0} = \boldsymbol{v}_0 - \boldsymbol{\nabla} \times \boldsymbol{b}_0$. This set of equations can be regarded as a closure model of the Hall–MHD equations, which are now general in two respects: 1) it is a closure of the full set of equations, since the feedback of the micro–scale is consistently included in the evolution of both $\boldsymbol{H}$ and $\boldsymbol{U}$; 2) the role of the Hall current (especially in the dynamics of the micro–scale) is also properly accounted for (see [244, 245] for details).

We now choose the constants $a$ and $d$ so that the two Beltrami scales become vastly separated (since these constants reflect the values of the invariant helicities, it is through $a$ and $d$ that the helicities control the final results). In the astrophysically relevant regime of disparate scales (the size of the structure is much greater than the ion skin depth), we shall deal with two extreme cases : (i) $a \sim d \gg 1$ , $(a-d)/a\,d \ll 1$ $(\lambda \sim d,\ \ \mu \sim (a-d)/a\,d$ ), and (ii) $a \sim d \ll 1$ , $(a-d)/a\,d \gg 1$ $(\lambda \sim (a-a^{-1}),\ \ \mu \sim (d-a)$ ). At this time, we would like to draw the reader's attention to the origin of scale separation in the original equilibrium system – it is the Hall term that imposes the micro scale (ion skin–depth) on the macroscopic MHD equilibrium.

Consistent with the main objectives of this study, we will now assume that the original equilibrium is predominantly micro–scale (condition applicable for many astrophysical systems), i.e, the basic reservoir from which we will generate macro scale fields is, indeed, at a totally different scale. Neglecting the macro scale component altogether, the assumed

equilibria becomes simpler with the velocity and magnetic fields linearly related as

$$\boldsymbol{v}_0 = \boldsymbol{b}_0 \left(\lambda + a^{-1}\right) \tag{3.58}$$

leading to

$$\boldsymbol{v}_{e0} = \boldsymbol{v}_0 - \boldsymbol{\nabla} \times \boldsymbol{b}_0 = \boldsymbol{b}_0 \; a^{-1} \tag{3.59}$$

$$\dot{\tilde{\boldsymbol{b}}} = \left(a^{-1}\boldsymbol{H} - \boldsymbol{U}\right) \cdot \boldsymbol{\nabla} \boldsymbol{b}_0 \tag{3.60}$$

$$\dot{\tilde{\boldsymbol{v}}} = \left(\boldsymbol{H} - \left(\lambda + a^{-1}\right) \boldsymbol{U}\right) \cdot \boldsymbol{\nabla} \boldsymbol{b}_0. \tag{3.61}$$

Notice the preponderance of nonlinear terms in the evolution equations for $\boldsymbol{U}$ and $\boldsymbol{H}$ . One would expect that these terms will certainly play a very important part in the eventual saturation of the macroscopic fields, but in the early acceleration stage when the ambient short scale energy is much greater than the newly created macroscopic energy, these terms will not be significant. Deferring the fully nonlinear to a later stage, we shall limit ourselves to a "linear" treatment here. Neglecting the nonlinear terms and manipulating the system of equations, we readily derive (after "solving" for and eliminating the short scale fluctuating fields)

$$\ddot{\boldsymbol{H}} \simeq \left(1 - \frac{\lambda}{a} - \frac{1}{a^2}\right) \langle \boldsymbol{\nabla} \times (\boldsymbol{H} \cdot \boldsymbol{\nabla}) \boldsymbol{b}_0 \times \boldsymbol{b}_0 \rangle \,, \tag{3.62}$$

$$\begin{aligned} \ddot{\boldsymbol{U}} \simeq \Big\langle \left(\lambda + a^{-1}\right) \left(\boldsymbol{\lambda} \dot{\tilde{\boldsymbol{v}}} - \boldsymbol{\nabla} \times \dot{\tilde{\boldsymbol{v}}}\right) - \left(\lambda + a^{-1}\right) \boldsymbol{\nabla} (\boldsymbol{b}_0 \cdot \dot{\tilde{\boldsymbol{v}}}) \times \boldsymbol{b}_0 \Big\rangle \\ - \left\langle (\lambda \dot{\tilde{\boldsymbol{b}}} - \boldsymbol{\nabla} \times \dot{\tilde{\boldsymbol{b}}}) \times \boldsymbol{b}_0 \right\rangle . \end{aligned} \tag{3.63}$$

where the spatial averages are yet to be performed. We use the standard isotropic ABC solution of the single Beltrami system,

$$\begin{aligned} b_{0x} &= \frac{b_0}{\sqrt{3}} \left[\sin \lambda y + \cos \lambda z\right], \\ b_{0y} &= \frac{b_0}{\sqrt{3}} \left[\sin \lambda z + \cos \lambda x\right], \\ b_{0z} &= \frac{b_0}{\sqrt{3}} \left[\sin \lambda x + \cos \lambda y\right]. \end{aligned} \tag{3.64}$$

to compute the spatial averages. After some tedious but straightforward algebra, we arrive at the final acceleration equations

$$\ddot{\boldsymbol{U}} = \frac{\lambda}{2}\frac{b_0^2}{3}\boldsymbol{\nabla}\times\left[\left(\left(\lambda+\frac{1}{a}\right)^2-1\right)\boldsymbol{U}-\lambda\boldsymbol{H}\right] \tag{3.65}$$

$$\ddot{\boldsymbol{H}} = -\lambda\frac{b_0^2}{3}\left(1-\frac{\lambda}{a}-\frac{1}{a^2}\right)\boldsymbol{\nabla}\times\boldsymbol{H}. \tag{3.66}$$

where $b_0^2$ measures the ambient micro scale magnetic energy (also the kinetic energy because of (11)). The coefficients in these equations are determined by $a$ and $d$ ($\lambda = \lambda(a,d)$).

We see that, to leading order, $\boldsymbol{H}$ evolves independently of $\boldsymbol{U}$ but the reverse is not true: the evolution of $\boldsymbol{U}$ does require knowledge of $\boldsymbol{H}$.

In the dynamo context, the Hall–currents in the micro–scale are known to modify the $\alpha$ coefficient so that it survives the standard cancellation of the kinetic and magnetic contributions for Alfvénic perturbations [243]. It is also known that, depending on the state of the system, the Hall effect (by replacing the bulk kinetic helicity by the electron flow helicity) can cause large enhancement or suppression of the dynamo action as compared to the standard MHD [245].

Writing (18) and (19) as

$$\ddot{\boldsymbol{H}} = -r\,(\boldsymbol{\nabla}\times\boldsymbol{H})\,, \qquad \ddot{\boldsymbol{U}} = \boldsymbol{\nabla}\times[s\,\boldsymbol{U}-q\boldsymbol{H}], \tag{3.67}$$

where

$$r = \lambda\frac{b_0^2}{3}(1-\lambda\,a^{-1}-a^{-2})\,, \qquad s = \lambda\frac{b_0^2}{6}[(\lambda+a^{-1})^2-1]\,, \qquad q = \lambda^2\frac{b_0^2}{6}\,, \tag{3.68}$$

and fourier analyzing, one obtains

$$-\omega^2 \boldsymbol{H} = -i\, r\, (\boldsymbol{k} \times \boldsymbol{H}) \ , \qquad -\omega^2 \boldsymbol{U} = i\boldsymbol{k} \times (s\, \boldsymbol{U} - q\boldsymbol{H}). \tag{3.69}$$

yielding the growth rate,

$$\omega^4 = r^2 k^2 \ , \qquad \omega^2 = -|r|\, (k) \ , \tag{3.70}$$

at which $\boldsymbol{H}$ and $\boldsymbol{U}$ increase. The growing macro fields are related to one another by

$$\boldsymbol{U} = \frac{q}{s+r}\ \boldsymbol{H}. \tag{3.71}$$

We shall now show how a choice of $a$ and $d$ fixes the relative amounts of microscopic energy in the ambient fields and consequently in the nascent macroscopic fields $\boldsymbol{U}$ or $\boldsymbol{H}$. We persist with our two extreme cases:

(i) For $a \sim d \gg 1$ , the inverse micro scale $\lambda \sim a \gg 1$ implying $\boldsymbol{v_0} \sim a\, \boldsymbol{b_0} \gg \boldsymbol{b_0}$, i.e, the ambient micro–scales fields are primarily kinetic. These type of conditions may be met in stellar photospheres, where the turbulent velocity field at some stage can be dominant although some $\boldsymbol{b_0}$ is present as well. For these parameters, it can be easily seen that the generated macro–fields have precisely the opposite ordering, $\boldsymbol{U} \sim a^{-1}\boldsymbol{H} \ll \boldsymbol{H}$. This is an example of the straight dynamo mechanism. Micro scale fields with kinetic dominance create, preferentially, macro scale fields that are magnetically dominant — super–Alfvénic "turbulent flows" lead to steady flows that are equally sub–Alfvénic (remember we are using Alfvénic units). It is extremely important, however, to emphasize that the dynamo effect (dominant in this regime) must always be accompanied by the generation of macro–scale plasma flows. This realization can have serious consequences for defining the initial setup for the later dynamics in the stellar atmosphere. The presence of an initial macro–scale velocity field during the flux emergence processes is, for instance, always guaranteed by the mechanism exposed above. The implication is that all models of chromosphere

heating / particle acceleration should take into account the existence of macro–scale primary plasma flows (even weak) and their self–consistent coupling (see [72, 219, 241] and references therein).

(ii) For $a \sim d \ll 1$ the inverse micro scale $\lambda \sim a - a^{-1} \gg 1$. Consequently $\boldsymbol{v}_0 \sim a\,\boldsymbol{b}_0 \ll \boldsymbol{b}_0$, and the ambient energy is mostly magnetic. These conditions might pertain in certain domains in the photospheres or chromospheres, where the turbulent velocity field may exist, but the turbulent magnetic field is the dominant component. This micro–scale magnetically dominant initial system creates macro–scale fields $\boldsymbol{U} \sim a^{-1}\boldsymbol{H} \gg \boldsymbol{H}$ that are kinetically abundant. The situation has fully reversed from the one discussed in the previous example — starting from a strongly sub–Alfvénic turbulent flow, the system generates a strongly super–Alfvénic macro–scale flow; this mode of conversion could be called the "reverse dynamo" mechanism. In the region of a given astrophysical system where the fluctuating/turbulent magnetic field is initially dominant, the magneto–fluid coupling induces efficient/significant acceleration and part of the magnetic energy will be transferred to steady plasma flows. The eventual product of the "reverse dynamo" mechanism is a steady super–Alfvénic flow — a macro flow accompanied by a weak magnetic field (compare with [238] for a magnetically driven dynamo. In this study magnetic field growth on much larger scales, and significant velocity fluctuations with finite volume averaged kinetic helicity are found). It is tempting to stipulate that "reverse dynamo" may be the explanation for the observations that fast flows are generally found in weak field regions of the solar atmosphere [233].

This simple analysis has led to, what we believe, are several far-reaching results: (1) the dynamo and "reverse dynamo" mechanisms have the same origin – they are manifestation of the magneto–fluid coupling; (2) The proportionality of $\boldsymbol{U}$ and $\boldsymbol{H}$ implies that they must be present simultaneously, and the greater the macro–scale magnetic field (generated locally), the greater the macro–scale velocity field (generated locally); (3) the growth rate of the macro–scale fields is defined by DB parameters (hence, by the ambient magnetic and generalized helicities) and scales directly with the ambient

turbulent energy $\sim b_0^2$ ($v_0^2$). Thus, the larger the initial turbulent (microscopic) magnetic energy, the stronger the acceleration of the flow. We believe that these novel results will surely help in advancing our understanding of the evolution of large–scale magnetic fields and their opening up with respect to the fast particle escape from the stellar coronae. This effect may also have important impact on the dynamical and continuous kinetic energy supply of plasma flows observed in various astrophysical systems. We would add here that in this study both the initial and final states have finite heliciies (magnetic and kinetic). The helicity densities are dynamical parameters that evolve self–consistently during the process of flow generation. It is also important to notice that the end product of the reverse dynamo action is a macroscopic flow (produced from a microscopic helical magnetic field) while for "inverse dynamo" [238] it is still the macroscopic magnetic field but produced from a velocity field with helicity.

We end the analytical section by a remark on the nonlinear terms in Eqs. (7,10) that do not appear later. It is amazing that the linear solution given in Eqs. (22-24) makes the nonlinear terms strictly zero. Thus the solution discussed in the last section is an exact (a special class) solution of the nonlinear system and thus remains valid even as $\boldsymbol{U}$ and $\boldsymbol{H}$ grow to larger amplitudes. This interesting but peculiar property that a basically linear solution solves the nonlinear problem pertains to both MHD and HMHD. In MHD, for example, it manifests itself as Walen's nonlinear Alfven wave [249, 250] while in HMHD it is revealed through the recently discovered solution of [242].

### 3.4.2 A Simulation Example

In order to strengthen and support the conclusions of the simple analytical model, we now present some representative results from our 2.5 D numerical simulation of the general two-fluid equations in Cartesian Geometry [72]. For a description of the code, the reference [241] should also be consulted. The simulation system is somewhat different because of the existence of an ambient embedding macroscopic field. We find that, when such a field is present, the basic qualitatively features of the dynamo and reverse dynamo

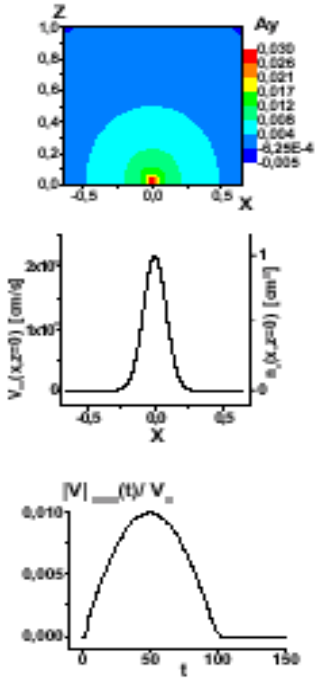


Fig. 1

Figure 3-12: Upper plot: contour plot for the $y$– component of vector potential $A_y$ (flux function) in the $x-z$ plane for an initial distribution of ambient arcade–like magnetic field. The field has a maximum $B_{max}(x_0 = 0, z_0 = 0) = 100\,\mathrm{G}$ . Middle plot: initial symmetric profiles of the radial velocity $V_z$, and density $n$. The respective maxima (at $x$=0) are $\sim 2\,km/s$ and $10^{12}\,cm^{-3}$ . Lower plot corresponds to time evolution of initial flow: $V_z(t, z = 0) = V_{0z}\sin(\pi t/t_0)$; $V_z(t > t_0) = 0$; $t_0 = 100\,\mathrm{s}$ .

mechanisms do not change much but the algebra is considerably more complicated and will be presented in a longer study later.

The simulation system contains several effects not included in the analysis; it has, for instance, dissipation and heat flux in addition to the vorticity and the Hall terms.The plasma is taken to be compressible and embedded in a gravitational field; this provides an extra possibility for micro–scale structure creation. Transport coefficients for heat conduction and viscosity are taken from [59].

The simulation presented here deals with the trapping and amplification of a primary flow impinging on a single closed–line structure. The choice of initial conditions is guided by the observational evidence [200, 233] of the self–consistent process of acceleration and trapping/heating of plasma particles in the finely structured solar atmosphere. The simulation begins with a weak symmetric up–flow (initially Gaussian, $|\mathbf{V}|_{0max} \ll C_{s0}$, where $C_{s0}$ is an initial sound velocity) with its peak located in the central region of a single closed magnetic field structure (location of field maximum $B_{0z} = 100\,G$ – upper plot of Fig.3.12 for the vector potential (flux function) defining the 2D arcade). This field was assumed to be initially uniform in time. The magnetic field is represented as : $\mathbf{B} = \boldsymbol{\nabla} \times \mathbf{A} + B_z\,\hat{\mathbf{z}}$ with $\mathbf{A}(0; A_y; 0)$; $\mathbf{b} = \mathbf{B}/B_{0z}$; $b_x(t, x, z \neq 0) \neq 0$. From numerous runs on the flow–field evolution, we have chosen to display the results corresponding to the following initial and boundary flow parameters: $V_{0max}(x_o, z = 0) = V_{0z} = 2.18 \cdot 10^5\,cm/s$; $n_{0max} = 10^{12}\,cm^{-3}$; $T(x, z = 0) = const = T_0 = 10\,eV$. The background plasma density is $n_{bg} = 0.2 n_{0max}$. In simulations $n(x, z, t = 0) = n/n_{0max}$ is an exponentially decreasing function of $z$. Experience was a guide to for imposing the following boundary condition, $\partial_x(x = \pm\infty, z, t) = 0$ which was used with sufficiently high accuracy for all parameters $(\mathbf{A}, T, \mathbf{V}, \mathbf{B}, n)$ . The initial velocity field has a pulse–like distribution (middle and lower plots of Fig.3.13) with a time duration $t_0 = 100\,s$.

It is found that:

(1) the acceleration is significant in the vicinity of the magnetic field–maximum (originally present or newly created during the evolution) with strong deformation of field lines and energy re–distribution due to magneto–fluid coupling and dissipative effects.

(2) Initially, a part of the flow is trapped in the maximum field localization area, accumulated, cooled and accelerated (plots corresponding to $t = 100\,s$ in Fig.3.13). The accelerated flow reaches speeds greater than 100 km/s in less than 100 s (in agreement with recent observations [1, 247, 246] and references therein).

(3) After this stage the flow passes through a series of quasi–equilibria. In this relatively extended era ($\sim 1000\,s$) of stochastic/oscilating acceleration, the intermittent flows con-

tinuously acquire energy (see Fig.3.14 for the flow kinetic and magnetic energy maxima and also Fig.3.13 results at $t = 1000\,s$).
(4) The flow starts to accelerate again (Fig.3.14(a-c) for the velocity field evolution). This process is completely consistent with the analytical prediction; the acceleration is highest in the strong field regions (newly generated, Fig.3.13). At this moment the accelerated daughter flows (macro–scale) are decoupled from the mother flow carrying currents and modifying the initial arcade field creating new $b_{max}$ localization areas that span the region between . $0.05\,R_s$ and $\sim 0.01\,R_s$ from the interaction surface.

The extensive simulation runs also show that when dissipation is present, the hall term (proportion to $\alpha_0$), through the mediation of micro–scale physics, plays a crucial role in the acceleration/heating processes. The existence of initial fast acceleration in the region of maximum localization of the original magnetic field, and the creation of new areas of macro–scale magnetic field localization (Fig.3.13, panel for $A_y$) with simultaneous transfer of the magnetic energy (oscillatory, micro–scale) to flow kinetic energy (Fig.3.13, panel for $|\boldsymbol{V}|$ and Fig.3.14 results) are manifestations of the combined effects of the dynamo and reverse dynamo phenomena. The maintenance of quasi–steady flows for rather significant period is also an effect of the continuous energy supply from fluctuations (due to the dissipative, Hall and vorticity effects). These flows are likely to provide a very important input element for understanding the finely structured atmospheres with their richness of dynamical structures as well as for the mechanisms of heating, and possible escape of plasmas.

Notice, that in the simulation the actual magnetic and generalized helicity densities are dynamical parameters. Thus even if they are not in the required range initially, their evolution could bring them in the range where they could satisfy conditions needed to efficiently generate flows. The required conditions could be met at several stages. This could, perhaps, explain the existence of several phases of acceleration. Dissipation effects

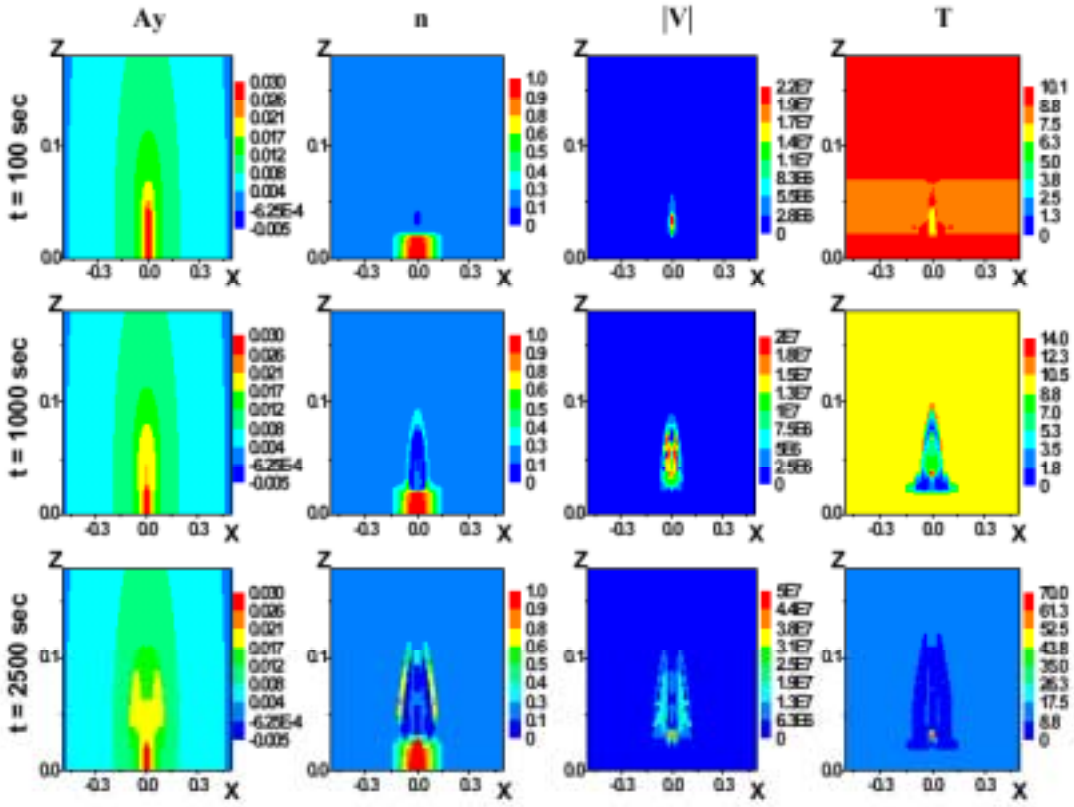


Figure 3-13: $x - z$ contour plots at 3 time–frames: $t = 100\,s$; $1000\,s$; $2500\,s$ for the dynamical evolution of $A_y$ (first panel from the left), $n$ (second panel), $|\boldsymbol{V}|$ (third panel) and $T$ (last panel) for flow – arcade field interaction. The realistic viscosity and heat–flux effects as well as the Hall term ($\alpha_0 = 3.3 \cdot 10^{-10}$) are included in the simulation. Primary flow (type displayed in Fig.3.12) is accelerated as it makes a way through the magnetic field with an arcade–like structure (Fig.1). The primary flow, locally sub–Alfvénic, is accelerated reaching significant speeds (& 100 km/s) in a very short time (. 100 s). Initially the effect is strong in the strong field region (center of the arcade). There is a critical time (. $1000\,s$) when the accelerated flow bifurcates in 2; the original arcade field is deformed correspondingly. After the bifurcation, strong magnetic field localization areas, carrying currents, are created symmetrically about $x = 0$. Post–bifurcation daughter flows are localized in the newly created magnetic field localization areas. The maximum density of each daughter flow is of the order of the density of the mother–flow. Daughter–flows have distinguishable dimensions $\sim 0.05\,R_s$. At $t$ & 1000 s, the velocities reach $\sim 500$ km/s or even greater (. 800 km/s) values. The distance from surface where it happens is & $0.01\,R_s$ . In the regions of daughter flows localization there is a significant cooling while the nearby regions are heated.

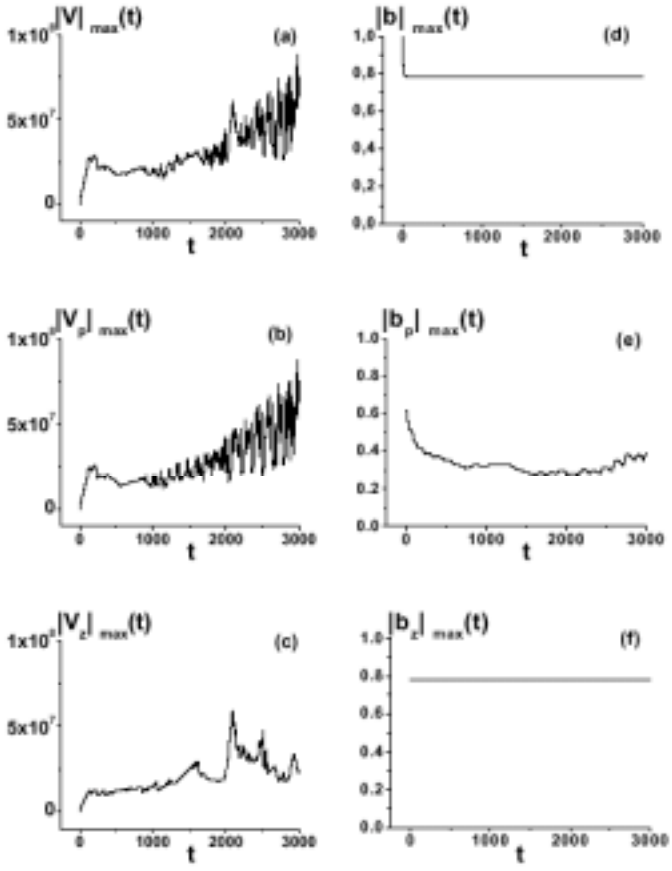


Figure 3-14: Evolution of maximum values of $|\mathbf{V}|$, $|\boldsymbol{V}_p| = (V_x^2 + V_y^2)^{1/2}$, $V_z$ ((a–c)) and $|\mathbf{b}|$, $|\boldsymbol{b}_p| = (b_x^2 + b_y^2)^{1/2}$, $b_z$ ((d–f)) in time. (a),(d) – It is shown that much of the transfer from magnetic field energy happens while the first and very fast ($\sim 100\,s$) acceleration stage; (e),(b) – later, the dissipation of perpendicular (towards height) magnetic field fluctuations lead to the maintenance of the quasi–equilibrium fast perpendicular flows for a period of $\sim 1000\,s$ and then the effective acceleration of flow follows; (c),(f) – maximum value of magnetic field component along height is not changed and radial component of velocity field dissipates effectively. It should be emphasized that these maximum values of both field parameters change the localization dynamically and follow the relationship found analytically – fast flows (see Fig.3.13) are observed in the regions of macro scale magnetic field maximum localization (initially given or later generated).

could play a fundamental role in setting up these distinct stages; it could, for example, modify the generalized vorticity that will finally lead to a modification of field lines and even to the creation of micro scales (shocks or fast fluctuations).

From an analysis of the two–fluid equations, we have extracted, in this study, the "reverse–dynamo" mechanism — the amplification/generation of fast plasma flows in astrophysical systems with initial turbulent (micro scale) magnetic fields. This process is simultaneous with, and complimentary to the highly explored dynamo mechanism. It is found (both analytically and numerically) that the generation of macro–scale flows is an essential consequence of the magneto–fluid coupling, and is independent of the initial and boundary conditions. The generation of macro scale magnetic fields and flows goes hand in hand; the greater the macro–scale magnetic field (generated locally) the greater the macro–scale velocity field (generated locally). The acceleration due to the reverse dynamo is directly proportional to the initial turbulent magnetic energy. When the microscopic magnetic field is initially dominant, a major part of its energy transforms to macro–scale flow energy; a weak macro–scale magnetic field is generated along with.

The reverse dynamo mechanism, providing an unfailing source for macro–scale plasma flows, is likely to be an important mechanism for understanding a host of phenomena in astrophysical systems.

## 3.5 Dynamical Creation of Channels for the Particle Escape in the Solar Atmosphere

In this section we investigate the conditions under which a stream of high speed charged particles may create temporary escape channels in a region nested with closed magnetic fields of varying scales. This active mode of particle escape (as opposed to the escape from open field regions) may become a critical ingredient in building a theory of stellar winds. Temporary channel creation, for example, could be the crucial mechanism needed to explain the recent suggestions that the fast solar wind seems to emerge from all latitudes [251] inspite of the observational consensus that, barring the polar regions, the solar surface (on the average) is studded with magnetic structures with closed fields (even the so called Coronal Holes) [252, 1, 200, 203, 234].

If a given stream of particles were to punch out its own channels of escape in a short–lived, dynamic process, we could certainly explain the emergence of fast outflows from regions of the solar atmosphere with no observable long–lived (quasi–static) open–fields; the flow enters an area, quickly distorts the field topology, creates a channel, escapes and leaves the field lines to mend themselves. This kind of phenomenon will happen with statistical uniformity over the entire low atmosphere and the fast outflows would appear to come from regions permeated by primarily closed field line structures.

Before delineating the physical model we would like to state that there is convincing observational evidence for the presence of flows everywhere in the solar atmosphere (see e.g. [1, 253, 246, 120]). In addition, various theoretical models for up–flow/jet production permeate the literature (the catastrophe models, magnetic reconnections, [231] on dynamical leakage of magnetic twists produced in the sub-photosphere, cascade of shock wave interactions [246], magneto–fluid coupling [218, 240] and etc.). Extra details about flow creation are beyond the scope of this study.

The current model harnesses the ability of flows to complement the magnetic field in the creation of the amazing richness observed in astrophysical plasma systems like the

solar corona. A minimum two–fluid model with arbitrary flows seems to be sufficient to reveal the breadth of phenomena made possible by the combined actions of the flow–velocity and the magnetic fields (see e.g, [72] in which the trapping and primary heating of relatively weak (extremely sub–Alfv/'enic) flows in strong magnetic fields is emphasized). For channel creation, the flows must be relatively strong (Alfv/'enic flows) pushing their way through regions of relatively weaker fields. Under certain conditions, the fields are deformed enough to create escape channels; the detailed nature of a channel depends on initial, and boundary conditions.

The 2 dimensional (2D) simulation code reported in [72] and based on the physics model presented there, is our basic tool for investigation. Though the current calculation is carried out in the solar context, the explored physics is quite general. We use quasi–neutrality : $n_e \simeq n_i = n$ $(\nabla \cdot \mathbf{j} = 0)$ but allow the proton $(V_i)$ and the electron $(V_e = (V - j/en)$ flow velocities to be different. The electron and the proton temperatures are taken to be equal such that the pressure $p = p_i + p_e \simeq 2\,nT,\ T = Ti \simeq Te$. The analysis can be readily extended to allow different temperatures for different species [215, 229, 230, 209]. The dimensionless two-fluid equations describing the flow–field interaction can be read off from [72]. The flow requirements were found to be quite consistent with the latest observational data. It was, however, shown that in the absence of "anomalous viscosity", the only way to enhance the dissipation rates (to the observed values) through viscosity is to create spatial gradients of the velocity field that are on a scale much shorter than that of the structure length. Thus, the viability of this two–fluid approach depends wholly on the existence of mechanisms that induce short–scale velocity fields. Theoretical foundations showed that the short–scale velocity fields are self–consistently generated in the two–fluid system.

A high–speed flow must overcome both gravity and the magnetic field to emerge from the solar atmosphere. Overcoming gravity, imposes a stiff lower bound on the flow velocity. Negotiating the magnetic field is even harder; preliminary studies show that flows with reasonable densities and velocities $\leq 400\,km/sec$ can not destroy or deform

closed magnetic fields structures sufficiently to meet escape conditions. Estimates based on the observed magnetic field strengths show that even in weak field regions ($\sim (1-5)\,G$) flows must be rather strong to punch holes. If the up–flow creation and acceleration mechanisms were operative at low heights from the solar surface the flow–magnetic field interaction could lead to conditions more favorable to particle–escape.

The assumed high speed flows, interacting with the co–existing closed fields provide initial conditions for our numerical work. The creation of flows is a major subject beyond the scope of this study. Some recent observational findings for CH and the "quiet Sun" are highly revealing [256, 258, 257].

The results of two distinct representative simulations will be presented: i) the flow interacting with a single structure providing an example of field–deformation, and ii) the flow passing through a region nested with varying scale closed fields creating escape–channels. The initial solar magnetic field [72] was modelled as a 2D arcade with circular field lines in the $x$–$z$ plane (see e.g. Fig.3.15 for the vector potential/flux function). The field attains its maximum value $B_{\mathsf{max}}(x_o, z = 0)$ at $x_{\mathsf{0}}$ at the center of the arcade, and is a decreasing function of the height $z$ (radial direction).

Note that the 2D Cartesian nature of our code does not allow us to Explore large distances from the surface due to interference with the boundaries. Although we present here only the symmetric cases, the simulation of asymmetric situations is straightforward. In carrying out the simulations an important assumption was made: the diffusion time of magnetic field is longer than the duration of the interaction process (it would require $T$ to be at least a few $eV$–s.)

We first study the dynamics of a spatially localized flow (initially a Gaussian motivated by observations - e.g. jets, spicules) entering an arcade–like single closed field line structure. Two scenerios emerge:

1) Flow is strong ($|\mathbf{V}_{\mathsf{0}}|_{max} \sim 600\,km/sec,\ n_{\mathsf{0}} \sim 10^{\mathsf{8}}\,cm^{-\mathsf{3}}$ – first picture of Fig.3.15) and its peak is located in the central region of the arcade magnetic field structure, the

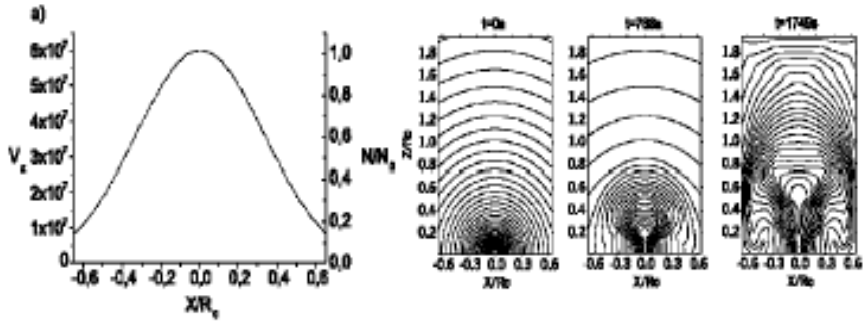

Figure 3-15: Magnetic field deformation: Initial distribution of the flow kinetic energy ($|\mathbf{V_0}|_{max}(x=0) = 600\,km/sec,\ n_0 \sim 10^8\,cm^{-3}$,) and the evolution of the arcade–like magnetic structure for 3 time–frames: $t = 0; 768; 1749\,sec$; the structure had initially $B_{0max}(0, Z=0) = 5\,G$. Strong shear is created in the central region of the structure resulting in the plasmoid–type configuration not leading to the particle escape. *The heights are measured from the Sun's surface.*

original field ($B_{0max} = 5\,G$) shown in second picture of Fig.3.15. is seriously deformed, and its central region is transformed to one with more or less parallel field lines. The local channel, however, does not go all the way but may extend to a respectable height. The resulting plasmoid–type configuration, though, may not lead to particle escape. In all such cases one finds that narrower the flow pulse, the sharper the created shear and stronger the flow, the faster the deformation process.

2) Several flow pulses arrive simultaneously towards a single arcade structure, they may create sheared narrow sub-regions with opposite polarity. The magnetic "well" displayed in Fig.3.16 (which shows the deformation process for three time–frames: $t = 0; 768, 1749\,sec$) was formed by two identical pulses (Fig.3.16, $|\mathbf{V_0}|_{max} \sim 600\,km/sec,\ n_0 \sim 10^8\,cm^{-3}$) located symmetrically on the opposite sides of the arcade-center ($B_{0max} = 5\,G$).

In both cases, the flows were not able to punch channels through a single closed field structure although the ambient field was quite thoroughly deformed. This is true even when we put somewhat larger but realistic amount of energy in the flows; the flow cannot

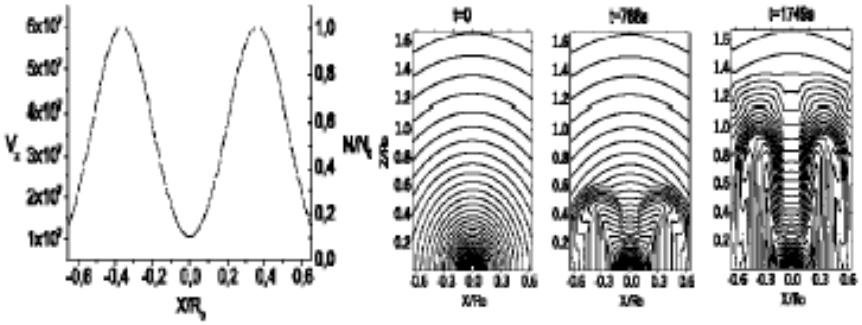

Figure 3-16: Magnetic field (with parameters of Fig.3.15) deformation by two–pulse flow ($|\mathbf{V_0}|_{max} = 600\,km/sec,\ n_0 \sim 10^8\,cm^{-3}$). Strong shear is created in the central region of the structure resulting in the well–type configuration. No particle escape.

overcome the magnetic field in a direct "collision'.

The direct attempt by a relatively strong flow to force its way through a moderate–strength single magnetic field structure seems to result in complete failure (everywhere the flow is sub–Alfénic!); the field is highly distorted but does not quite yield. What structure (prevalent in the atmosphere), then, may prove more cooperative for our goal? Recent literature is extremely helpful in this quest. It has been suggested in [253] that the coexistence of strong– and weak–field components observed in the quiet–Sun photospheric field [259] has a counterpart in the corona. It was shown that the observed predominance of the radial component of the quiet coronal magnetic field is defined, again, by the weak–field component. Coupling these observations with the models of high–speed up–flow generation, it seems rather reasonable to study the passage of this strong flow through an area nested with several arcade-magnetic field structures. Although it is only the 3D simulations that can reproduce most of the observational features of the channel escape process, we believe that the current 2D code is sufficient to determine whether an escape–channel can be created.

From our extensive simulation runs we choose two representative case studies: 1) the flows interacting with two neighboring arcade–structures, and 2) the flows interacting

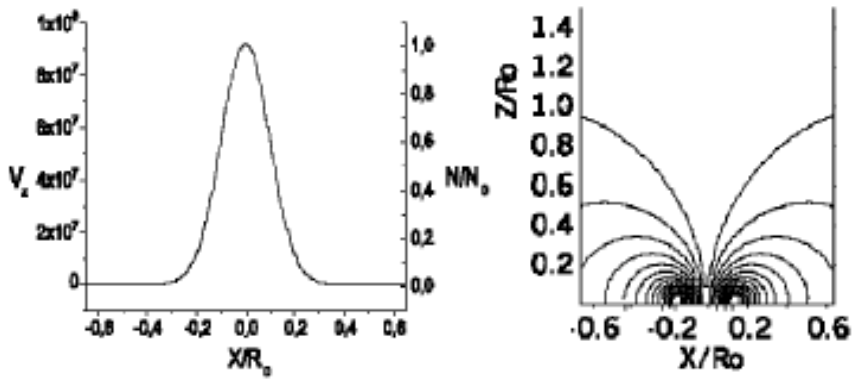


Figure 3-17: Initial flow and 2 identical arcade–magnetic structures of: $B_{0max} = 3\,G$, flow $|\mathbf{V}_0|_{max} = 920\,km/sec,\ n_0 = 2 \cdot 10^7\,cm^{-3}$; background plasma density $= 5 \cdot 10^6\,cm^{-3}$ at the height where strong flows can be found.

with four neighboring arcades. For optimum effect we locate the maxima of the flow pulses in the weak–field region in between the neighboring arcades (where the flows are locally Alfvenic). We present the results of spatially symmetric initial conditions; the inhomogeneous initial conditions do lead to different evolutions, but channel creation remains a common feature.

The fate of the system of Fig.3.17 the two neighboring arcade–structures invaded in the middle (weak field regions ($B_{0max} = 3\,G$)) by a fast flow $|\mathbf{V}_0|_{max} \sim 900\,km/sec,\ n_0 = 2 \cdot 10^7\,cm^{-3}$), is shown in Fig.3.18 The flow is able to stretch and drastically deform the structures and, in a reasonably short time ($\sim 50\,min$), creates a 3D channel (the last time–frame of Fig.3.18). The channel itself is practically cold for distances of a few $R_\odot$. The neighboring regions are comparably hotter: at the structure "coronal base" (created in this dynamical process), one can distinguish rather hot ($T \sim 10^6\,K$) areas where a part of the flow was trapped and thermalized [72]. Note, that if the simulation were done in cylindrical $(r, \phi)$ geometry, we could see the widening of the channel with increasing $r$. We should also add here that if the short scales created in the velocity fields due to Hall term and vorticity effects, and secondary processes like wave generation in the channel

were also taken into account, one could get hotter channels of escape (the subject of a future submission).

One of the more interesting consequences of the channel–creation dynamics is displayed in the two pictures of Fig.3.19 –there is a sharp decrease in density along the channel (after the usual shock front area due to the interaction of flow with background plasma) with a clearly distinguishable ballistic deceleration of the initial flow. At heights $\geq 2\,R_{\odot}$ from the Sun's surface the flow speed ($\sim 800\,km/sec$) has only marginally decreased; the fast flow expends a negligible fraction of its energy in creating a channel for its escape.

The response of 4 arcade–structures (Fig.3.20) to the onslaught of the flow is rather inhomogeneous and complicated; several channels are created in the region of the initial flow (Fig.3.21). The central channel seems a bit pressed due to combined interactions – but this could be just an artifact of the Cartesian geometry used here. In the dynamical evolution of this system, there is a ballistic deceleration of the flow in each one of the channels; the deceleration is faster in the central channel (Fig.3.21). One can also see that, at longer times, the 4 arcade–structures will be permeated by intermittent flows. This picture could be seen as a possible depiction of the complex and very diverse dynamical structure of the recently observed Coronal Holes.

Note that for all our runs the flows were, initially, constant in time. We understand that up–flows from the chromosphere/TR have finite life times; the temporary channel creation process, therefore, will last only for the time dictated by the duration and other characteristics of the impinging flow–pulse. We now list several other omissions of this preliminary study: anisotropies of velocities and temperature (source of wave generation and instabilities), ionization, multi–species dynamics, flux emergence etc. are not

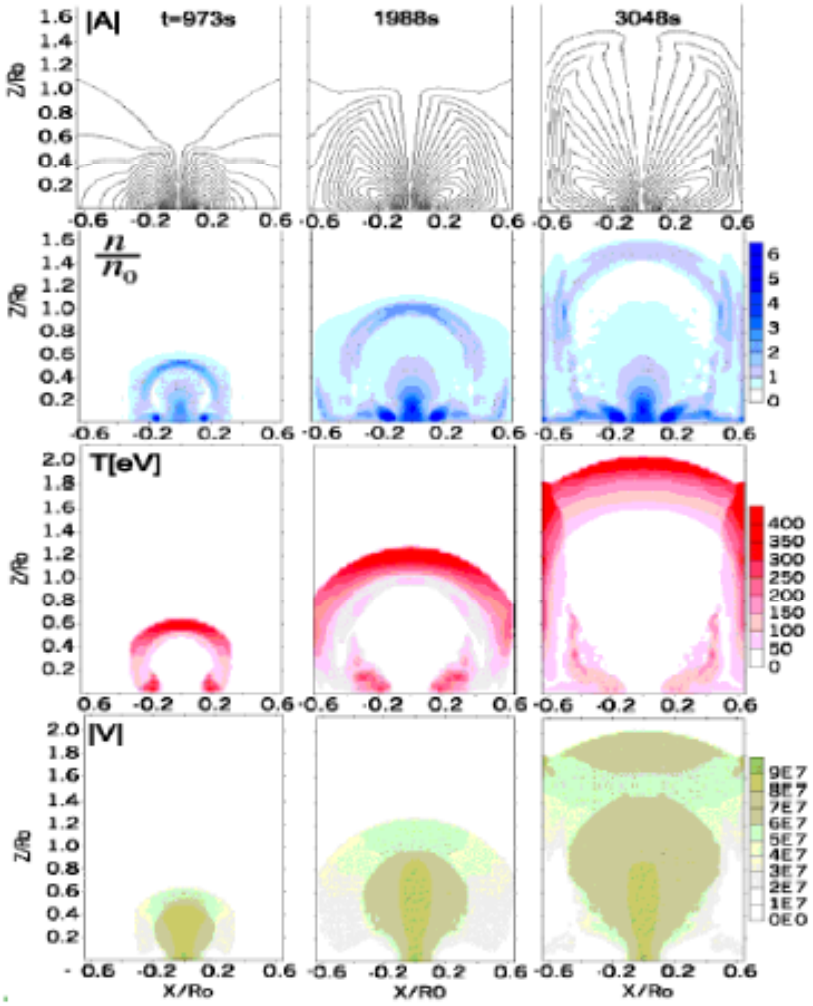


Figure 3-18: Dynamical Creation of Flow channels in the system of Fig.3.18 Plots for the vector potential $A$; the density $n$, the temperature $T$, and the speed $|\mathbf{V}|$ for 3 time frames $t = 973; 1988; 3048\, sec$. The channel for particle escape may be clearly seen. *Note*: The shock seen at the leading edge is an artifact due to the interaction of the flow with the background plasma (necessary for the smooth working of simulation code).

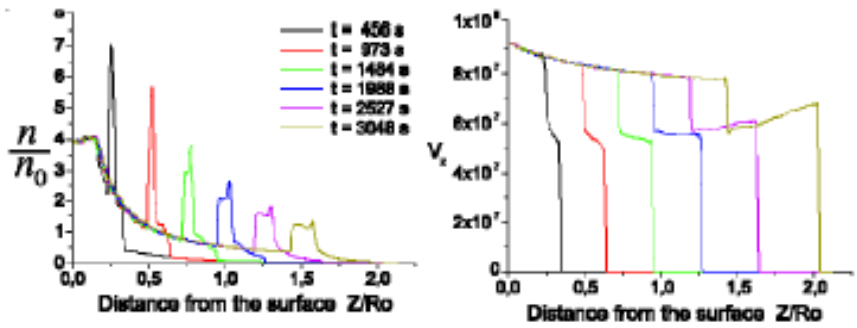


Figure 3-19: Evolution of: density $n(x=0,z)$, radial velocity $V_z(x=0,z)$ in the center of the escape channel of Fig.3 along the radial distance $z$. A sharp decrease in density and the accompanying ballistic deceleration of the initial flow is revealed. $z$–projection of the shock explained in Fig.3.18 is seen.

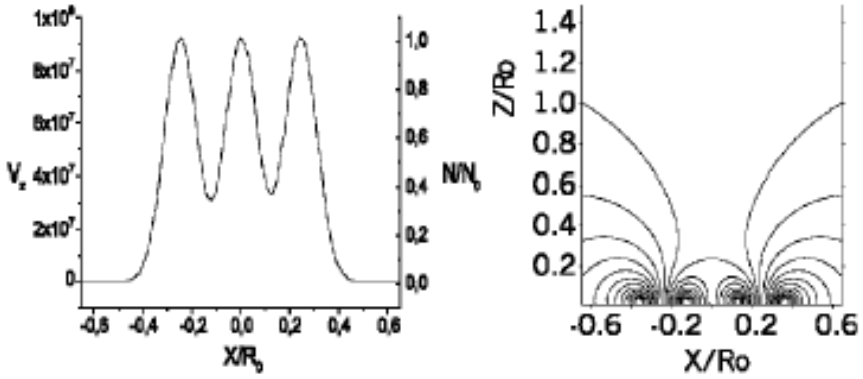


Figure 3-20: The 4–arcade + 3–pulse system. Boundary conditions for the initial flow (spatially non–uniform): $|\mathbf{V}_0|_{max} = 920\,km/sec$ , $n_0 = 2 \cdot 10^7\,cm^{-3}$; background density $= 5 \cdot 10^6\,cm^{-3}$; and initial condition for $A$ ( $(B_{0max} = 4\,G)$.

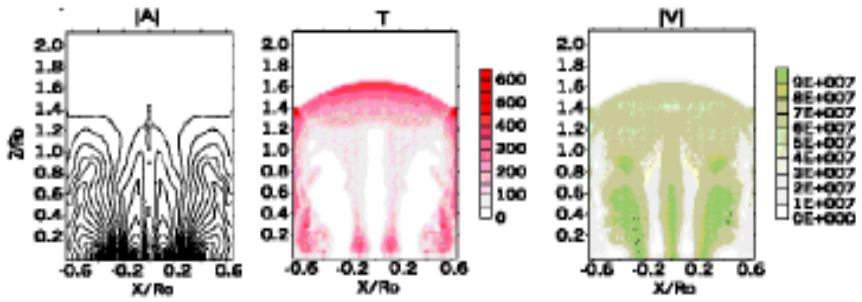


Figure 3-21: Inhomogeneous temporary channel creation in a structure of four identical arcades. The plots of the vector potential, temperature, velocity at $t = 2335\,sec.$ Deceleration is ballistic; the flow occupies practically the entire region.

included. Either of these could influence the channel–creation dynamics. We, however, believe that our simple model has adequately shown that sufficiently strong flows are capable of engineering their escape (self–induced transparency) from an area nested with a variety of co-existing closed field structures of different scales prevalent in the solar atmosphere.

## 3.6 1D analysis for Solar Wind Origin

Given a high speed solar emanation with sufficient radial speed that it can overcome Sun's gravity, the only barrier it must cross to reach us as the fast solar wind, is the magnetic field. Since the magnetic forces are "strong" in general, the only way for these particles to escape the solar atmosphere is to be either born, or to be kicked into the regions where the fields are essentially radial.

Thus the existence of the so called "coronal holes" (suggested by Parker and others), which are precisely such regions of nearly radial or open fields, is a necessary condition for particle escape, and therefore, for the solar wind formation. The polar regions automatically satisfy this requirement. It would appear that we are running headlong into a conflict with the very experimental fact that had motivated us to seek a new origin of the SW, i.e., the fast solar wind seems to come from all over the surface and not just from some specific regions (like the poles). And the coronal holes, even if they were to exist, could not occupy the entire solar surface, much of which is known to harbor closed field line structures (loops, arcades and etc.). In fact, it is believed that the "coronal holes" (CH) are limited to about 20 p.c. of the solar surface.

We believe that there is a very reasonable resolution of this difficulty. Although the CH–s cover only a small fraction of the solar surface, their locations on the solar surface is very much a function of time (excepting that of the polar regions, of course). Since the interior processes which lead to the creation of magnetic fields (open and closed), must be, in general, statistically random, the CH regions will also be randomly distributed. Averaged over some sufficiently long time interval, the CH will, then, uniformally cover (in a statistical sense) the entire surface of the Sun. Coupling it with the very plausible assumption that the primary emanations are emitted with equal probability over the surface, we may be able to understand why the fast solar wind seems to originate from the entire solar surface.

In this study, we do not intend to tie ourselves to any particular mechanism for the primary emanations. We are concerned, here, much more with an investigation

of the phenomena that magnetofluids can display. Below we give an extremely simple extrapolation from the general equations for the already created radial particle escape channels.

The bulk of the fast wind will consist of particles that escape through the open field regions. Since there is no accumulation of particles in these regions, we can safely neglect the the self–field $\mathbf{b}_f$ of the flow. In principle, even for small initial flow–currents $\mathbf{j}_f$ (a measure of the differential electron–proton motion), the magnetic force $\mathbf{j}_f \times \mathbf{b}_s$ is not negligible, and must be appropriately modeled. From the preceding discussion, we had concluded that in the regions from which the particles can escape (to eventually form the solar wind), this force also has to be negligibly small. The vanishing of this force can be used, perhaps, as the best operational definition of a coronal hole (CH). With the effect of the magnetic field gone, a pure radial dependence of the physical quantities may be enough to capture the essence of the plasma dynamics in these regions.

However there is a class of coronal holes where the field lines are nearly open. Such small–scale configurations are met in the background corona in the streamer belt areas. In these areas, the loops are very stretched (the distances between the footpoints are much less than the loop–heights), and the $\mathbf{j} \times \mathbf{b}$ force may not be negligible in the upper reaches of the region. In these regions, the conditions for particle escape may still exist but due to stronger dissipation effects the velocity of the particles may be less than they had initially.

A few remarks on the possibility of plasma heating in the regions of open field lines, are in order. The observations and models discussed in Hundhausen (1977) and Bravo & Stewart (1997) showed the dependence of the SW temperature and density (as well as the velocity) on the coronal hole sizes, their divergence, and also on the solar activity period. From Eq. (1.9), we can see that even for a purely radial dependence of the flow variables $(\mathbf{V}, \mathbf{j}_f)$, it is possible to have some temperature enhancement (over and above the intrinsic temperature that the flow may be born with) by the dissipation of a part of the flow energy. But this effect can not be strong. The observations also bear this out;

the coronal holes and the polar gaps are found to be relatively dark.

In purely open–field regions, the magnetic field curvature effects are weak near the solar surface and may become significant only far from the surface by virtue of the Solar rotation effects. Therefore, for an enquiry into the origin of the fast SW, the details of heating are not a major issue. We shall, however, come back to the heating problem when we investigate general coronal structures in the next section.

Let us also mention that, using Eq. (1.6), we could obtain different final temperatures for the species even if they had equal temperatures initially, because the heating mechanism proposed here (the conversion of the flow kinetic energy to heat) favors protons over electrons. This difference could remain significant for the escaping particles (SW particles, for example) because their densities are too low for an inter–species energy equiliberation. For the trapped particles, on the other hand, this difference can not be essential because the high plasma density will shorten the relaxation times, and both species will acquire the same final temperature.

To describe the solar wind, we now proceed to extract an extremely simple model from our general equations. In the wake of the preceding discussion, we assume

$$T = \text{const}, \qquad \mathbf{b}_f \to 0 \tag{3.23}$$

in the regions of the open magnetic fields.

Let us study the flow–magnetic field interaction in the equatorial plane (Weber & Davis 1967) where we have only radial dependence (in spherical coordinates). Let the solar field $\mathbf{b}_s$, and the normalized flow velocity $\mathbf{u} = \mathbf{V}/\sqrt{\beta}$, be represented as:

$$\mathbf{u} = (u_r(r),\ 0,\ u_\phi(r)), \qquad \mathbf{b}_s = (b_{sr}(r),\ 0,\ b_{s\phi}(r)), \tag{3.24}$$

where [from Eq. (1.15)]

$$b_{sr} = \frac{b_\odot}{r^2}. \tag{3.25}$$

Other relevant equations follow from Eqs. (1.13) and (1.16), after neglecting dissipation,

$$\frac{\partial u_r}{\partial t} + u_r \frac{\partial u_r}{\partial r} - \frac{u_\phi^2}{2} +$$

$$+ \frac{\partial}{\partial r} \ln\ N - (\alpha\beta)^{-1}\ \frac{r^2}{N}\ j_{f\theta}\ b_{s\phi} - 2\frac{\partial}{\partial r}\left[\frac{r_c}{r} + \ln\ r\right] = 0, \tag{3.26}$$

$$\frac{\partial}{\partial t} u_\phi + \frac{u_r}{r}\frac{\partial}{\partial r}(r\ u_\phi) = -(\alpha\beta)^{-1}\ \frac{r^2}{N}\ j_{f\theta}\ b_{sr}, \tag{3.27}$$

$$\frac{\partial N}{\partial t} + \frac{\partial}{\partial r}(N\ u_r) = 0. \tag{3.28}$$

where $N = n \cdot r^2$, and $t \rightarrow t \cdot \sqrt{\beta}$, where $r_c$ is the distance at which the gravitational and the pressure gradient force are numerically equal. These equations have to be solved in conjunction with the following boundary conditions:

$$u_r(1AU) \equiv u_{r\infty} = \frac{(750\ \mathrm{km/s})}{c_s}; \qquad u_\phi(R_\odot) = \Omega_s R_\odot;$$

$$b_{s\phi}(R_\odot) = 0; \qquad j_{f\theta}(R_\odot) = ?, \tag{3.29}$$

where the first boundary condition is dictated by the observed solar wind speed. In (3.29), the subscript "$\odot$" ($r = 1$) denotes the solar surface, $\Omega_s$ is the solar rotation frequency. For completeness, the quantities $b_{s\phi}$, and $j_{f\theta}$ have to be modeled. It is now necessary to stipulate that the intrinsic flow currents (which, in fact, depend on the solar particle emanation mechanisms) are insignificant(or are parallel to the magnetic field) so that the magnetic force influence on the particle propagation is weak. Otherwise particles won't be able to escape to create fast SW with the required characteristics.

Let us further ignore the rotation of the Sun ($\Omega_s \rightarrow 0$) so that the solar magnetic field lines are purely straight, and $b_{s\phi}(r) \rightarrow 0$. Consequently $u_\phi(r) \rightarrow 0$ , and we are left to solve Eqs. (3.26) and (3.28) without the terms containing $b_{s\phi}(r)$ and $u_\phi(r)$. We remind the reader that all this truncation is being done just to show, in a very simple scenario, the origin of the solar wind.

If time–dependence were neglected, these equations are precisely the ones that Parker

(1958) had in his original calculation. We shall soon show where and how do we differ from his conclusions.

A closed form solution for the radial speed and density can be readily written down for the time–independent case. The analytic form (can be seen in Parker (1958)), however, is not particularly useful in visualizing the radial variation. Therefore we present here the results of numerical simulation of the time–dependent system. For this purpose we have taken $r_\infty = 200$. We use two different temperatures $T = 2 \cdot 10^5\,\mathrm{K}$, and $T = 10^6\,\mathrm{K}$; the first choice corresponds to the current observational value, while the second reflects the temperatures used in earlier times (essentially the temperature of the coronal particles which were supposed to be accelerated to create the fast wind).

For the lower temperature case, the time asymptotic solution (starting from a variety of initial conditions) leads to the upper curve ($r_c = 24,\ u_\infty = 12,\ V_{r\infty} = 750\,\mathrm{km/s}$, $c_s = 63\,\mathrm{km/s}$) of Fig. 3.22. Notice that the flow velocity is maximum (950 km/s) at the solar surface, decelerates due to gravity, and soon reaches a plateau value. What is interesting is that there is just the expected region of deceleration but none of acceleration at these lower temperatures.

This is, of course, in some contrast to what pertains for the higher temperature ($T = 10^6\,\mathrm{K},\ r_c = 4.8,\ u_\infty = 5.4,\ c_s = 140\,\mathrm{km/s}$) case shown as the lower curve in Fig.3.22. Starting from a velocity maximum at the solar surface ($V_{r\odot} = 720\,\mathrm{km/s} < V_{r\infty} = 750\,\mathrm{km/s}$), the flow experiences a rapid deceleration up to $r_c = 4.8$ to the velocity $V_r(r_c) = 590\,\mathrm{km/s} < V_{r\infty}$ and then a slow but significant acceleration to the SW velocity $= V_{r\infty}$.

Note that a similar class of solutions for the solar wind were very much there in the general solution given by Parker (1958). But because of the poor observational data available at that time, these solutions were ignored; it was hard, then, to believe that such high speed particles can exist at the solar surface. Lack of evidence of high speed particles near the Sun was, perhaps, the determining factor which biased the leaders in this field towards the “acceleration" dominated theories of the solar wind. An essential

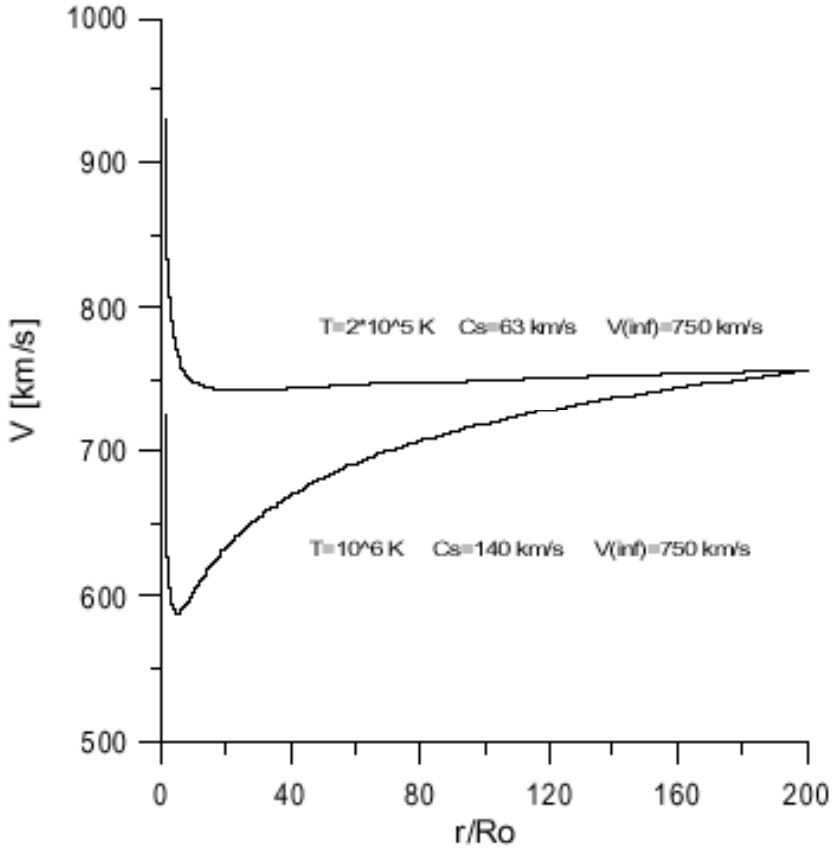


Figure 3-22: Radial plots of the solar wind speed for temperature $T = 2 \cdot 10^5\, K$ [$C_s =$ 63 km/s] and $T = 10^6\, K$ [$C_s = 140\,\mathrm{km/s}$]. The asymptotic speed $V_\infty = 750\,\mathrm{km}$ is the boundary condition at $1AU$. These are the time asymptotic plots.

part of these theories was to look for mechanisms of plasma acceleration to arrive at the fast SW velocity observed at 1 AU (see Parker 1992; Axford & McKenzie 1992; Tu & Marsch 1997; Mckenzie, Banaszkiewicz & Axford 1995).

And if the fast solar emanations exist, the solar wind follows naturally, in fact, rather trivially. Our only addition to the earlier system is a different set of boundary conditions at the solar surface. And these boundary conditions follow from the basic program that we had proposed in the beginning of this study, i.e., to accord a kind of a primacy to the flows. It is of utmost importance that observations seem to support the existence of these flows.

We have carried out extensive numerical experiments to show the stability as well as the accessibility of our solar wind solutions. Starting from a diverse set of initial conditions (some differing quite a bit from the eventual steady state solution) we were able to demonstrate that, indeed, the stationery solutions are the time asymptotic solutions of the initial value problem. The time history of a typical solution (for the lower temperature) is illustrated in Fig.3.23. We start from a spatially constant initial condition and see the system evolve to the asymptotic state in a fairly short time. In Fig.3.24, we show an example where the stability of this solution is tested by imposing a sinusoidal perturbation at time $t = 0$. Notice that the perturbations dies away leaving the stationary solution as the final state. This happens even when the perturbations are "large."

The continuity equation allows us to estimate (for a given solution) the flow density at the solar surface from a knowledge of the SW density at IAU (infinity in our calculations). Using the relation, $n_\odot V_{r\odot} R_\odot^2 = n_\infty V_{r\infty}(1\text{ AU})^2$, we find $n_\odot = 1.5 \cdot 10^5$ cm$^{-3}$ for $T = 1.5 \cdot 10^5$ K and the pertaining flow velocity value at the solar surface, $V_{r\odot} = 930$ km/s. The upper limit on the electron density in the CH bottom can be estimated using the empirical models relating the brightness and the electron density distribution in the corona, averaged for an activity cycle (Nikolskaya & Val'chuk 1997a). This method provides the value $n_e \simeq 5 \cdot 10^5$ cm$^{-3}$ at the bottom of the coronal holes . Thus, the plasma

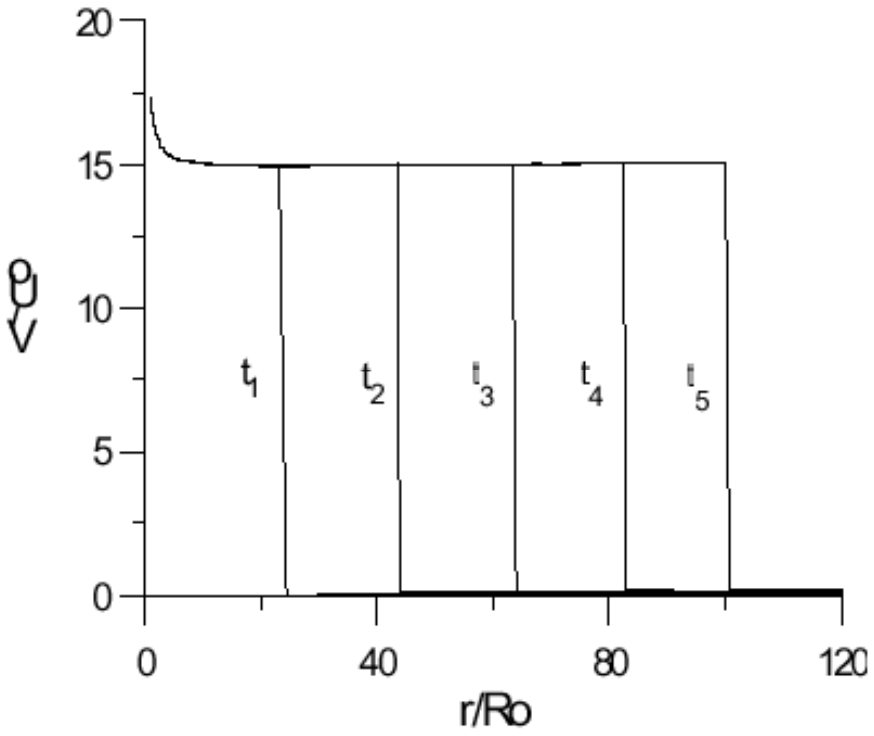


Figure 3-23: Fig.3.23 Radial plot of the normalized solar wind speed at different times in the evolution for $T = 2 \cdot 10^5$ K. The initial profile is $V_r = \text{const}$ for all $r$. As time becomes larger, the profile tends to become more and more like the upper curve in Fig.3.22.

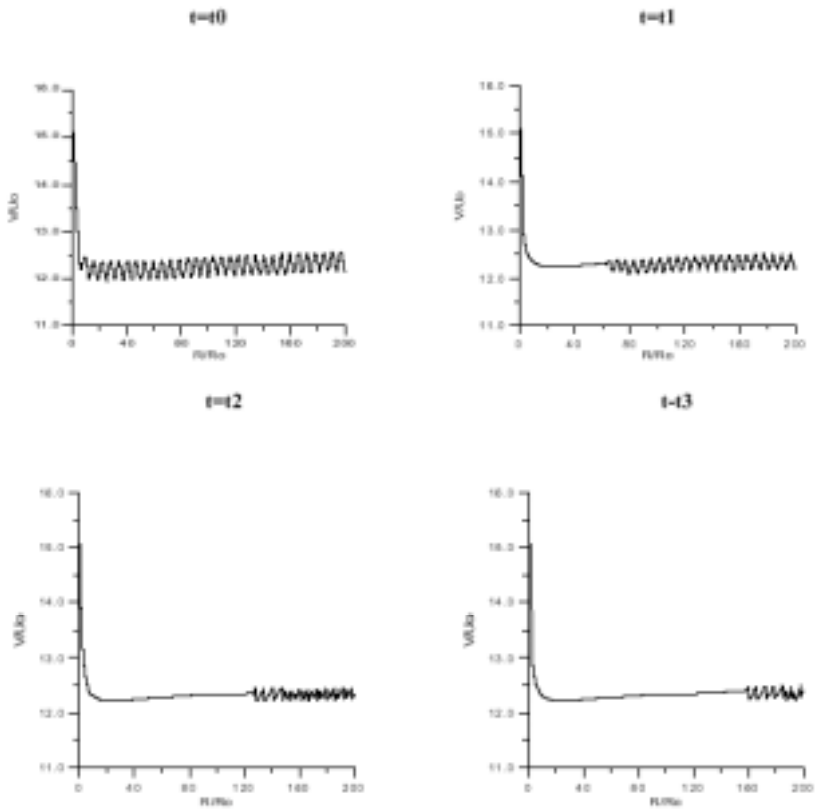


Figure 3-24: Radial plots of the normalized solar wind speed for different times. A sinusoidal perturbation is imposed on the upper solution displayed in Fig.3.22. Note that the perturbation decreases as the time goes on proving the stability of the solution

density of the primary emanations may be expected to lie in the range $(1.5 \div 5) \cdot 10^5$ cm$^{-3}$.

In our model for the origin of the solar wind we have not worried much either about the acceleration or the heating of the solar wind particles. We have also "neglected" the magnetic field effects. Naturally all these processes do take place and must find their way in any complete modeling of the solar wind. Our aim, in this section, was a bit limited; we wanted to present a possible zeroth order theory of the SW origin. Our choice to attempt to establish an unencumbered, primitive, origin theory was, partially dictated by historical reasons. We do know that Parker's original solution was subsequently extended

and modified in many ways—the energy balance equation (even two energy equations for the two species) was incorporated to give temperature effects, and the effects of magnetic field were also added. The CH–s were modeled for which a 2D MHD model was set up by Pneuman and Kopp (1971). But despite these modifications, the origin of the fast SW remained an enigma. The indications were that a different element (primary flows) may be necessary to resolve the issue. All the other effects may be necessary to understand the details of the characteristics of the solar wind but may not be crucial to lead us to its origin.

On a more technical side, it appears from Figs.3.22–3.23, that there exists the possibility of dissipative heating of the SW because of the variation of the radial velocity. However for the lower temperature (currently accepted) case, the gradients are quite weak (on the scale of $r_c$), and the classical dissipation turns out to be negligible.

We must, however, remark that the observations do show some temperature variation in the distant reaches of the coronal holes (Bravo & Stewart 1997). It is, in fact, expected that both heating and magnetic field effects may become important in such regions because of the relatively strong radial divergence of the field lines and the concomitant self–consistent flow vorticity. These effects require a multidimensional treatment and will be discussed in the context of the general corona.

## 3.7 Conclusions for Structure Creation in Solar Atmosphere

In this study we have investigated the conjecture that both the SW and the structures which comprise the solar corona (for the quiescent Sun) owe their origin to particle (plasma) flows emanating from the Sun's surface. These primary emanations are the sources which are expected to provide, on a continuous basis, much of the required material and energy. From a general framework describing a plasma with flows, we have been able to "derive" several of the essential characteristics of the solar wind, and of the coronal structures.

The principal distinguishing component of our model is the full treatment accorded to the velocity fields associated with the directed plasma motion (originally present or generated dynamically as shown in our model). It is the interaction of the fluid and the magnetic aspects of plasma that ends up creating so much diversity in the solar atmosphere.

This study has led to the following preliminary results:

1. The possibility of transient fast flow generation/acceleration of primary flows due to magneto-fluid coupling is explored. It is shown for the first time, that transient fast flows can generated low in the atsmosphere with observed parameters (ate the distances $\sim 0.01 R_s$.

2. The dynamical creation of particle escape channels for specific boundary conditions for the flow-closed magnetic field interactions is demonstrated.

3. In the created channels for particle escape – open magnetic field regions (neglecting curvature and heating effects), we obtain stable time asymptotic solutions with characteristics of the recently observed Fast Solar Wind. For the Primary emanations escaping through these regions to eventually appear as FSW, the maximum velocity was found at the solar surface. For example, for the observed FSW parameters: $V(1\mathrm{AU}) \sim 750 \div 800\,\mathrm{km/s}$; $T = 2 \cdot 10^5\,\mathrm{K}$, the surface velocity and density turn out to

be respectively $\sim 1000\,\mathrm{km/s}$, and $\sim (2 \div 5) \cdot 10^5\,\mathrm{cm}^{-3}$. The transient fast flow velocity first decelerates due to gravity but soon reaches the asymptotic (spatially) plateau value; there is no evidence of an acceleration region at this (and lower) temperature.

4. By using different sets of boundary conditions, it is possible to construct various kind of 2D loop and arcade configurations.

5. In the closed magnetic field regions of the solar atmosphere, the transient flows can accumulate to give sufficient material supply to the corona. Simultaneously with the accumulation, the flows, through viscous dissipation, can provide an efficient and sufficient source for the primary heating of the plasma. The stronger the spatial gradients of the flow, the greater is the rate of the dissipation of the kinetic energy into heat.

6. The magnetofluid equilibria reveal that for extreme sub–Alfvénic flows (most of the created corona flows) the velocity field can have a substantial, fastly varying (spatially) component even when the magnetic field may be mostly smooth. Viscous damping associated with this fast component could be a major part of the primary heating needed to create and maintain the bright, visible Corona. The far–reaching message of the equilibrium analysis is that neglecting viscous terms in the equation of motion may not be a good approximation until a large part of the primary flow kinetic energy has been dissipated.

7. The qualitative statements on plasma heating, made in points 4 and 5, were tested by a numerical solution of the time–dependent system. In case of sub–Alfvénic primary flows we find that the particle–accumulation begins in the strong magnetic field regions (near the solar surface), and soon spans the entire volume of the closed magnetic field regions. It is also shown that, along with accumulation, the viscous dissipation of the kinetic energy contained in the primary flows heats up the coronal structures to the observed temperatures, i.e., in the very first (and fast) stage of the coronal creation, much of the flow kinetic energy is converted to heat. This happens on a very short distance from the solar surface (transition region)—$0.03R_s$. The end of this transition region defines the base of the corona. In the transition region, the flow velocity has very

steep gradients. After the transition, the dissipation is insignificant, and in a very short time a nearly uniform (with insignificantly decreasing density and temperature on the radial distance) hot layer is created around the Sun—this is the equilibrium corona. The transition region from the solar surface to the equilibrium corona is also characterized by strongly varying (along both radial and transverse directions) temperature and density. Depending on the magnetic field configuration, the base of the hot region (of the bright corona) of a given structure acquires its appropriate density and temperature.

# Basic Results

1. An integrated Magneto–Fluid model, that accords full treatment to the Velocity fields associated with the directed plasma motion, is developed to investigate the dynamics of stellar coronal structures.

2. It is established that the interaction of the fluid and the magnetic aspects of plasma may be a crucial element in creating the diversity in the solar atmosphere.

3. It is shown that the structures which comprise the solar corona can be created by particle (plasma) flows observed near the Sun's surface — the primary heating of these structures is caused by the viscous dissipation of the flow kinetic energy.

4. A generalized Schrödinger–Boussinesq system of coupled equations is derived that describes the coupling between the high-frequency electromagnetic wave and low–frequency electron–acoustic wave arising from the cold plasma component.

5. The possibility of soliton formation in hot electron–positron un–magnetized plasma with small fraction of cold electron–ion plasma is investigated. The relevance of these results to astrophysical situations is pointed out.

6. It is shown, that by relating the velocity and the magnetic fields, the Hall term in the two–fluid model leads to a singular perturbation that enables the formation of an equilibrium given by a pair of two different Beltrami fields. This new set of relaxed states

includes a variety of plasma states that could explain a host of interesting phenomena. The H-mode (high-confinement) boundary layer, where a diamagnetic structure is self-organized under the coupling of the magnetic field, flow, electric field, and pressure, is an example. The theory also predicts the possibility of producing high beta equilibrium.

7. By modeling the closed field structures by "slowly" evolving Double–Beltrami two-fluid equilibria (created by the interaction of the magnetic and velocity fields), the conditions for catastrophic transformations of the original state are derived. It is shown that a catastrophic loss of equilibrium occurs when the macro–scale of a closed structure, interacting with its local surroundings, decreases below a critical value; the catastrophe is possible only if the total energy of the structure (for given helicities) also exceeds a well–defined threshold. It is shown that at the transition much of the magnetic energy of the original state is converted to the flow kinetic energy.

8. The differnt route to catastrophe within the developed theoretical framework when the characteristic length scales are not separable into micro and macro lengths is demonstrated.

9. The new approach to the quasistatic magnetic (QSM) field generation in the underdense cold unmagnetized electron plasma by subpicosecond relativistically strong c.p short EM pulses is developed. It is shown that due to the possibility of electron cavitation for narrow and intense beams, the increase in the generated magnetic field slows down as the beam intensity is increased. The structure of the magnetic field closely resembles that of the field produced by a solenoid. In extremely dense plasmas, highly intense EM pulses in the self-channeling regime can generate magnetic fields $\sim 100\, MG$ and greater.

10. Investigating the different initial density profiles for laser-produced plasmas, where the density scale length is typically of the order of that of the laser beam amplitude and taking into account the electron cavitation by relativistically strong short EM pulses, it is shown the advantage of the convex initial density profile compared to the concave one (or to the initially homogeneous plasma) to generate immense magnetic

fields ($\sim 200\,MG$ and greater) in the self-channeling regime by the currently available intense EM pulses.

11. The generation of generalized vorticity and quasi–static magnetic field by short relativistically strong EM pulse propagating in dissipative under–dense cold unmagnetized plasma is shown. It is demonstrated that due to dissipation the generated quasi–static axial current becomes the source for azimuthal quasi–static magnetic (QSM) field leading to the helical structure of magnetic field (exists even in weakly relativistic case).

12. For the first time, it is shown that a plasma flow (locally sub–Alfvénic) is accelerated while interacting with emerging/ambient arcade–like closed field structures. The time–scale for creating reasonably fast flows ($\gtrsim 100\,$km/s) is dictated by the initial ion skin depth while the amplification of the flow depends on local plasma $\beta$.

13. For the first time, it is shown that distances over which the flows become "fast" are $\sim 0.01\,R_s$ from the interaction surface; the fast flow localizes (with dimensions $\lesssim 0.05\,R_S$) in the upper central region of the original arcade. For fixed initial temperature, the final speed of the accelerated flow $\gtrsim 500\,$km/s, and the modification of the field structure are independent of the time-duration of the initial flow. In the presence of dissipation, these flows are likely to play a fundamental role in the heating of the finely structured Solar atmosphere.

14. It is shown that a generalized magneto-Bernoulli mechanism (which converts thermal energy into kinetic energy, or to the general magnetofluid rearrangement of a relatively constant kinetic energy, i.e., going from an initial high-density low-velocity state to a low-density high-velocity state) can effectively generate high-velocity flows in the solar subcoronal regions; sharp amplification of the flow speed is accompanied by a significant fall in density.

15. For the first time, the "reverse–dynamo" mechanism — the amplification/generation of fast plasma flows by micro scale (turbulent) magnetic fields via magneto–fluid coupling is recognized and explored/developed. It is shown that macroscopic magnetic fields and flows are generated simultaneously and proportionately from microscopic fields and

flows. The stronger the micro–scale driver, the stronger are the macro–scale products. Stellar and astrophysical applications are suggested.

16. Using a dissipative two–fluid code in which the flows are treated at par with the currents, the theory for dynamical temporary channel creation in a region nested with a variety of co–existing closed–field line structures is developed. It is shown, that this self-induced transparency may provide an attractive mechanism for the creation of transient (local) fast solar outflows.

17. Based on the conjectured and recently observed existence of plasma flows low in the atmosphere, a model for the Origin of the Solar Wind, and the creation and heating of the coronal structures is developed. Preliminary results reproduce many of the salient observational features.

# Acknowledgements

At the end I would like to express my enormous gratitude to all my collaborators and co-authors for finding the adequate interest to our joint ideas and work. Specifically I am grateful to my teacher Nodar Tsintsade for the inspirations, supervision and guiding my early studies. Especially I would thank my collaborator Vazha Berezhiani from Andronikashvili Institute of Physics for his fruitful joint work, the investigations we carried together and readiness to support the new initiatives. I would also thank my colleague Tamar Pataraia for her support; Jimsher Javakhishvili from I. Javakhishvili Tbilisi State University and seniors from Plasma physics department of the Andronikashvili Institute of Physics that greatly contributed in establishing me as a scientist: Davy Tskhakaya, Givi Suramlishvili, Vladimir Paverman, Tsiala Loladze, Ekaterina Khirseli, Ivane Murusidze and David Garuchava. I would like to thank all other members of this department that helped me to learn a lot of physics on the Laser-plasma interactions and plasma ignition problems: Gela Gelashvili, Eduard Barkhudarov, Tariel Chelidze, Sulkhan Nanonbashvili, George Rostomashvili, Nikoloz Kervalishvili and Vladimir Kortkhonjia. I highly appreciate my collaborators from otehr departments of Andronikashvili Instiute of Physics Solomon Mikeladze, Ketevan Sigua and Zaza Rostomashvili for the cooperation and sucessful joint work.

I express my gratitude to the scientists from other centers of Georgia for their co-

operation. Especially I am thankful to my colleagues from Abastumani Astrophysical Observatory Tbilisi laboratory where I always felt great interest to my personal achivements and work from: Jumber Lominadze, Elguja Tsikarishvili, Gia Machabeli, Avtandil Pataraya, George Chagelishvili, George Melikidze, Andria Rogava, Bidzina Chargeishvili and Revaz Chanishvili.

I am extremely grateful to my western, Japanese and Russian co-authors that extensively collaborated with me in carrying out the investigations presented in the thesis: S. M. Mahajan (Univ. Texas, US), Z. Yoshida (Univ. Tokyo, Japan), R. Miklaszewski (Warsaw,Poland), K.I. Nikol'skaya (IZMIRAN), S. Ohsaki (Univ. Tokyo, Japan), M. Iqbal (Pakistan), H. Kaya (TUBITAK, Turkey).

Finally I would like to stress my specific thanks to my parents, my daughter, brother and entire family for the spirit and conditions that I had when growing; the encouragement and personal examples, love and support I feel permanently.

# Bibliography


[1] Schrijver, C.J., Title, A.M., Berger, T.E., Fletcher,L., Hurlburt, N.E., Nightingale, R.W., Shine, R.A., Tarbell, T.D., Wolfson, J., Golub, L., Bookbinder, J.A., Deluca, E.E., McMullen, R.A., Warren, H.P., Kankelborg, C.C., Handy B.N. and DePontieu, B. "A new view of the solar outer atmosphere by the Transition Region and Coronal Explorer". 1999, Solar Phys., 187, 261-302.

[2] Aschwanden, M.J., Tarbell, T.D., Nightingale, R.W., Schrijver, C.J., Title, A., Kankelborg, C.C., Martens, P. and Warren, H. P. "Time Variability of the "Quiet" Sun Observed with TRACE. II. Physical Parameters, Temperature Evolution, and Energetics of Extreme-Ultraviolet Nanoflares". 2000, Astrophys. J., 535, 1047-1065.

[3] Golub, L., Bookbinder, J., DeLuca, E., Karovska, M., Warren,H., Schrijver, C.J., Shine, R., Tarbell, T., Title, A., Wolfson, J., Handy, B. and Kankelborg, C. "A new view of the solar corona from the transition region and coronal explorer (TRACE)". 1999, Phys. Plasmas, 6, 2205-2216.

[4] Beckers, J.M. "Solar Spicules". 1972, Ann. Rev. A& A 10, 73; 1979, Astrophys. J., 203, 739.

[5] Bohlin, J.D. In *Coronal Holes and High Speed Solar Wind Streams*, edited by J.B. Zirker (Colorado Assoc. Univ. Press, Boulder, CO 1977), p.27.

[6] Withbroe, G.L., Jaffe, D.T., Foukal, P.V., Huber, M.C.E., Noyes, R.W., Reeves, E.M., Schmahl, E.J., Timothy, J.G. and Vernazza, J.E. "Extreme-ultraviolet transients observed at the solar pole". 1976, Astrophys. J., 203, 528-532.

[7] Withbroe, G.L. "The role of spicules in heating the solar atmosphere Implications of EUV observations". 1983, Astrophys. J., 267, 825-836.

[8] Wilhelm, K., Marsch, E., Dwivedi, B.N., Hassler, D.M., Lemaire,P., Gabriel, A.H. and Huber, M.C.E. "The Solar Corona above Polar Coronal Holes as Seen by SUMER on SOHO". 1998, Astrophys. J., 500, 1023.

[9] Pneuman, G.W. and Orrall, F.Q. In *Physics of the Sun*, edited by P.A. Sturrock (Dordrecht: Reidel, 1986), Vol. II, p.71.

[10] Shibata, K. In *Solar and Astrophysical Magnetohydrodynamic Flows*, edited by K.C. Tsinganos (Dordrecht: Kluwer, 1996), p.217.

[11] Thomas, J.H. In *Solar and Astrophysical Magnetohydrodynamic Flows*, edited by K.C. Tsinganos (Dordrecht: Kluwer, 1996), p.39.

[12] Southwell, K. "Slow and Fast Solar Wind". 1997, Nature, 390, 235.

[13] Oluseyi, H.M., Walker II, A.B.C., Santiago, D.I., Hoover, R.B. and Barbee Jr., T.W. "Observation and Modeling of the Solar Transition Region. II. Identification of New Classes of Solutions of Coronal Loop Models". 1999, Astrophys. J., 527, 992-999.

[14] Feldman, U., Widing, K.G. and Warren, H.P. "Morphology of the Quiet Solar Upper Atmosphere in the $4\times10^4<T_e<1.4\times10^6$K Temperature Regime". 1999, Astrophys. J., 522, 1133-1147.

[15] Peter, H. and Judge, P.G. "On the Doppler Shifts of Solar Ultraviolet Emission Lines". 1999, Astrophys. J., 522, 1148-1166.

[16] Woo, R. and Habbal, S.R. "Imprint of the Sun on the Solar Wind". 1999, Astrophys. J., 510, L69-L72.

[17] Scudder, J. D. "On the causes of temperature change in inhomogeneous low-density astrophysical plasmas". 1992, Astrophys. J., 398, 299-318.

[18] Feldman, W.C., Gosling, J.T., McComas, D.J. and Philips, J.L. "Evidence for ion jets in the high-speed solar wind". 1993, J. Geophys. Res. 98, 5593-5605.

[19] Feldman, W.C., Habbal, S.R., Hoogeveen, G. and Wang, Y.-M. "Experimental constraints on pulsed and steady state models of the solar wind near the Sun". 1997, J. Geophys. Res., 102, 26905-26918.

[20] Li, X., Habbal, S.R. and Hollweg, J.V. "Heating and cooling of protons by turbulence-driven ion cyclotron waves in the fast solar wind". 1999, J. Geophys. Res. 104, 2521-2536.

[21] Hu, Y.Q. and Habbal, S. R. "Resonant acceleration and heating of solar wind ions by dispersive ion cyclotron wav". 1999, J. Geophys. Res. 104, 17,045.

[22] Bravo, S. and Stewart, G.A. "Fast and Slow Wind from Solar Coronal Holes". 1997, Astrophys. J., 489, 992.

[23] Sturrock, P.A. and Hartle, R.E. "Two-Fluid Model of the Solar Wind". 1966, Phys. Rev. Lett. 16, 628-631.

[24] Banaszkiewicz, M., Czechowski, A., Axford, W.I., McKenzie, J.F. and Sukhorukova, G.V. 1997, 31st ESLAB Symposium. (Noordwijk, Netherlands) ESTEC SP-415, 17.

[25] Browning, P. and Priest, E.R. "Kelvin-Helmholtz instability of a phased-mixed Alfven wave". 1984, A&A, 131, 283-290.

[26] Cally, P.S. "A Sufficient Condition for Instability in a Sheared Incompressible Magnetofluid". 2000, Solar Phys. 194, 189-196.

[27] Davila, J.M. "Heating of the solar corona by the resonant absorption of Alfven waves". 1987, Astrophys. J., 317, 514-521.

[28] Goedbloed, J.P. "Spectrum of ideal magnetohydrodynamics of axisymmetric toroidal systems". 1975, Phys. Fluids, 18, 1258-1268.

[29] Goossens, M. In *Advances in Solar System MHD*, ed. E.R. Priest and A.W. Hood (Cambridge), 137 (1991).

[30] Heyvaerts, J. and Priest, E.R. "Coronal heating by phase-mixed shear Alfven waves". 1983, A&A, 117, 220-234.

[31] Hollweg, J.V. "Resonances of coronal loops". 1984, Astrophys. J., 277, 392-403.

[32] Litwin, C. and Rosner, R. "Alfven Wave Transmission and Heating of Solar Coronal Loops". 1998, Astrophys. J., 499, 945.

[33] Parker, E.N. "Dynamics of the Interplanetary Gas and Magnetic Fields". 1958, Astrophys. J., 128, 664.

[34] Parker, E.N. *Interplanetary Dynamical Processes* (New York/London: Interscience Publishers 1963).

[35] Parker, E.N. "Topological Dissipation and the Small-Scale Fields in Turbulent Gase". 1972, Astrophys. J., 174, 499.

[36] Parker, E.N. "Nanoflares and the solar X-ray corona". 1988, Astrophys. J. 330, 474-479.

[37] Parker, E.N. "The X ray corona, the coronal hole, and the heliosphe". 1992, J. Geophys. Res., 97, 4311-4316.

[38] Parker., E.N.. *Spontaneous Current Sheets in Magnetic Fields* (Oxford University Press 1994).

[39] Parnell, PC.E., Smith, J., Neukirch, T. and Priest, E.R. "The structure of three-dimensional magnetic neutral points". 1996, Phys. Plasmas, 3, 759-770.

[40] Priest, E.R. and Demoulin, P. "Three-dimensional magnetic reconnection without null points. 1. Basic theory of magnetic flipping". 1995, J. Geophys. Res., 100, 23443-23464.

[41] Priest, E.R. and Titov, V.S. "Linear theory of steady X-point magnetic reconnection". 1996, Phil. Trans. R. Soc. Lond. A., 354, 2951.

[42] Craig, I.J.D. and Fabling, R.B. "Exact Solutions for Steady State, Spine, and Fan Magnetic Reconnection". 1996, Astrophys. J., 462, 969.

[43] Galsgaard, K. and Nordlund, A. "Heating and activity of the solar corona 1. Boundary shearing of an initially homogeneous magnetic field". 1996, J. Geophys. Res., 101, 13445-13460 .

[44] Mikic, Z., Schnack, D. and Van Hoven, G. "Dynamical evolution of twisted magnetic flux tubes. I - Equilibrium and linear stability". 1990, Astrophys. J., 361, 690-700.

[45] Schindler, K., Hesse, M. and Birn, J. "General magnetic reconnection, parallel electric fields, and helicity". 1988, J. Geophys. Res., 93, 5547-5557.

[46] Van Ballegooijen, A.A. "Cascade of magnetic energy as a mechanism of coronal heating". 1986, Astrophys. J., 311, 1001-1014.

[47] Heyvaerts, J. and Priest, E.R. "Coronal heating by reconnection in DC current systems - A theory based on Taylor's hypothesis". 1984, A& A, 137, 63-78; "A self-consistent turbulent model for solar coronal heating". 1993, Astrophys. J., 390, 297-308.

[48] Sudan, R.N. "Stability of field-reversed, force-free, plasma equilibria with mass flow". 1979, Phys. Rev. Lett., 79, 1277-1281; Sudan, R.N. and Spicer, D.C. "Conventional solar flare theory re-examined". 1997, Phys. Plasmas, 4(5), 1929-1935.

[49] Pfirsch, D. and Sudan, R.N. "Small scale magnetic flux-averaged magnetohydrodynamics". 1994, Phys. Plasmas, 1(8), 2488-2514; "Stability of force-free Taylor states in a new version of magnetic flux-averaged magnetohydrodynamics". 1996, Phys. Plasmas, 3(1), 29-34.

[50] Tsuneta, S. "Interacting Active Regions in the Solar Corona". 1996, Astrophys. J., 456, L63.

[51] Priest, E.R. "How is the Solar Corona Heated ?" 1997, Fifth SOHO Workshop (Oslo) (ESA SP–404), 93.

[52] Rosner, R., Tucker, W.H. and Vaiana, G.S. "Dynamics of the quiescent solar corona". 1978, Astrophys. J., 220, 643-665.

[53] Neupert, W.M., Nakagawa, Y. and Rust, D.M. "Energy balance in a magnetically confined coronal structure observed by OSO-7". 1975, Solar. Phys., 43, 359-376.

[54] Nikol'skaya, K.I. 1985, Astron. Zh., 62, 562; In *Mechanisms of Chromospheric and Coronal Heating*, ed. P. Ulmschneider, E. R. Priest and R. Rosner (Heidelberg: Springer, 1991), 113.

[55] Habbal, S.R. "Small scale structures in the solar corona". 1994, Space Sci. Rev. 70, 37.

[56] Foukal, P. *Solar Astrophysics* (New York Chichester Brisbane Toronto Singapore: A Wiley–Interscience Publication, 1990).

[57] Richtmyer, R.D. and Morton, K.W. *Difference Methods for Initial–Value Problems* (Interscience Publishers a division of John Wiley and Sons, New York, London, Sydney, 1967).

[58] Zalesak, S.T. "Fully multidimensional flux-corrected transport algorithms for fluids". 1979, J.Comp.Phys. 31, 335-362.

[59] Braginski, S.I. *Transport Processes in a Plasma*, in Reviews of Plasma Physics, edited by M.A. Leontovich (Consultants Bureau, New York, 1965), Vol.1, p. 205. 50

[60] Cox, D. P. and Tucker, W. H. "Ionization Equilibrium and Radiative Cooling of a Low-Density Plasma". 1969, Astrophys. J. 157, 1157.

[61] Potasch, S.R. "Radiative Cooling". 1965, Bull. Astron. Inst. Netherlands 18,8.

[62] Tucker, W. H. and Koren, M. "Radiation from a High-Temperature Low-Density Plasma: the X-Ray Spectrum of the Solar Corona". 1971, Astrophys. J. 168,283.

[63] McWhirter, R. W. P., Thonemann, P. C. and Wilson, R. "The heating of the solar corona. II - A model based on energy balance". 1975, Astron. Astrophys. 40,63-73.

[64] Taylor, J. B. "Relaxation of Toroidal Plasma and Generation of Reverse Magnetic Fields". 1974, Phys. Rev. Lett., 33, 1139; "Relaxation and magnetic reconnection in plasmas". 1986, Rev. Mod. Phys., 58, 741-763 .

[65] Faddeev, L. and Niemi, Antti J. "*Magnetic Geometry and the Confinement of Electrically Conducting Plasma".* 2000, Phys. Rev.Lett. 85, 3416-3419.

[66] Steinhauer, L. C. and Ishida, A. "Relaxation of a Two-Specie Magnetofluid". 1997, Phys. Rev. Lett. 79, 3423-3426 .

[67] Mahajan, S.M. and Yoshida, Z. "Double Curl Beltrami Flow: Diamagnetic Structures". 1998, Phys. Rev. Lett. 81, 4863-4866 .

[68] Mahajan, S.M. and Yoshida, Z. "A collisionless self-organizing model for the high-confinement (H-mode) boundary layer". 2000, Phys. Plasmas, 7(2), 635-640.

[69] Yoshida, Z. and Mahajan, S.M. "Simultaneous Beltrami conditions in coupled vortex dynamics". 1999, Journal Of Mathematical Physics, 40 (10), 5080-5091.

[70] Mahajan, S.M., Miklaszewsky, R., Nikol'skaya, K.I. and Shatashvili, N.L. 1999, *Primary Flows, the Solar Corona and the Solar Wind*. Preprint IFSR ♯ 857,Univ.of Texas, Austin, February 1999.

[71] Mahajan, S.M., Miklaszewsky, R., Nikol'skaya, K.I. and Shatashvili, N.L. 2000, "Primary Plasma Outflow and the Formation and Heating of the Solar Corona; The High Speed Solar Wind Formation". In *Structure and Dynamics of the Solar Corona*, eds. B.P.Philipov, V.V. Fomichev, G.N., Kulikova, (Troitsk of Moscow Reg.), p.117.

[72] Mahajan, S.M., Miklaszewski, R., Nikol'skaya, K.I. and Shatashvili, N.L. "Formation and primary heating of the solar corona: Theory and simulation". 2001, Phys. Plasmas, 8, 1340-1357.

[73] Mahajan, S.M., Miklaszewski, R., Nikol'skaya, K.I. and Shatashvili, N.L. "Formation and heating of the solar corona - theory and simulation". 2002, Adv. Space Res. 30(3) 571-576.

[74] Woltjer, L. "A theorem on force-free magnetic fields". 1958, In Proc. Nat. Acad. Sci. U.S.A. 44, 489.

[75] Priest, E.R. "Magnetohydrodynamics" in *Plasma Astrophysics* by J. G. Kirk, D. B. Melrose, E. R. Priest, ed. A.O. Benz and T. J.–L. Courvoisier (Springer-Verlag, 1994), p. 1.

[76] Finn, J.M. and Antonsen, "Turbulent relaxation of compressible plasmas with flow". T.M. 1983, Phys. Fluids, 26, 3540-3552.

[77] Begelman, M.C., Blandford, R.D. and Rees, M.D. "Theory of extragalactic radio sources". 1984, Rev. Mod. Phys. 56, 255-351 .

[78] Berezhiani, V.I. and Mahajan, S.M. "Large amplitude localized structures in a relativistic electron-positron ion plasma". 1994, Phys. Rev. Lett. 73, 1110-1113.

[79] Berezhiani, V.I. and Mahajan, S.M. "Large relativistic density pulses in electron-positron-ion plasmas". 1995, Phys. Rev. E, 52, 1968-1979.

[80] Javakhishvili, D.I. and Tsintsadze, N.L. 1973, Zh. Eksp. Teor. Fiz. 64, 1314, [1973, Sov. Phys. JETP, 37, 666].

[81] Kartal, S, Tsintsadze, L.N. and Berezhiani, V.I. "Localized structures of electromagnetic waves in hot electron-positron plasmas". 1995, Phys. Rev. E , 53, 4225-4228.

[82] Khirseli, E.M. and Tsintsadze, N.L. "Nonlinear waves in a two-temperature electron plasma". 1980-1084, Fizika Plazmy, 6, 1081 [1980, Sov. J. Plasma Phys. 6, 595].

[83] Lakhina, G.S. and Buti, B. "Generation of a d.c. field by nonlinear electromagnetic waves in relativistic plasmas". 1981, Astrophys. Space Sci. 79, 25-36.

[84] Lominadze, D.C., Machabeli, G.Z., Melikidze, G.I. and Pataraya, A.D. "Pulsar-magnetosphere plasma". 1986, Sov. J. Plasma Phys. 12, 712-1249.

[85] Michel, F.C. "Theory of pulsar magnetospheres". 1982, Rev. Mod. Phys. 54, 1-66.

[86] Rees, M.J. 1983, in G.W. Gibbons, S.W. Hawking and S.Siklos (eds.), *The Very Early Universe*, Cambridge University Press, Cambridge.

[87] Tajima, T. and Taniuti, T. "Nonlinear interaction of photons and phonons in electron-positron plasmas". 1990, Phys. Rev. A. 42, 3587-3602.

[88] Holcomb, K. A. and Tajima, T. "General-relativistic plasma physics in the early Universe". 1989, Phys. Rev. D 40, 3809-3818.

[89] Goldreich, P. and Julian, W. H. "Pulsar Electrodynamics". 1969, Astrophys. J. 157, 869.

[90] Miller, H. R. and Wiita, P. J. 1987, "Active Galactic Nuclei" (Springer, Berlin).

[91] Surko, C. M., Leventhal, M. and Passner, A. "Positron plasma in the laboratory". 1989, Phys. Rev. Lett. 62, 901-904.

[92] Surko, C. M. and Murphy, T. J. "Use of the positron as a plasma particle". 1990, Phys. Fluids B 2, 1372-1375.

[93] Greeves, R. G., Tinkle, M. D. and Surko, C. M. "Creation and uses of positron plasmas". 1994, Phys. Plasmas, 1439-1446.

[94] Kennel, C. F. and Pellat, R. "Relativistic nonlinear plasma waves in a magnetic field". 1976, J. Plasma Phys. 15, 335-355.

[95] Leboeuf, J. N., Ashour-Abdalla, M., Tajima, T., C. Kennel, F. Coroniti, F. and Dawson, J. M. "Ultrarelativistic waves in overdense electron-positron plasmas".1982, Phys. Rev. A 25, 1023-1039.

[96] Gedalin, M. E., Lominadze, J. G., Stenflo, L. and Tsitovich, V. N. "Nonlinear wave conversion in electron-positron plasmas". 1985, Astrophys. Space Sci. 108, 393-400.

[97] Berezhiani, V.I., Skarka, V. and Mahajan, S. M. "Relativistic solitary wave in an electron-positron plasma". 1993, Phys. Rev. E 48, R3252-R3255.

[98] Kates, R. E. and Kaup, D. J. "Nonlinear modulational stability and propagation of an electromagnetic pulse in a two-component neutral plasma". 1989, J. Plasma Phys. 42, 507-519.

[99] Gomberoff, L. and Galvão, R. M. O. "Modulational instability of a circularly polarized wave in a magnetized electron-positron plasma with relativistic thermal energies". 1997, Phys. Rev. E 56, 4574-4580.

[100] Shukla, P. K., Rao, N. N., Yu, M. Y. and Tsintsadze, N. L. "Relativistic nonlinear effects in plasmas". 1986, Phys. Rep. 138, 1-149.

[101] Kates, R. E. and Kaup, D. J. "Influence of an ambient magnetic field on the nonlinear modulational stability of circularly polarized electromagnetic pulses in a two-component neutral plasma". 1989, J. Plasma Phys. 42, 521-530.

[102] Shatashvili, N. L., Javakhishvili, J. I. and Kaya, H. "Nonlinear Wave Dynamics in Two-Temperature Electron-Positron-Ion Plasma". 1997, Astrophys. Space Sci. 250, 109-115.

[103] Shatashvili, N. L., Javakhishvili, J. I. and Kaya, H. "Nonlinear Wave Dynamics in Two-Temperature Electron-Positron-Ion Plasma". 1996, In *Proc. ICPP, Nagoya, Japan.* p.946 (1996). ArXiv: astro-ph/9810180.

[104] Kuznetsov, S. V. "Theory of envelope solitons of electromagnetic waves". 1982, Fiz. Plasmy 8, 352-356. [1982, Sov. Phys. JETP 8, 199].

[105] Rao, N. N. and Shukla, P. K. "Coupled Langmuir and ion-acoustic waves in two-electron temperature plasmas". 1997, Phys. Plasmas 4, 636-645.

[106] Rasmussen, J. Juul and Rypdal, K. "Blow-up in nonlinear Schrödinger equations-I. A general review". 1986, Phys. Scr. 33, 481.

[107] Chian, A. C. L. and Kennel, C. F. "Self-modulational formation of pulsar microstructures". 1983, Astrophys. Space Sci. 97, 9-18.

[108] Mikhailovskii, A. B., Onishchenko, O. G. and Tatarinov, E. G. "Alfven solitons in a relativistic electron-positron plasma. II. Kinetic theory ". 1985, Plasma Phys. Controlled Fusion 27, 539-556.

[109] Gangadhara, R. T., Krishnan, V. and Shukla, P. K. "The modulation of radiation in an electron-positron plasma". 1993, Mon. Not. R. Astron. Soc. 262, 151-163.

[110] Shatashvili, N. L. and Tsintsadze, N. L. "Nonlinear Landau damping phenomenon in a strongly turbulent plasma". 1982, Phys. Scr. T2/2, 511-516.

[111] Shatashvili, N.L.and Rao, N.N. "Localized nonlinear structures of intense electromagnetic waves in two-electron-temperature electron-positron-ion plasmas". 1999, Phys. Plasmas, 6, 66-71.

[112] Arnold, V.I. and Khesin, B.A. 1998, "Topological Methods in Hydrodynamics", Springer–Verlag: New York Berlin Heidelberg 1998, 72.

[113] Aschwanden, M.J., Nightingale, R.W. and Alexander, R.W. "Evidence for Nonuniform Heating of Coronal Loops Inferred from Multithread Modeling of TRACE Data". 2000a, Astophys. J., 541, 1059-1077.

[114] Aschwanden, M.J., Tarbell, T.D., Nightingale, R.W. *et al.*, "Time Variability of the "Quiet" Sun Observed with TRACE. II. Physical Parameters, Temperature Evolution, and Energetics of Extreme-Ultraviolet Nanoflares". 2000b, Astrophys. J. 535, 1047-1065.

[115] Birn, J., Gosling, J.T., Hesse, M., Forbes, T.G. and Priest, E.R. "Simulations of Three-Dimensional Reconnection in the Solar Corona". 2000, Astrophys. J. 541, 1078-1095.

[116] Chen, P.F. and Shibata, K. "An Emerging Flux Trigger Mechanism for Coronal Mass Ejections". 2000, Astrophys. J., 545, 524-531.

[117] Chen, J. "Physics of Coronal Mass Ejections: A New Paradigm of Solar Eruptions". 2001, Space Sci. Rev., 95, 165-190 .

[118] Choe, G.S. and Cheng, C.Z. "A Model of Solar Flares and Their Homologous Behavior". 2000, Astrophys. J., 541, 449-467.

[119] Christopoulou, E.B., Georgakilas, A.A. and Koutchmy, S. "Fine Structure of the Magnetic Chromosphere: Near-Limb Imaging, Data Processing and Analysis of Spicules and Mottles". 2001, Solar Phys., 199, 61-80 .

[120] Goodman, M.L. "The Necessity of Using Realistic Descriptions of Transport Processes in Modeling the Solar Atmosphere, and the Importance of Understanding Chromospheric Heating". 2001, Space Sci. Rev., 95, 79-93 .

[121] Jordan, R., Yoshida, Z. and Ito, N. "Statistical mechanics of three-dimensional magnetohydrodynamics in a multiply connected domain". 1998, Physica D, 114, 251-272.

[122] Forbes, T.G. and Isenberg, P.A. "A catastrophe mechanism for coronal mass ejections". 1991, Astrophys. J., 373, 294-307.

[123] Forbes, T.G. and Priest, E.R. "Photospheric Magnetic Field Evolution and Eruptive Flares". 1995, Astrophys. J., 446, 377.

[124] Ito, N. and Yoshida, Z. "Statistical mechanics of magnetohydrodynamics". 1996, Phys. Rev. E, 53, 5200-5206.

[125] Klimchuk, J.A. and Sturrock, P.A. "Force-free magnetic fields - Is there a 'loss of equilibrium'?". 1989, Astrophys. J. , 345, 1034-1041.

[126] Kusano, K., Suzuki, Y. and Nishikawa, K. "A solar flare triggering mechanism based on the Woltjer-Taylor minimum energy principle". 1995, Astrophys. J., 441, 942-951.

[127] Kusano, K. and Nishikawa, K. "Bifurcation and Stability of Coronal Magnetic Arcades in a Linear Force-free Field". 1996, Astrophys. J., 461, 415.

[128] Yoshida, Z. and Mahajan, S.M. "Variational Principles and Self-Organization in Two-Fluid Plasmas". 2002, Phys. Rev. Lett. 88, 095001.

[129] Montgomery, D., Turner, L. and Vahala, G. "Three-dimensional magnetohydrodynamic turbulence in cylindrical geometry". 1978, Phys. Fluids, 21, 757-764.

[130] Orlando, S., Peres, G. and Serio, S. "Models of stationary siphon flows in stratified, thermally conducting coronal loops. 1: Regular solutions". 1995a, Astrophys. and Astronomy, 294, 861-873 .

[131] Orlando, S., Peres, G. and Serio, S. 1995b, Astrophys. and Astronomy, 300, 549.

[132] Parker, E.N. "Inferring Mean Electric Currents in Unresolved Fibril Magnetic Fields". 1996, Astrophys. J., 471, 489.

[133] Roald, C.B., Sturrock, P.A. and Wolfson, R. "Coronal Heating: Energy Release Associated with Chromospheric Magnetic Reconnection". 2000, Astrophys. J., 538, 960-967.

[134] Rosner, R., Tucker, W.H. and Vaiana, G.S. "Dynamics of the quiescent solar corona". 1978, Astrophys. J., 220, 643-665.

[135] Sakurai, T. "Magnetic equilibria and instabilities". 1989, Solar Phys., 121, 347-360.

[136] Steinhauer, L.C. and Ishida, A. "Relaxation of a Two-Specie Magnetofluid". 1997, Phys. Rev. Lett.,79, 3423-3426 .

[137] Taylor, J.B. "Relaxation of Toroidal Plasma and Generation of Reverse Magnetic Fields". 1974, Phys. Rev. Lett. , 33, 1139-1141.

[138] Yoshida, Z. and Giga, Z. 1990, Math. Z. 204, 235.

[139] Wilhelm, K. "Solar spicules and macrospicules observed by SUMER". 2000, Asrophys. and Astronomy, 360, 351-362 .

[140] Winebarger, A.M., DeLuca, E.E. and Golub, L. "Apparent Flows above an Active Region Observed with the Transition Region and Coronal Explorer". 2001, Astrophys. J., 553, L81-L84.

[141] Yoshida, Z., Mahajan, S.M., Ohsaki, S., Iqbal, M. and Shatashvili, N. "Beltrami fields in plasmas: High-confinement mode boundary layers and high beta equilibria". 2001, Phys. Plasmas, 8, 1559-2131.

[142] Mourou, G. and Umstadter, D. "Development and applications of compact high-intensity lasers". 1992, Phys. Fluids B, 4, 2315-2325.

[143] http://www.rl.ac.uk/lasers

[144] Perry, M. and Mourou, G. "Terawatt to petawatt subpicosecond lasers". 1994, Science, 264, 917-924 .

[145] Tabak, M. et al., "Ignition and high gain with ultrapowerful lasers". 1994, Phys. Plasma, 1, 1626-1634.

[146] Borovskii, A.V., Korobkin, V.V. and Prokhorov, A.M. "On possible applications of the self-channeling in matter of high-power ultrashort laser pulses". 1994, Zh. Eksp. Teor. Fiz. 106, 148 [ 1994, JETP, 79, 81-87].

[147] Berezhiani, V.I., Tskhakaya, D.D. and Shukla, P.K. "Pair production in a strong wake field driven by an intense short laser pulse". 1992, Phys. Rev. A 46, 6608-6612.

[148] Borisov, A.B. et al., "Observation of relativistic and charge-displacement self-channeling of intense subpicosecond ultraviolet (248 nm) radiation in plasmas". 1992, Phys. Rev. Lett. 68, 2309-2312.

[149] Chiron, A. et al., "Experimental observations and simulations on relativistic self-guiding of an ultra-intense laser pulse in underdense plasmas". 1996, Phys. Plasma, 3, 1373-1401.

[150] Nakajima, K. et al., "Observation of Ultrahigh Gradient Electron Acceleration by a Self-Modulated Intense Short Laser Pulse". 1995, Phys. Rev. Lett. 74, 4428-4431.

[151] Tajima, T. and Dawson, J.M. "Laser electron accelerator". 1979, Phys. Rev. Lett. 43, 267-270.

[152] Gorbunov, L.M. and Kirsanov, V.I. "The excitation of plasma waves by an electromagnetic wave packet". 1987, Zh. Eksp. Teor. Fiz. 93, 509-518 [1987, Sov. Phys. JETP, 66, 290].

[153] Bulanov, S.V., Kirsanov, V.I. and Sakharov, A.S. "Excitation of ultrarelativistic Langmuir waves by an electromagnetic radiation pulse". 1989, Pis'ma Zh. Eksp. Teor. Fiz. 50, 176-178 [1989, Sov. JETP Letters 50, 198].

[154] Berezhiani, V.I. and Murusidze, I.G. "Relativistic wake-field generation by an intense laser pulse in a plasma". 1990, Phys. Lett. A 148, 338-340.

[155] Sprangle, P., Esarey, E. and Ting, A. "Nonlinear theory of intense laser-plasma interactions". 1990, Phys. Rev. Lett. 64, 2011-2014.

[156] Litvak, A.G. 1969, Zh. Eksp. Teor. Fiz. 57, 629 [1970, Sov. Phys. JETP 30, 344].

[157] Max, C., Arons, J. and Langdon, A. "Self-Modulation and Self-Focusing of Electromagnetic Waves in Plasmas". 1974, Phys. Rev. Lett. 33, 209-212 .

[158] Garuchava, D.P., Rostomashvili, Z.I. and Tsintsadze, N.L. "Self-focusing of strong electromagnetic beams in an inhomogeneous plasma". 1986, Fiz. Plazmy 12, 1341-1347 [1986, Sov. J. Plasma Phys. 12, 776].

[159] Barnes, D.C., Kurki-Suonio, T. and Tajima, T. 1987, IEEE Trans. Plasma Sci. PS-15, 154.

[160] Sun, G.Z., Ott, E., Lee, Y.C. and Guzdar, P. "Self-focusing of short intense pulses in plasmas". 1987, Phys. Fluids, 30, 526-532.

[161] Borisov, A.B. et al., "Relativistic and charge-displacement self-channeling of intense ultrashort laser pulses in plasmas". 1992, Phys. Rev. A, 45, 5830-5845.

[162] Brandi, H.S. et al., "Relativistic and ponderomotive self-focusing of a laser beam in a radially inhomogeneous plasma. I. Paraxial approximation". 1993, Phys. Fluids B, 5, 3539-3550.

[163] Komashko, A. et al., "Relativistic self-focusing in a plasma". 1995, Pis'ma Zh. Eksp. Teor. Fiz., 62, 849 [1995, JETP Lett., 62, 860-865].

[164] Shukla, P.K., Rao, N.N., Yu, M.Y. and Tsintsadze, N.L.. "Relativistic nonlinear effects in plasmas". 1986, Phys. Rep., 138, 1-149.

[165] Wilks, S.C. , Kruer, W.L., Tabak, M. and Langdon, A.B. "Absorption of ultra-intense laser pulses". 1992, Phys. Rev. Lett., 69, 1383-1386.

[166] Sudan, R.N. "Mechanism for the generation of 109 G magnetic fields in the interaction of ultraintense short laser pulse with an overdense plasma target". 1993, Phys. Rev. Lett., 70, 3075-3078.

[167] Tsintsadze, L.N. and Shukla, P.K. "A novel mechanism for strong magnetic field generation by ultra-intense laser pulses". 1994, Phys. Lett. A, 187, 67-70.

[168] Lehner, T. "Intense magnetic field generation by relativistic ponderomotive force in an underdense plasma". 1994, Physica Scripta, 49, 704.

[169] Berezhiani, V.I., Tskhakaya, D.D. and Auer, G. "Some remarks on spontaneous magnetic field generation and the nonlinear dynamics of a Langmuir plasma". 1987, J. Plasma Phys., 38, 139-153.

[170] Askar'yan, G.A., Bulanov, S.V., Pegoraro, F. and Pukhov,A.M. 1995, Comments Plasma Phys. Controlled Fusion, 17, 35.

[171] Askar'yan, G.A., Bulanov, S.V., Pegoraro, F. and Pukhov,A.M., "Nonlinear evolution of ultrastrong laser pulses in a plasma. New phenomena of magnetic interaction between strong electromagnetic beams". 1995, Fizika Plazmy, 21, 884 [1995, Plasma Phys. Rep. 21, 835-846].

[172] Gorbunov, L., Mora, P. and Antonsen,Jr., T.M. "Magnetic Field of a Plasma Wake Driven by a Laser Pulse". 1996, Phys. Rev. Lett., 76, 2495-2498.

[173] Bulanov, S.V. et al., "Electron Vortices Produced by Ultraintense Laser Pulses". 1996, Phys. Rev. Lett., 76, 3562-3565.

[174] Pitaevskii, L.P. 1960, Zh. Eksp. Teor. Fiz., 39, 1450 [1961, Sov. Phys. JETP, 39, 1008].

[175] Steiger, A.D. and Woods, C.H. "Intensity-Dependent Propagation Characteristics of Circularly Polarized High-Power Laser Radiation in a Dense Electron Plasma". 1972, Phys. Rev. A, 45, 1467-1474.

[176] Abdullaev, A.Sh. and Frolov, A.A. "The inverse Faraday effect in a relativistic electron plasma". 1981, Zh. Eksp. Teor. Fiz., 81, 927-932 [1981, Sov. Phys. JETP, 54, 493].

[177] Abdullaev, A.Sh., Aliev, Yu.M. and Frolov, A.A. "Generation of quasi-static magnetic fields by strong circularly polarized electromagnetic radiation in a relativistic magnetoactive plasma". 1986, Fiz. Plasmy, 12, 827-835 [1986, Sov. J. Plasma Phys., 12, 476].

[178] Bychenkov, V.Yu., Demin, V.I. and Tikhonchuk, V.T. "Electromagnetic field generation by an ultrashort laser pulse in a rarefied plasma". 1994, Zh. Eksp. Teor. Fiz. 105, 118 [1994, JETP, 78, 62-67].

[179] Gorbunov, L.M. 1976, Sov. Phys. Usp., 16, 217.

[180] Tsintsadze, N.L. and Tskhakaya, D.D. "On the theory of electrosound waves in a plasma". 1977, Sov. Phys. JETP, 45, 252-255.

[181] Bourdier, A. and Fortin, X. "Nonlinear linearly polarized standing waves in a cold-electron overdense plasma". 1979, Phys. Rev. A, 20, 2154-2161.

[182] Berezhiani, V.I. and Murusidze, I.G. "Relativistic wake-field generation by an intense laser pulse in a plasma". 1990, Phys. Lett.148, 338-340.

[183] Abdullaev, A.Sh. and Frolov, A.A. "Theory of inverse Faraday effect in an inhomogeneous plasma". 1981, Pis'ma Zh. Eksp. Teor. Fiz., 33, 107 [1081, JETP Lett., 33, 101-102].

[184] Mora, P. and Antonsen, Jr., T.M. "Electron cavitation and acceleration in the wake of an ultraintense, self-focused laser pulse". 1996, Phys. Rev. E, 53, R2068-R2071.

[185] Gorbunov, L., Mora, P. and Antonsen, Jr., T.M. "Magnetic Field of a Plasma Wake Driven by a Laser Pulse". 1996, Phys. Rev. Lett. 76, 2495-2498.

[186] Tripathi, V.K. and Liu, C.S. "Self-generated magnetic field in an amplitude modulated laser filament in a plasma". 1994, Phys.Plasmas, 1(4), 990-992.

[187] Tsintsadze, L.N. and Shukla, P.K. "A novel mechanism for strong magnetic field generation by ultra-intense laser pulses". 1994, Phys. Lett. A 187, 67-70.

[188] Lehner, T. "Intense magnetic field generation by relativistic ponderomotive force in an underdense plasma". 1994, Physica Scripta, 49, 704.

[189] Rizzato, F.B. "Weak nonlinear electromagnetic waves and low-frequency magnetic-field generation in electron-positron-ion plasmas". 1988, J.Plasma Phys. 40(2), 289-298.

[190] Sheng, Z.M. and Meyer-ter-Vehn, J. "Inverse Faraday effect and propagation of circularly polarized intense laser beams in plasmas". 1996, Phys. Rev. E. 4, 1833-1842.

[191] Berezhiani, V.I., Mahajan, S.M. and Shatashvili, N.L. "Theory of magnetic field generation by relativistically strong laser radiation". 1997, Phys. Rev. E, 55(1), 995-1001.

[192] Berezhiani, V. I., Mahajan, S. M. and Shatashvili, N.L. "Quasistatic Magnetic Field Generation in Initially Inhomogeneous Plasma". 1998, Physica Scripta, T75, 280-282.

[193] Deschamps, J., Fitaire, M. and Lagoutte, M. "Inverse Faraday Effect in a Plasma". 1970, Phys. Rev. Lett. 25, 1330-1332.

[194] Bonnaud, G., Brandi, H.S., Manus, C., Mainfray, G. and Lehner,T. "Relativistic and ponderomotive self-focusing of a laser beam in a radially inhomogeneous plasma. II. Beyond the paraxial approximation". 1994, Phys.Plasmas, 1, 968-989.

[195] Kostyukov, I., Shvets, G., Fisch, N.J. and Rax, J.M. "Inverse Faraday effect in a relativistic laser channel". 2001, Laser and Particle Beams, 19, 133-136.

[196] Haines, M.G. "Generation of an Axial Magnetic Field from Photon Spin". 2001, Phys. Rev. Letters, 87, 135005-135008.

[197] Tsintsadze, N.L., Mima, K., Tsintsadze, L.N., et al. "Generation of magnetic field, vortices and relativistic particles by the nonpotential ponderomotive force". 2002, Phys. of Plasmas, 9 (10), 4270.

[198] Najmudin, Z. et al. "Investigating the Inverse Faraday Effect with an intense short pulse laser". 2000, Bulletin of APS, 5, 129.

[199] Landau, L.D. and Lifshitz, E.M., *The Classical Theory of Fields*, Pergamon, New York (1976).

[200] Aschwanden, M.J., Poland A.I., and Rabin D.M. "The New Solar Corona". 2001a, Ann. Rev. Astron. Astrophys., 39, 175-210.

[201] Aschwanden, M.J. "An Evaluation of Coronal Heating Models for Active Regions Based on Yohkoh, SOHO, and TRACE Observations". 2001b, Astrophys. J, 560, 1035-1044.

[202] Brynildsen, N., Maltby, P., Kjeldseth-Moe, O. & Wilhelm, K. "Dual Flows with Supersonic Velocities in the Sunspot Transition Region". 2004, Astrophys. J., 612, 1193-1195.

[203] Chertok, I.M., Mogilevsky, E.I, Obridko, V. N., Shilova, N. S. and Hudson, H. S. "Solar Disappearing Filament Inside a Coronal Hole". 2002, Astrophys. J., 567, 1225-1233.

[204] Cox, D.P. and Daltabutt, E. "Radiative Cooling of a Low-Density Plasma". 1971, Astrophys. J., 167, 113.

[205] De Moortel, I., Parnell, C.E. and Hood, A.W. "Determination of coronal loop properties from trace observations". 2003, Solar Phys. 215, 69-86.

[206] Falconer, D.A., Moore, R.L., Porter, J.G. and Hathaway, D.H. "Solar Coronal Heating and the Magnetic Flux Content of the Network". 2003, Astrophys. J., 593, 549-563.

[207] Feldman, U., Landi, E. and Curdt, W. "Nonthermal Mass Motions within the High-Temperature Plasmas above a Complex Solar Active Region". 2003, Astrophys. J., 585, 1087-1094.

[208] Goodman, M.L. "On the Mechanism of Chromospheric Network Heating and the Condition for Its Onset in the Sun and Other Solar-Type Stars". 2000, Astrophys. J., 533, 501-522.

[209] Hollweg, J.V., "Potential wells, the cyclotron resonance, and ion heating in coronal holes". 1999, J. Geophys. Res., 104, 505-520.

[210] Liu, Y., Jiang, Y., Ji, H., Zhang, H. and Wang, H. "Observational Evidence of a Magnetic Flux Rope Eruption Associated with the X3 Flare on 2002 July 15 ". 2003, Astrophys. J., 593, L137-L140.

[211] Magara,T. and Longcope, D.W. "Injection of Magnetic Energy and Magnetic Helicity into the Solar Atmosphere by an Emerging Magnetic Flux Tube". 2003, Astrophys. J., 586, 630-649.

[212] Mahajan, S.M., Miklaszewski, R., Nikol'skaya, K.I. and Shatashvili, N.L. "Dynamical Creation of Channels for Particle Escape in the Solar Corona". 2003, ArXive: astro-ph/0308012, 35 pages.

[213] Mahajan, S.M., Miklaszewski, R., Nikol'skaya, K.I. and Shatashvili, N.L. "The coronal hole creation: theory and simulation". 2002, Adv. Space Res. Vol. 30(3), pp. 545-550.

[214] Mahajan, S.M., Shatashvili, N.L., Mikeladze, S.V. and Sigua, K.I. "Acceleration of Plasma Flows Due to Reverse Dynamo Mechanism". 2005, Astrophys. J., 632, No.1.

[215] McKenzie, J.F., Sukhorukova, G.V. and Axword,W.I.. "The source region of the fast solar wind". 1998, Astronomy and Astrophys. 330, 1145-1148.

[216] Nikol'skaya, K.I., and Valchuk, T.E. 1998, Geomagnetizm and Aeronomy, 38, No. 2, 14.

[217] Nitta, N.V., Cliver, E. W. and Tylka, A.J. "Low Coronal Signatures of Large Solar Energetic Particle Events". 2003, Astrophys. J. , 586, L103-L106.

[218] Ohsaki, S., Shatashvili, N.L., Yoshida, Z., and Mahajan, S.M. "Magnetofluid Coupling: Eruptive Events in the Solar Corona". 2001, Astrophys. J., 559, L61-L65.

[219] Ohsaki, S., Shatashvili, N.L., Yoshida, Z., and Mahajan, S.M. "Energy Transformation Mechanism in the Solar Atmosphere Associated with Magnetofluid Coupling: Explosive and Eruptive Events". 2002, Astrophys. J., 570-407.

[220] Poedts, S., Rogava, A.D. and Mahajan, S. M. "Shear-flow-induced Wave Couplings In The Solar Wind". 1998, Astrophys. J. , 505, 369-375.

[221] Raymond, J.C., Cox, D.P. and Smith, B.W. "Radiative cooling of a low-density plasma". 1976, Astrophys. J., 204, 290-292.

[222] Richtmyer, R.D. and Morton, K.W. "Difference Methods for Initial–Value Problems". Interscience, New York, 1967.

[223] Sakai, J.I. and Furusawa, K. "Nonuniform Heating of Coronal Loop Footpoints and Formation of Loop Threads Associated with Up- and Downflows in the Solar Chromosphere". 2002, Astrophys. J., 564, 1048-1053.

[224] Socas–Navarro, H., and Sanchez Almeida, J. "Magnetic Fields in the Quiet Sun: Observational Discrepancies and Unresolved Structure". 2003, Astrophys. J. , 593, 581-586.

[225] Socas–Navarro, H., and Sanchez Almeida, J. "Magnetic Properties of Photospheric Regions with Very Low Magnetic Flux". 2002, Astrophys. J. , 565, 1323-1334.

[226] Socas–Navarro, H., Martinez Pillet, V. and Lites, B.W. "Magnetic Properties of the Solar Internetwork". 2004, Astrophys. J., 611, 1139-1148.

[227] Socas–Navarro, H. "Multiline Stokes Analysis for the Study of Small-Scale Solar Magnetic Fields". 2004, Astrophys. J., 613, 610-614.

[228] Socas–Navarro, H. and Lites, B.W. "Observational Evidence for Small-Scale Mixture of Weak and Strong Fields in the Quiet Sun". 2004, Astrophys. J., 616, 587-593.

[229] Tu, C.-Y. and Marsch, E.. "Two-Fluid Model for Heating of the Solar Corona and Acceleration of the Solar Wind by High-Frequency Alfven Waves". 1997, Solar Phys., 171, 363-391.

[230] Tu, C.-Y. and Marsch, E. "On cyclotron wave heating and acceleration of solar wind ions in the outer corona". 2001, J. Geophys. Res., 106, 8233-8252 .

[231] Uchida Y., Miyagoshi, T., Yabiku T., Cable S., and Hirose S. 2001, Publ. Astron. Soc. Japan, 53, 331.

[232] Winebarger, A.R., Warren, H., Van Ballagooijen, A., DeLuca E.E., and Golub, L. "Steady Flows Detected in Extreme-Ultraviolet Loops". 2002, Astrophys. J., 567, L89-L92.

[233] Woo, R., Habbal, S.R. & Feldman, U. "Role of Closed Magnetic Fields in Solar Wind Flow". 2004, Astrophys. J., 612, 1171-1174.

[234] Zhang, J., White, S.M. and Kundu, M.K. "Two-Temperature Coronal Models from SOHO/EIT Observations". 1999, Astrophys. J., 527, 977-991.

[235] Yang, G., Xu, Y., Cao, W., Wang, H., Denker, C. and Rimmele, T.R. "Photospheric Shear Flows along the Magnetic Neutral Line of Active Region 10486 prior to an X10 Flare". 2004, Astrophys. J., 617, L151-L154.

[236] Yoshida, Z., Ohsaki, S. and Mahajan, S.M. "Scale hierarchy created in plasma flow". 2004, Phys. Plasmas, 11, 3660.

[237] Bellot Rubio, L.R., Rodriguez Hidalgo, I., Collados, M., Khomenko, E. and Ruiz Cobo, B. "Observation of Convective Collapse and Upward-moving Shocks in the Quiet Sun". 2001, Astrophys. J., 560, 1010-1019.

[238] Blackman, E.G. and Field, G.B. "Dynamical magnetic relaxation: A nonlinear magnetically driven dynamo". 2004, Phys. of Plasmas, 11, 3264.

[239] Blackman, E.G. "Bihelical magnetic relaxation and large scale magnetic field growth". 2005, Phys. Plasmas, 12, 012304.

[240] Mahajan, S.M., Nikol'skaya, K.I., Shatashvili, N.L. & Yoshida, Y. "Generation of Flows in the Solar Atmosphere Due to Magnetofluid Coupling". 2002, Astrophys. J., 576, L161-L164.

[241] Mahajan, S.M., Shatashvili, N.L., Mikeladze, S.M. and Sigua, K.I. "Acceleration of Plasma Flows in the Solar Atmosphere Due to Magnetofluid Coupling - Simulation and Analysis". 2005, Astrophys. J. (submitted). ArXiv: astro–ph/0502345, 33 pages.

[242] Mahajan, S.M. and Krishan, V. "Exact solution of the incompressible Hall magnetohydrodynamics". 2005, Mon. Not. R. Astron. Soc., 359, L27-L29.

[243] Mininni, P. D., Gomez, D. O. and Mahajan, S.M. "Dynamo Action in Hall Magnetohydrodynamics". 2002, Astrophys. J., 567, L81-L83.

[244] Mininni, P. D., Gomez, D.O. and Mahajan, S.M. "Role of the Hall Current in Magnetohydrodynamic Dynamos". 2003, Astrophys. J., 584, 1120-1126.

[245] Mininni, P. D., Gomez, D.O. and Mahajan, S.M. "Waves, Coriolis Force, and the Dynamo Effect". 2005, Astrophys. J., 619, 1019-1018.

[246] Ryutova, M. and Tarbell, T. "MHD Shocks and the Origin of the Solar Transition Region". 2003, Phys. Rev. Lett., 90, 191101.

[247] Seaton D.B., Winebarger, A.R., DeLuca, E.E., Golub, L., and Reeves, K.K. 2001, Astrophys. J., "Active Region Transient Events Observed with TRACE". 563, L173-L177.

[248] Socas–Navarro, H. and Sainz, M. "Shocks in the Quiet Solar Photosphere: A Rather Common Occurrence". 2005, Astrophys. J., 620, L71-L74.

[249] Wallen, C. 1944. Ark. Mat. Astron. Fys., 30A, No.15.

[250] Wallen, C. 1945. Ark. Mat. Astron. Fys., 31B, No.3.

[251] Habbal, S.H. and Woo, R., "Connecting the Sun and the Solar Wind: Comparison of the Latitudinal Profiles of Coronal and Ulysses Measurements of the Fast Wind". 2001, Astrophys. J., 549, L253-L256.

[252] Lin, H., Penn,M.J. and Tomczyk, S. "A New Precise Measurement of the Coronal Magnetic Field Strength". 2000, Astrophys. J., 541, L83-L86.

[253] Habbal, S.H., Woo, R. and Arnaud, J., "On the Predominance of the Radial Component of the Magnetic Field in the Solar Corona". 2001, Astrophys. J., 558, 852-858.

[254] Ofman, L. and Davila, J.M., "Three-Fluid 2.5-dimensional Magnetohydrodynamic Model of the Effective Temperature in Coronal Holes". 2001, Astrophys.J., 553, 935-940.

[255] Granmer, S., Field, G.B. and Kohl, J.L., "Spectroscopic Constraints on Models of Ion Cyclotron Resonance Heating in the Polar Solar Corona and High-Speed Solar Wind". 1999, Astrophys. J., 518, 937-947.

[256] Doschek, G.A., *et al.*, "Properties of Solar Polar Coronal Hole Plasmas Observed above the Limb". 2001, Atrophys. J., 546, 559-568.

[257] Grall, R.R., *et al.*, "Rapid acceleration of the polar solar wind". 1996, Nature, 379, 429.

[258] Ofman, L., *et al.*, "IPS Observations of the Solar Wind Velocity and the Acceleration Mechanism", in *The 31st ESLAB Symposium on Correlated Phenomena at the Sun, Heliosphere and in Geospace*, ed. A. Wilson. ESTEC, Noordwijk, The Netherlands, 22-25 September 1997, 361, (1997).

[259] Lin, H. "On the Distribution of the Solar Magnetic Fields". 1995, Astrophys. J., 446, 421-429.